The Angiogenic Potential of Human Dental Pulp Stem Cells Cultured on 3D Silk Scaffolds

---

Dissertation

zur

Erlangung der naturwissenschaftlichen Doktorwürde
(Dr. sc. nat.)

vorgelegt der

Mathematisch-naturwissenschaftlichen Fakultät

der

Universität Zürich

von

Anna Maria Woloszyk

aus
Deutschland

Promotionskomitee

Prof. Dr. Michael Hengartner

Prof. Dr. Thimios Mitsiadis

Prof. Dr. Ralph Müller

Prof. Dr. Christian von Mering

Prof. Dr. Sabine Werner

PD Dr. Nagihan Bostanci

Zürich, 2016

Table of Contents

1. Summary 5
2. Zusammenfassung 6
3. Introduction 8
   3.1 Regenerative medicine and tissue engineering 8
   3.2 Stem cells 9
      3.2.1 Embryonic stem cells 10
      3.2.2 Adult stem cells and their niches 12
      3.2.3 Mesenchymal stem cells 14
      3.2.4 Induced pluripotent stem cells 15
   3.3 Dental mesenchymal stem cells 16
      3.3.1 The origin of dental stem cells - the tooth 16
      3.3.2 Dental pulp stem cells 17
      3.3.3 Stem cells from human exfoliated deciduous teeth 18
      3.3.4 Periodontal ligament stem cells 18
      3.3.5 Stem cells from the apical papilla 19
      3.3.6 Dental follicle stem cells 19
      3.3.7 Dental stem cell banking 20
   3.4 Vascularization 21
      3.4.1 Vascularization strategies for tissue engineering 23
         3.4.1.1 Scaffolds for the engineering of vascularized tissues 24
         3.4.1.2 Cell-based strategies for the engineering of vascularized tissues 25
         3.4.1.3 Growth factors 26
   3.5 Chorioallantoic membrane assay 26
4. Aims of the project 28
5. Materials and Methods 30
   5.1 Production of silk fibroin scaffolds 30
   5.2 Cell isolation, culture, and sorting 30
   5.3 Cell characterization 31
      5.3.1 Flow cytometry 31
      5.3.2 Immunocytochemistry 31
   5.4 Cell proliferation assay 31
   5.5 Cell cytotoxicity assay 32
   5.6 Cryopreservation of cells 32

5.7 Differentiation assays 32
5.7.1 Osteogenic differentiation 32
5.7.2 Chondrogenic differentiation 33
5.7.3 Adipogenic differentiation 33
5.8 Cell seeding 34
5.9 Chorioallantoic membrane assay 34
5.10 In vivo assay 35
5.11 Analyses 36
5.11.1 MicroFil® perfusion and microCT imaging 36
5.11.2 Histology and histomorphometrical analysis 36
5.11.2.1 Hematoxylin and Eosin staining 36
5.11.2.2 Manual blood vessel analysis 37
5.11.2.3 Picrosirius Red staining 37
5.11.2.4 Quantitative assessment of the collagen content 37
5.11.2.5 Von Kossa staining 37
5.11.3 Immunohistochemistry 37
5.11.4 Immunofluorescence 38
5.11.5 RNA isolation and quantitative real-time polymerase chain reaction 39
5.12 Statistical analysis 39
6. Results 40
6.1 In vitro characterization of hDPSCs 40
6.1.1 Cell morphology and proliferation of freshly isolated hDPSCs 40
6.1.2 Cell proliferation and cytotoxicity of hDPSCs 41
6.1.3 Expression of cell surface markers 42
6.1.4 Immunocytochemical analysis of unsorted hDPSCs and sorted hDPSCs 43
6.1.5 In vitro differentiation potential of unsorted hDPSCs and sorted hDPSCs 44
6.1.5.1 Osteogenic differentiation 44
6.1.5.2 Chondrogenic differentiation 45
6.1.5.3 Adipogenic differentiation 45
6.1.6 Cell survival of unsorted hDPSCs and sorted hDPSCs on 3D silk scaffolds in vitro 46
6.2 Histological and molecular analysis of 3D silk scaffolds cultured in ovo 48
6.2.1 Tissue morphology and histomorphometrical blood vessel analysis 48
6.2.2 Characterization of the extracellular matrix 50
6.2.3 Identification and characterization of vessel structures 51
6.2.4 Identification of stem cells of mesenchymal origin 52
6.2.5 Gene expression analysis 54

6.3 Histological and molecular analysis of 3D silk scaffolds cultured in vivo 55
6.3.1 Tissue morphology and histomorphometrical blood vessel analysis 55
6.3.2 Characterization of the extracellular matrix 58
6.3.3 Identification and characterization of vessel structures 60
6.3.4 Identification of stem cells of mesenchymal origin 61
6.3.5 Preliminary gene expression analysis 62
6.3.6 Mineralization 63
6.4 Visualization of the vascular network within hDPSC-seeded 3D silk scaffolds cultured in ovo 64
7. Discussion 66
7.1 Tissue integration and vascularization of 3D silk scaffolds 66
7.2 Human cell contribution to vascular structures within the 3D silk scaffold 69
7.3 Presence of potential progenitor cell reservoirs within cell-seeded 3D silk scaffolds 70
7.4 3D imaging of the developing vasculature within stem cell-seeded scaffolds cultured in ovo 71
7.5 Conclusion 72
8. Acknowledgments 74
9. List of Abbreviations 75
10. List of Figures 78
11. List of Tables 80
12. Curriculum Vitae 81
13. References 86
14. Appendix 99
14.1 Publications 99
14.1.1 Schiraldi et al., Eur Cell Mater, 2012 99
14.1.2 Mitsiadis et al., Nanomedicine, 2012 115
14.1.3 Woloszyk et al., PLoS One, 2014 127
14.1.4 Kivrak Pfiffner et al., Tissue Eng Part C, 2015 137
14.1.5 Mitsiadis and Woloszyk, Front Physiol, 2015 146
14.1.6 Woloszyk and Buschmann et al., Front Physiol, 2016 149
14.1.7 Woloszyk et al., Front Physiol, 2016 157

1. Summary

Current treatment after the loss of tissues or organs is mostly limited to the use of tissue autografts (e.g. skin) and organ allografts (e.g. kidney). However, the availability of grafts is restricted due to donor shortage as well as donor site morbidity. Recent advances in tissue engineering and regenerative medicine offer promising strategies for the generation of biological substitutes, which could help to overcome the mentioned problems. The core elements of tissue engineering are multipotent stem cells that have been discovered within the adult body and modern biocompatible materials, optionally combined with growth factors. While first cell-based treatments for the regeneration of avascular tissues (e.g. cartilage) are starting to enter the clinics, the engineering of vascularized tissues or even full organs remains a key challenge, as fast oxygen and nutrient supply of an implant is essential for its long-term survival and successful healing.

In this study we investigated the angiogenic potential of human dental pulp stem cells (hDPSCs) cultured on 3D silk scaffolds, since the dental pulp presents an easily accessible source of autologous multipotent mesenchymal stem cells, which have been previously shown to possess pro-angiogenic properties, and silk is a biomaterial that is approved for clinical use. We hypothesized that hDPSCs are able to attract the host's vasculature and can contribute to the neovascularization of the silk implant while recreating their stem cell niche within the biomaterial without any additional supplements.

HDPSC-seeded silk scaffolds attracted more vessels than empty scaffolds within the same incubation period in both chicken and mouse host organisms, resulting in better and faster integration of the implants into the surrounding tissue. Human cells were found to participate in functional blood vessels, expressing vWF, and being involved in the production of collagen type IV and laminin, the two main components of the vascular basement membrane. Increased collagen types I and III content, which plays an important role in wound healing processes, was present in cell seeded samples potentially improving the quality of the extracellular matrix that was produced within the scaffold. Furthermore, some cells of human origin within the scaffolds still expressed markers typical for undifferentiated mesenchymal cells, suggesting the presence of potential stem cell niches.

Taken together, the results suggest that the presence of hDPSCs supports and improves the vascular and tissue integration of the 3D silk scaffold within the host tissue, which is an essential factor for the development of future cell-based treatment strategies of tissue loss caused by injury or disease.

2. Zusammenfassung

Die heutigen Behandlungsmethoden, die nach dem Verlust von Gewebe oder eines Organs zur Verfügung stehen, beschränken sich grösstenteils auf die Transplantation von patienteneigenem Gewebe (z.B. Haut) und die Transplantation von Spenderorganen (z.B. Niere). Diese stehen jedoch nicht in ausreichender Menge zur Verfügung und verursachen zusätzlich Wunden an der Entnahmestelle, die zu Komplikationen führen können. Jüngste Fortschritte im Bereich des Tissue Engineering und der Regenerativen Medizin bieten vielversprechende Strategien für die Herstellung von biologischem Gewebeersatz, die helfen könnten die genannten Probleme zu lösen. Kernbestandteile des Tissue Engineering sind multipotente Stammzellen, die auch bei Erwachsenen entdeckt wurden, als auch moderne biokompatible Materialien, die optional mit Wachstumsfaktoren kombiniert werden können. Während erste zell-basierte Behandlungsmethoden für die Regeneration von gefässfreien Geweben (z.B. Knorpel) bereits in der Praxis angewandt werden, bleibt das Herstellen von durchbluteten Geweben oder gar ganzen Organen weiterhin eine wesentliche Herausforderung, da eine schnelle Sauerstoff- und Nährstoffversorgung eines Implantats für dessen langfristiges Überleben sowie für eine erfolgreiche Heilung unerlässlich ist.

In dieser Studie haben wir das angiogene Potential von humanen dentalen Pulpa-Stammzellen (hDPSZ), die auf einem 3D Seiden-Biomaterial kultiviert wurden, untersucht. Die Zahnpulpa ist eine leicht zugängliche Quelle zur Isolation von autologen multipotenten mesenchymalen Stammzellen, von denen man bereits weiss, dass sie ein pro-angiogenes Potential besitzen; Seide wiederum ist ein bereits klinisch zugelassenes Biomaterial. Wir haben die Hypothese aufgestellt, dass hDPSZ in der Lage sind Gefässe des Wirtsorganismus zum Einwachsen in das 3D Seiden-Biomaterial anzuregen und direkt zur Bildung neuer Gefässe beitragen zu können, während sie ihre eigene Stammzellnische innerhalb des Biomaterials ohne den Einsatz von Zusatzstoffen nachbilden.

Wir konnten zeigen, dass hDPSZ-besiedelte 3D Seiden-Biomaterialzylinder zu einer stärkeren Gefässbildung innerhalb des Biomaterials als zell-freie Konstrukte führten, sowohl nach Implantation auf der Chorioallantois-membran eines Hühnereis als auch subkutan in der Maus. Dies resultierte in einer besseren und schnelleren Integration des Implantats in das umliegende Gewebe. Humane Zellen waren an der Bildung von funktionsfähigen Blutgefässen beteiligt, exprimierten vWF und produzierten Kollagen Typ IV sowie Laminin, zwei der Hauptkomponenten der vaskulären Basalmembran. Ein erhöhter Kollagengehalt (Typ I und III), der bei der Wundheilung eine wichtige Rolle spielt, war in den zell-besiedelten Proben vorhanden und kann potentiell zur Qualitätsverbesserung der Zellmatrix, die innerhalb des Konstrukts produziert wird,

beitragen. Des Weiteren haben einige der Zellen humanen Ursprungs immer noch Marker exprimiert, die für undifferenzierte mesenchymale Stammzellen charakteristisch sind und daher suggerieren, dass potentielle Stammzellnischen vorhanden sind.

Zusammenfassend lässt sich sagen, dass die Anwesenheit von hDPSZ die vaskuläre als auch die Gewebsintegration eines 3D Seiden-Biomaterials innerhalb eines Wirtsorganismus unterstützen und verbessern kann. Dieses Wissen stellt einen essentiellen Faktor für die Entwicklung von zukünftigen zell-basierten Behandlungsverfahren von Gewebsverlusten nach Verletzung oder Krankheit dar.

3. Introduction

3.1 Regenerative medicine and tissue engineering

The idea of generating artificial tissues, organs or entire organisms dates back to ancient times. A first reference of organ regeneration can be found as early as in Greek mythology. As an eternal punishment by Zeus, Prometheus is chained to a rock and is attacked by an eagle every night who pecks away his daily regrowing liver (Chen and Chen, 1994). The famous painting 'Healing of Justinian' by Fra Angeliac, showing the transplantation of a homograft limb onto an injured soldier, represents another historical example of the early vision of regenerative medicine. This fundamental desire of people to generate, heal, and regenerate body parts fueled the emergence of all the related disciplines in engineering, medicine, and life sciences, whose principles are combined in regenerative medicine and tissue engineering. Consequently, the term regenerative medicine is used to define a field in health sciences that aims to replace or regenerate human cells, tissues, or organs to restore or establish normal function (Mason and Dunnill, 2008). Tissue engineering in turn is considered a subfield of regenerative medicine, focusing strictly on the *ex vivo* engineering of tissues by seeding cells on or into supporting biomaterials, optionally including soluble molecules to encourage cell proliferation and differentiation, as well as tissue growth (Katari et al., 2015) before being used as a graft. In contrast, regenerative medicine includes also *in vivo* regeneration by cell recruitment, gene manipulation, or combinations of these two elements (Orlando et al., 2011).

One of the first tissue engineering experiments was performed in 1988 (Vacanti et al., 1988). Mouse and rat hepatocytes, pancreatic islet cells, and cells from the small intestine were seeded onto biodegradable synthetic scaffolds, showing cell viability in culture, partial proliferation, as well as engraftment and vascularization of hepatocyte-seeded scaffolds *in vivo*. This and similar experiments (Cao et al., 1997) laid the foundation for the first tissue engineered product, i.e. artificial skin containing living keratinocytes and fibroblasts known as Apligraf™ (Alvarez et al., 1998), approved by the FDA in 1998. Bioengineered vessels (Shin'oka et al., 2001), bladder and urethra tissue (Atala et al., 2006; Raya-Rivera et al., 2011), as well as autologous nasal cartilage tissues for facial reconstruction (Fulco et al., 2014) represent further milestones in tissue engineering. Recently, the first stem cell-based product has been approved by the European Commission, namely Holoclar® (EMEA/H/C/002450), which uses autologous stem cells in order to enable patients with severe corneal injury to regain sight (Pellegrini and De Luca, 2014). An exemplary product falling under the definition of regenerative medicine is the INFUSE® bone graft (Medtronic), an absorbable collagen sponge carrying recombinant human bone morphogenetic

protein 2 (BMP2) that induces stem cell differentiation into osteoblasts, which results in accelerated bone healing. The FDA approved it to be administered in lumbar spinal fusion procedures, in bone fractures, and in dental restoration (McKay et al., 2007; Mundy, 1999).

The development of successful stem cell-based therapies is paving the way for personalized medicine, where each patient's genetic makeup is taken into consideration for a more precise, predictable, and powerful health care. Autologous stem cell-based products (e.g. Holoclar®) allow for therapies without the risk of immune rejections or toxicity caused by the transplant and will play an important role in future treatment of congenital and acquired diseases, as well as in the regeneration of injury- or disease-induced tissue loss.

Early tissue engineering approaches were using differentiated cell types isolated from the same tissues that needed to be repaired. However, since the first isolation of human embryonic stem cells in 1998 (Thomson et al., 1998), extensive work in regenerative medicine has focused on the application of these cells and other undifferentiated cells of adult origin in stem cell-based therapies aiming to regenerate lost or diseased tissues (Berthiaume et al., 2011).

3.2 Stem cells

The presence of stem cells in living organisms is essential in many ways. During embryogenesis they are the body's raw materials that give rise to all the cells, organs, and tissues in the fetus's body, whereas later in the adult body, stem cells are responsible for tissue maintenance and regeneration (Pessina and Gribaldo, 2006). Common properties of all stem cells are their unique ability to self-renew by going through numerous cell division cycles while remaining undifferentiated, as well as their potential to differentiate into specialized cell types under the influence of intrinsic and extrinsic signals (Morrison et al., 1997; Watt and Hogan, 2000; Weissman, 2000). Based on their plasticity, stem cells are classified as totipotent if they can give rise to an entire organism (i.e. cells of the zygote/morula during the first four days after fertilization) (Seydoux and Braun, 2006), as pluripotent if they can differentiate into cells of the three germ layers (e.g. embryonic stem cells isolated from the inner cell mass of the blastocyst forming on day five after fertilization) (Thomson et al., 1998), and as multipotent if they can produce differentiated cells from a closely related lineage system (e.g. mesenchymal stem cells isolated from bone marrow) (Weissman et al., 2001). Oligo- and unipotent stem cells possess limited differentiation capacities and can produce only a few cell types or only one cell type, respectively, but still have self-renewal capacity, which distinguishes them from non-stem cells (Wagers and Weissman, 2004).

3.2.1 Embryonic stem cells

Cultures of pluripotent stem cells from mouse embryos were first established in 1981 (Evans and Kaufman, 1981) laying the basis for regenerative medicine, tissue repair, modern stem cell research and gene therapy applications. Moreover, the development of genetically modified mice from embryonic stem cells became an important tool for studying genes involved in many human diseases (the Nobel Prize in Physiology or Medicine 2007 was jointly awarded to Mario R. Capecchi, Sir Martin J. Evans, and Oliver Smithies). The technologies developed for the isolation, culture, and maintenance of mouse embryonic stem cell lines ultimately led to the isolation of pluripotent embryonic stem cells from the inner cell mass of human blastocysts (Thomson et al., 1998). Due to their unique ability to differentiate into any cell of the three germ layers (endoderm, mesoderm, and ectoderm) as well as their indefinite proliferation capacity, these pluripotent stem cells could potentially be used for the generation of cells and tissues for cell-based therapies to treat diseases such as macular degeneration, spinal cord injury, stroke, burns, heart disease, and diabetes (Chang et al., 2013; Hamrahi et al., 2012; Lambert et al., 2015; Priest et al., 2015; S. D. Schwartz et al., 2015; Szot et al., 2014). However, the prospect of using embryonic stem cells also induced an ethical and moral debate, as potential life has to be destroyed first before embryonic stem cells can be used for research or for the treatment of diseases (Wobus and Boheler, 2005). Additional therapeutic problems related to embryonic stem cells are genetic and epigenetic concerns, the development of tumors as a result of uncontrolled differentiation, and the graft-versus-host reaction when allogeneic stem cells are transplanted, which all have to be solved in order to apply these cells in clinics (Wobus and Boheler, 2005). Despite these issues, findings from embryonic stem cell research are essential for the progress and development of therapeutic applications of adult stem cells, just as the isolation of human embryonic stem cells would not have been possible without the initial isolation of embryonic stem cells from mice.

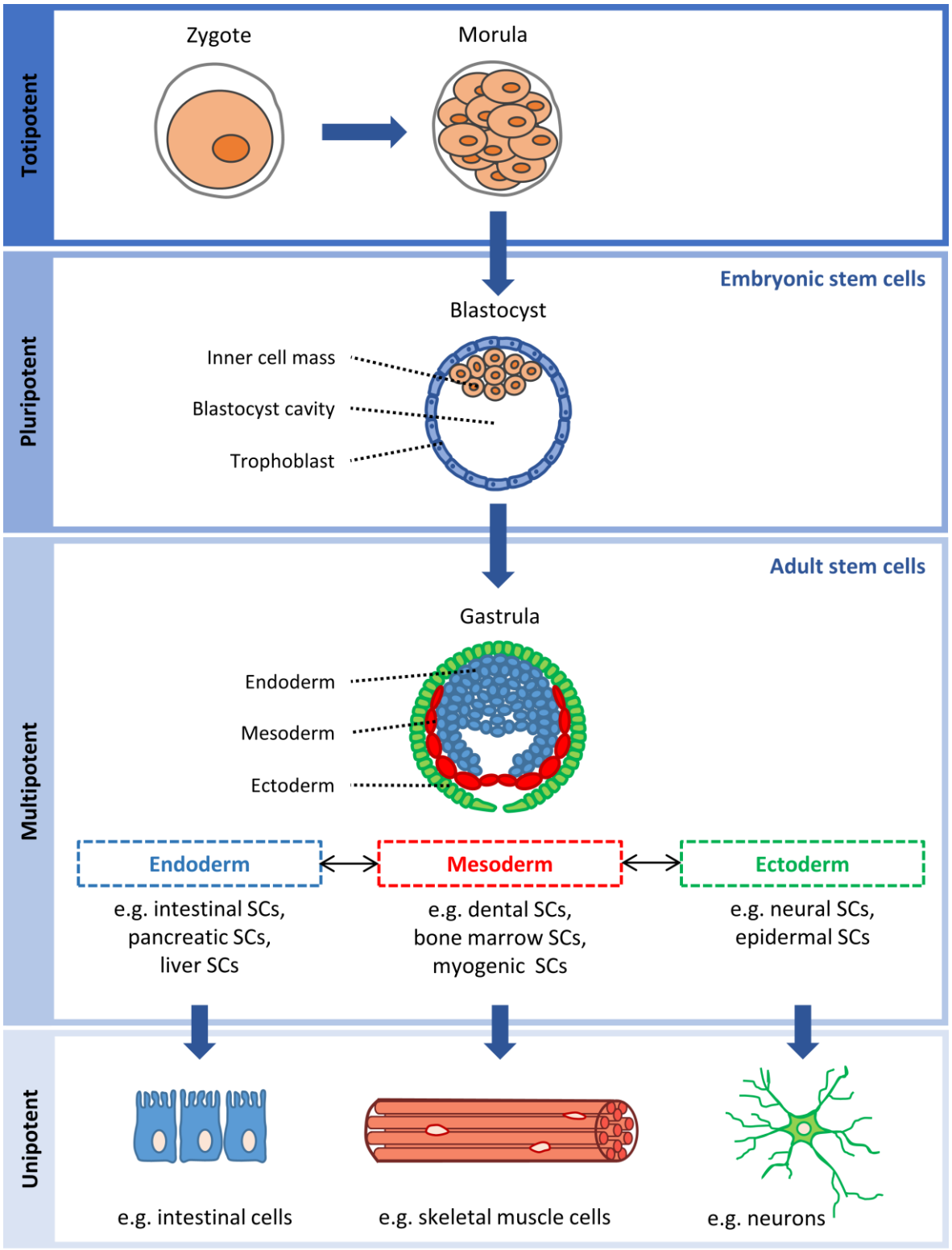

Figure 3.1. Stem cells classified by their potency. The totipotent zygote divides to form the inner cell mass (ICM) containing pluripotent embryonic stem cells, and the trophoblast of the blastocyst. During embryogenesis the stem cells of the ICM continue to differentiate into more specific cell types and give rise to multipotent and unipotent adult stem cells, which remain within tissues and organs for tissue homeostasis. SCs, stem cells. Modified figure (Eckfeldt et al., 2005).

3.2.2 Adult stem cells and their niches

Tissue homeostasis throughout life includes the regular elimination and replacement of differentiated cells preserving the form and function of developed tissues and organs by cell turnover (Pellettieri and Alvarado, 2007; Watt and Driskell, 2010), but also the repair of tissues after injury or disease (Caplan, 1991; Pittenger, 1999). Even organs that were previously considered non-renewing, like brain and heart, were found to exhibit cell turnover (Kajstura et al., 1998; Lois and Alvarez-Buylla, 1993). These processes require the presence of adult stem cells, which have been discovered in various tissues including lung, intestine, pancreas, liver, mammary glands, umbilical cord blood, bone marrow, heart, muscle, adipose tissue, tooth, brain, skin, and eye (Bianco et al., 2001; Burke et al., 2007; Gilbert et al., 2010; Gronthos et al., 2000; Haegebarth and Clevers, 2009; Lau et al., 2012; O. K. Lee et al., 2004; Merkle et al., 2007; Messina et al., 2004; Nadri et al., 2008; Welm et al., 2003; Zuk et al., 2002). Collected evidence suggests that most, if not all tissues may contain stem cells with the potential to repair damaged tissue (Raff, 2003). In this context, organs with a higher cell turnover, like skin, the hematopoietic system, and the lining of the intestine are assumed to have a higher regenerative capacity than tissues with slower self-renewal rates, like heart tissue or the spinal cord (Pellettieri and Alvarado, 2007; Poss, 2010).

Initially, adult stem cells were believed to be exclusively multi- or unipotent stem cells that give rise to mature cell types of their tissue of origin without crossing germ layer boundaries (Hombach-Klonisch et al., 2008; Wagers and Weissman, 2004). However, various cell differentiation studies using adult stem cell populations have provided evidence for so-called transdifferentiation, i.e. “the conversion of a cell of one tissue lineage into a cell of an entirely distinct lineage, with concomitant loss of the tissue-specific markers and function of the original cell type, and acquisition of markers and function of the transdifferentiated cell type” (Wagers and Weissman, 2004). Especially mesenchymal and hematopoietic bone marrow stem cells were reported to transdifferentiate into hepatocytes (R. E. Schwartz et al., 2002), endothelial and myocardial cells (Jackson et al., 2001), neuronal and glial cells (Sanchez-Ramos et al., 2000), and epithelial cells of the liver, gastrointestinal tract, lung, and skin (Krause et al., 2001). Although the concept of adult stem cell plasticity is still controversial (Chagastelles and Nardi, 2011), it is accepted that some types of adult stem cells (e.g. mesenchymal stem cells) do have an extended plasticity and may therefore be good candidates for cell-based therapies (Meirelles and Beyer Nardi, 2009). Compared to embryonic stem cells, adult stem cells could be used for autologous transplantations, limiting the risk of immunological rejection and avoiding many ethical issues of religious, historical, cultural, and medical origin (Brignier and Gewirtz, 2010). Furthermore, their lower differentiation potential reduces the risk of tumor formation (Smith, 2001).

Adult stem cells reside in so-called stem cell niches within the individual tissues and organs (Mitsiadis et al., 2007; Watt and Hogan, 2000), which are considered to be an anatomical structure harboring stem cells but even more a microenvironment regulating stem cell behavior, i.e. proliferation, differentiation, survival, and localization. The concept of a stem cell niche was first introduced by Schofield in 1978 (Schofield, 1978), who hypothesized the existence of a microenvironment required for the maintenance of stem cells. Within this highly regulated microenvironment, the residing stem cells interact with stromal support cells and tissue-specific cells by direct cell-cell contact through cadherins and integrins, as well as through secreted soluble factors, such as chemokines, growth factors, and hormones (Fig. 3.2). A three-dimensional (3D) scaffolding is provided by extracellular matrix (ECM) proteins, which play a key role in creating cell-guiding gradients of soluble growth factors and whose stiffness and elasticity, as well as its topography and shear forces provide mechanical cues that directly affect stem cell fate, a process known as mechanotransduction (Ingber, 1997). Blood vessels allow the transport of systemic signals and the recruitment of inflammatory and other circulatory cells into the niche (Jones and Wagers, 2008). Cells of the innate and adaptive immune system dynamically regulate the niche during inflammation or tissue damage (Lane et al., 2014) and even distant physiological cues, e.g. after injury, can reach the niche through neural inputs (Scadden, 2006). Another important feature of the stem cell niche is the presence of low oxygen tensions (i.e. hypoxia), which has been found to be essential for the maintenance of stem cells' multipotency as well as self-renewal capacities. Additionally, cell proliferation, differentiation, and quiescence are directly influenced by cellular metabolism (Lane et al., 2014). Stem cell fate is also regulated by extrinsic cues (e.g. through signaling pathways) and intrinsic genetic signals, as well as by the interaction of both intrinsic and extrinsic factors. Positive and negative feedback mechanisms regulate stem cell self-renewal and differentiation through autocrine, paracrine, and endocrine signaling, thus keeping the ratio of self-renewing and differentiating stem cells in balance.

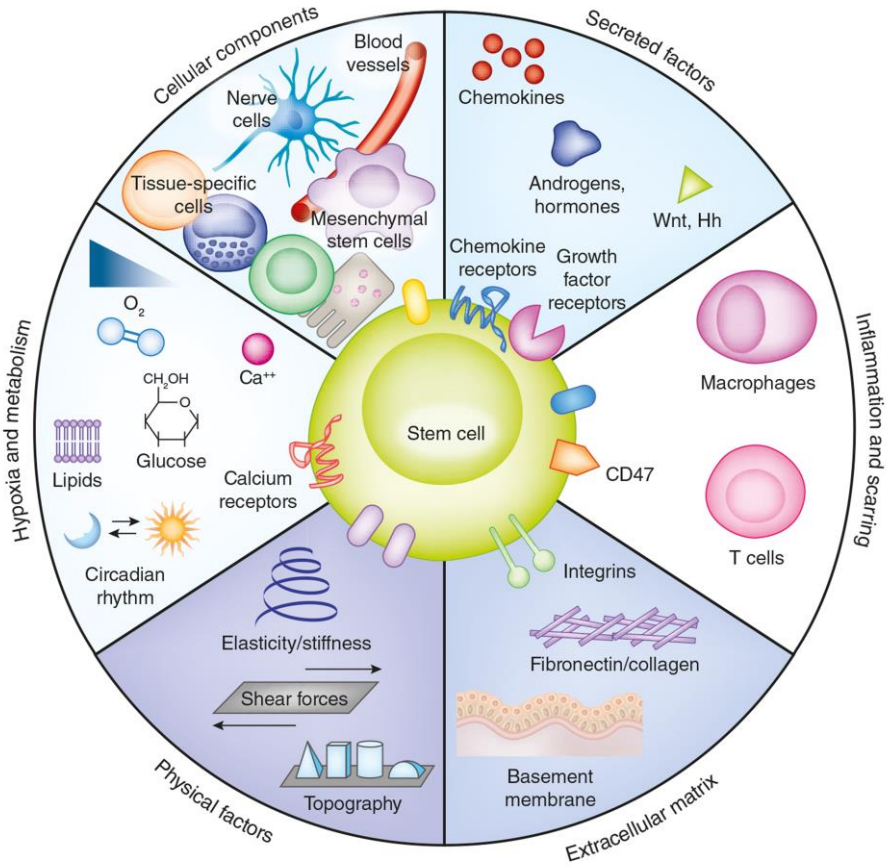

Figure 3.2. Composition of the stem cell niche. Cellular components, secreted factors, immunological control, ECM, physical parameters, and metabolic control regulate stem cell behavior and provide an anatomical structure that protects and maintains stem cells as well as their multipotency and self-renewal (Lane et al., 2014).

3.2.3 Mesenchymal stem cells

Multipotent mesenchymal stem cells (MSCs) are adult stem cells that were initially isolated from the bone marrow of mice by Friedenstein and co-workers in 1966, who described them as clonal, plastic adherent cells capable of forming colonies and differentiating into osteoblasts (Friedenstein et al., 1966). For many years, bone marrow stem cells (BMSCs) were considered the golden standard for mesenchymal stem cell research due to their high expansion potential and reproducible isolation procedures. Apart from differentiating into osteoblasts, MSCs were also found to give rise to other lineages of the connective tissue, such as the adipogenic, the chondrogenic, and the myogenic lineage (Pittenger, 1999). Furthermore, reports about the transdifferentiation potential of MSCs (Heo et al., 2013; Liang et al., 2015; Pokrywczynska et al., 2015; Xin et al., 2015) increased the interest of using MSCs for the development of stem cell-based regenerative therapies. Knowledge gained in numerous studies has led to the development

of many potential stem cell-based therapies being tested in clinical trials and the approval of a first MSC-based product, Prochymal® (Osiris Therapeutics, Inc., Columbia MD, USA), for the treatment of acute graft-vs-host disease in Canada and New Zealand (Vaes et al., 2012).

Since the cell populations isolated from bone marrow are not homogenous and a unique combination of surface markers for the isolation of a pure MSC population is still missing, minimal criteria for defining MSCs have been determined by the International Society for Cellular Therapy (Dominici et al., 2006). According to these criteria, MSCs have to be plastic adherent under normal culture conditions, they should express CD73, CD90, CD105 and lack CD11b, CD14, CD19, CD34, CD45, or CD79α, and HLA-DR surface molecules. Finally, MSCs must differentiate *in vitro* into osteoblasts, adipocytes, and chondrocytes.

3.2.4 Induced pluripotent stem cells

Stem cell-based regenerative medicine has been revolutionized by reprogramming mature cells into so-called induced pluripotent stem cells (iPS cells), a technology, pioneered by Shinya Yamanaka and colleagues (the Nobel Prize in Physiology or Medicine 2012 was jointly awarded to Shinya Yamanaka and Sir John Gurdon). Initially, mouse embryonic and adult fibroblast were used for the induction of the first pluripotent stem cells from differentiated cells (Takahashi and Yamanaka, 2006), followed soon by the first human iPS cells generated from human adult fibroblasts (Takahashi et al., 2007). The iPS technology holds great promise as the generated cells can give rise to any cell type, similar to embryonic stem cells, while being ethically unproblematic. As any adult cell can be used for the generation of iPS cells independent of their differentiation status, patient-matched pluripotent stem cell lines could be used for personalized regenerative cell therapies one day (Robinton and Daley, 2012). However, their pluripotency is considered not only a benefit, but also a risk for teratoma formation, which cannot be fully controlled with currently available reprogramming methods. Although the initial protocol for generating iPS cells, which was based on retroviral gene delivery, has been improved over the years, technical limitations and safety concerns for the clinical use of iPS cells need to be addressed first (Ji et al., 2016).

3.3 Dental mesenchymal stem cells

3.3.1 The origin of dental stem cells - the tooth

Teeth are specialized organs of the orofacial complex located in the oral cavity (Fig. 3.3). In each tooth four different tissues can be distinguished, which are the mineralized enamel, cementum, and dentin, as well as the soft dental pulp. These tissues start forming between the 10th and the 12th week of fetal development as a result of sequential and reciprocal interactions between the ectoderm-derived oral epithelium and the neural crest-derived ectomesenchyme (Mitsiadis and Graf, 2009). Enamel develops from ectoderm, while all the other structures of the tooth are of ectomesenchymal origin (Jiménez-Rojo et al., 2012).

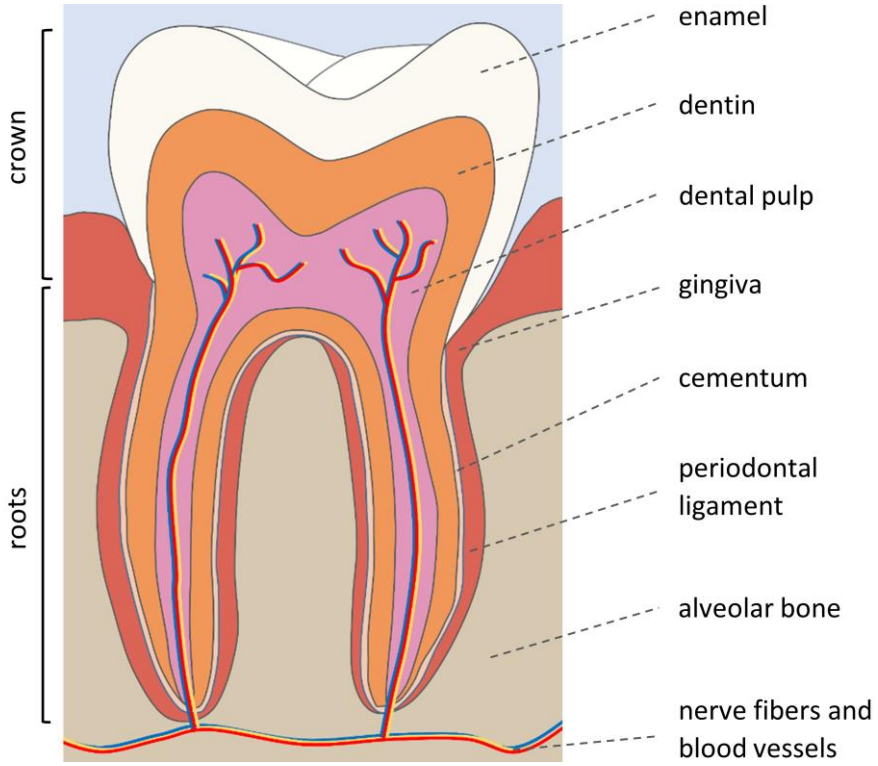

Figure 3.3. Schematic representation of the anatomy of a human tooth. The periodontal ligament attaches the tooth to the surrounding gingiva and alveolar bone. Nerve fibers and blood vessels enter the tooth through the apexes of the roots. Modified figure (Mitsiadis et al., 2012).

In fully developed teeth the tooth crown is covered by enamel, which is the hardest and most mineralized tissue of the human body and does not contain any cells. A thin layer of cementum is lining the outer layer of the roots of a tooth and is part of the periodontium that is responsible for proper tooth attachment to the alveolar bone of the jaw. Dentin can be found in both crown and roots, just below the enamel and cementum layers, respectively. Located in the center of the tooth, the dental pulp is a soft connective tissue constituting the vital part of the tooth. Vascularization and innervation of the pulp are essential as they ensure nutrition and sensation,

respectively (Nanci, 2012). Structurally, four areas can be distinguished (Nanci, 2012). The innermost pulpal core, which contains the majority of the vascular supply and nerves, is surrounded by a cell-rich zone, including mainly fibroblasts and undifferentiated mesenchymal stem cells. The third layer is known as the cell-free zone of Weil, which harbors capillaries and small nerve fibers. Odontoblasts, the dentin producing cells, form the outer layer of the dental pulp and send cellular projections into channels called dentinal tubules of the mineralized dentin. The pulp as a whole is connected with the surrounding tissues exclusively through the apexes of the roots, which makes it difficult to treat pulpitis, a common tooth disease, without degenerating the tooth.

Apart from their main function in mastication and speech, healthy teeth also play an important role in keeping our facial profile and a pleasant appearance. Additionally, postnatal or adult human teeth were found to harbor multipotent dental mesenchymal stem cell populations that can be isolated from the different tissue structures and are believed to be a promising cell source for applications in stem cell- based regenerative therapies (Tatullo et al., 2015).

3.3.2 Dental pulp stem cells

In 2000, Gronthos and colleagues were the first to isolate adult human dental stem cells, termed dental pulp stem cells (DPSCs), from the only vital part of the mineralized tooth, the dental pulp (Gronthos et al., 2000) (Fig. 3.4). Assumptions about the presence of stem cells in the dental pulp were based on the observation of reparative dentin formation after tooth injury. Further studies led to the conclusion that odontoblast apoptosis occurring after tooth injury activates DPSCs, which start proliferating, migrating, and differentiating into odontoblasts producing a thin layer of reparative dentin to close the pulp chamber (Mitsiadis et al., 2011). A precise characterization of this newly discovered stem cell population *in vitro* confirmed their self-renewal capability and multi-lineage differentiation capacity (Gronthos et al., 2002). Due to the lack of specific dental stem cell markers, identification relies on morphology, selective adherence, and their differentiation potential (Mitsiadis et al., 2011). DPSCs show phenotypic characteristics similar to BMSCs and were found to express more than 4000 known human genes on a comparable level as BMSCs (S. Shi et al., 2001). Additionally, a donor-matched comparison of DPSCs and BMSCs isolated from a single adult Sprague-Dawley rat revealed faster population doubling time and a higher percentage of stem/progenitor cells in DPSC populations (Alge et al., 2010). Furthermore, these cells can be induced *in vitro* to differentiate into osteo-/dentinogenic, adipogenic, chondrogenic, myogenic, and neurogenic lineages (About, Bottero, et al., 2000; d'Aquino et al.,

2007; Gronthos et al., 2002; Huang et al., 2006; Laino et al., 2005; Woloszyk et al., 2014; W. Zhang et al., 2006). *In vivo* they were shown to form a dentin-pulp-like complex, odontoblast-like cells, and mineralized bone-like tissue (Huang et al., 2009). Therefore, these cells are considered to be a promising cell source especially for vascularized dental pulp (Hilkens et al., 2014; Huang et al., 2010; Iohara et al., 2009) and bone tissue engineering (d'Aquino et al., 2007, 2009; Graziano et al., 2008; Woloszyk et al., 2014).

3.3.3 Stem cells from human exfoliated deciduous teeth

Similar to permanent teeth, the dental pulps of exfoliated human deciduous teeth also contain a population of multipotent stem cells, known as stem cells from human exfoliated deciduous teeth (SHEDs) (Miura et al., 2003) (Fig. 3.4). Apart from their self-renewal capacity with a higher proliferation rate than DPSCs, they were shown to differentiate towards the neurogenic, adipogenic, and osteogenic lineage *in vitro*. Unlike DPSCs, SHEDs failed to reconstitute a dentin-pulp-like complex *in vivo* but were found to induce new bone formation by recruiting murine host osteogenic cells (Miura et al., 2003). More recent studies have used SHEDs for the successful repair of critical-size calvarial defects with substantial bone formation in mice (Seo et al., 2008), as well as in a rat model of Parkinson's disease, where SHEDs differentiated into dopaminergic neuronal-like cells, mitigating the symptoms of the disease (Wang et al., 2010). When transplanted into completely transected adult rat spinal cords, SHEDs promoted locomotor recovery by differentiating into mature oligodendrocytes and by inhibiting multiple axon growth inhibitors as well as the spinal cord injury-induced apoptosis of neurons, astrocytes, and oligodendrocytes (Sakai et al., 2012). In regenerative dentistry-based studies, SHED-seeded biodegradable PLLA-scaffolds inserted into human tooth slices were transplanted into immunodeficient mice, which resulted in the formation of a dental pulp-like tissue (Cordeiro et al., 2008).

3.3.4 Periodontal ligament stem cells

The periodontal ligament is composed of fibrous connective tissue fibers, with neural and vascular components, that spans between the tooth root cementum and the alveolar bone (Fig. 3.4). Its primary function lies in the dynamic but strong attachment of the tooth to the surrounding alveolar bone, while contributing to tooth homeostasis, nutrition, and repair of damaged tissues at the same time (Shimono et al., 2003). Periodontal ligament stem cells (PDLSCs) can be isolated

from the root surface of extracted teeth and have been shown to differentiate into adipogenic and osteogenic lineages *in vitro* (Seo et al., 2004). One potential application of PDLSCs could be the regeneration of the periodontal ligament itself in patients suffering from periodontitis (Y. Liu et al., 2008; Menicanin et al., 2014).

3.3.5 Stem cells from the apical papilla

During the development of permanent teeth, the growing roots are apically covered by a smooth-surfaced soft tissue, the so-called apical papillae (Fig. 3.4). Stem cells from the apical papilla (SCAPs) are considered to have a higher regeneration potential than DPSCs due to their higher proliferation rate and telomerase activity, as well as their enhanced migration capacity, which might be related to the developing stage of their tissue of origin (Sonoyama et al., 2006, 2008). This cell population can give rise to osteo-/odontogenic as well as adipogenic lineages upon induction *in vitro* and the cells stain positive for several neural markers without neurogenic stimulation (Abe et al., 2007). Due to their origin from the neural crest, their expression of numerous neurogenic markers, and SCAP-mediated neurite outgrowth and axonal targeting, SCAPs have been recently applied in a rat hemisection model and were found to improve gait in spinally injured rats, while reducing glial reactivity at the same time (De Berdt et al., 2015).

3.3.6 Dental follicle stem cells

Apart from the apical papillae, dental mesenchymal stem cells can also be isolated from another developing dental tissue, known as the dental follicle (Fig. 3.4). This ectomesenchymal tissue surrounds the developing tooth germ prior to eruption and gives rise to the periodontal ligament, alveolar bone, and cementum of the functional tooth (Morsczeck et al., 2005). In co-cultures with DPSCs, dental follicle stem cells (DFSCs) were observed to increase their migration activity and velocity, while surrounding the present DPSCs, which resembles *in vivo* developmental processes (Schiraldi et al., 2012). Under specific culture conditions, DFSCs can differentiate towards several mesenchymal-derived cell types, such as osteoblasts, chondrocytes, and adipocytes *in vitro* (Kémoun et al., 2007). Therefore, their potential to contribute to bone regeneration was recently investigated in a rat cranial critical-size defect, where bone regeneration was only observed in defects treated with DFSCs-seeded polycaprolactone scaffolds but not in empty scaffolds (Rezai-Rad et al., 2015).

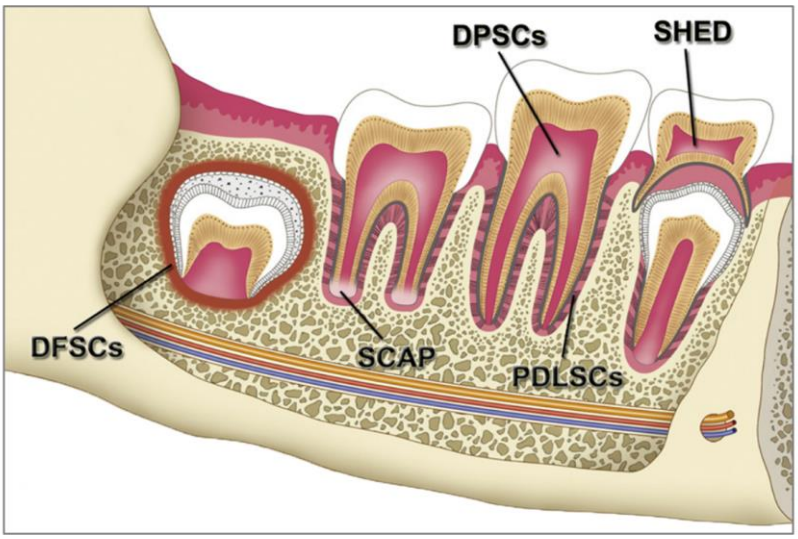

Figure 3.4. Sources of adult dental mesenchymal stem cells in the oral cavity. DFSCs, dental follicle stem cells; DPSCs, dental pulp stem cells; PDLSCs, periodontal ligament stem cells; SCAP, stem cells from the apical papilla; SHED, stem cells from human exfoliated deciduous teeth. Modified figure (Egusa et al., 2012).

3.3.7 Dental stem cell banking

For potential future applications in autologous cell-based treatments, multipotent adult stem cells can be stored in so-called cell banks. Structurally intact living cells and tissues can be preserved by using very low temperatures, usually -196°C when stored in liquid nitrogen. For a flexible use of autologous multipotent stem cells in regenerative medicine and tissue engineering, the optimization of cryopreservation methods is crucial. Even though dental stem cells can be isolated from any intact tooth and its surrounding tissues at any point of life, studies have shown that the regenerative capacity of stem cells is diminishing with age (Oh et al., 2014). Therefore, the cryopreservation of stem cells isolated from either deciduous teeth or developing tissues like the dental follicle or dental pulp of unerupted molars is potentially better than the ones from older fully developed teeth. Apart from deciduous teeth, the most suitable type of teeth for potential cryopreservation of adult stem cells are wisdom teeth, as their extraction is one of the most common dental surgical procedures, with 60-85% of the population having one or more wisdom teeth removed (American Association of Oral and Maxillofacial Surgeons). Unlike stem cells derived from bone marrow, dental stem cells can be isolated non-invasively from 'medical waste' without causing extra pain or morbidity and without the need for general anesthesia. Companies offering the isolation, testing, and preservation of dental pulp stem cells from deciduous and extracted teeth are already on the market (e.g. StemSave, Inc, New York, NY, USA). Although it is common practice to isolate the cells before freezing, several studies have shown that the

cryopreservation of either the whole tooth or the dental pulp tissue followed by cell isolation after freezing might yield even better results (H. S. Lee et al., 2015; Woods et al., 2009).

3.4 Vascularization

Blood vessel formation is essential in both physiological and pathological processes. Haematopoietic cells circulating within the vasculature supply the surrounding tissues with oxygen and nutrients, transport hormones, remove waste products and CO_2, and protect the body from infections (Carmeliet and Jain, 2011). Vascular structures are formed in two ways, through vasculogenesis and through angiogenesis, both being conserved in embryonic and adult blood vessel formation. In embryonic vasculogenesis, the vascular system starts developing from small blood islands of mesoderm-derived angioblasts around day 18 (Larsen, 1998). These endothelial progenitor cells differentiate into endothelial cells and create vesicular structures, which fuse to form the primary vascular blood plexus (Risau, 1997) (Fig. 3.5 A). Although it was generally accepted for many years that vasculogenesis takes place only during embryonic development, several studies in the 1990s have presented evidence for a similar process taking place, postnatally. In 1994, it was reported for the first time that a vascular graft implanted in both the arterial and venous systems of a dog showed a so-called fallout endothelialization, i.e. scattered islands of confluent endothelium developed from cells deposited from the circulation on the inside of the implant, in addition to the expected ingrowth of neighboring vessels (Q. Shi et al., 1994). After the identification of an antigenic profile on peripheral blood mononuclear cells similar to the one typically found on embryonic angioblasts (Asahara, 1997), the assumption that these circulating cells are adult endothelial progenitor cells contributing to adult/postnatal vasculogenesis gained further support (Asahara and Kawamoto, 2004; Kässmeyer et al., 2009) (Fig. 3.5 B).

Once a primary capillary network is established, new capillaries are formed from these pre-existing structures during both embryonic development as well as adult life through angiogenesis. The extension of the vasculature includes vessel enlargement, sprouting, bridging, and intussusception (division of individual capillaries into two separate vessels), which results in a hierarchically branched vascular system (Adams and Alitalo, 2007) (Fig. 3.5 C). Vessel branching requires tip cell formation, the degradation of the surrounding ECM by specific proteases, and proliferation of the cells behind the tip cell, which invades the avascular tissue (Carmeliet and Jain, 2011). Maturation of newly formed blood vessels requires the recruitment of mural cells (pericytes and vascular smooth muscle cells; vSMCs) as well as the production of extracellular

matrix proteins, mainly collagen type IV and laminin that assemble into the so-called basal lamina (Gaengel et al., 2009). Pericytes form a single, often discontinuous, cell layer on the outer wall of blood vessels providing structural support and interacting with the underlying endothelial cells (Armulik et al., 2005). While pericytes are typically found around blood capillaries, pre-capillary arterioles, and post-capillary venules (Allt and Lawrenson, 2001), vSMCs are rather associated with larger vessels, i.e. arteries and veins, where they form multiple continuous layers (Fig. 3.5 D). However, it is believed that a continuum of phenotypes ranging from the typical pericyte to the classical vSMC exists. vSMCs play a key role in the local control of blood flow by contraction and relaxation, and together with pericytes they are responsible for the synthesis and the maintenance of the extracellular components of the vascular wall that build up the basal lamina (Armulik et al., 2005).

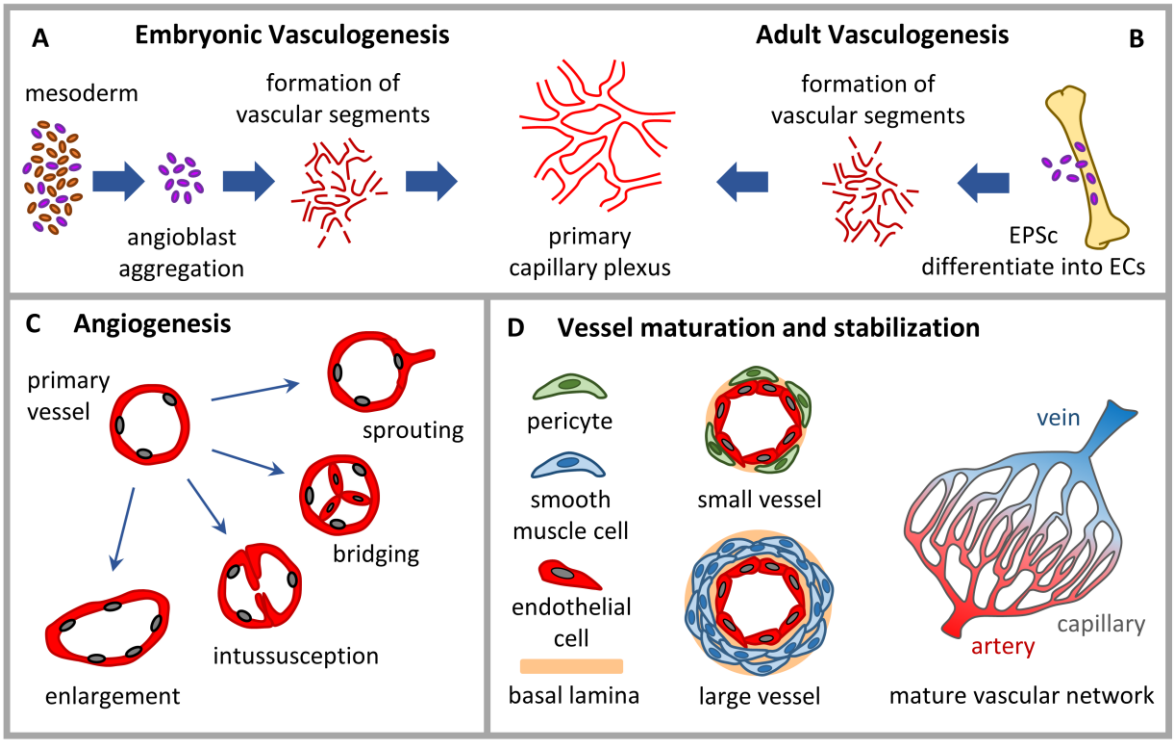

Figure 3.5. Development of the vascular system. *De novo* formation of vessels in (A) embryonic vasculogenesis and (B) adult vasculogenesis. (C) Extension of the primary capillary plexus by angiogenesis. (D) Vessel maturation and stabilization by recruitment of mural cells (pericytes and smooth muscle cells) and formation of a basal lamina resulting in a mature vascular network of arteries, capillaries, and veins. EPCs, endothelial progenitor cells; ECs, endothelial cells. Modified figure (Korpisalo and Ylä-Herttuala, 2010; Pardali et al., 2010).

The main constituents of the vascular basal lamina include collagen type IV and laminin, which form independent networks that are linked by nidogens and the heparin sulfate proteoglycan perlecan, resulting in a dense highly cross-linked sheet of 50-100 nm in thickness. Apart from

providing mechanical support and dividing tissues into compartments, the vascular basal lamina also regulates cell behavior by modulating cell attachment, spreading, migration, matrix synthesis, and tube formation (Kalluri, 2003). The inner wall of all blood vessels is lined by endothelial cells, which form a selectively permeable barrier allowing the transport of molecules between blood and tissues. Additionally, they regulate blood coagulation and fibrinolysis, as well as the vascular tone, and participate in inflammatory reactions (Michiels, 2003).

3.4.1 Vascularization strategies for tissue engineering

Successful engineering of functional tissue substitutes and transplantable organs depends on rapid blood vessel formation towards the transplanted tissue as sufficient oxygen and nutrient supply is essential for the long-term survival of the implant. Except for very few tissues such as skin, cartilage, or cornea, most tissues of the body are vascularized by a dense network of capillaries with a maximum distance of 200 nm, correlating with the diffusion limit of oxygen (Carmeliet and Jain, 2000; Novosel et al., 2011). Since spontaneous vascular ingrowth into the implant from the host tissue is limited to several tenths of micrometers per day, the improvement and acceleration of implant vascularization remains a key challenge in tissue engineering (Rouwkema et al., 2008).

In the last two decades, various vascularization strategies for tissue engineering have been proposed, tested, and refined. Based on the tissue engineering triad (Murphy et al., 2013), they include approaches focusing on the scaffold design, (progenitor) cell-based techniques, and the delivery of angiogenic (growth) factors, either alone or in combination. Vascularization is either initiated *in vitro* by engineering pre-vascularized constructs before implantation, or starts *in vivo* directly at the defect site or alternatively at a vascularization site for *in vivo* pre-vascularization (Lovett et al., 2009; Phelps and García, 2010; Rouwkema et al., 2008) (Fig. 3.6).

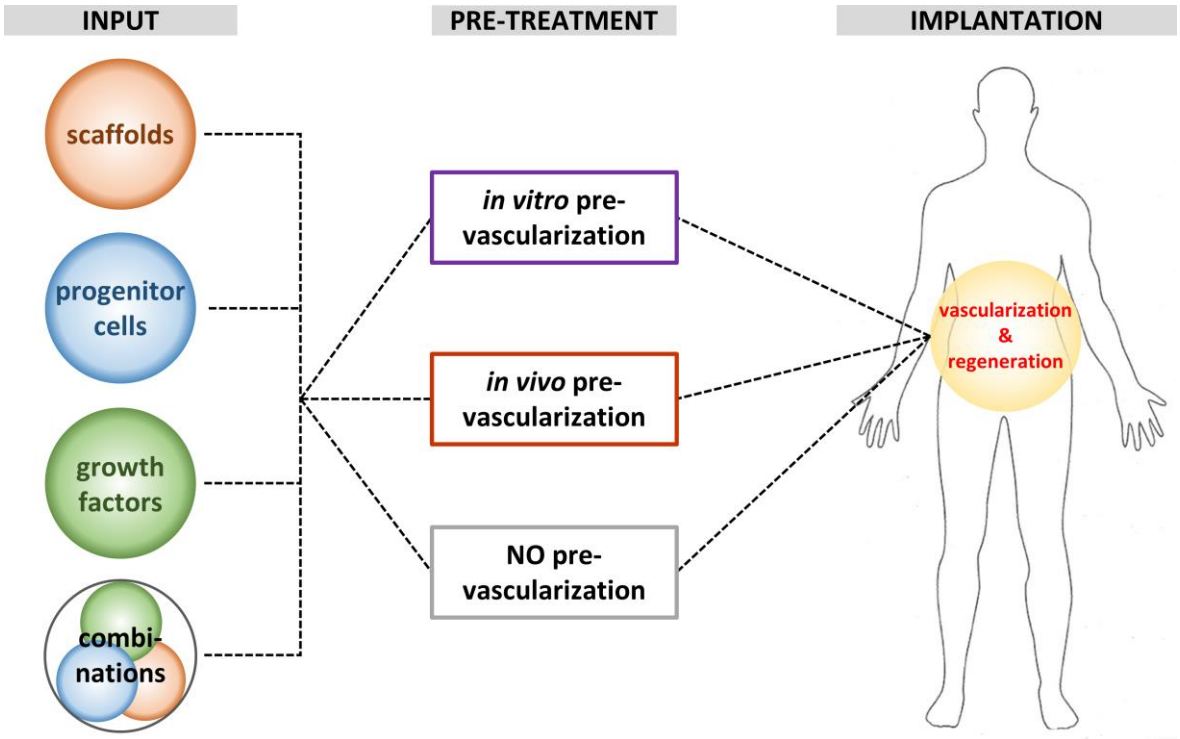

Figure 3.6. Vascularization strategies for tissue engineering. Scaffolds, (progenitor) cells, and growth factors can be used either alone or in combination. Potential implants can be pre-vascularized *in vitro* or *in vivo* before being implanted at the defect site or can be implanted directly without pre-vascularization (Rouwkema et al., 2008).

3.4.1.1 Scaffolds for the engineering of vascularized tissues

Scaffolds are 3D frame structures used in tissue engineering, serving as templates for tissue regeneration, which guide the growth of new tissue (O'Brien, 2011). The ideal scaffold for an engineered tissue would be the ECM of the tissue it is meant to replace. While it remains difficult to produce the ECM of native tissues, the development and use of new scaffolds has produced many promising alternatives, with the aim to resemble the original as closely as possible. These include decellularized ECM, stacks of cell sheets with their own secreted ECM, as well as a wide range of porous scaffolds and self-assembling hydrogels, consisting of either one or combinations of more than one material (Chan and Leong, 2008). Required scaffold properties include biocompatibility, degradability without toxic by-products, adequate mechanical properties, and tissue-specific scaffold architecture (O'Brien, 2011). These properties are mainly determined by the choice of material(s) and the fabrication process.

For successful vascularization of scaffold-based implants, porosity is "a critical determinant of blood-vessel ingrowth" (Rouwkema et al., 2008). Scaffolds with pores larger than 250 µm were shown to accelerate vessel ingrowth significantly when compared to scaffolds with smaller pores

(Laschke and Menger, 2012). Besides porosity, also the pore interconnectivity plays an important role to allow for proper cell migration and vascularization (Rouwkema et al., 2008). Common fabrication techniques used for the production of porous scaffolds are electrospinning, solvent casting/particle leaching, thermally-induced phase separation, melt molding, gas foaming, emulsion freeze-drying, 3D printing, selective laser sintering, and stereolithography (Janik and Marzec, 2015; Loh and Choong, 2013). Three groups of biomaterials used for the fabrication of scaffolds can be distinguished: ceramics, synthetic polymers, and natural polymers (O'Brien, 2011). Ceramic scaffolds (e.g. hydroxyapatite, tri-calcium phosphate, bioglass) are characterized by a high mechanical stiffness and are mainly applied in dental and orthopaedic surgery to treat bone defects. Popular synthetic polymers are polystyrene, poly-l-lactic acid (PLLA), polyglycolic acid (PGA), and poly-lactic-co-glycolic acid (PLGA). Their architectural and degradation properties can be easily modified and their 3D structure is highly reproducible; however, their reduced bioactivity might result in immune rejection. Naturally-derived biopolymer scaffolds include proteins, such as silk, collagen, and gelatin, as well as polysaccharides like hyaluronan, cellulose, and amylose as their raw materials. These materials are bioactive and biodegradable, but the production of homogenous and reproducible structures is often difficult, and mechanical stability is limited (Novosel et al., 2011; O'Brien, 2011).

3.4.1.2 Cell-based strategies for the engineering of vascularized tissues

The use of cell-based techniques to generate vascularized tissues has several advantages. Relevant cells can be isolated from various tissues for autologous cell therapy, including endothelial precursor cells from circulating blood (Asahara et al., 2011), endothelial cells from human umbilical vein (Novosel et al., 2011) or from the microvasculature of adipose tissue and skin (Hewett, 2009), as well as multipotent adult stem cells, which decreases the risk for immune rejection and increases the biocompatibility of the implant. Furthermore, the use of cell-based grafts can stimulate the endogenous release of angiogenic growth factors induced by the experienced hypoxia at the implant site, triggering the ingrowth of new blood vessels from the surrounding tissue (Laschke et al., 2006). Additionally, cells can be transfected to overexpress angiogenic factors resulting in the release of cytokines that can regulate endothelial cell migration, proliferation, and maturation into tubular vessels in a controlled way (Lovett et al., 2009). To achieve vascularization, the cells can be grown *in vitro* as spheroid co-cultures or as simple mix co-cultures of endothelial (precursor) cells with tissue-specific cells, which can produce capillary-like sprouts, especially in the presence of angiogenic factors, such as vascular endothelial growth factor (VEGF) or basic fibroblast growth factor (bFGF) (Lovett et al., 2009). However, rather than being applied alone, cells are mainly used to functionalize scaffolds by seeding them

with endothelial cells only or as co-cultures with pericytes, vSMCs, fibroblasts, mesenchymal stem cells, osteoblasts, or other specialized cells. Cell-seeded scaffolds can be implanted directly or further processed for *in vitro* pre-vascularization before implantation (Costa-Almeida et al., 2014).

3.4.1.3 Growth factors

The application of growth factors is another possibility to functionalize a previously produced scaffold by loading or chemically coupling angiogenic factors, such as VEGF, bFGF, and platelet-derived growth factor (PDGF) (Lovett et al., 2009). These can attract endothelial (precursor) cells from existing vasculature of the host tissue or can induce the secretion of several factors by activating signaling pathways, thereby accelerating the onset of angiogenesis towards the inside of the graft and the maturation of newly formed vessels (Rouwkema et al., 2008). Recombinant proteins can be delivered either through passive diffusion or are released locally in response to cellular demand when degraded by matrix metalloproteinases secreted by ingrowing endothelial cells (Ehrbar et al., 2004). However, the use of growth factors for the vascularization of engineered tissues also requires a strict coordination of the correct signaling factors, dosing, and exposure time points (Phelps and García, 2010).

The presented strategies can be combined in various ways to bring together the advantages of scaffolds, cells, and growth factors to encourage the formation of vessel networks inside the graft. However, not only vessel formation, but also the maturation and functionality of the engineered or ingrown vessels from the host are important. Finally, for clinical success, the manufacturing technology of scaffolds and growth factors should be commercializable and the procedures for generating personalized grafts clinically applicable.

3.5 Chorioallantoic membrane assay

The study of vascularization is based on so-called angiogenesis assays. One of the well-established assays is the chorioallantoic membrane (CAM) assay (Fig. 3.7). During the development of the chicken three extraembryonic membranes are formed: the yolk sac membrane, the amnion, and the CAM. The CAM is highly vascularized and serves as a transient gas exchange surface during the incubation period, similar to the lung (Romanoff, 1960). Originally, the CAM assay was used in order to study the developmental potential of embryonic tissue grafts (Laschke et al., 2006). As chicken embryos become immunocompetent only by day 18 of their development (Janković et al., 1975), various biological processes where vascularization plays a role can be studied, including insufficient vascularization (e.g. ischemic disorders) or excessive vessel formation (e.g. cancer),

with the goal to either enhance or decrease vessel growth, respectively (Ribatti, 2014). In tissue engineering, experimental models are required to study blood vessel ingrowth into engineered tissue implants. Compared to other *in vivo* angiogenesis assays (e.g. dorsal skinfold chamber, subcutaneous implantation in mice), the CAM assay is a simple, cost-effective, and highly reproducible method, which does not require an ethical approval when performing experiments in chicken embryos until embryonic day 14 (Swiss animal care guidelines, TSchV, Art. 112). Additionally, the chicken embryo serves as a natural bio-incubator, as grafted tissues and cells can be sustained without any additional media supply. Even though the incubation time on the CAM is limited to a period of about one week, it constitutes an excellent screening method, which allows the study of cell behavior, i.e. proliferation, migration, and differentiation, within 3D biomaterials during the early phase of vascularization. Apart from the effect of different cell populations, also the influence of growth factors, gene therapy, as well as the architecture and material properties of scaffolds on blood vessel ingrowth can be investigated. Various available *in situ* imaging and quantification methods including magnetic resonance imaging of the blood flow (Kivrak Pfiffner et al., 2015) enhance the scientific impact and the range of application of the CAM assay. Following the '3Rs' principles of replacement, refinement, and reduction of animal use in research, the CAM assay provides a valuable intermediate platform for rapid assessments prior to pre-clinical studies in mammals (Nowak-Sliwinska et al., 2014).

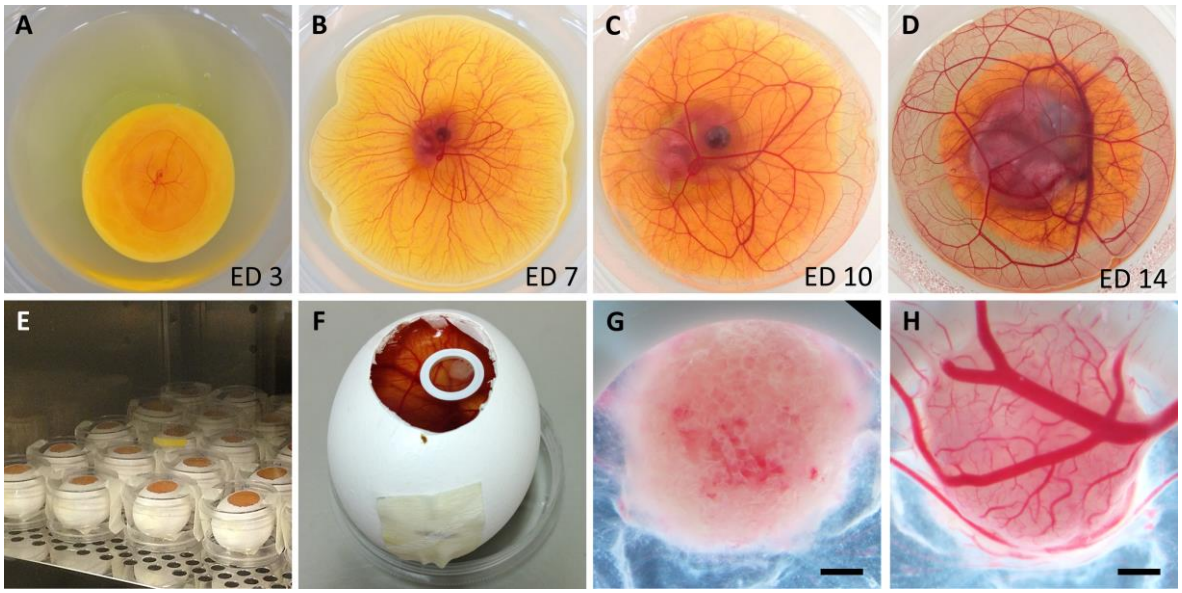

Figure 3.7. Chorioallantoic membrane assay. (A-D) Fertilized chicken egg cultured in a plastic dish on embryonic day 3 (ED 3) (A), ED 7 (B), ED 10 (C), and ED 14 (D). (E) Egg incubation after opening the shell. (F) Egg with a sample placed within a silicone ring after 1 week of incubation. (G, H) Vascularized scaffold after 1 week of incubation as seen from the top (G) and the bottom (H). Scale bar = 1 mm.

4. Aims of the project

The requirement for tissue and organ replacement is high and is expected to increase due to population ageing, especially in highly developed countries. Advances in tissue engineering and regenerative medicine can offer new therapies for the treatment of tissue or organ loss induced by injury or disease. Hence, the shortage of donor tissues and organs could be overcome by applying the principles of cell transplantation, bioengineering, and material science, and combining them to generate biological substitutes with the potential to regenerate and replace lost tissues and organs. The discovery of various multipotent stem cell populations in the adult body has provided ethically unproblematic cell sources that could potentially be used for autologous cell-based therapies with a reduced risk for immune rejection. The selected cell population should not only be easily accessible, but should also have a good proliferative potential to obtain high cell numbers in cell culture, as well as the required differentiation potential. Additionally, rapid vascularization and integration of a tissue engineered transplant into the surrounding host tissues is a prerequisite for its long-term survival.

Teeth present an easily accessible cell source, as deciduous teeth or commonly extracted (wisdom) teeth could be banked for autologous or maybe even allogeneic therapeutic use in the future without any additional discomfort for the patient once tissue or organ replacement is necessary later in life. Multipotent mesenchymal stem cells isolated from the human dental pulp reside in perivascular stem cell niches and have been shown to express angiogenic factors, suggesting an angiogenic potential of human dental pulp stem cells (hDPSCs).

In the present study we hypothesize that hDPSCs are able to attract the host's vasculature and contribute to the vascularization of a three-dimensional (3D) silk scaffold while recreating their own stem cells niche within the biomaterial without any additional supplements. In this context, also the question if using a $CD34^+/CD90^+$ sorted hDPSC population is beneficial for the vascularization and integration efficiency of the implant when compared to unsorted hDPSCs should be answered. Therefore, freshly isolated hDPSCs will be characterized and sorted before seeding unsorted and sorted cells on 3D silk scaffolds placed on the chorioallantoic membrane of fertilized chicken eggs (i.e. *in ovo* culture). By analyzing the expression of endothelial stem cell markers, components of the extracellular matrix, as well as stem cell markers, the tissue structures inside the biomaterial will be characterized to test our hypothesis. Following this analysis, empty and cell-seeded silk scaffolds will be implanted subcutaneously in immunocompromised mice in order to assess the validity of the results obtained *in ovo* as well as to assess the long-term effect that unsorted and sorted hDPSC populations will have on the tissue

integration of 3D silk scaffolds. Finally, MicroFil® perfusion followed by a visualization and analysis by microcomputed tomography will be adapted and applied to *in ovo* cultured samples in order to evaluate the vascular network within the scaffolds.

5. Materials and Methods

5.1 Production of silk fibroin scaffolds

Silk fibroin scaffolds were produced using the salt leaching technique as previously described (Hofmann et al., 2007; Nazarov et al., 2004; Sofia et al., 2001). Silkworm cocoons (Trudel Inc., Zurich, Switzerland) were boiled twice for 1 h in 0.02 M sodium carbonate (Fluka AG, Buchs SG, Switzerland) and rinsed with ultrapure water (UPW) to extract sericin. After drying, the silk was dissolved in 9 M lithium bromide and dialyzed against UPW for 36 h using a Slide-A-Lyzer™ Dialysis Cassette (Fisher Scientific AG, Wohlen, Switzerland) followed by lyophilization (Alpha 1-2, Martin Christ GMBH, Osterode am Harz, Germany). A 17% (w/v) silk fibroin solution was prepared by dissolving lyophilized silk in 1,1,1,3,3,3-hexafluoro-2-propanol (HFIP) (abcr GmbH & Co., Karlsruhe, Germany). This solution was added to Teflon containers filled with sodium chloride (200-300 mm in diameter) (Sigma-Aldrich Chemie GmbH, Buchs SG, Switzerland) at a ratio of 1:20 (silk fibroin:NaCl). After complete evaporation of HFIP, conformational transition from α- to β-sheet domains was induced by immersing the blocks in 90% methanol (Sigma-Aldrich Chemie GmbH, Buchs SG, Switzerland) for 30 min (Sofia et al., 2001). The scaffolds were dried for at least 48 h before sodium chloride was leached out in five changes of UPW within 48 h resulting in scaffolds with more than 90% porosity (Nazarov et al., 2004). Wet silk fibroin scaffolds were cut into cylinders of 5 mm diameter and 3 mm height by using a mold, a razor blade, and a biopsy punch. These scaffolds were sterilized by autoclaving at 121°C and 1 bar for 20 min.

5.2 Cell isolation, culture, and sorting

The procedure for anonymized cell collection was approved by the Kantonale Ethikkommission of Zurich (reference number 2012-0588) and performed with patients' written consent.

Human dental pulps were obtained from healthy teeth of adult patients within 24 h after the extraction of impacted wisdom teeth. After the removal of the dental pulp from the tooth, human dental pulp stem cells (hDPSCs) were isolated as previously described (Gronthos et al., 2000; Tirino et al., 2012). Dental pulps were enzymatically digested in a solution of 3 mg/mL collagenase type I (Life Technologies Europe B.V., Zug ZG, Switzerland) and 4 mg/mL dispase (Sigma-Aldrich Chemie GmbH, Buchs SG, Switzerland) for 1 h at 37°C. For a single-cell suspension the solution was filtered through a 70 µm strainer (Falcon, Corning, Root Längenbold LU, Switzerland) and plated in a 35 mm Petri dish after washing away the enzyme solution. Sorted hDPSCs (s-hDPSCs) were obtained by isolating a $CD34^+/CD90^+$ subpopulation using antibodies (CD34: Miltenyi Biotec,

Bergisch Gladbach, Germany; CD90: BD Biosciences, Allschwil BL, Switzerland) and fluorescence-activated cell sorting (FACS) (FACSAria™, Beckton, Dickinson and Company, Franklin Lakes, NJ, USA). Unsorted and sorted were expanded using DMEM/F12 (Sigma-Aldrich Chemie GmbH, Buchs SG, Switzerland), 10% fetal bovine serum (FBS) (Biochrom AG, Berlin, Germany), 1% Penicillin/Streptamycin (P/S) (Sigma-Aldrich Chemie GmbH, Buchs SG, Switzerland), and 0.5 µg/mL fungizone (Thermo Fisher Scientific AG, Reinach BL, Switzerland) with medium changes every 3-4 days and were passaged at 80-90% confluency.

5.3 Cell characterization

5.3.1 Flow cytometry

For flow cytometric characterization unsorted hDPSCs (uns-hDPSCs) were stained with CD34 antibodies conjugated to PE (Miltenyi Biotec, Bergisch Gladbach, Germany) and CD45 antibodies conjugated to APC-Cy7, as well as with CD90 antibodies conjugated to FITC and CD105 antibodies conjugated to PerCP-Cy5.5 (CD45, CD90, CD105: BD Biosciences, Allschwil BL, Switzerland) according to the manufacturers' protocols. Cell debris and dead cells were excluded from the analysis based on scatter signals and 7-aminoactinomycin D staining (Thermo Fisher Scientific AG, Reinach BL, Switzerland).

5.3.2 Immunocytochemistry

For immunocytochemical characterization uns-hDPSCs and s-hDPSCs were grown on 8-well glass slides (Millipore, Merck & Cie, Schaffhausen SH, Switzerland) for 24 h and were stained with anti-Nestin (1:100; MA1-110, Thermo Fisher Scientific AG, Reinach BL, Switzerland) anti-Sox2 (1:200; ab59776, Abcam plc, Cambridge, United Kingdom), and anti-Vimentin (1:300; M0725, Dako, Glostrup, Denmark) antibodies. The primary antibodies were detected using secondary antibodies conjugated to Alexa Fluor® 488 (Thermo Fisher Scientific AG, Reinach BL, Switzerland). Cell nuclei were stained with 4',6-diamidino-2-phenylindole (DAPI; Thermo Fisher Scientific AG, Reinach BL, Switzerland). Slides were mounted with Vectashield® (Reactolab, S.A., Servion VD, Switzerland).

5.4 Cell proliferation assay

Uns-hDPSCs isolated from wisdom teeth of three patients were seeded in 24-well-plates at a density of 2 x 10^4 cells/well in 400 µL of hDPSC growth medium, respectively. On day 1, day 3, and

day 7, the medium was changed before 40 µL of MTT (3-(4,5-dimethylthiazol-2-yl)-2,5-diphenyltetrazolium bromide) was added followed by an incubation at 37°C for 3 h. After the medium was removed, the formed formazan crystals were solubilized by adding 200 µL of acidic isopropanol per well and incubating for 15 min at RT in the dark. The solution was transferred to wells of a 96-well-plate and the absorbance of the converted dye was measured at 570 nm with background subtraction at 690 nm.

5.5 Cell cytotoxicity assay

Uns-hDPSCs were seeded in wells of a 96-well-plate at a density of 5 x 10^3 cells/well in 100 µL of growth medium (see section 5.2). On day 1, day 3, and day 7, supernatant was collected and used to determine lactate dehydrogenase (LDH) cytotoxicity according to the manufacturer's instructions (Thermo Fisher Scientific AG, Reinach BL, Switzerland). Absorbance was measured at 490 nm with background subtraction at 680 nm.

5.6 Cryopreservation of cells

At passage 2 (P2), the cells were detached from the culture flasks by tripsinization. In detail, the cell monolayer was washed with PBS twice before trypsin (Sigma-Aldrich Chemie GmbH, Buchs SG, Switzerland) was added for 3 min at 37°C for cell detachment and was stopped by the addition of growth medium. Next they were pelleted (5 min, 1,500 rpm, RT) and resolved in a concentration of $1 \cdot 10^6$ cells/400 µL growth medium. Labeled cryotubes were placed in a freezing container and filled with 100 µL of a 1:1 mix containing pure FBS and 50 µL of dimethyl sulfoxide (Sigma-Aldrich Chemie GmbH, Buchs SG, Switzerland). 400 µL of the cell suspension were added to each cryotube for a final volume of 500 µL. The freezing container was kept at -80°C for approximately 4 h before transferring the cryotubes into a liquid nitrogen storage tank.

5.7 Differentiation assays

5.7.1 Osteogenic differentiation

Uns-hDPSCs and s-hDPSCs were seeded in 24-well-plates at a density of 2 x 10^4 cells/well in 400 µL of growth medium (see section 5.2), respectively, and were incubated for 24 h. On the next day, the growth medium was replaced by DMEM high glucose containing 10% FBS and

1% P/S as well as a mix of ingredients for osteogenic differentiation, which were 0.1 mM L-ascorbic acid, 10 mM β-glycerophosphate, and 10 nM dexamethasone (all Sigma-Aldrich Chemie GmbH, Buchs SG, Switzerland). Controls were cultured with the same basic media without the addition of the osteogenic ingredients. Medium was changed every 3-4 days. After 21 days of culture, the cells were washed in PBS and fixed in 4% paraformaldehyde (PFA) for 30 min at RT. The PFA solution was washed away and Alizarin Red S staining solution (Sigma-Aldrich Chemie GmbH, Buchs SG, Switzerland) was added to the cells followed by an incubation in the dark for 45 min at RT. The cells were washed four times with distilled water (dH_2O) and pictures were taken immediately for documentation. Extracellular calcium deposits appeared bright orange-red.

5.7.2 Chondrogenic differentiation

0.5 x 10^6 of uns-hDPSCs and s-hDPSCs were pelleted in 15 mL Falcon tubes (Falcon, Corning, Root Längenbold LU, Switzerland) by centrifugation (5 min, 1500 rpm, RT). The supernatant (500 µL) was not removed and the cap was kept loose for gas exchange. After 48 h, the growth medium was replaced by chondrogenesis differentiation medium (StemPro® Chondrogenesis Differentiation Kit, Thermo Fisher Scientific AG, Reinach BL, Switzerland), which was changed every 2-3 days. Controls were grown in DMEM low glucose with GlutaMAX™ (Thermo Fisher Scientific AG, Reinach BL, Switzerland) containing 10% FBS and 1% P/S. After 21 days of culture, the cell pellets were washed in PBS and fixed in 4% PFA for 30 min at RT. They were washed in PBS and embedded in cryo embedding medium (Medite GmbH, Burgdorf, Germany) in order to cut 10 µm sections (Cryostat CM3050 S, Leica Biosystems AG, Muttenz BL, Switzerland) for Alcian Blue staining (Sigma-Aldrich Chemie GmbH, Buchs SG, Switzerland). Blue staining indicated the synthesis of proteoglycans by chondrocytes.

5.7.3 Adipogenic differentiation

Uns-hDPSCs and s-hDPSCs were seeded in 48-well-plates at a density of 2 x 10^4 cells/well in 200 µL of DPSC growth medium. Before changing the regular growth medium to adipogenesis differentiation medium (StemPro® Adipogenesis Differentiation Kit, Thermo Fisher Scientific AG, Reinach BL, Switzerland), the cells were cultured for 3 more days until 75% confluency. The differentiation medium was changed every 3-4 days. After 21 days, the differentiation was stopped and Oil Red O staining was performed to confirm adipogenic differentiation. The cell monolayers were washed with PBS, fixed with PFA for 30 min at RT, and were washed with dH_2O before adding 60% isopropanol for 5 min at RT. The isopropanol was replaced by freshly prepared Oil Red O staining solution followed by an incubation of 15 min at RT. After the staining, the cells

were first washed with dH_2O until the water became clear, and were then covered with PBS for microscopic analysis and documentation. Lipid vesicles in mature adipocytes stained bright red.

5.8 Cell seeding

The cells were seeded on sterile silk fibroin scaffolds at a density of 1 x 10^6 cells per scaffold in a volume of 60 µL of growth medium (see section 5.2). For cell attachment, the seeded scaffolds were placed in a humidified incubator for 1 h at 37°C. Non-attached cells were washed away from the scaffolds, which were incubated for additional 24 h at 37°C before being placed on the chorioallantoic membrane (CAM) of fertilized chicken eggs (see 5.9) or subcutaneously in 7 week-old BALB/c Nude Mice (see 5.10). Scaffolds for the *in vivo* experiment contained cells labeled with 1,1'-Dioctadecyl-3,3,3',3'-Tetramethylindocarbocyanine Perchlorate (DiI) according to the manufacturer's protocol (Thermo Fisher Scientific AG, Reinach BL, Switzerland).

5.9 Chorioallantoic membrane assay

No approval is necessary when performing experiments in chicken embryos until embryonic day 14 (ED 14) according to Swiss animal care guidelines (TSchV, Art. 112). Fertilized Lohman white LSL chicken eggs (Animalco AG, Staufen AG, Switzerland) were pre-incubated for 3 days at 38°C at a rotation speed of 360°/4 h (Bruja 3000, Brutmaschinen-Janeschitz GmbH, Hammelburg, Germany). On ED 3, the eggs were processed for *in ovo* (Fig. 5.1) cultivation. Before opening the eggs, the egg shell was wiped with 70% ethanol. *In ovo* cultivation required the opening of the shell using Scotch™ tape and scissors after removing 4 mL of albumen through a small hole in the shell to lower the developing embryo. The egg was stabilized in a 60 mm Petri dish lid and the opening was covered with a second 60 mm Petri dish lid, which was fixed to the bottom lid with tape. The eggs were incubated at 37°C. On ED 7, empty and cell-seeded scaffolds were placed on the CAM (1-2/egg) in the middle of previously placed silicone rings (taken from sterile cryovials) to ensure a flat surface and were incubated for 7 days until ED 14.

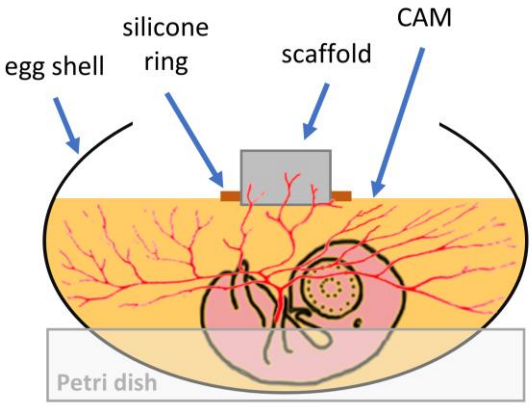

Figure 5.1. Scheme of the experimental setup. The scaffold is placed in the middle of a silicone ring on top of the CAM of a fertilized egg grown inside the egg shell (*in ovo*) for histological and molecular analysis or for MicroFil® perfusion followed by microCT scanning. CAM, chorioallantoic membrane.

5.10 In vivo assay

All animal experiments were carried out in accordance with the Swiss Animal Welfare Law and in compliance with the regulations of the Cantonal Veterinary office of Zurich and with the permission of the Animal Ethics Committee (license number: 11/2014). 12 nude mice (BALB/c Nude Mice - CAnN. Cg-Foxn1nu/Crl, Charles River, Cologne, Germany) were used at 7 weeks of age. Buprenorphine (0.1 mg/kg bodyweight) was injected subcutaneously one hour before the surgery. For surgery, the mice were anesthetized using isoflurane (3-5% for induction and 1-3% for maintenance). The mice were placed on a warming pad in a prone position and four subcutaneous pouches were prepared to hold the scaffolds on the back of the mice. Subsequently, the wounds were closed with an absorbable polyglycolic acid suture (Resorba Wundversorgung GmbH + Co. KG, Nürnberg, Germany). After cleaning the surgical site, the mice were kept on a warming pad under observation until they regained consciousness. For pain management, Buprenorphine (0.1 mg/kg bodyweight) was injected subcutaneously 8 h after the surgery. Moreover, Buprenorphine (1 mg/kg bodyweight) was added to the drinking water and the level was marked to make sure that the mice consume the water containing the analgesic. Posture, stiches, and wound healing were controlled during the days following the surgery (score sheet).

5.11 Analyses

5.11.1 MicroFil® perfusion and microCT imaging

On ED 14, the chicken embryos were perfused with a mix of the MicroFil® components (Flow Tech, Inc., Carver MA, USA). The silicone rubber injection compound (yellow) was diluted 10-fold in MV-Diluent and 10% (by weight) of MV-Curing Agent was added right before use. Working time of the MicroFil® was at least 20 min and started with the addition of the MV-Curing agent. The MicroFil® mix was filled into a 5 mL syringe (B. Braun Melsungen AG, Melsungen, Germany) to which a three-way valve (Discofix® C; B. Braun Melsungen AG, Melsungen, Germany) with a 10 cm tube was attached for more flexibility between the 30G ½" needle (Beckton, Dickinson and Company, Franklin Lakes, NJ, USA) and the syringe. Using a stereoscope, a branch of the vitelline vasculature matching the diameter of the needle was fixed with blunt end tweezers and the needle was carefully inserted into the vessel. A small drop of superglue was applied where the needle entered the vasculature. The MicroFil® mix was carefully injected into the vasculature until the pressure increased. If the filling of the vasculature was not sufficient after the first injection, MicroFil® was injected a second time into a non-perfused vessel. Next, the tube was removed from the needle, which remained in the CAM. A fresh needle was attached to the tube before continuing with the injection. The perfused chicken embryo was placed overnight at 4°C for complete curing of the MicroFil®. On the next day, the perfused scaffold samples were cut out from the CAM using scissors, washed in PBS, fixed in 4% PFA, washed in PBS, and placed in 70% ethanol until imaging. MicroCT scanning (µCT 40; Scanco Medical AG, Brüttisellen ZH, Switzerland) was performed at an isotropic resolution of 20 µm, an energy level of 70 kVp, an intensity of 114 µA, and 300 ms integration time.

5.11.2 Histology and histomorphometrical analysis

Samples for histological stainings were washed in PBS and fixed in 4% PFA ON at 4°C right after extraction. The constructs were embedded in paraffin and sectioned at 5 µm thickness. Before staining, the sections were deparaffinized and rehydrated.

5.11.2.1 Hematoxylin and Eosin staining

Hematoxylin is a basic dye used to stain acidic structures like DNA and RNA, which appear in a blue-purple color. Eosin is an acidic dye staining basic structures like proteins in varying degrees of pink. Therefore, Hematoxylin and Eosin (H&E) staining was used to visualize cell nuclei (blue-purple) and the cytoplasm as well as the extracellular matrix (pink). Deparaffinized and rehydrated slides were immersed in hematoxylin for 1 min 30 sec, rinsed in four changes of tap

water, washed in dH_2O for 3 min, placed in Eosin for 1 min, before they were dehydrated and mounted using Eukitt® (Sigma-Aldrich Chemie GmbH, Buchs SG, Switzerland).

5.11.2.2 Manual blood vessel analysis

The number of vessels and the percent vessel per scaffold area were determined by counting the number of vessels in longitudinal sections taken from the center of the scaffold. Each vessel was marked in black and ImageJ v1.48s (National Institutes of Health, USA) was used to analyze the number of marked vessels and their total area. Three sections of three *in ovo* cultured samples and three sections of two *in vivo* cultured samples were used resulting in nine and six evaluated sections per group, respectively.

5.11.2.3 Picrosirius Red staining

Picrosirius Red is used to detect collagen, which is stained in a red color. Dewaxed and rehydrated sections were immersed in hematoxylin to stain nuclei. Next, the slides were washed in four changes of tap water, rinsed in dH_2O, stained in Sirius Red solution for 1 h at RT, washed twice in acidified water, dehydrated, cleared in xylene, and mounted using Eukitt®.

5.11.2.4 Quantitative assessment of the collagen content

Picrosirius Red-stained sections were used for estimating the collagen (type I and III) content within the scaffold area, isolated from microscopical pictures recorded with a slide scanner (Axio Scan.Z1, Carl Zeiss AG, Feldbach ZH, Switzerland). The pictures were processed in imageJ and thresholded in order to determine the percentage of red-stained areas within the scaffold.

5.11.2.5 Von Kossa staining

Deparaffinized and rehydrated samples were incubated in 1% silver nitrate solution for 20 min under ultraviolet light. After washing in dH_2O, the unreacted silver was removed by incubating the sections with 5% sodium thiosulfate for 5 min. Eosin was used for counterstaining before mounting the slides using Eukitt®. Phosphate depositions indicating mineralization appear in brown/black color.

5.11.3 Immunohistochemistry

Immunohistochemistry was performed on deparaffinized and rehydrated sections. Endogenous peroxidases were quenched by incubating the sections in 3% H_2O_2 in ice-cold methanol for 45 min. If necessary, antigens were retrieved by applying either sodium citrate buffer, pH 6.0 and heat or trypsin solution, pH 7.8 at 37°C (for details see Table 5.1). To reduce non-specific staining,

the sections were incubated in 20% normal goat serum/PBS for 20 min at RT. Vectastain ABC and Vectastain ABC-AP kits (Reactolab, S.A., Servion VD, Switzerland) were used for the staining procedure. The primary antibody was applied ON at 4°C or for 1 h at RT. For the development of the staining either 3-amino-9-ethylcarbazole (AEC; Reactolab, S.A., Servion VD, Switzerland), or 3,3'-diaminobenzidine (DAB; Sigma-Aldrich Chemie GmbH, Buchs SG, Switzerland), or 5-bromo-4-chloro-3-indolyl phosphate/nitro blue tetrazolium chloride (BCIP/NBT; Reactolab, S.A., Servion VD, Switzerland) were chosen as chromogenic substrates. Omission of the primary antibody served as a negative control. Stained sections were mounted in Eukitt®. Pictures were taken using the Leica DM6000 FS microscope, the Leica DFC350FX camera, and the Leica Application Suite (LAS) software (Leica Microsystems AG, Heerbrugg SG, Switzerland).

primary antibody	reference number	company	antigen retrieval	conc.	incubation time	chromogen
NuMA	GTX113510	GeneTex	trypsin	1:500	ON	AEC
Collagen IV	ab6586	abcam	trypsin	1:750	ON	BCIP/NBT
Laminin	ab11575	abcam	trypsin	1:200	ON	BCIP/NBT
vWF	ab6994	abcam	trypsin	1:300	ON	BCIP/NBT

Table 5.1. Antibodies used for immunohistochemistry. AEC, 3-amino-9-ethylcarbazole; BCIP, 5-bromo-4-chloro-3-indolyl phosphate; conc., concentration; NBT, nitro blue tetrazolium chloride; NuMA, nuclear mitotic apparatus protein 1; ON, overnight; vWF, von Willebrand Factor.

5.11.4 Immunofluorescence

Immunofluorescent stainings were performed on deparaffinized and rehydrated slides. If necessary, antigens were retrieved by applying either sodium citrate buffer, pH 6.0 and heat or trypsin solution, pH 7.8 at 37°C (for details see Table 5.2). To reduce non-specific staining, the sections were blocked in 20% normal goat serum/PBS for 20 min at RT. The sections were incubated with the primary antibody ON at 4°C followed by incubation in the secondary antibody (1:250; Thermo Fisher Scientific AG, Reinach BL, Switzerland) for 1 h at RT, and DAPI staining to visualize the nuclei.

primary antibody	reference number	company	antigen retrieval	conc.	incubation time	secondary antibody
Nestin	MA1-110	ThermoFS	citrate buffer	1:100	ON	Alexa Fluor® 488
NuMA	GTX113510	GeneTex	citrate buffer	1:400	ON	Alexa Fluor® 568
Sox2	ab59776	abcam	citrate buffer	1:200	ON	Alexa Fluor® 488
Vimentin	M 0725	Dako	citrate buffer	1:300	ON	Alexa Fluor® 488

Table 5.2. Antibodies used for immunofluorescence. conc., concentration; NuMA, nuclear mitotic apparatus protein 1; ON, overnight; Sox2, SRY (sex determining region Y)-box 2; ThermoFS, Thermo Fisher Scientific.

5.11.5 RNA isolation and quantitative real-time polymerase chain reaction

RNA was extracted from *in ovo* and *in vivo* cultivated samples using the RNeasy Plus Universal Mini Kit (Qiagen AG, Hombrechtikon ZH, Switzerland) and quantified using the UVS-99 micro-volume UV/Vis spectrophotometer (ACTGene Inc., Piscataway NJ, USA). If necessary, samples were purified by ethanol precipitation. The iScript cDNA Synthesis Kit (Bio-Rad Laboratories AG, Cressier FR, Switzerland) was used to reverse-transcribe 1 µg of extracted RNA into cDNA. The primers were designed to be specific for human sequences without targets in the chicken or mouse genome. Specificity of the primers was checked with the Primer-Basic Local Alignment Tool (Primer-BLAST; http://www.ncbi.nlm.nih.gov/tools/primer-blast/). Quantitative real-time polymerase chain reaction (qRT-PCR) (Eco Real-Time PCR System, Illumina Inc., San Diego CA, USA) was performed using the Power SYBR Green Master Mix (Life Technologies Europe B.V., Zug ZG, Switzerland), 2 µM of primers (Table 5.3), and a 1:10 dilution of the cDNA in a total volume of 10 µL. Target gene expression was normalized to the expression of the control gene (beta-Actin). The $2^{-\Delta\Delta CT}$ method (Livak and Schmittgen, 2001) was used to calculate relative changes in gene expression.

Gene	Accession no.	Forward primer 5'-3'	Reverse primer 5'-3'
beta-Actin	NM_001101.3	AAA CTG GAA CGG TGA AGG TG	AGA GAA GTG GGG TGGCTT TT
Nanog	NM_024865.3	TTT GTG GGC CTG AAG AAA ACT	AGG GCT GTC CTG AAT AAG CAG
Nestin	NM_006617.1	CCT GCA AAA GGA GAA TCA AG	GTT CTC AAT GTC TCT TGG TC
TGFb1	NM_000660.5	GCC ACA GAT CCC CTA TTC AA	GTC TCC CGG CAA AAG GTA G
VEGFA	NM_001287044.1	CCA GGC CCT CGT CAT TG	AAG GAG GAG GGC AGA ATC AT
RUNX2	NM_001015051.3	AGC AAA GCC GCT TCC TCT CT	CGG AGG GCA CTG GTC CAT AC

Table 5.3. Human-specific primer sequences used for gene expression analyses. *RUNX2*, runt-related transcription factor 2; *TGFb1*, transforming growth factor beta 1; *VEGFA*, vascular endothelial growth factor A.

5.12 Statistical analysis

For a comparison of the groups a one-way analysis of variance (ANOVA) was performed using GraphPad Prism v6.05 (GraphPad Software, Inc., La Jolla, CA, USA). A Bonferroni's multiple comparison test was conducted to determine significant differences between the groups. Data were considered significant at $p < 0.05$ (*) and highly significant at $p < 0.01$ (**).

6. Results

6.1 In vitro characterization of hDPSCs

Cultures of human dental pulp stem cells (hDPSCs) were established by enzymatically digesting dental pulps previously removed from extracted impacted molars of adult patients within 24 hours. The cells were expanded until passage 3 (P3) before being cryopreserved for further characterization and experimental use.

6.1.1 Cell morphology and proliferation of freshly isolated hDPSCs

In monolayer cultures of freshly isolated hDPSCs grown on plastic Petri dishes, first colony forming units were observed three days after plating (Fig. 6.1). Adherent cells showed a typical fibroblast-like morphology similar to bone marrow stem cells (BMSCs). Dead cells, non-adhering cells, and cells that cannot survive in a growth medium consisting of Dulbecco's Modified Eagle Medium/Nutrient Mixture F-12 (DMEM/F12) supplemented with 10% serum and 1% L-glutamine were washed away when the growth medium was changed. A frequent problem when culturing cells of oral origin is mycoplasma contamination, as these bacteria are commonly found in the human oral cavity. Therefore, the medium of the primary cell cultures was regularly tested for the presence of mycoplasma using specific primers recognizing DNA fragments from the most common types of mycoplasma. Affected cultures were discarded.

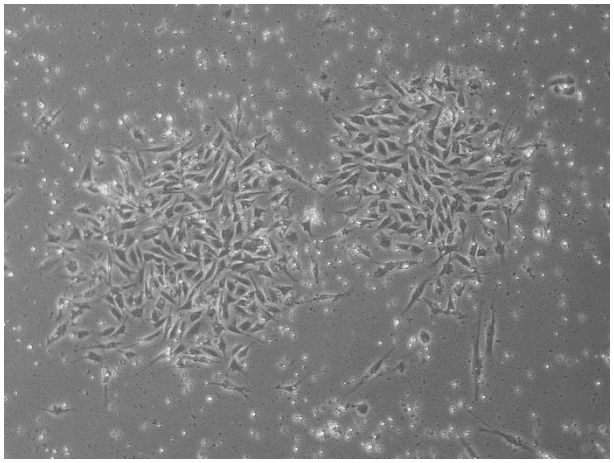

Figure 6.1. Two colony forming units of primary hDPSCs three days after cell isolation from the dental pulp.

To keep the cells at an optimal density for continued growth and to stimulate further proliferation, the cells were passaged at a confluency of 80-90%. Cell numbers and time until reaching the right cell density for passaging were recorded for all the isolated hDPSC populations (Fig. 6.2). Initially, an average of 2×10^5 cells after an average time of almost ten days were counted when passaging the freshly isolated cells for the first time. At passage 2, the average cell number increased to 3×10^6 in approximately six days. In the final passage 3, the cells reached an average number of 19×10^6 in four to five days, and were frozen in portions of 1×10^6 cells for cryopreservation. Their exponential growth behavior resulted in a 97-fold increase in cell number from passage 1 to 3 within 21 days on average.

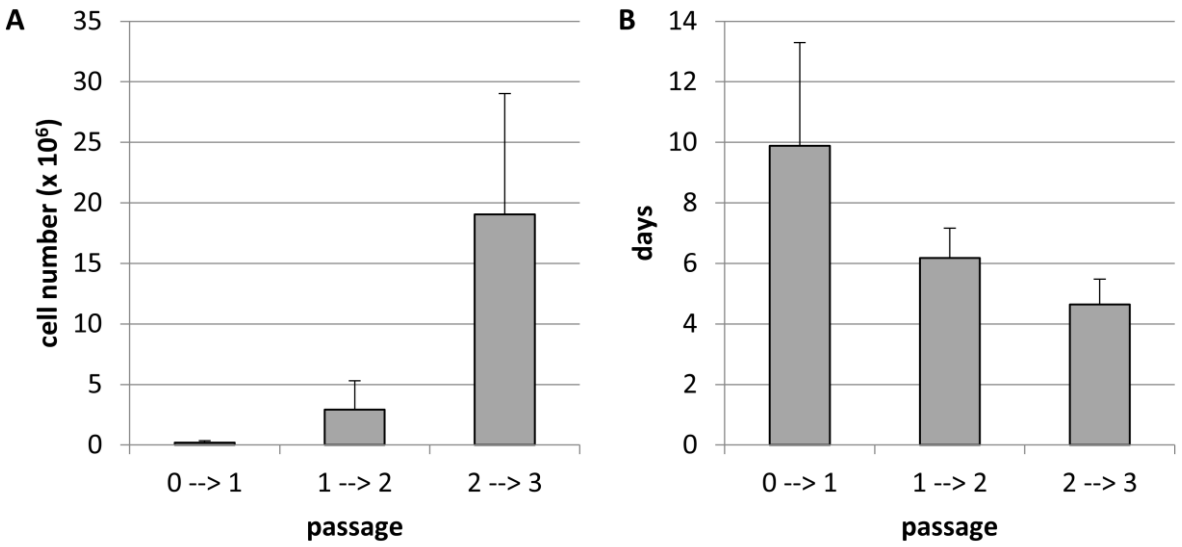

Figure 6.2. Proliferation behavior of freshly isolated hDPSCs. (A) Average cell number recorded at each passage. (B) Average time period between passages. Data is shown as mean ± SD, n = 17.

6.1.2 Cell proliferation and cytotoxicity of hDPSCs

Cells of three different patients were used to compare their proliferation rates and possible cytotoxicity during cell culture by using the MTT and the LDH assay, respectively (Fig. 6.3).

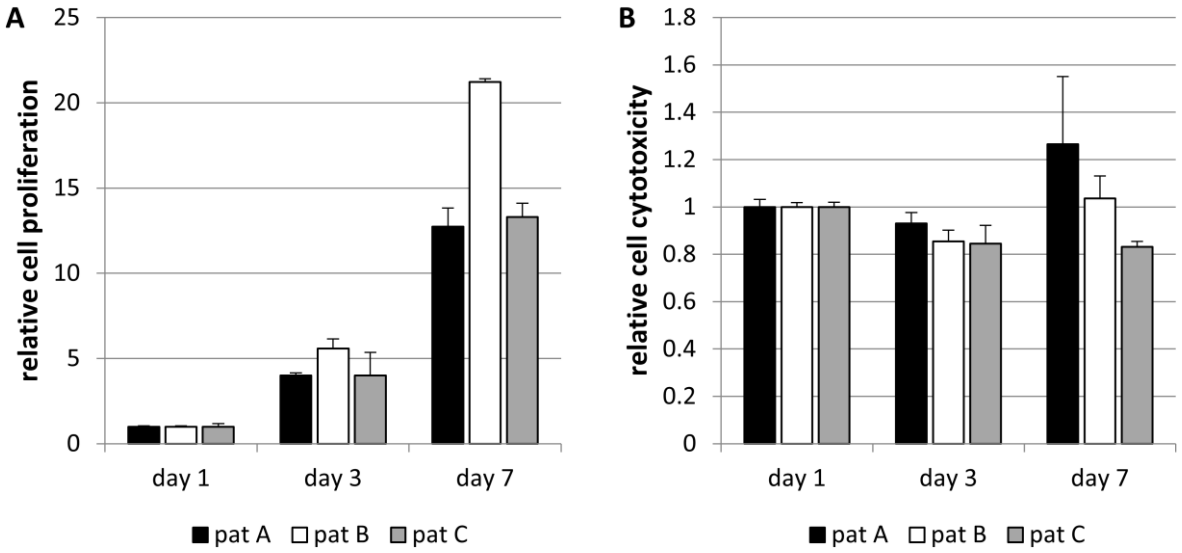

Figure 6.3. Cell proliferation and cytotoxicity of hDPSCs. (A) Cell proliferation measurement based on the MTT assay, where cell metabolic activity is assessed. (B) Cell cytotoxicity assay based on the concentration of lactate dehydrogenase (LDH), which is released by stressed and dead cells into the medium. Data is shown as mean ± SD, n = 3. No statistically significant differences between the patients were found.

No statistically significant differences were observed between the cell proliferation and LDH activity of the hDPSCs from three different donors. On average, cell numbers showed a 4.5-fold and 15.7-fold increase on day 3 and day 7, respectively, when compared to day 1 (Fig. 6.3 A). At the same time the average LDH activity, indicating possible cytotoxicity, did not increase but remained stable during seven days of culture in all the tested cells (Fig. 6.3 B). These results suggest similar behavior of hDPSCs isolated from different patients.

6.1.3 Expression of cell surface markers

Unsorted hDPSCs (uns-hDPSCs) were analyzed for their expression of typical cell surface markers identifying mesenchymal stem cells. Samples of uns-hDPSCs isolated from three different patients were used and showed similar cell surface marker profiles. An exemplary profile is presented in Figure 6.4.

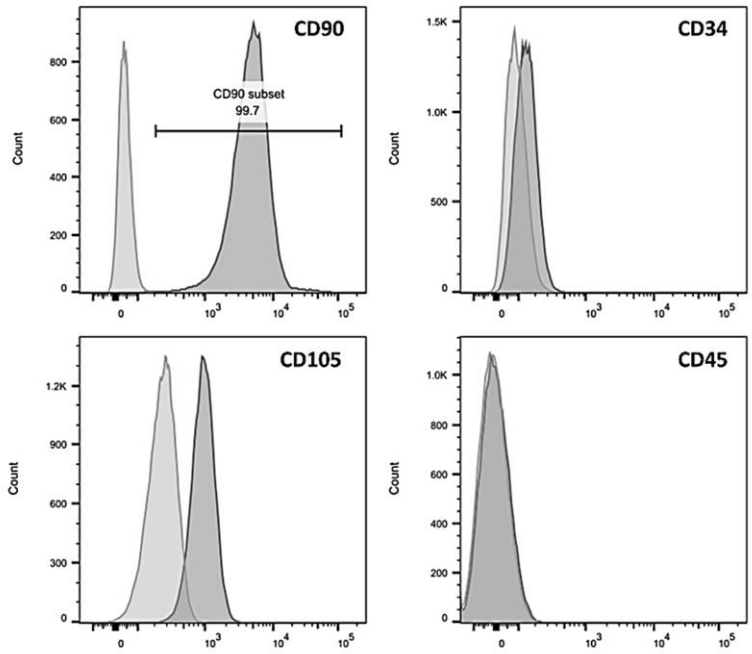

Figure 6.4. Cytofluorimetric analysis of CD90, CD105, CD34, and CD45 expression on unsorted hDPSCs. Histograms represent the fluorescence intensity on the x-axis and the number of cells on the y-axis. Unstained control cells and cells marked with antibodies are shown in light grey and dark grey color, respectively.

All tested samples were positive for the mesenchymal stem cell markers CD90 and CD105, while being negative for the hematopoietic stem cell marker CD45. A small percentage of cells was also positive for CD34, which has been shown to be expressed on a small proportion of various cell populations, distinguishing a subset of cells with enhanced progenitor activity (Sidney et al., 2014). The percentage of $CD34^{+}/CD90^{+}$ cells chosen for a sorted population of hDPSCs was 14.76% (Fig. 6.5).

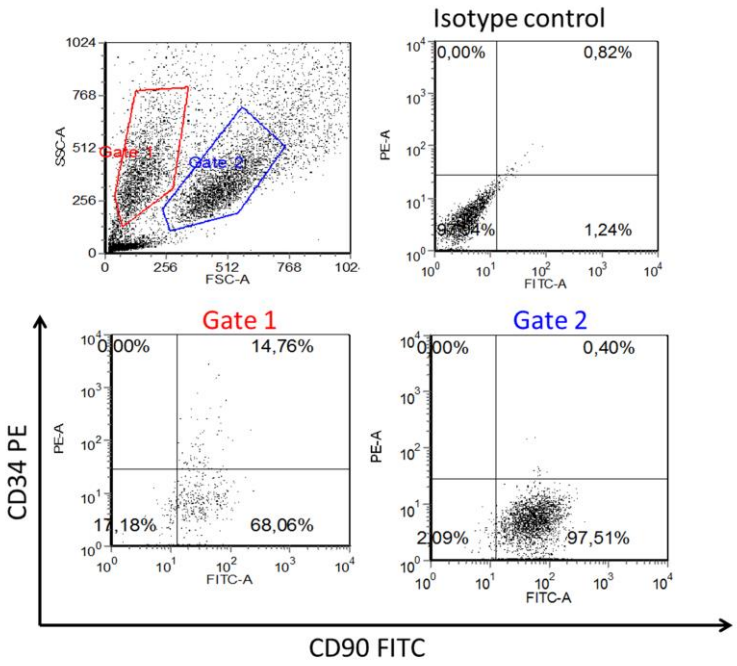

Figure 6.5. Fluorescence-activated cell sorting (FACS) plots for the sorting of hDPSCs. FITC-A, fluorescein isothiocyanate area; FSC-A, forward scatter area; PE-A, phycoerythrin area; SSCA, side scatter area.

6.1.4 Immunocytochemical analysis of unsorted hDPSCs and sorted hDPSCs

To further characterize the cells, their expression of Nestin, Sox2, and Vimentin were examined by immunocytochemical analysis (Fig. 6.6). Uns-hDPSCs were compared with $CD34^{+}/CD90^{+}$ sorted hDPSCs (s-hDPSCs) in order to elucidate if using sorted stem cell populations is advantageous for the vascularization efficiency of a 3D biomaterial when used as an implant.

Nestin is known as a marker for multi-lineage progenitor cells but is also expressed by nerve cells, which require Nestin for proper self-renewal. Both uns-hDPSCs and s-hDPSCs were positive for Nestin (Fig. 6.6 A, B). Sox2 is commonly expressed by embryonic stem cells and is used as a marker for the identification of undifferentiated pluripotent cells. The expression of this pluripotency marker in the tested cell groups (Fig. 6.6 C, D) suggests the existence of a primitive stem cell population in our cultures and indicates that the chosen culture conditions support self-renewing cells. Vimentin is the major intermediate filament protein of mesenchymal cells. Therefore, its expression confirms the mesenchymal character of hDPSCs (Fig. 6.6 E, F).

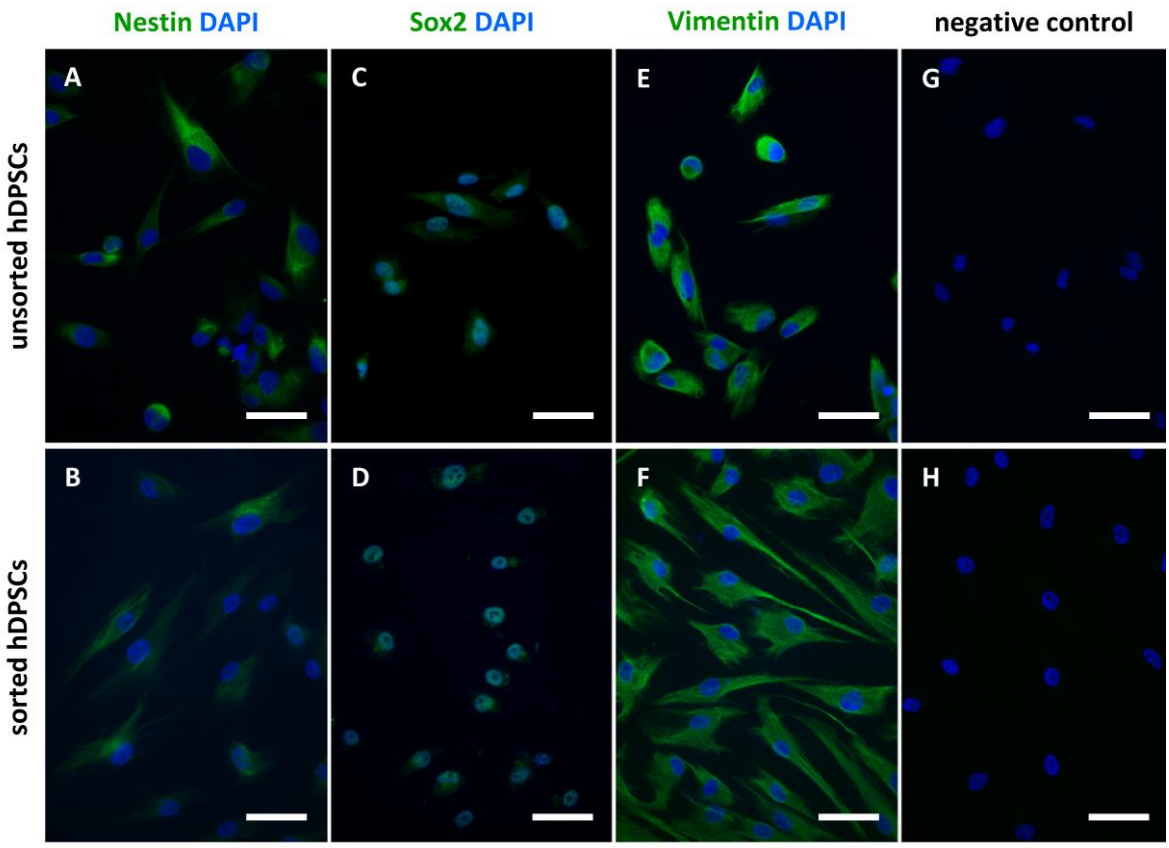

Figure 6.6. Immunocytochemistry showing Nestin, Sox2, and Vimentin expression. (A, B) Expression of Nestin. (C, D) Expression of Sox2. (E, F) Expression of Vimentin. (G, H) Negative controls. Cell nuclei are stained with DAPI. Scale bar = 50 µm.

6.1.5 In vitro differentiation potential of unsorted hDPSCs and sorted hDPSCs

One of the minimal criteria for the definition of multipotent mesenchymal stem cells is their ability to differentiate into several mesenchymal cell lineages, like osteoblasts, chondrocytes, and adipocytes. Therefore, the trilineage differentiation potential of monolayer cultures of the isolated uns-hDPSCs and s-hDPSCs was tested by culturing them in osteogenic, chondrogenic, and adipogenic differentiation media.

6.1.5.1 Osteogenic differentiation

Alizarin Red staining of hDPSCs cultured for 14 days in osteogenic media, containing ascorbic acid, β-glycerophosphate, and dexamethasone, was used to identify calcium deposits in the extracellular matrix (ECM) of successfully differentiated cells. Bright orange-red staining of calcified nodules was observed in both uns-hDPSCs (Fig. 6.7 A) and s-hDPSCs cultures (Fig. 6.7 B) grown in osteogenic medium, whereas control cultures (Fig. 6.7 C, D) remained unstained after washing away the Alizarin Red staining solution. S-hDPSCs showed bigger and a higher number of

calcified nodules than uns-hDPSCs. These results confirm the osteogenic differentiation potential of hDPSCs *in vitro*.

6.1.5.2 Chondrogenic differentiation

For chondrogenic differentiation, a commercially available Chondrogenesis Differentiation Kit was used. Instead of being cultured as monolayers, the cells were pelleted in conical Falcon tubes, where they formed visible cell aggregates within 24 hours of culture. After 21 days, the cell pellets were analyzed for the presence of acidic polysaccharides, stained in blue, which are building blocks of proteoglycans (mainly aggrecan) and are highly abundant in mature cartilage. Nuclei and the cytoplasm were counterstained with nuclear fast red, resulting in a red-pink background in non-differentiated areas. Both uns-hDPSCs (Fig. 6.7 E) and s-hDPSCs (Fig. 6.7 F) were successfully differentiated towards the chondrogenic lineage when cultured in chondrogenic medium as seen by an intense blue color within the cell pellets, however, weaker in cultures of s-hDPSCs than in uns-hDPSCs. Negative controls did not show any signs of chondrogenic differentiation (Fig. 6.7 G, H).

6.1.5.3 Adipogenic differentiation

Adipogenic differentiation was induced by using a commercially available Adipogenic Differentiation Kit. The cells were incubated for 21 days followed by an Oil Red O staining, which stains intracellular lipid vesicles in bright red, which are only present in successfully differentiated cells. Both uns-hDPSCs and s-hDPSCs showed only tiny spots of red staining (Fig. 6.7 I, J), but real lipid vesicles were not observed, which suggests that the differentiation might not be complete. S-hDPSCs showed a similar result even when cultured in control medium (Fig. 6.7 L), which might indicate that the observed red spots in cells cultured in adipogenic medium might not be specific.

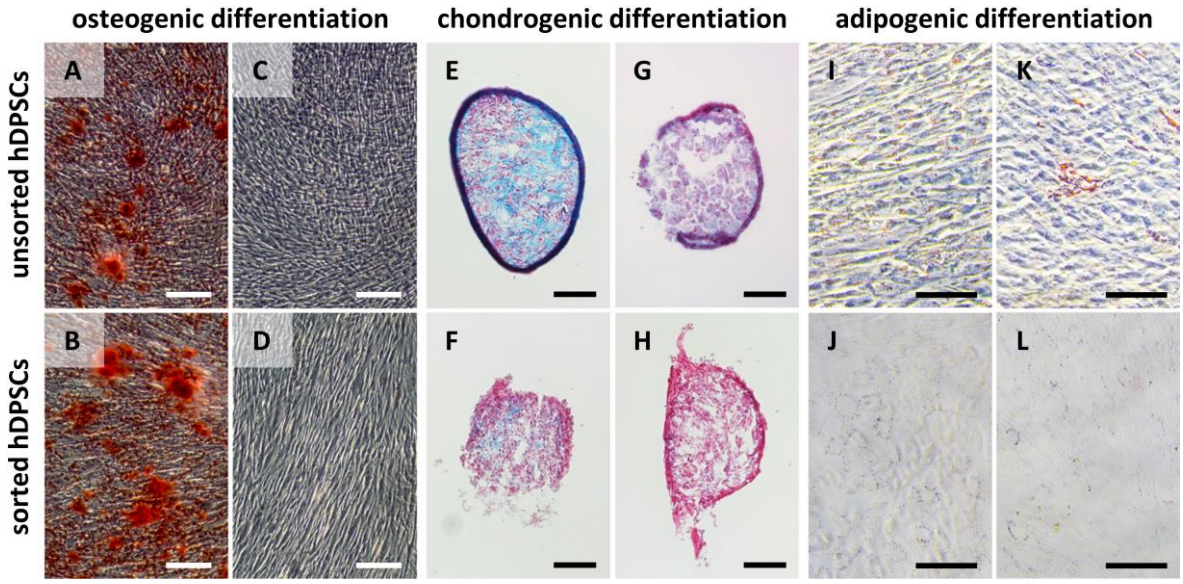

Figure 6.7. Trilineage differentiation potential of uns-hDPSCs and s-hDPSCs. (A, B) Alizarin Red S staining of cells cultured in osteogenic medium and (C, D) in control medium for 14 days *in vitro*. Extracellular calcium deposits are stained in bright orange-red, indicating successful osteogenic differentiation. Scale bar = 200 µm. (E-H) Chondrogenic differentiation assay of uns-hDPSCs and s-hDPSCs. Alcian Blue staining on sections of cell pellets cultured (E, F) in chondrogenic medium and (G, H) in control medium for 21 days *in vitro*. Acidic polysaccharides are stained in blue, indicating successful chondrogenic differentiation. Scale bar = 100 µm. (I-L) Adipogenic differentiation assay of uns-hDPSCs and s-hDPSCs. Oil Red O staining of cells cultured (I, J) in adipogenic medium and (K, L) in control medium for 21 days *in vitro*. Successful adipogenic differentiation is recognized by intracellular lipid vesicles stained in bright red, which was not complete in any of the samples. Scale bar = 100 µm.

6.1.6 Cell survival of unsorted hDPSCs and sorted hDPSCs on 3D silk scaffolds in vitro

The 3D silk scaffold used in this study is made of silk fibroin extracted from the cocoons of the silkworm *Bombyx mori*. Before having been used as a 3D biomaterial in tissue engineering (Altman et al., 2003), the material has been used in clinics for decades as a suture material, where it has proven its biocompatibility after the removal of sericin, a glue-like protein known to induce inflammatory responses. The crude material (Fig. 6.8 A left) was soaked in PBS before being cut into the final size of 3 mm height and 5 mm diameter (Fig. 6.8 A right) used for the following studies. Its properties are summarized in Figure 6.8 B and the 2D structure of an empty scaffold section is shown in Figure 6.8 C.

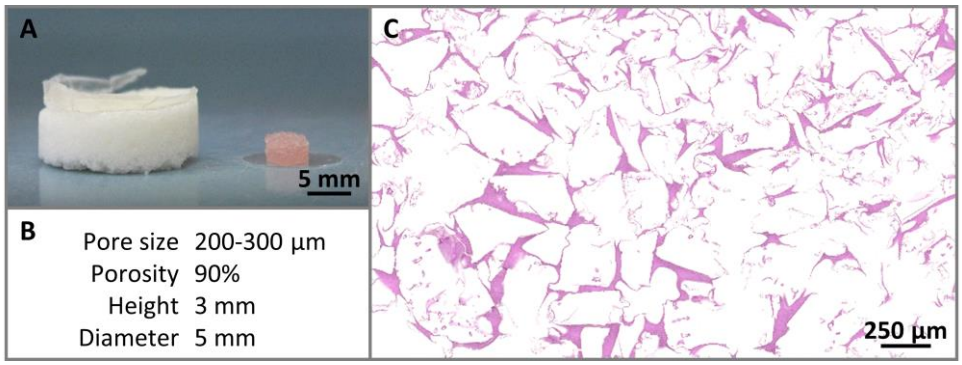

Figure 6.8. Silk scaffold biomaterial and its properties. (A) Left: crude material after production. Right: Medium-soaked scaffold after being cut into the final size of 3 mm height and 5 mm diameter. (B) Properties. (C) Hematoxylin and Eosin (H&E) staining of a section of the silk scaffold.

Cell growth within the 3D silk scaffolds was first observed in an *in vitro* setup before using the cell-seeded constructs for the planned studies. Using common cell proliferation assays like the MTT or the PicoGreen assay proved to be difficult due to the 3D architecture of the samples. Therefore, cell survival was assessed qualitatively from H&E-stained sections of silk scaffolds seeded with either uns-hDPSC or s-hDPSCs for one and seven days. One day after seeding single cell suspensions onto the silk scaffolds, the cells appeared in sphere-like aggregates attached to the fibers of the scaffold in both groups (Fig. 6.9 A, B). Within seven days of culture these aggregated cells proliferated and spread between the scaffold fibers, while producing their own ECM (Fig. 6.9 C, D). These results indicate that the environment provided by the silk scaffold is not limiting cell proliferation and allows for normal cell functioning.

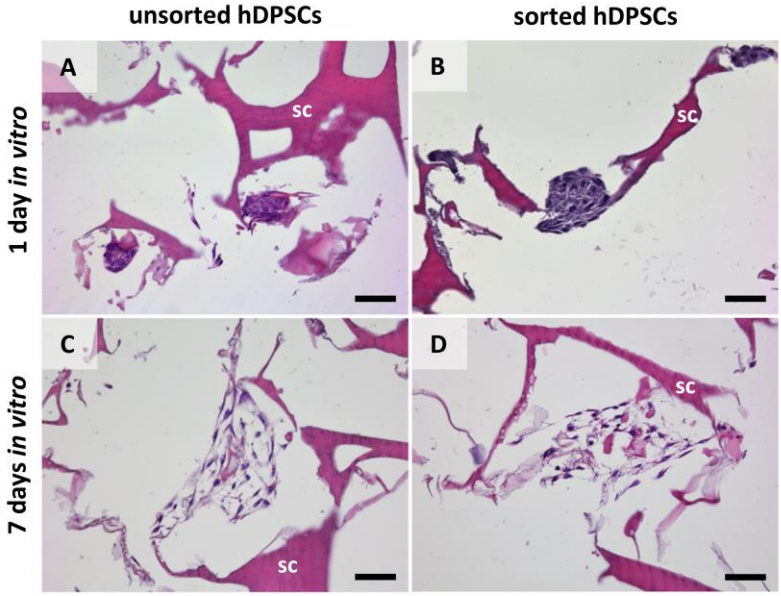

Figure 6.9. *In vitro* growth of cells seeded in 3D silk scaffolds. H&E-stained sections show typical cell arrangements as observed after one (A, B) and seven (C, D) days of culture. sc, silk scaffold fibers. Scale bar = 50 µm.

6.2 Histological and molecular analysis of 3D silk scaffolds cultured in ovo

Empty and cell-seeded scaffolds cultured *in ovo* were analyzed after 1 week to assess the quality of the tissues grown within the scaffold pores as well as the quantity of blood vessels, to characterize the extracellular matrix and the origin of the vessel structures, and to find out if and to what extent the implanted cells express markers of undifferentiated mesenchymal cells. Finally, the expression of selected genes in the human cells was investigated.

6.2.1 Tissue morphology and histomorphometrical blood vessel analysis

In order to qualitatively analyze the effect of cell-seeding of a 3D silk scaffold on vascularization and tissue integration, H&E-stained cross-sections of empty, uns-hDPSC-seeded, and s-hDPSC-seeded scaffolds were compared after their removal from the chorioallantoic membrane (CAM) of the fertilized eggs (Fig. 6.10 A). After 1 week of incubation a clear difference in the level of tissue growth within the scaffold was observed especially between the empty and the cell-seeded scaffolds (Fig. 6.10 B-D). The empty scaffold showed only minimal ingrowth of the CAM tissue at the interface between the scaffold and the CAM (Fig. 6.10 B) with the majority of the scaffold pores remaining empty. In contrast, most pores of cell-seeded scaffolds were filled with ingrowing tissue of chicken origin at the interface and with hDPSCs in the center and at the top of the scaffold (Fig. 6.10 C, D). The seeded cells were spread between the scaffold fibers (Fig. 6.10 c'', d'') and seemed to proliferate more efficiently and more homogenously within the scaffold than in scaffolds cultured *in vitro*.

Capillaries within the scaffold pores were found in all three groups (Fig. 6.10 b'-d'). The distribution of the vasculature along the horizontal axis of the scaffold was nearly homogeneous, whereas the vessel density decreased along the vertical axis from the bottom to the top of the scaffold. Blood vessels were only found in tissue- and/or cell-filled scaffold pores. Therefore, the empty scaffold was vascularized to a lower extent than the cell-seeded scaffolds. To quantify the degree of vascularization a histomorphometrical blood vessel analysis was performed. The percent area that the vessels occupy in the analyzed scaffold sections (Fig. 6.11 A) as well as the number of vessels per scaffold section (Fig. 6.11 B) were assessed. The number of vessels was normalized to a full scaffold section with an area of 15 mm^2 (3 mm height x 5 mm width) for all the evaluated samples. Lowest values for both vessel area and vessel number were obtained for the empty scaffolds, while the seeding of scaffolds with cells led to an increase of the vessel area within the scaffold by 1.6-fold and 1.5-fold for uns-hDPSCs and s-hDPSCs, respectively. Also the number of counted vessels was higher by 1.7-fold and 1.4-fold in uns-hDPSCs and s-hDPSCs, respectively, when compared to the empty scaffold. Scaffolds seeded with s-hDPSCs were slightly

less vascularized than scaffolds seeded with uns-hDPSCs. Interestingly, both graphs showed an almost proportional behavior among the groups, indicating that the counted blood vessels on average were of similar size in all the three groups. Even though no statistically significant differences in the histomorphometrical measurements among the groups were observed, cell-seeded scaffolds resulted in better tissue distribution within the scaffold pores and a higher number of vessels found within the scaffold.

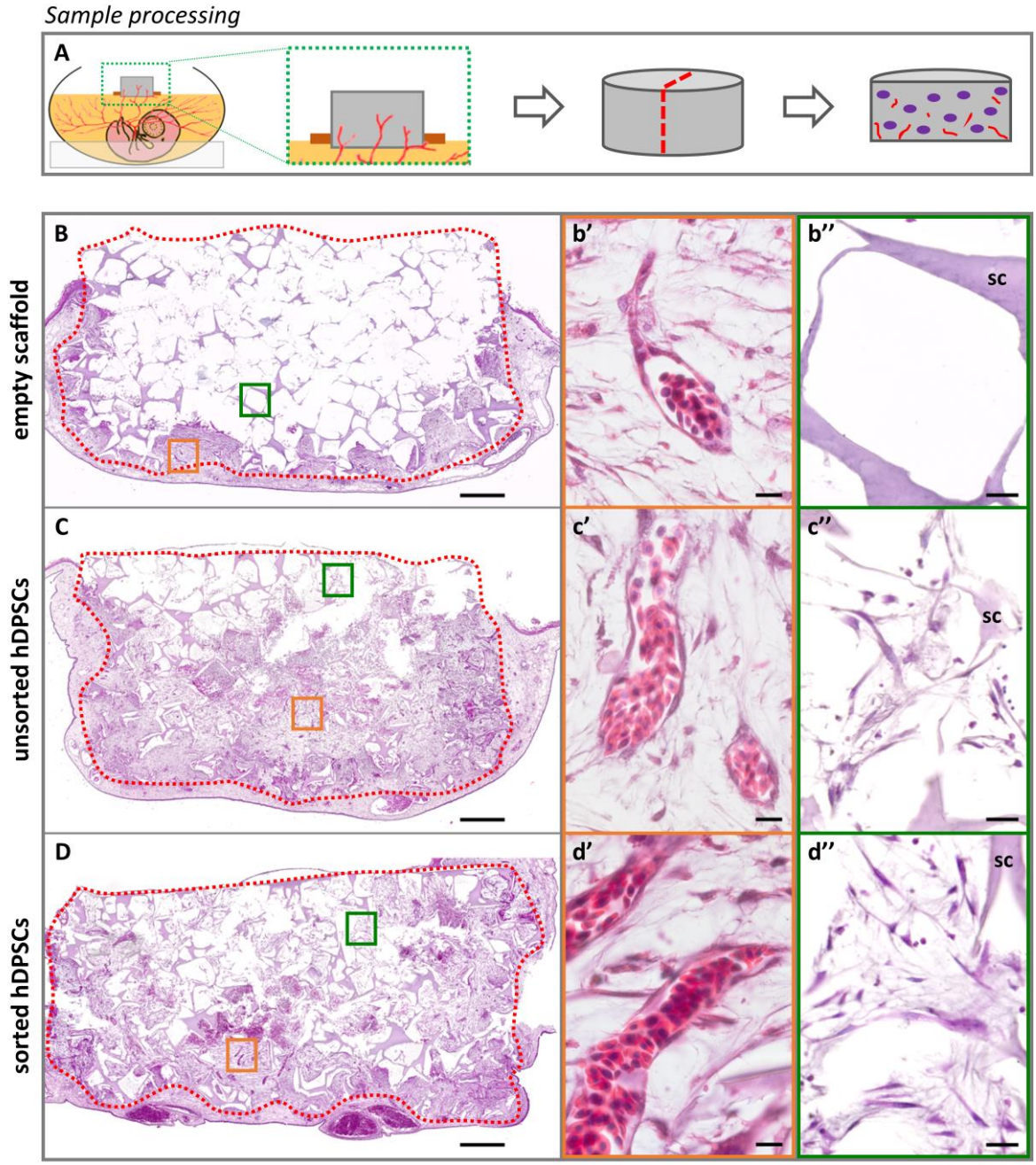

Figure 6.10. H&E staining of longitudinal sections after *in ovo* culture for 1 week. (A) Sample processing after the removal from the CAM of the fertilized egg. (B) Empty silk scaffold. (C) Silk scaffold seeded with uns-hDPSCs. (D) Silk scaffold seeded with s-hDPSCs. (B-D) Exemplary scaffold section overview. Red dotted lines indicate the outline of the scaffold. Scale bar = 500 µm. (b'-d') Magnifications showing single capillaries

in the area marked with an orange box in the corresponding overview picture. Scale bar = 10 µm. (b''-d'') Magnifications showing the empty pore and seeded cells spread between the scaffold fibers, respectively. Scale bar = 25 µm. sc, silk scaffold fibers.

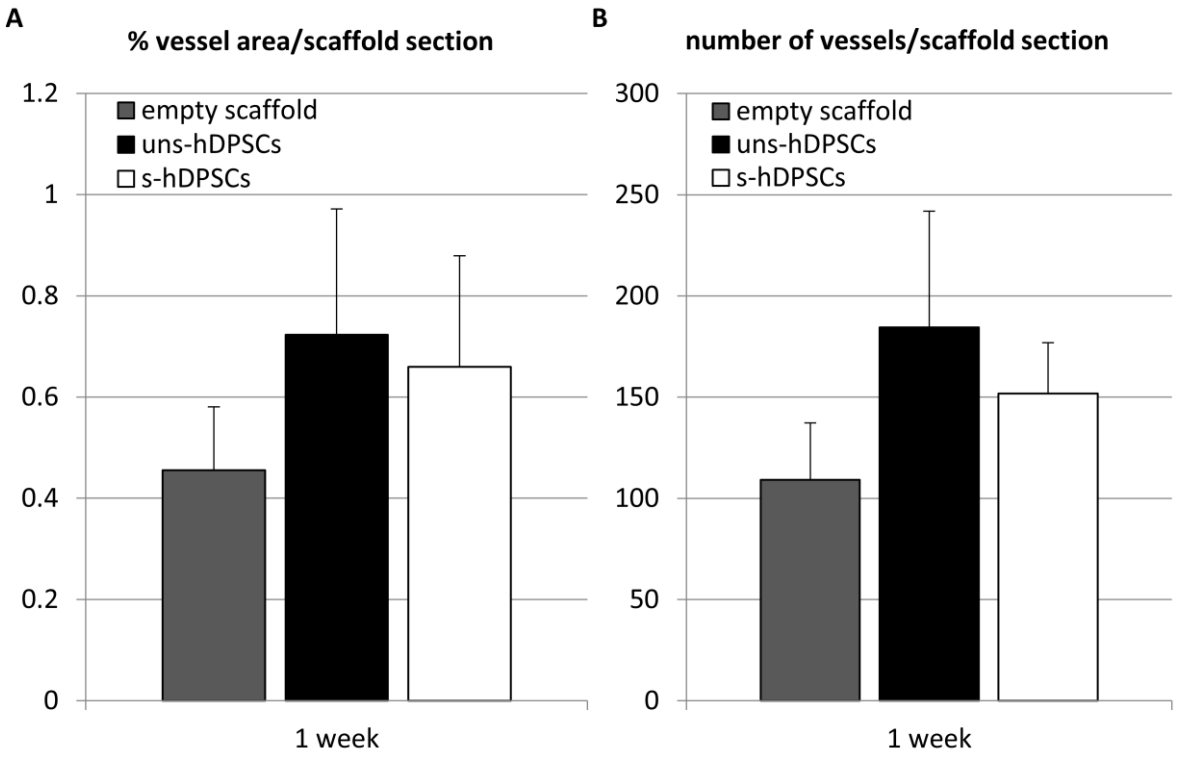

Figure 6.11. Histomorphometrical analysis of cell-seeded samples grown *in ovo* for 1 week. (A) Percent vessel area per scaffold section. (B) Number of vessels per scaffold section. Data is shown as mean ± SD, n = 3 (per n three complete sections were analyzed). No statistically significant differences between the groups were found.

6.2.2 Characterization of the extracellular matrix

To further analyze the tissue present within the scaffold, Picrosirius Red-stained sections identifying the collagen types I and III content of a matrix was assessed quantitatively in *in ovo* cultured samples. Together with collagen type II, collagen type I and III are the main collagens of connective tissue and constitute up to 90% of the collagens in the body and plays an important role during wound healing (Martin, 1997). In samples cultured for 1 week *in ovo* the presence of a collagenous matrix was lowest in empty scaffolds where only the collagen content within the CAM was measured as the rest of the scaffold remained empty (Fig. 6.12 A, a', D). In samples containing hDPSCs an increase of collagen of approximately 160% and 170% in scaffolds seeded with uns-hDPSCs (Fig. 6.12 B, D) or s-hDPSCs (Fig. 6.12 C, D), respectively, was observed. A closer

look at the ECM of the cells spread within the scaffold fibers revealed small islands of an increased collagen content as identified by a darker red staining (Fig. 6.12 b', c').

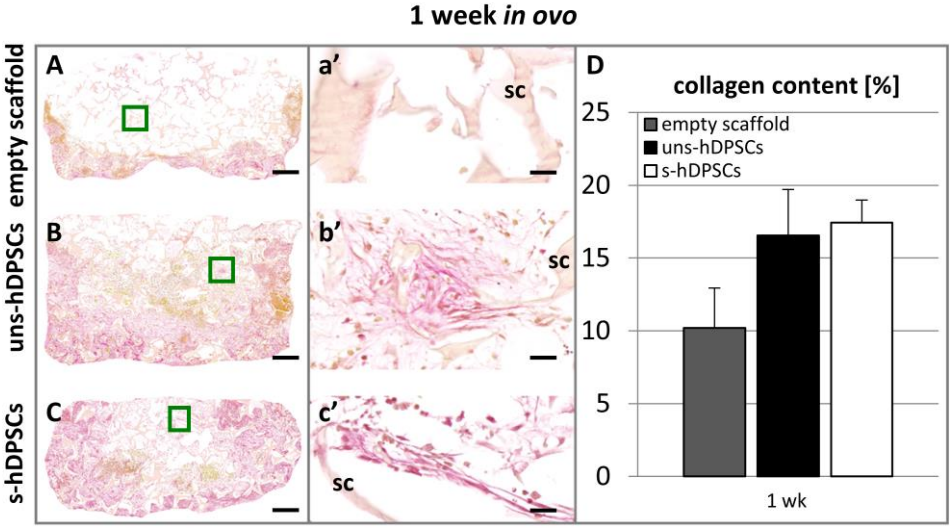

Figure 6.12. Collagen types I and III content in samples cultured *in ovo* for 1 week. In Picrosirius Red-stained sections collagen fibers appear red. The intensity of the color is proportional to the content of collagen. (A-C) Samples removed after 1 week of *in ovo* culture. Scale bar = 500 µm. (a'-c') Magnified areas of samples shown in A-C marked by a green box. Scale bar = 25 µm. (D) Quantification of the collagen content within the scaffold area. Data is shown as mean ± SD, n = 3 (per n three complete sections were analyzed). No statistically significant differences between the groups were found. sc, silk scaffold fibers.

6.2.3 Identification and characterization of vessel structures

The basement membrane is the ECM separating the endothelium from the underlying connective tissue. In vessels it appears as a sheet-like layer of laminin and collagen-rich (esp. collagen type IV) fibers formed by pericytes and endothelial cells, which can be identified using antibodies directed against epitopes of the corresponding proteins. Combined with a human-specific marker for the nuclear mitotic apparatus protein (NuMA), cells of human origin can be distinguished from cells of chicken origin. To answer the question if the human cells used to seed the 3D silk scaffolds do not only attract vessels growing in from the host tissue but if they are able to also contribute to newly developing vessels within the scaffolds, double-stainings using either anti-NuMA with anti-laminin or anti-NuMA with anti-collagen type IV antibodies were performed. Vessels were identified by a positive staining of either laminin (Fig. 6.13 A, a', B, b') or collagen type IV (Fig. 6.13 C, c', D, d') (stained in purple) and by blood cells of chicken origin present within the endothelial lumen. Human cell nuclei were visible in an orange-red color (Fig. 6.13) and were located very close and partially even as part of the endothelium, suggesting a potential pericyte or endothelial cell

function for the hDPSCs. Both components of the vascular basement membrane were identified in all cell-seeded samples. The anti-laminin antibody was not human-specific, staining both chicken and human laminin. Therefore, the distinction between human- and chicken-derived laminin was not possible. However, the anti-collagen type IV antibody did not show any staining in cell-free silk scaffolds, thus identifying human collagen type IV only.

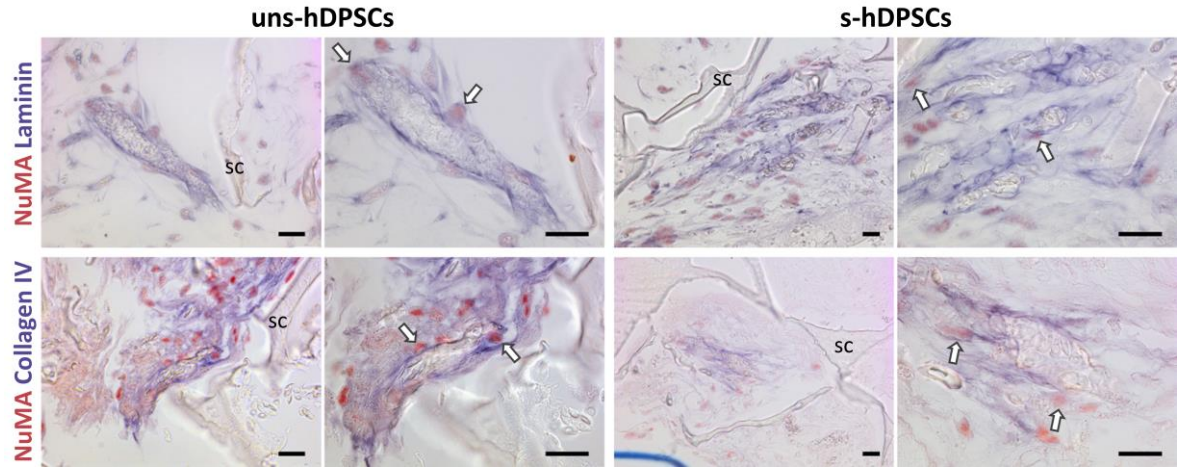

Figure 6.13. Immunohistochemistry showing laminin and collagen type IV expression in the basement membrane of capillaries within the scaffold material after *in ovo* implantation for 1 week. (A, B) NuMA (orange-red) and laminin (purple) staining of samples containing uns-hDPSCs (A) or s-hDPSCs (B). (C, D) NuMA and collagen type IV (purple) staining of samples containing uns-hDPSCs (C) or s-hDPSCs (D). (a' d') Magnifications of the area marked with a green dotted line in the corresponding overview picture. White arrows indicate cells of human origin involved in the vessel structures. Scale bar (all pictures) = 25 µm. sc, silk scaffold fibers.

6.2.4 Identification of stem cells of mesenchymal origin

When using undifferentiated stem cells for tissue engineering, a part of the cells should differentiate in order to recreate the tissue according to signals coming from the immediate environment, but part of the cells should also remain in an undifferentiated state in order to keep up tissue homeostasis. To assess if the cells seeded into the silk scaffold are able to remain undifferentiated, the sections were stained using anti-Nestin, anti-Sox2, and anti-Vimentin antibodies, which have been detected before in monolayer cultures of both uns-hDPSCs and s-hDPSCs (Fig. 6.6). Human origin of the cells was assessed with the anti-NuMA-antibody. Nestin was expressed in both cell populations, similar to the results previously observed in monolayer cultures (Fig. 6.14 A, B). However, the Sox2 stainings showed an unexpected staining pattern, where mostly the cytoplasm was stained, while only few cells were Sox2-positive in the nucleus of both uns-hDPSCs and s-hDPSCs (Fig. 6.14 C, D). Nestin- and Sox2-positive cells were mostly

localized where the human cells had not been in touch with chicken-derived tissue. Vimentin was used to identify cells of mesenchymal origin and follow their integration within the ingrowing tissue of the host (Fig. 6.14 E, F). The staining showed that the human cells were localized not only at the edges of the scaffold but also in the center and mixed with cells of chicken origin, which were identified by negative NuMA staining.

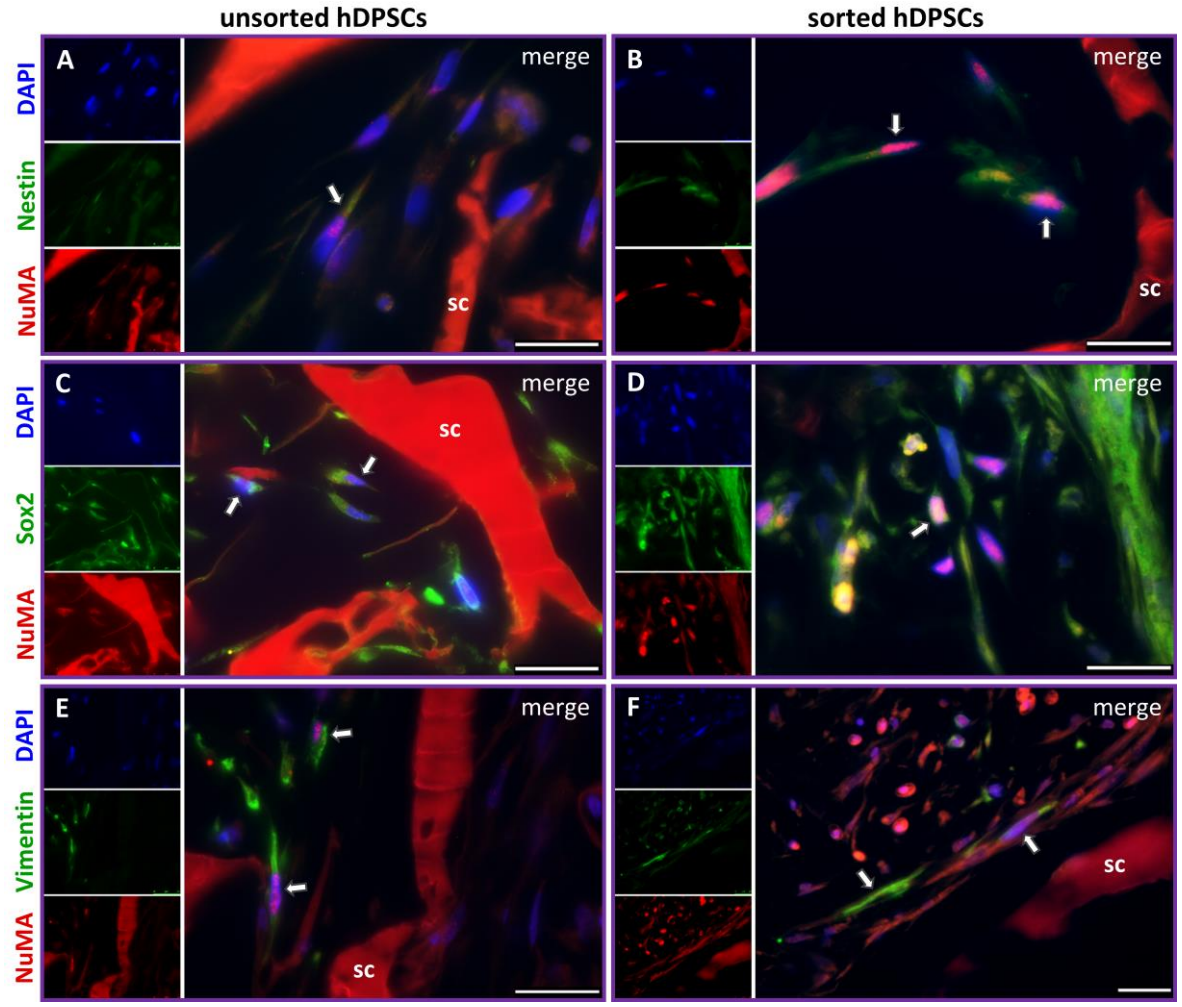

Figure 6.14. Immunofluorescence of stem cell markers and a mesenchymal cell marker of samples cultured *in ovo*. (A, B) NuMA (red) and Nestin (green) staining of samples containing uns-hDPSCs (A) or s-hDPSCs (B). (C, D) NuMA (red) and Sox2 (green) staining of samples containing uns-hDPSCs (C) or s-hDPSCs (D). (E, F) NuMA (red) and Vimentin (green) staining of samples containing uns-hDPSCs (E) or s-hDPSCs (F). Arrows indicate cells of human origin expressing Nestin, Sox2, or Vimentin. Small pictures on the left side of each picture show the three individual channels. Scale bar = 25 µm. sc, silk scaffold fibers.

6.2.5 Gene expression analysis

The expression of human *Nanog* and *Nestin* (stem cell markers), transforming growth factor beta 1 (*TGFb1*) and vascular endothelial growth factor A (*VEGFA*) (angiogenic cytokines), as well as runt-related transcription factor 2 (*RUNX2*) (key transcription factor of osteoblast differentiation) was analyzed in samples after 1 week of *in ovo* culture (Fig. 6.15). While the expression of *Nestin*, *TGFb1*, and *VEGFA* was 2-fold lower in s-hDPSCs than in uns-hDPSCs, *Nanog*- and *RUNX2*-expression were upregulated in s-hDPSCs when compared to uns-hDPSCs by a factor of 1.85 and 1.6, respectively. However, the observed differences between the two groups were not statistically significant, suggesting similar gene regulation in both cell populations. In comparison to monolayer cultures of uns-hDPSCs, all genes showed increased expression after *in ovo* incubation.

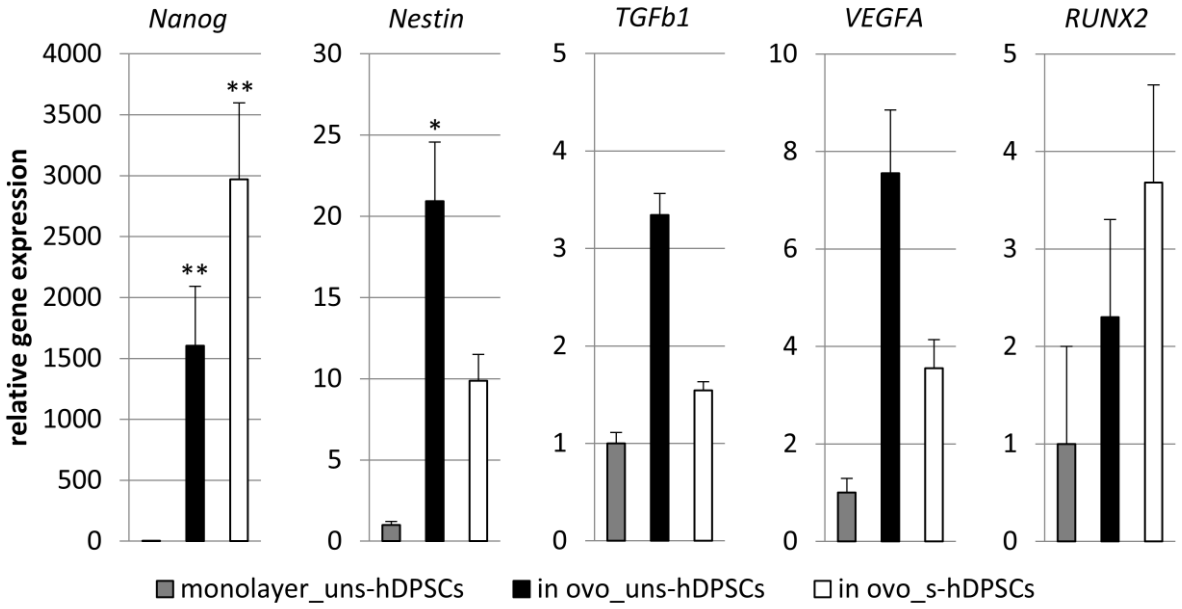

Figure 6.15. Gene expression analysis of cell-seeded samples grown *in ovo* for 1 week. Gene expression relative to uns-hDPSCs cultured as a monolayer. *RUNX2*, runt-related transcription factor 2; *TGFb1*, transforming growth factor beta 1; *VEGFA*, vascular endothelial growth factor A. Data is shown as mean ± SD, monolayer samples: n = 3, *in ovo* samples: n = 6. Asterisks indicate significant (*, $p < 0.05$) or highly significant (**, $p < 0.01$) differences between the groups.

6.3 Histological and molecular analysis of 3D silk scaffolds cultured in vivo

For a direct comparison of the results obtained from samples cultured *in ovo* with a more common angiogenesis assay, empty and cell-seeded samples that were prepared and analyzed in exactly the same way as for the *in ovo* study, were implanted subcutaneously in mice for a time period of 1 week. Furthermore, samples were cultured also for 4 weeks and 47 days in order to assess the long-term effect on tissue integration of uns-hDPSC- and s-hDPSC-seeded silk scaffolds within a typical time frame of wound healing.

6.3.1 Tissue morphology and histomorphometrical blood vessel analysis

After the removal of the implants from the subcutaneous pockets of immunocompromised mice, H&E-stained cross-sections of empty, uns-hDPSC-seeded, and s-hDPSC-seeded scaffolds were analyzed with a focus on tissue growth and vascularization (Fig. 6.16 A). Empty and cell-seeded samples removed after 1 week of *in vivo* culture demonstrated clear differences in the cell/tissue content within the scaffold pores (Fig. 6.16 B, E, H). While the seeded human cells were proliferating and spreading within the scaffold pores (Fig. 6.16 e'', h''), the pores in the empty scaffold were filled with acellular fibers appearing blue in the H&E staining (Fig. 6.16 b''). Additionally, s-hDPSCs seemed to proliferate a bit less than the uns-hDPSCs resulting in a higher percentage of scaffold pores that appeared empty (Fig. 6.16 H). Compared to *in ovo* cultured samples more pores containing dead cells were found after 1 week of implantation *in vivo*, which might be induced by the closed environment provided by the subcutaneous pocket. Similar to observations from the *in ovo* samples minimal ingrowth of host tissue was visible at the interface along the edges of the scaffold. Blood vessels were found exclusively at the border of the scaffold in all samples analyzed after 1 week of incubation (Fig. 6.16 b', e', h'). The vessel area in uns-hDPSC- and s-hDPSC-seeded scaffolds was 31 and 22 times higher, respectively, when compared to the empty scaffold (Fig. 6.17 A). The number of vessels showed an increase of 40- and 25-fold for uns-hDPSCs and s-hDPSCs, respectively (Fig. 6.17 B). In contrast to *in ovo* cultured samples the percent vessel area of scaffolds implanted *in vivo* for 1 week were lower by 98%, 57%, and 67% for empty, uns-hDPSC- and s-hDPSC-seeded scaffolds, respectively.

The next samples were analyzed after 4 weeks of implantation, as this is a time where the proliferative phase of wound healing is finishing. Even though differences between the empty scaffolds and the cell-seeded scaffolds were not as obvious as they have been after 1 week, still the empty scaffolds were showing more empty areas within the scaffold than the cell-seeded groups (Fig. 6.16 C, F, I). The tissue structure within the pores was less dense and less organized (Fig. 6.16. c''). Based on the H&E-stained sections samples seeded with s-hDPSCs were showing a

pore filling of almost 100% and a homogenously dense network of ECM throughout the whole scaffold (Fig. 6.16 i''). Also in uns-hDPSC-seeded scaffolds most pores were filled and even though the ECM was homogenously distributed, it appeared slightly less compact than the one seen in the other cell-seeded group (Fig. 6.16 f''). Blood vessels were present in all areas of the scaffold, including the center (Fig. 6.16 c', f', i'). The average percent vessel area for all the three groups was around 1%, while on average around 280 vessels were counted per scaffold section, with the lowest value found in empty scaffolds and the highest in samples containing uns-hDPSCs.

The third and final time point for sample analysis was chosen at 47 days, as we wanted to compare the degree of potential matrix mineralization with experiments we had previously performed for the same silk fibroin scaffolds seeded with hDPSCs, which were cultured statically and in bioreactors for 47 days *in vitro* (Woloszyk et al., 2014). Histologically, similar tissue structures and degrees of pore filling were found as in the samples analyzed after 4 weeks. The center of the empty scaffolds was clearly free of vessels and tissue (empty area in Fig. 6.16 D, d''), while most of the pores in cell-seeded scaffolds (Fig. 6.16 G, J) contained a homogenous ECM, again being more compact in s-hDPSC-seeded scaffolds than in the case of uns-hDPSCs (Fig. 6.16 g'', j''). The histomorphometric analysis of blood vessels seen in all the samples (Fig. 6.16 d', g', j') showed an increase of the total percent vessel area from 1 week to 47 days by 1.6-, 6.3-, and 4-fold for the empty, uns-hDPSC-, and s-hDPSC-seeded scaffolds, respectively (Fig. 6.16 A). Also the number of blood vessels rose by 129-fold (empty scaffold), by 5.7-fold (uns-hDPSCs), and by 4.1-fold (s-hDPSCs) (Fig. 6.16 B). The values obtained in cell-seeded scaffolds for vessel area and vessel number behaved proportionally, which demonstrates that the average size of blood vessels in those two groups were the same. The disproportionate increase observed in empty scaffolds appeared so much higher due to a very low number of blood vessels found in empty scaffolds after 1 week. Compared to the vessel area and number determined in samples incubated for 4 weeks, both values increased in samples collected after 47 days on average by 150%. Furthermore, in cell-seeded scaffolds analyzed after both 4 weeks and 47 days, almost no cell death within the scaffold pores was observed, indicating that the cells that survived the first week after implantation were sufficient for the development of vascularized tissue within the scaffolds.

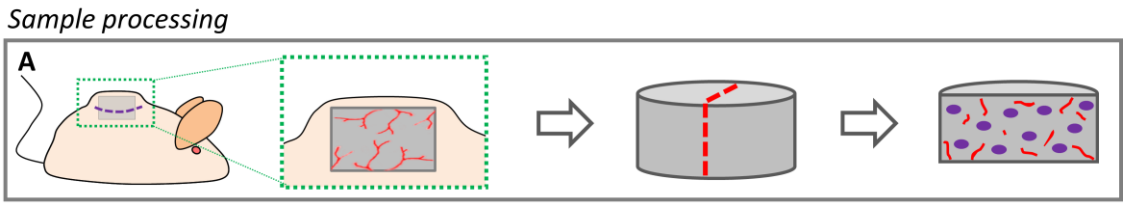

Figure 6.16 A. Sample processing after the excision of the implants from the subcutaneous pocket of an immunocompromised mouse.

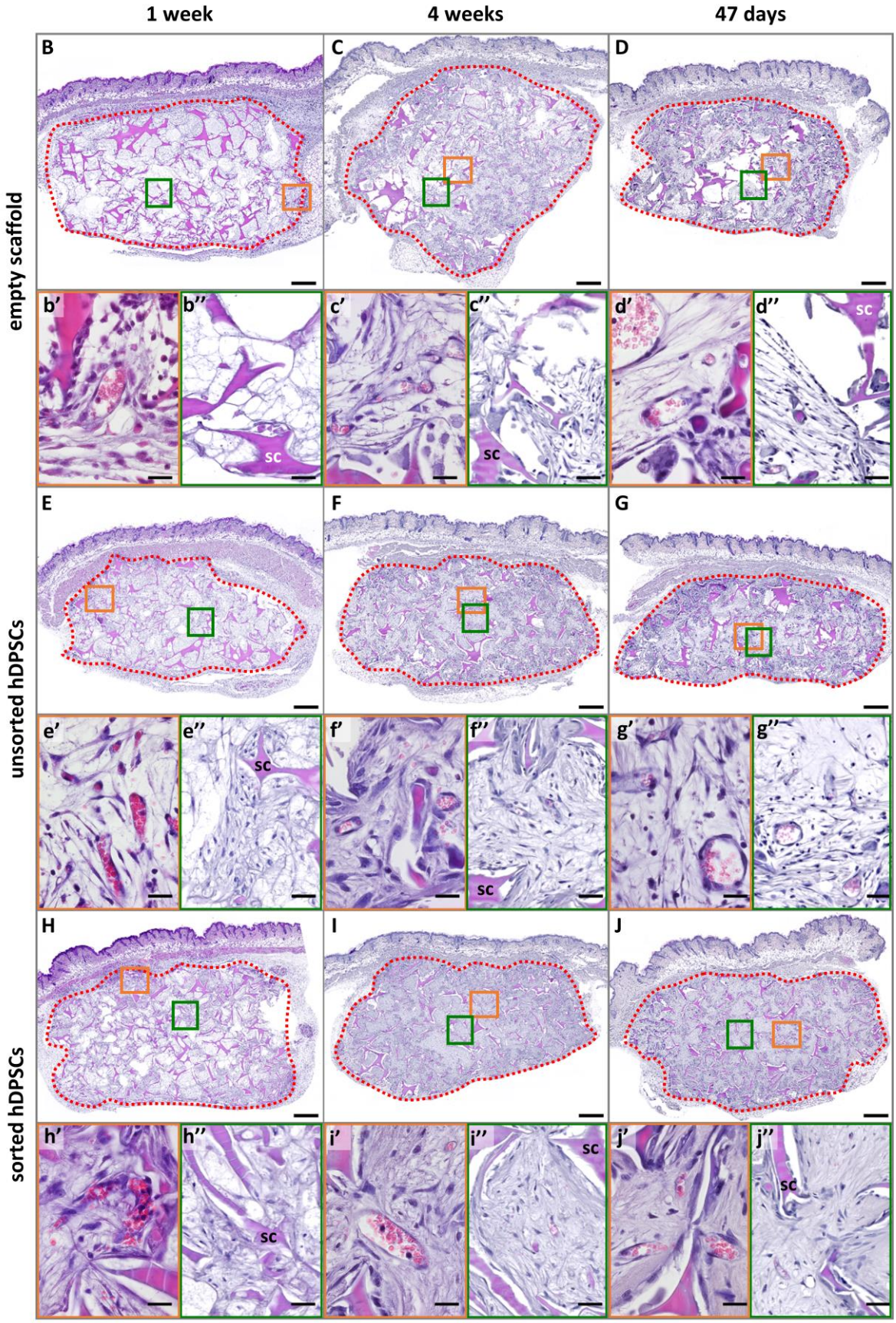

The corresponding figure legend can be found on the next page.

Figure 6.16 B-J (*see previous page*). H&E staining of longitudinal cross-sections cultured *in vivo*. (B-D) Empty silk scaffold incubated for 1 week, 4 weeks, and 47 days. (E-G) Silk scaffold seeded with uns-hDPSCs incubated for 1 week, 4 weeks, and 47 days. (H-J) Silk scaffold seeded with s-hDPSCs incubated for 1 week, 4 weeks, and 47 days. (B-J) Exemplary scaffold section overview. Red dotted lines indicate the outline of the scaffold. Scale bar = 500 µm. (b'-j') Magnifications showing single capillaries in the area marked with an orange box in the corresponding overview picture. Scale bar = 20 µm. (b''-j'') Magnifications showing the seeded cells spread between the scaffold fibers. Scale bar = 40 µm. sc, silk scaffold fibers.

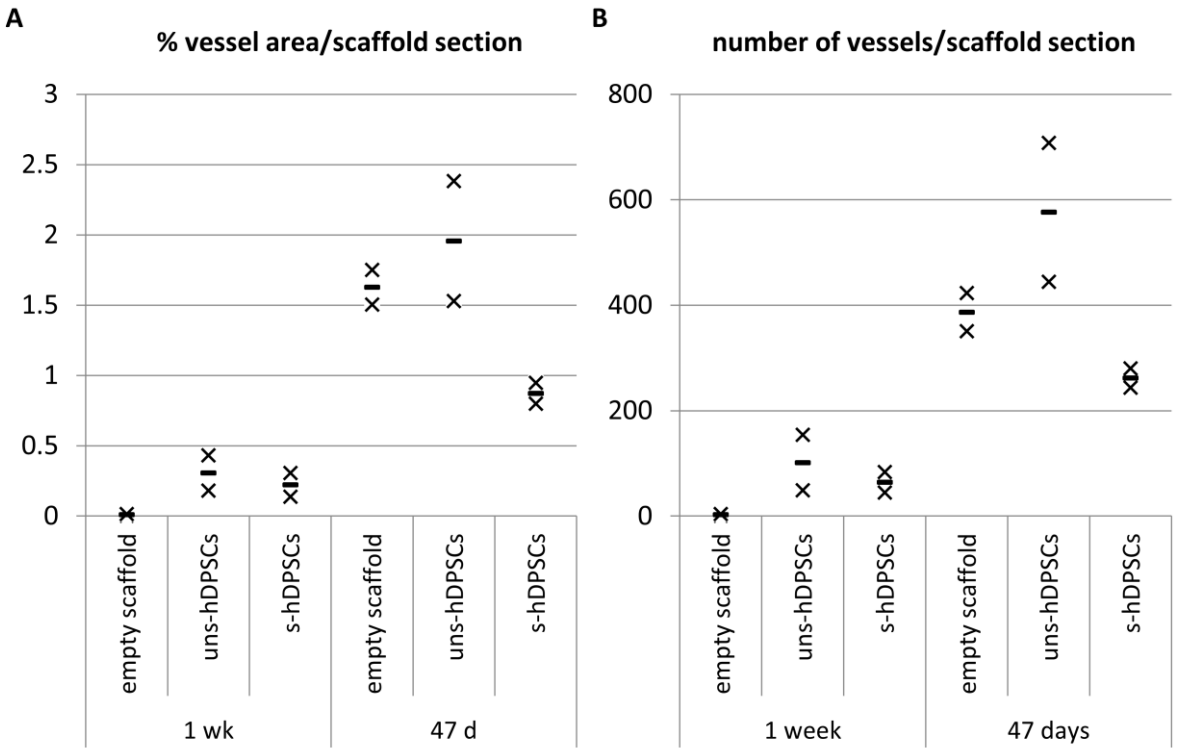

Figure 6.17. Histomorphometric analysis of cell-seeded samples grown *in vivo* for 1 week and for 47 days. (A) Percent vessel area per scaffold section (15 mm^2). (B) Number of vessels per scaffold section. Crosses indicate the values of two different samples (resulting from 3 analyzed sections per sample), black lines indicate the mean value.

6.3.2 Characterization of the extracellular matrix

Similar to the *in ovo* cultured samples also the samples implanted *in vivo* were stained with Picrosirius Red stain in order to measure the content of collagen types I and III of the matrix grown within the 3D silk scaffolds. In samples analyzed after 1 week of culture, the highest content of collagen was found in sections of scaffolds seeded with s-hDPSCs (Fig. 6.18 C, D). The measured collagen content in uns-hDPSC-seeded scaffolds was only slightly lower (Fig. 6.18 B, D),

while the empty scaffold showed a reduced collagen content of approximately 30% compared to the cell-seeded scaffolds (Fig. 6.18 A, D). Small islands of more intensely colored collagen fibers were observed being stretched between the scaffold fibers (Fig. 6.18 a', b', c'), similarly to the *in ovo* results. After 47 days of incubation, the staining seen in sections of all the three groups was significantly stronger (Fig. 6.18 E-G). As shown in the magnified areas (Fig. 6.18 e', f', g') also the matrix was much denser, especially in the scaffolds seeded with uns-hDPSCs (Fig. 6.18 f'), resulting in a percent difference of 20% and 12% when compared to empty and s-hDPSC-seeded scaffolds (Fig. 6.18 D), respectively. The collagen content was determined to be 1.9, 1.7, and 1.5 times higher for empty, uns-hDPSC-, and s-hDPSC-seeded scaffolds than in the corresponding 1 week-samples.

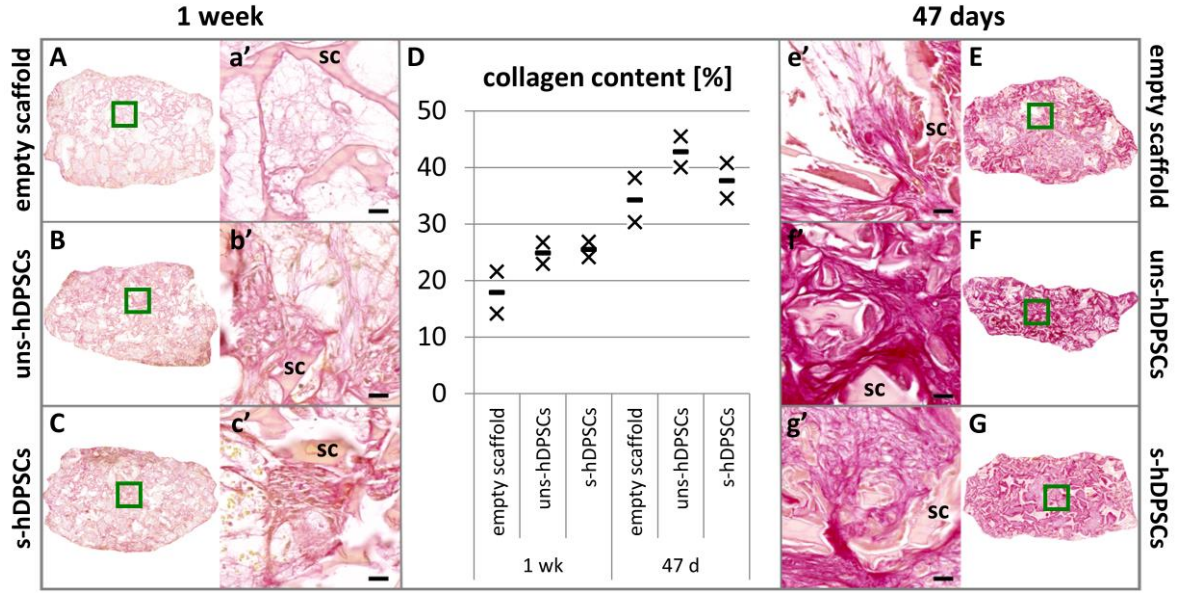

Figure 6.18. Collagen type I and III content in samples cultured *in vivo* for 1 week and 47 days. In Picrosirius Red-stained sections collagen type I and III fibers appear red. The intensity of the color is proportional to the content of collagen. (A-C) Samples removed after 1 week of culture. (D) Quantification of the collagen content within the scaffold area. Crosses indicate the values of two different samples (resulting from 3 analyzed sections per sample), black lines indicate the mean value. (E-G) Samples removed after 47 days of culture. (a'-c', e'-g') Magnified areas of samples shown in A-C and E-G marked by a green box. Scale bar = 25 µm. sc, silk scaffold fibers.

6.3.3 Identification and characterization of vessel structures

In order to investigate if the results observed *in ovo* are reproducible *in vivo*, the vessel structures growing within the scaffolds were characterized. We analyzed samples collected after 4 weeks, as the samples removed after only 1 week did not contain a sufficient number of vessels. The same antibodies were used as previously for the *in ovo* incubated samples to visualize cells of human origin (NuMA), the two main constituents of the vascular basement membrane (laminin and collagen type IV) and additionally the endothelial cell marker von Willebrand Factor (vWF), a glycoprotein that plays a major role in blood coagulation. Even though neither laminin (Fig. 6.19 A, a', B, b') nor collagen type IV (Fig. 6.19 C, c', D, d') were human-specific, the observed NuMA-positive human cell nuclei embedded in the vessels walls (white arrows in Fig. 6.19 a'-d') proved the ability of both uns-hDPSCs and s-hDPSCs to directly contribute to newly forming vessels within the scaffold. This finding was further supported by a positive vWF-staining of human-derived cells, which were observed in the vessel wall of tiny capillaries in both cell-seeded groups, indicating the differentiation into endothelial cells (white arrows in Fig. 6.19 e', f').

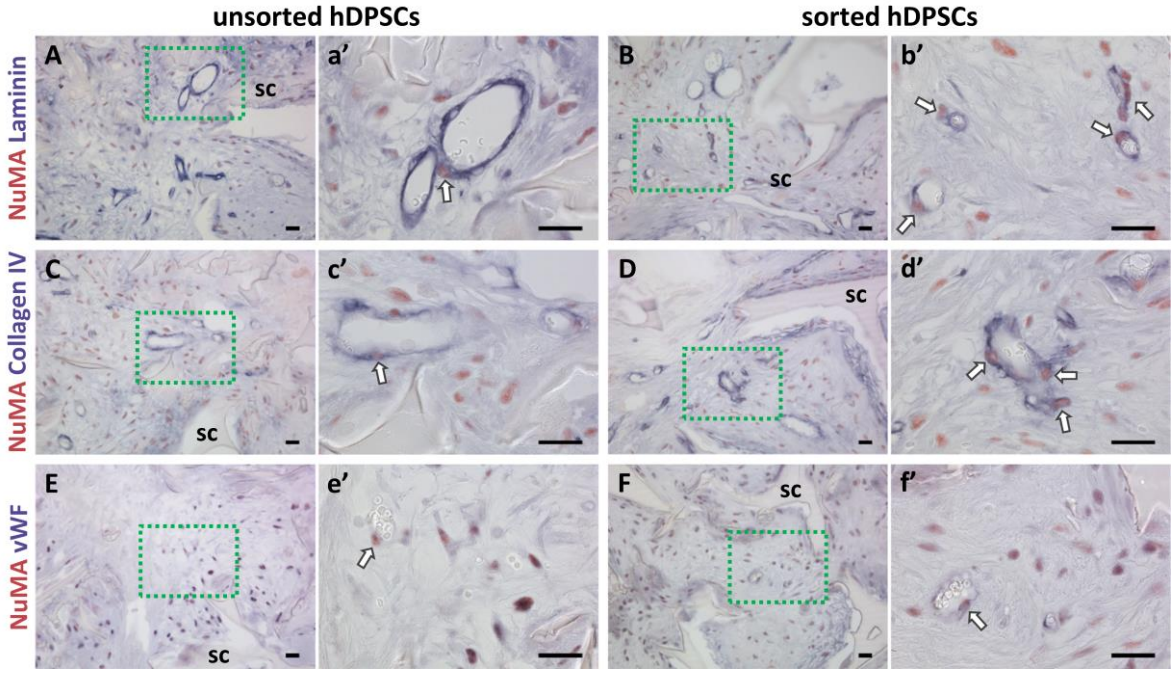

Figure 6.19. Immunohistochemistry showing laminin, collagen type IV, and vWF expression in the basement membrane of capillaries within the scaffold material after *in vivo* implantation for 4 weeks. (A, B) NuMA (orange-red) and laminin (purple) staining of samples containing uns-hDPSCs (A) or s-hDPSCs (B). (C, D) NuMA and collagen type IV (purple) staining of samples containing uns-hDPSCs (C) or s-hDPSCs (D). (E, F) NuMA and vWF (purple) staining of samples containing uns-hDPSCs (E) or s-hDPSCs (F). (a'-f') Magnifications of the area marked with a green dotted line in the corresponding overview picture. White arrows indicate cells of human origin embedded in the vessel wall. Scale bar (all pictures) = 25 µm. sc, silk scaffold fibers.

6.3.4 Identification of stem cells of mesenchymal origin

The goal was to confirm the presence of undifferentiated cells of mesenchymal origin expressing Nestin, Sox2, and Vimentin as previously observed *in ovo*. Instead of using the NuMA-antibody, the human origin of the seeded cells was tracked by staining the cells with DiI stain (1,1'-Dioctadecyl-3,3,3',3'-Tetramethylindocarbocyanine Perchlorate) prior to seeding them on the 3D silk scaffolds. After the experiment, the stain was detected in the red fluorescence channel (ex: 549 nm, em: 565 nm). The stainings were performed on samples collected after an *in vivo* incubation time of 4 weeks. In both uns-hDPSC- and s-hDPSC-seeded scaffolds, Nestin- and Vimentin-postive cells of human origin were observed (Fig. 6.20 A, B, E, F). Nestin-postive cells were mostly localized close to scaffold fibers and did not occur in a very high number, while Vimentin-positive cells were detected all over the scaffold pores throughout all the scaffold. Similar to the Sox2-staining performed in *in ovo* cultured samples, also in the *in vivo* samples Sox2 expression was not exclusively limited to the cell nucleus (Fig. 6.20. C, D) and only a few cells were found to show some Sox2-positive signal coming from the nucleus.

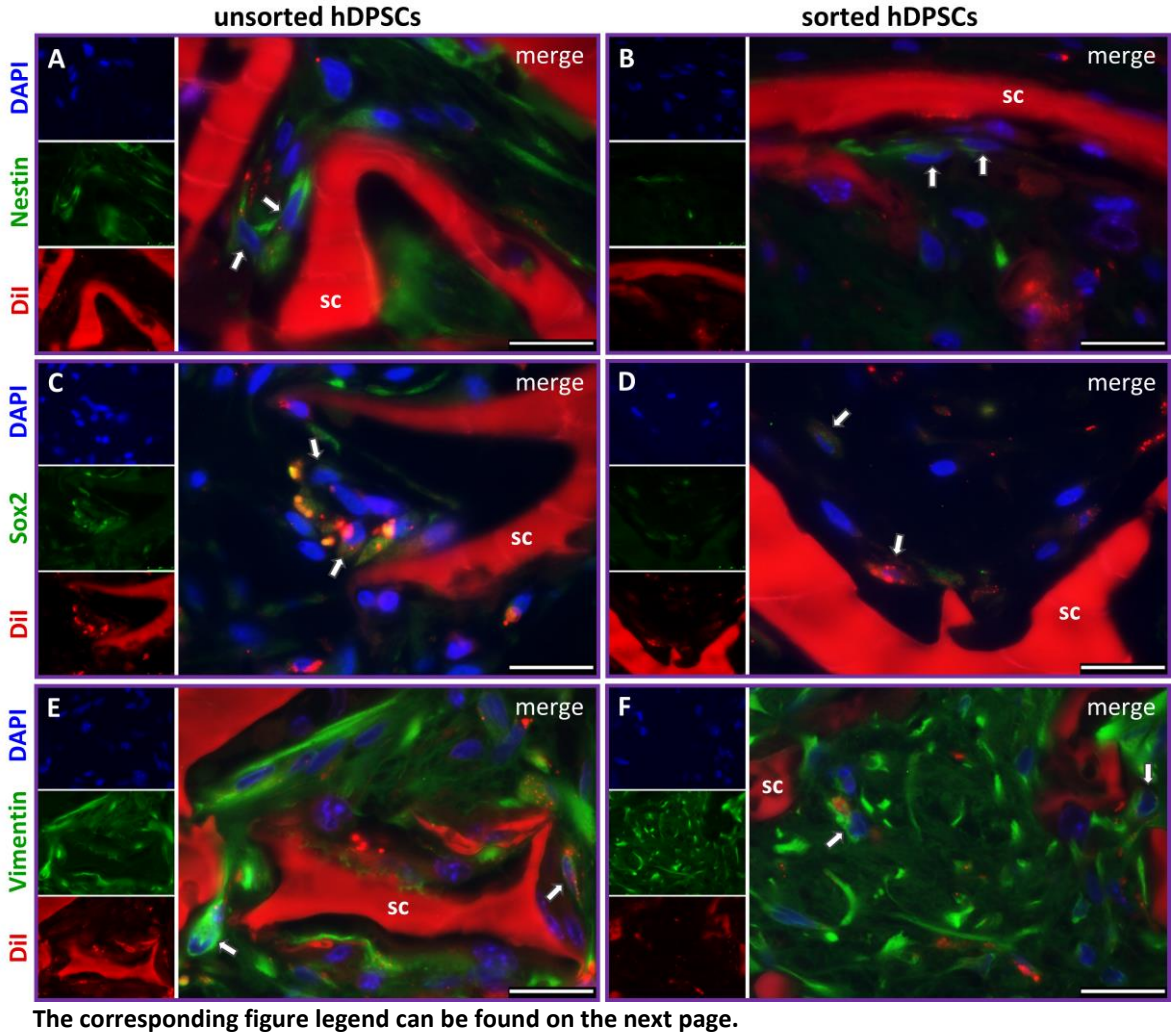

The corresponding figure legend can be found on the next page.

Figure 6.20. Immunofluorescence of stem cell markers and a mesenchymal cell marker of samples cultured *in vivo*. (A, B) DiI (red) and Sox2 (green) staining of samples containing uns-hDPSCs (A) or s-hDPSCs (B). (C, D) DiI (red) and Nestin (green) staining of samples containing uns-hDPSCs (C) or s-hDPSCs (D). (E, F) DiI (red) and Vimentin (green) staining of samples containing uns-hDPSCs (E) or s-hDPSCs (F). Arrows indicate cells of human origin expressing Sox2, Nestin, or Vimentin. Small pictures on the left side of each picture show the three individual channels. Scale bar = 25 µm. sc, silk scaffold fibers.

6.3.5 Preliminary gene expression analysis

Gene expression analysis was performed for samples obtained after 4 weeks of incubation. As only one sample per group was available for analysis only preliminary results can be presented (Fig. 6.21). The same set of genes was analyzed as previously in *in ovo* cultured samples.

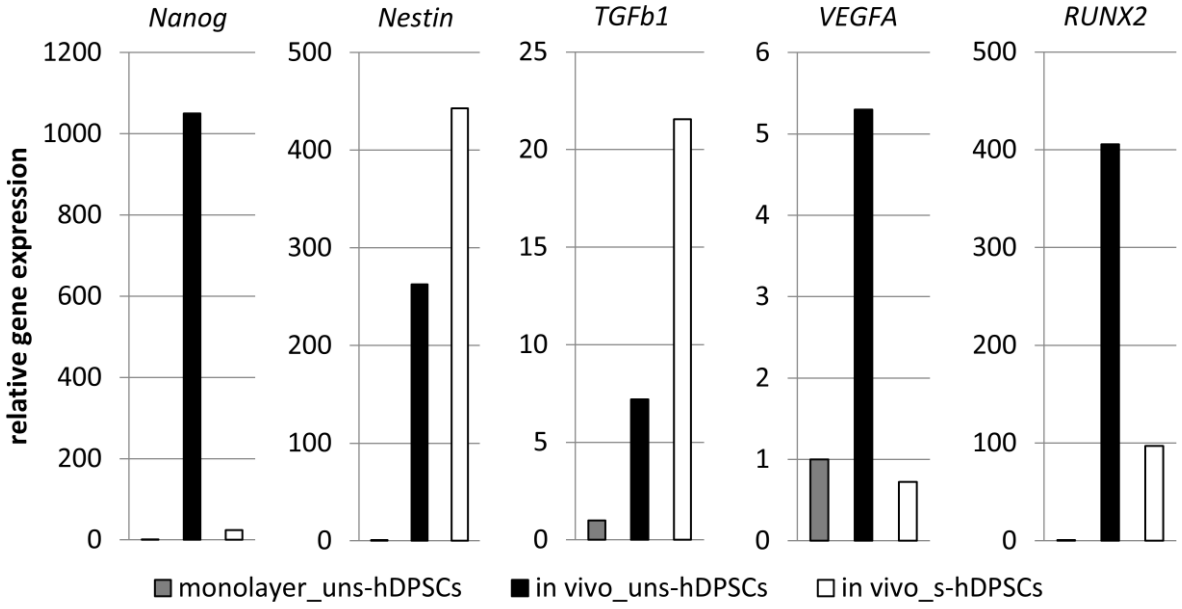

Figure 6.21. Preliminary gene expression analysis of cell-seeded samples grown *in vivo* for 4 weeks. Gene expression relative to uns-hDPSCs cultured as a monolayer. *RUNX2*, runt-related transcription factor 2; *TGFb1*, transforming growth factor beta 1; *VEGFA*, vascular endothelial growth factor A. Data is shown as mean for monolayer samples (n = 3) and measurement from one single sample per group for *in vivo* samples (n = 1).

Nanog-expression was higher in both *in vivo* groups than in monolayer cultures but lower than in both *in ovo* groups, suggesting a lower differentiation potential and self-renewal ability, even stronger in the s-hDPSCs than in uns-hDPSCs. However, *Nestin*-expression was found to be much higher in both *in vivo* groups than in the *in ovo* groups, which in contrast to the lower *Nanog*-expression indicates an increase in pluripotency and self-renewal ability. *TGFb1* was expressed higher in the *in vivo* groups than in both *in ovo* groups, while *VEGFA*-expression was lower,

especially in s-hDPSC-seeded scaffolds after *in vivo* incubation. This might indicate a *TGFb1*-induced inhibition of *VEGF*. Furthermore, an increase in *RUNX2*-expression was observed when compared to *in ovo* samples, stronger in uns-hDPSCs than in s-hDPSCs.

6.3.6 Mineralization

To test if the formation of ectopic bone does occur in samples implanted in a non-mineralized environment, we prolonged the *in vivo* experiment to a period of 47 days as we had previously shown that silk scaffolds containing hDPSCs can produce mineralized matrix when cultured statically in non-osteogenic medium *in vitro* (Woloszyk et al., 2014). Therefore, a microCT scan of the samples removed after 47 days was performed prior to histological analysis. Except for one sample that showed a minimal bone volume of 0.19 mm^3 (Fig. 6.22), which accounts for as little as 0.3% of the total volume of the scaffold (58.9 mm^3), no mineralized nodules were found in any of the other samples. Histological analysis of the mineral-containing sample showed that the nodules were located at the edges of the scaffold and therefore were most probably of mouse-origin and less likely a product of the seeded human cells.

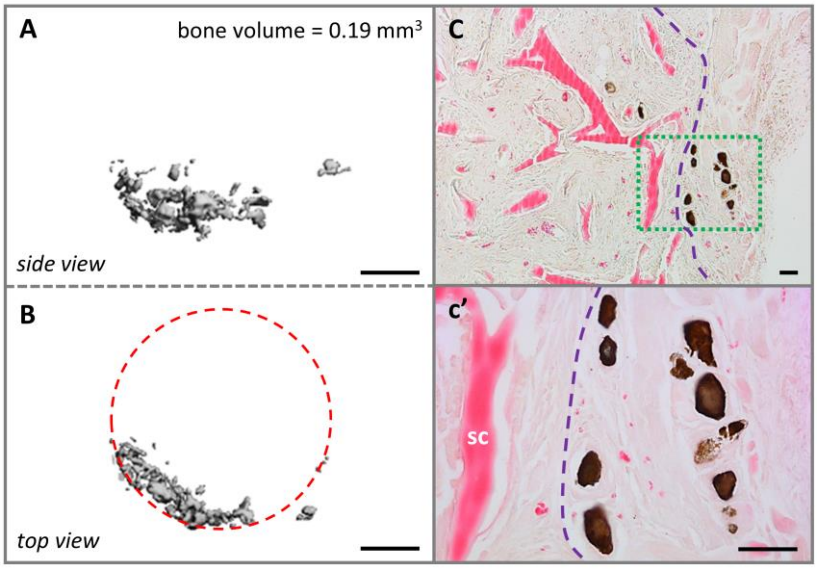

Figure 6.22. MicroCT analysis of samples cultured *in vivo* for 47 days. (A) Side view of the mineralized nodules found in one of the scaffolds seeded with uns-hDPSCs. Scale bar = 1 mm. (B) Top view of the same sample. The red dashed line indicates the outline of the scaffold. Scale bar = 1 mm. (C) Von Kossa staining showing the mineralized nodules in brown-black color within the sample. Purple dashed line indicated the border between the host tissue on the right and the implant on the left. Scale bar = 50 µm. (c') The magnification of the area marked with a green dotted line in the corresponding overview picture shown in C. Scale bar = 50 µm. sc = silk scaffold fibers.

6.4 Visualization of the vascular network within hDPSC-seeded 3D silk scaffolds cultured in ovo

We have used the CAM assay *in ovo* setup (Fig. 5.1) to study the vascularization of a 3D biomaterial when placed in a vascularized host environment. The perfusion of the vascular system was performed without pre-perfusion with PBS, instead the blood was directly replaced by the injected MicroFil® (Fig. 6.23 A). The perfusion efficiency with MicroFil® initially diluted according to the manufacturer's recommendation (i.e. 1:1) was improved by using a 10-fold dilution of the silicone rubber injection compound in MV-diluent, which required an increased amount of MV-Curing Agent of 10% instead of 5% (by weight). If perfusion with the yellow MicroFil® was not complete after the first injection (Fig. 6.23 B), as seen by the presence of blood-filled vessels (red), a second injection site was chosen to increase the number of perfused vessels (Fig. 6.23 C). The microCT scan showed the MicroFil® perfused 3D vasculature growing into the scaffold (red area in Fig. 6.23 E) from the bottom and from the sides within 1 week of *in ovo* culture. While the macroscopical image of the same sample within the CAM (Fig. 6.23 D) provides only the information about the vascularization visible on the surface of the CAM, the microCT image visualizes the whole 3D vascular network. Interestingly, there seems to be one large vessel encircling the scaffold, from which new capillaries are sprouting into the scaffold (white arrows in Fig. 6.23 E). The generated microCT data could be further used for complete morphometric characterization of the vascular network, including the vessel number, vessel diameter, vessel density, vessel length, as well as the number of branching points.

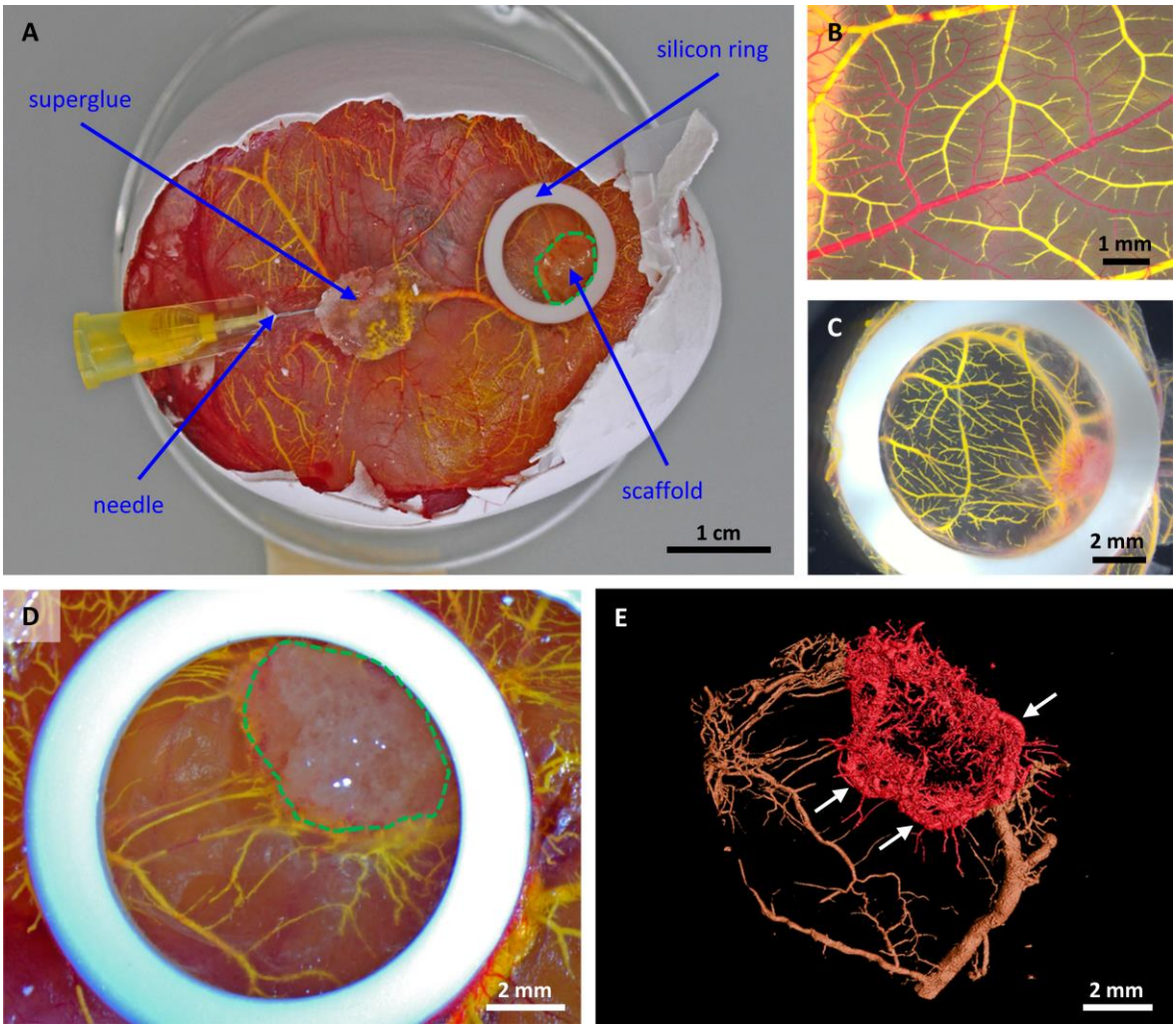

Figure 6.23. MicroFil® perfusion and microCT scan of a 3D silk scaffold incubated *in ovo* for 1 week. (A) Setup for the perfusion of the chorioallantoic membrane vasculature. The scaffold is placed in the middle of a silicone ring for *in ovo* culture. For proper perfusion a 30G ½" needle is fixed with a drop of superglue before MicroFil® (yellow) injection. (B) Perfused (yellow) and non-perfused (red) vessels after one injection showing incomplete perfusion. (C) Exemplary sample after two injections of MicroFil®. (D) Macroscopic view of an *in ovo*-cultured scaffold (green dashed line) immediately after perfusion with yellow MicroFil®. The silicone ring is seen in white, vasculature in yellow. (E) Microcomputed tomography image of the vascular cast within the scaffold marked in red. Vasculature outside the scaffold area is marked in brown. New capillaries are sprouting into the scaffold from one large vessel that encircles the scaffold (white arrows).

7. Discussion

Successful engineering of vascularized tissues and organs remains one of the key challenges in regenerative medicine (Dew et al., 2015; Mitsiadis et al., 2012; Novosel et al., 2011) even though many promising approaches have been developed and applied with the aim to improve and accelerate the vascularization of potential tissue engineered implants (Dew et al., 2015). Throughout the years, various combinations of biomaterials, cells, and growth factors have been investigated using established as well as newly developed angiogenesis assays in order to gain new insights into the processes involved in neovascularization (Laschke and Menger, 2015). Especially the use of multipotent stem cells, which can be differentiated into the desired tissue-specific cells (incl. endothelial cells), optionally with the help of transcription and growth factors, has become a core element in tissue engineering (Almubarak et al., 2016; Jin et al., 2016).

As stem cell populations are known to possess a natural differentiation potential influenced by their immediate environment, in the present study we hypothesized that human dental pulp stem cells (hDPSCs) are able to improve the vascularization of a three-dimensional (3D) silk biomaterial by attracting the host's vasculature and can contribute to the vascularization while recreating their stem cell niche within the biomaterial without any additional supplements.

7.1 Tissue integration and vascularization of 3D silk scaffolds

In order to study the effect that hDPSCs have on the tissue integration and vascularization of 3D silk scaffolds, we compared cell-seeded scaffolds with empty scaffolds after an implantation period of 1 week *in ovo*. Clear differences between empty and cell-seeded scaffolds were observed, regarding the degree of pore filling, amount of blood vessels within the scaffold, and the collagen content of the extracellular matrix (ECM). All the listed parameters showed higher values in cell-seeded than in empty scaffolds, proving that the presence of cells accelerated and improved the tissue and vascular integration of the 3D silk scaffold when used as an implant for potential tissue regeneration. This finding corresponds with previous reports, where cell-seeded synthetic or natural porous biomaterials as well as other types of silk fibroin scaffolds have been combined with undifferentiated or differentiated cells in order to functionalize the implants and induce a better integration in the host organism. For example, co-cultures of osteoblast and endothelial cells have been used to enhance the neovascularization as well as the cellular ingrowth of the host tissue of a synthetic polyester-urethane scaffold (DegraPol®) cultured *in ovo* (Buschmann et al., 2011). In another study, porous collagen scaffolds seeded with either amniotic

fluid- or dental pulp-derived stem cells improved the healing outcome when implanted into a critical-sized bone defect in rat calvariae when compared to empty collagen scaffolds (Maraldi et al., 2011). Even when silk fibroin micronets were pre-cultured with already differentiated non-endothelial cells, in this case osteoblasts, host endothelial cells were found to migrate, proliferate, and vascularize the cell-seeded biomaterial significantly better than cell-free control scaffolds (Ghanaati et al., 2011). Cells present in a manufactured biomaterial might help to 'vitalize' the scaffold structures. By secreting hypoxia-induced growth factors and cytokines, the implanted cells can trigger angiogenesis in the host's vasculature, facilitating the ingrowth of the host's tissue.

Apart from attracting vessels and enhancing tissue ingrowth from the host, the seeded cells should also proliferate, differentiate, as well as synthesize and secrete their own ECM (Geckil et al., 2011; O'Brien, 2011), creating the tissue from inside the scaffold as seen in our cell-seeded samples. This process requires a scaffold that provides the cells with the right biophysical cues (Gasiorowski et al., 2013), while allowing for good diffusion so that the cells can be properly supplied until functional vascularization can take over. In samples cultured *in vivo*, we had observed how some of the cells did not survive the first week of incubation, resulting in areas of cell death. However, in samples recovered after 4 weeks and 47 days, the appearance of the cells as well as the surrounding matrix was completely normal throughout the entire scaffold. This finding indicates that cells surviving within the scaffold during the initial days after transplantation were able to proliferate sufficiently to repopulate the entire silk scaffold, most probably supported by the advanced degree of scaffold vascularization. A previous study has shown how a higher scaffold macroporosity (i.e. 25% instead of 15%) can accelerate blood vessel development and therefore improve cell survival within the scaffold (Walthers et al., 2014).

The produced ECM within our samples was identified to contain collagen types I and III in both the *in ovo* and the *in vivo* setup after 1 week, with a strong increase observed *in vivo* after 47 days. In wound healing, fibroblasts initially produce collagen type III, which is gradually replaced by the stronger collagen type I, a process that can be detected by an increase in the ratio of collagen type I/collagen type III during scar maturation (Cheng et al., 2011). However, also mesenchymal stem cells have been shown to synthesize collagen types I and III (Ku et al., 2006; L. Zhang et al., 2008). In our previous *in vitro* study hDPSCs cultured on 3D silk scaffolds under static and dynamic conditions in either normal or osteogenic medium for 47 days have been observed to produce collagen types I and III, which was strongest in samples cultured in osteogenic medium (Woloszyk et al., 2014). Naturally, collagen type I fibrils also serve as a template for the nucleation and growth of apatite during the mineralization process of bone and tooth structures (Silver and

Landis, 2011) and therefore the presence of collagen type I is required before mineralization can be initiated. As collagen type I is the most abundant protein (up to 90%) in all types of connective tissues (Hall, 1981), the presence of collagen type I does not necessarily imply mineralization or bone formation. In the present study, spontaneous minimal mineralization was found in only one single sample. All the other scanned samples remained unmineralized within 47 days of *in vivo* implantation, even though collagen type I was present and *RUNX2* gene expression was detected in both uns-hDPSCs and s-hDPSCs. This finding could be explained by the fact that the cells seeded into the 3D silk scaffolds were not supplemented with any osteogenic or other differentiation-inducing factors at any time of the experiment. Furthermore, the subcutaneous implantation site is not mineralized either, which is why the implants did not receive any osteoinductive signals from the immediate surrounding host tissue. Other studies, where hDPSCs alone or seeded into scaffolds had been used for bone tissue engineering approaches, always included a pre-incubation of the cells in osteoinductive medium. D'Aquino et al. used an increased amount of fetal bovine serum (FBS) (20% instead of 10%) for osteogenic differentiation and cultured hDPSCs for 60 days *in vitro* to obtain 3D woven bone tissue chips. These were implanted subcutaneously into immunosuppressed rats and were shown to yield vascularized bone after 45 days of transplantation (d'Aquino et al., 2007). Similarly, hDPSCs and human amniotic fluid stem cells seeded on silk fibroin scaffolds, which were implanted into critical-sized cranial defects in immunocompromised rats for 4 weeks, had been pre-incubated in osteogenic medium and improved the healing outcome by producing mineralized tissue (Riccio et al., 2012). When no pre-differentiation of hDPSCs took place, no distinct hard tissue formation was found under *in vivo* conditions in any of the tested scaffold materials (Niu et al., 2014; Zhang et al., 2011). Even in a first clinical trial, which has been performed several years ago, autologous hDPSCs isolated from a maxillary molar had been pre-cultured in medium containing 20% FBS that had shown osteoinductive properties in earlier studies for at least 21 days. Subsequently, these cells were seeded on commercially available collagen scaffolds (i.e. Gingistat®), which were used to reconstruct alveolar bone after the extraction of mandibular teeth in the same patient (d'Aquino et al., 2009). The control site (opposite mandibular wisdom tooth) was filled with a cell-free collagen-sponge. A follow-up study after three years proved increased bone formation. However, the bone was more compact than normal spongy alveolar bone when cells had been transplanted together with the collagen scaffold than at the control site (Giuliani et al., 2013).

Taken together, the presented findings combined with what is known in the literature suggest that cell seeding is beneficial for the tissue and vascular integration of biomaterials implanted in a host organism with the goal to improve the healing of a tissue defect. Furthermore, spontaneous differentiation of mesenchymal stem cells of dental or other origin into bone tissue is limited,

especially when the site of transplantation is not mineralized. Therefore, in the case of bone tissue engineering, osteogenic differentiation would have to be induced *in vitro* before implantation takes place.

7.2 Human cell contribution to vascular structures within the 3D silk scaffold

According to our hypothesis the seeded hDPSCs should not only attract tissue and vessel ingrowth into the scaffold, but also contribute directly to the vascular structures by environment-induced differentiation into endothelial cells or pericytes. In fact, our results support this hypothesis, as hDPSCs have been observed to be embedded in the vascular basement membrane of *in ovo* cultured samples after only 1 week of incubation, where they were involved in the production of basement membrane components of functional blood-perfused vessels. The integration of human cells into the vessel wall was confirmed and even more evident in samples cultured *in vivo* for 4 weeks. These findings are in agreement with those of d'Aquino et al., where human cell-derived vessel structures within hDPSC-produced scaffold-free bone chips were observed in immunocompromised rats after 45 days (d'Aquino et al., 2007). HDPSC-derived vascularized bone tissue has also been generated when hDPSCs-seeded collagen scaffolds were implanted in critical-sized bone defects in rats for 8 weeks, where the human origin of endothelial cells within the newly formed bone tissue was proved using an anti-human mitochondrial protein (Maraldi et al., 2011). A more recent study used a combination of hDPSCs with 45S5 Bioglass scaffolds to grow vascularized tissue in a diffusion chamber that was implanted intraperitoneally in immunocompromised mice for 8 weeks (El-Gendy et al., 2015). In contrast to the previously mentioned two studies, the latter one was the first showing hDPSC-derived capillaries without pre-incubating the cells in differentiation medium prior to implantation, supporting our own findings.

The angiogenic growth factors vascular endothelial growth factor A (*VEGFA*) and transforming growth factor beta 1 (*TGFb1*) genes were found to be expressed by human cells within our cell-seeded construct after implantation. VEGF is the key mediator of angiogenesis (Ferrara, 1996) and is expressed by hDPSCs without the need of induction (Bronckaers et al., 2013). Furthermore, Bento et al. showed that the VEGF/MEK1/ERK signaling pathway is a key regulator of the endothelial differentiation of dental pulp stem cells (Bento et al., 2013; Virtej et al., 2013). TGFb1 is known to induce angiogenesis through an indirect mechanism, by recruiting inflammatory cells that secrete VEGF and/or other angiogenesis inducers (Ferrari et al., 2012). Additionally, an earlier study had found evidence for a biphasic effect of TGFb1 on *in vitro* angiogenesis, as high

concentrations of TGFb1 inhibited VEGF-induced angiogenesis, while low concentrations stimulated angiogenesis (Derringer and Linden, 2004; Pepper et al., 1993).

Collectively, the findings provide evidence that hDPSCs are able to contribute to vascular structures as endothelial cells and pericytes, resulting in functional blood-perfused mosaic structures of human- and host-derived cells. HDPSC-derived laminin and collagen type IV form the vascular basement membrane, which stabilizes neovasculature and is a sign of vascular maturation. In our study we were able to show that these processes start as early as 1 week after *in ovo* implantation of the cell-seeded silk scaffold. Interestingly, the ability of hDPSCs to contribute to vessel structures after either short (1 week) or long (8 weeks) periods of incubation seems to be material independent, as similar results have been generated in a variety of materials, including silk fibroin, collagen, and 45S5 Bioglass scaffolds or osteoinduced hDPSC-derived bone chips.

7.3 Presence of potential progenitor cell reservoirs within cell-seeded 3D silk scaffolds

Most adult tissues have been shown to harbor progenitor cells, which are responsible for functional tissue homeostasis throughout life (Watt and Driskell, 2010). Therefore, tissue-engineered constructs should not only support the healing of a defect temporarily, but should also be able to continue the natural occurring tissue homeostasis for physiological functionality. Here, stainings performed on *in ovo* and *in vivo* incubated samples indicated that part of the seeded cells kept their initial characteristics of (multi-lineage) progenitor cells of mesenchymal origin. Based on previous studies, Nestin-expression in adult tissues, including the dental pulp, has been described to be mostly restricted to areas of regeneration and to be upregulated after injury, contradicting the initial believe of Nestin being an exclusive marker for neural stem cells (About, Laurent-Maquin, et al., 2000; Lizier et al., 2012; Wiese et al., 2004). In our samples, also *Nestin* gene expression supported the positive Nestin-expression obtained by immunofluorescent stainings. Sox2-immunostainings showed a predominant cytoplasmic localization in samples retrieved after implantation *in ovo* and *in vivo*. In contrast, clear expression of Sox2 in the nuclei had been observed in both cell populations (uns-hDPSCs and s-hDPSCs) *in vitro*, indicating an initial multipotent and self-renewing phenotype (Fong et al., 2008). Sox2-expression at various passages of dental pulp cells has been previously investigated by Liu et al. (L. Liu et al., 2011). Nuclear localization of Sox2 was observed at early passages (P0-P2), while in later passages (up to P7) Sox2 was translocated to the cytoplasm, ‘implying the potential loss of pluripotency along

extended passaging' (L. Liu et al., 2011). Therefore, the Sox2 staining pattern in our samples might be indicative for a gradual loss of their differentiation potential. The mesenchymal character of the implanted cells was tracked following Vimentin-expression, which was found to be positive in cells before as well as after *in ovo* and *in vivo* implantation. These results align with previously reported Vimentin-expression patterns of hDPSCs examined at early and late passages, where also Nestin-expression was observed to be stably expressed (Lizier et al., 2012).

Considering our findings in the light of previous reports, we can conclude that potential progenitor cell reservoirs of mesenchymal origin are still present within the 3D silk scaffolds after *in ovo* and *in vivo* culture, even though these properties might be gradually decreasing in the course of differentiation.

7.4 3D imaging of the developing vasculature within stem cell-seeded scaffolds cultured in ovo

Studying the spatio-temporal aspects of the vascularization of tissue engineered constructs requires proper tools for the visualization of vessels within such implants, which is essential for predicting and understanding the outcome of new regenerative approaches before their application in clinics. In the present study, one of the aims was to combine existing tools, i.e. MicroFil® perfusion and microcomputed tomography (microCT) scanning and analysis with the chorioallantoic membrane (CAM) assay, to develop a time- and cost-efficient technique for testing and visualizing the potential effect that selected scaffolds, cells, and growth factors might have on the vascularization efficiency of an *in vitro* engineered implant.

Casting techniques have been used extensively to study the vascular architecture in health and disease, ranging from whole organisms to specific organs and organ structures. Combining the use of a radiopaque perfusion substance (i.e. MicroFil®) with modern microCT imaging and analysis has improved our knowledge on tissue anatomy, physiology, and pathology. Additionally, the perfused specimen can be used for further histological analyses, thereby reducing the amount of required samples. Therefore, it has been applied in various fields, including embryonic vascular development (Anderson-Berry et al., 2005), cancer research (Xuan et al., 2007), cardiac disease models (Sangaralingham et al., 2012), and tissue engineering (Bolland et al., 2008; Stoppato et al., 2013). For example, angiogenesis has been visualized by microCT in MicroFil®-perfused tissue engineered constructs implanted subcutaneously into immunosuppressed mice. Both natural and synthetic materials used showed an increase in the vessel number within the implants when

seeded with bone marrow stromal cells (BMSCs) (Bolland et al., 2008). More recently, the same technique was used to compare the vascularization in pure poly (D,L)-lactic acid (PDLLA) scaffolds with PDLLA combined with silk fibers. The latter was demonstrated to promote vascular ingrowth when implanted subcutaneously into rats (Stoppato et al., 2013). However, the mentioned studies were always using rodents as hosts of the implants, which require extensive animal care-taking, ethical approvals, as well as surgical skills and equipment. Moreover, usually a longer incubation period is necessary in order to analyze the angiogenic effect of engineered implants. In contrast, the CAM assay is a simple, cost-effective, and highly reproducible method, which does not require approval when performing experiments in chicken embryos until reaching the last third of their development before hatching (i.e. embryonic day 14) (Swiss animal care guidelines, TSchV, Art. 112). Even though the incubation time on the CAM is limited to a period of about 7 days, it constitutes an excellent screening method to study the early phase of the vascular integration of a 3D biomaterial by the host. Following the '3Rs' principles of replacement, refinement, and reduction of animal use in research, the CAM assay combined with MicroFil® perfusion and microCT analysis as described in this work could provide a valuable intermediate platform for initial assessments prior to pre-clinical studies in mammals. Even repeated monitoring could be possible, if an *in vivo*-applicable contrast agent (e.g. AuroVist 15 nm, ExiTron nano 12000) was administered to the chicken embryo vasculature followed by an ultra-high resolution microCT scan.

7.5 Conclusion

The presented work is the first experimental study combining hDPSCs with 3D silk scaffolds in order to investigate the early phase of tissue integration and vascularization using the CAM assay. Apart from cell-mediated vessel attraction, our study focused on the potential of hDPSCs to contribute to ingrowing vessels from the host as well as to maintain a pool of stem cells within the biomaterial. Our findings showed a higher degree of scaffold integration and vascularization in the presence of cells, which further allowed for the creation of new mosaic vessels of host and human origin inside a biomaterial that is approved for clinical use. Additionally, evidence for remaining human multipotent stem cells of mesenchymal origin was provided. The long-term fate of the cell-scaffold-constructs was observed after subcutaneous implantation in mice. The lack of mineralization in the absence of osteogenic factors during the pre-culture of the cell-seeded scaffolds proves that this process can be controlled by adjusting pre-culture conditions. No obvious difference was observed between unsorted hDPSCs and CD34+/CD90+ sorted hDPSCs.

Further optimization of the 3D vessel imaging technique of *in ovo* cultivated samples would result in a valuable analytical tool with the power to reduce animal use in research.

In conclusion, autologous multipotent stem cells isolated from human dental pulp are easily accessible and have the potential to support the tissue integration and vascularization of future implants for clinical treatment of tissue defects after injury or disease.

8. Acknowledgments

First of all, I want to thank my supervisor and mentor Prof. Thimios Mitsiadis for his guidance, support, and encouragement throughout this challenging project. His comments and suggestions have always been of great help during my research and the relaxed and open-minded atmosphere he created in the lab provided a productive work environment. Working in the small but very international group of the Institute of Oral Biology has been a great experience and has taught me many important scientific as well as non-scientific lessons.

I am grateful to the members of my PhD committee, Prof. Michael Hengartner, Prof. Ralph Müller, Prof. Christian von Mering, Prof. Sabine Werner, and Dr. Nagihan Bostanci, who accompanied this project during the annual committee meetings. Your input and questions, as well as the resulting discussions were indispensable and an important point of reference.

This project could not have been accomplished without our collaborators. Therefore, I thank Prof. Gianpaolo Papaccio and his entire team at the Second University of Naples, who taught me in the beginning how to isolate and culture human dental pulp stem cells during my short term scientific mission in Naples, Italy. For providing teeth I would like to thank PD Dr. Dr. Bernd Stadlinger and of the Clinic for Dental Medicine. I especially want to thank Dr. Johanna Buschmann from the University Hospital Zurich, who taught me everything about the CAM assay and provided her lab and materials for the first sets of experiments. Furthermore, I wish to thank Prof. Ralph Müller, Prof. Sandra Hofmann, and Dr. Jolanda Baumgartner from the Institute of Biomechanics (ETH) for the production of the silk scaffolds used in this project and for performing important microCT scans. The Trudel Silk Inc. (Zurich, CH) is highly acknowledged for providing silk cocoons. For performing the surgeries for the *in vivo* part of my project I wish to thank Dr. Lucia Jiménez-Rojo.

I want to thank my PhD colleagues, Dr. Anna Filatova, Dr. Zoraide Granchi, Despoina Natsiou, and Dr. Pierfrancesco Pagella, who were far more than only colleagues to me. I am glad they were with me on this interesting journey.

For administrative help I would like to thank Angela Di Pietro and Christine Lämmler, as well as Dr. Susanna Bachmann, Coordinator of the PhD Program in Molecular Life Sciences. For the most precious troubleshooting in any kind of situation Martin Gander deserves a special Thank You!

In particular, I would like to thank Dr. Vaida Glatt for believing in me and for supporting me from afar.

Most of all I would like to thank my family, especially my parents and sister, for their constant love, care, and support during this thesis and on my way to it.

9. List of Abbreviations

3D	three-dimensional
AEC	3-amino-9-ethylcarbazole
APC-Cy7	alophycocyanin: Cy-7 tandem conjugate
BCIP	5-bromo-4-chloro-3-indolyl phosphate
bFGF	basic fibroblast growth factor
BMP2	bone morphogenetic protein 2
BMSC(s)	bone marrow stem cell(s)
CAM	chorioallantoic membrane
CD	cluster of differentiation
cDNA	complementary deoxyribonucleic acid
CO2	carbon dioxide
conc.	concentration
DAPI	4',6-diamidino-2-phenylindole
DFSC(s)	dental follicle stem cell(s)
dH2O	distilled water
DiI	1,1' dioctadecyl-3,3,3',3'-tetramethylindocarbocyanine perchlorate
DMEM	Dulbecco's Modified Eagle's medium
DMEM/F12	Dulbecco's Modified Eagle's medium/nutrient mixture F-12
DNA	deoxyribonucleic acid
DPSC(s)	dental pulp stem cell(s)
ECM	extracellular matrix
ECs	endothelial cells
ED	embryonic day
EPCs	endothelial progenitor cells
FBS	fetal bovine serum
FITC	fluorescein isothiocyanate conjugate
hDPSC(s)	human dental pulp stem cell(s)
H&E	Hematoxylin and Eosin
HLA-DR	human leukocyte antigen - D related
ICM	inner cell mass

iPS cells	induced pluripotent stem cells
LDH	lactate dehydrogenase
MSC(s)	mesenchymal stem cell(s)
MTT	3-(4,5-dimethylthiazol-2-yl)-2,5-diphenyltetrazolium bromide
n	sample number
NBT	nitro blue tetrazolium chloride
NuMA	nuclear mitotic apparatus protein 1
ON	overnight
P	cell passage
PBS	phosphate buffered saline
PE	phycoerythrin
PerCP-Cy5.5	peridinin-chlorophyll-protein complex: CY5.5 conjugate
PDLSC(s)	periodontal ligament stem cell(s)
PFA	paraformaldehyde
PGA	polyglycolic acid
PLGA	poly-lactic-co-glycolic acid
PLLA	poly-L-lactic acid
P/S	penicillin/streptomycin
qRT-PCR	quantitative real-time polymerase chain reaction
RNA	ribonucleic acid
RT	room temperature
RUNX2	runt-related transcription factor 2
s-hDPSC(s)	CD34+/CD90+ sorted human dental pulp stem cell(s)
SCAP(s)	stem cell(s) from the apical papilla
sc	silk scaffold fibers
SCs	stem cells
SD	standard deviation
SHEDs	stem cell(s) from human exfoliated deciduous teeth
Sox2	SRY (sex determining region Y)-box 2
TGFb1	transforming growth factor beta 1
uns-hDPSC(s)	unsorted human dental pulp stem cell(s)

VEGF	vascular endothelial growth factor
VEGFA	vascular endothelial growth factor A
vSMC(s)	vascular smooth muscle cell(s)
vWF	von Willebrand Factor

10. List of Figures

Figure 3.1. Stem cells classified by their potency 11

Figure 3.2. Composition of the stem cell niche 14

Figure 3.3. Schematic representation of the anatomy of a human tooth 16

Figure 3.4. Sources of adult dental mesenchymal stem cells in the oral cavity 20

Figure 3.5. Development of the vascular system 22

Figure 3.6. Vascularization strategies for tissue engineering 24

Figure 3.7. Chorioallantoic membrane assay 27

Figure 5.1. Scheme of the experimental setup 35

Figure 6.1. Two colony forming units of primary hDPSCs three days after cell isolation from the dental pulp 40

Figure 6.2. Proliferation behavior of freshly isolated hDPSCs 41

Figure 6.3. Cell proliferation and cytotoxicity of hDPSCs 41

Figure 6.4. Cytofluorimetric analysis of CD90, CD105, CD34, and CD45 expression on unsorted hDPSCs 42

Figure 6.5. Fluorescence-activated cell sorting (FACS) plots for the sorting of hDPSCs 43

Figure 6.6. Immunocytochemistry showing Nestin, Sox2, and Vimentin expression 44

Figure 6.7. Trilineage differentiation potential of uns-hDPSCs and s-hDPSCs 46

Figure 6.8. Silk scaffold biomaterial and its properties 47

Figure 6.9. In vitro growth of cells seeded in 3D silk scaffolds 47

Figure 6.10. H&E staining of longitudinal sections after in ovo culture for 1 week 49

Figure 6.11. Histomorphometrical analysis of cell-seeded samples grown in ovo for 1 week 50

Figure 6.12. Collagen types I and III content in samples cultured in ovo for 1 week 51

Figure 6.13. Immunohistochemistry showing laminin and collagen type IV expression in the basement membrane of capillaries within the scaffold material after in ovo implantation for 1 week 52

Figure 6.14. Immunofluorescence of stem cell markers and a mesenchymal cell marker of samples cultured in ovo 53

Figure 6.15. Gene expression analysis of cell-seeded samples grown in ovo for 1 week 54

Figure 6.16. H&E staining of longitudinal cross-sections cultured in vivo 57

Figure 6.17. Histomorphometric analysis of cell-seeded samples grown in vivo for 1 week and for 47 days 58

Figure 6.18. Collagen type I and III content in samples cultured in vivo for 1 week and 47 days ... 59

Figure 6.19. Immunohistochemistry showing laminin, collagen type IV, and vWF expression in the basement membrane of capillaries within the scaffold material after in vivo implantation for 4 weeks 60

Figure 6.20. Immunofluorescence of stem cell markers and a mesenchymal cell marker of samples cultured in vivo 61

Figure 6.21. Preliminary gene expression analysis of cell-seeded samples grown in vivo for 4 weeks 62

Figure 6.22. MicroCT analysis of samples cultured in vivo for 47 days 63

Figure 6.23. MicroFil® perfusion and microCT scan of a 3D silk scaffold incubated in ovo for 1 week 65

11. List of Tables

Table 5.1. Antibodies used for immunohistochemistry.....38

Table 5.2. Antibodies used for immunofluorescence.....38

Table 5.3. Human-specific primer sequences used for gene expression analyses.....39

12. Curriculum Vitae

PERSONAL INFORMATION

Name:	Anna Maria Woloszyk
Date of Birth:	18 April 1985
Place of Birth:	Budapest, Hungary
Nationality:	German, Polish
Address:	Pflugstrasse 4, 8006 Zürich (ZH), Switzerland
Phone	+41 (0)76 7400248 (mobile phone) +41 (0)44 6345753 (office)
E-Mail:	anna.wolo@gmail.com (private) anna.woloszyk@uzh.ch (University of Zurich)

EDUCATION

05/2012 -Present	PhD candidate at the Molecular Life Science Graduate School, ETH/University of Zurich, Zurich, Switzerland
04/2011	Master of Science (Diplom-Ingenieur) in Biotechnology, Technische Universität Berlin, Berlin, Germany
10/2008	Bachelor of Science (Vordiplom) in Biotechnology, Technische Universität Berlin, Berlin, Germany

WORK EXPERIENCE AND TRAINING

05/2012 – Present	Institute of Oral Biology, Department of Orofacial Development & Regeneration, Center of Dental Medicine, University of Zurich, Zurich, Switzerland (Supervisor: Prof. Dr. Thimios Mitsiadis) PHD CANDIDATE *Project title: The angiogenic potential of human dental pulp stem cells cultured on 3D silk scaffolds.*
04/2011 – 04/2012	Julius Wolff Institute, Charité - Universitätsmedizin Berlin, Berlin-Brandenburg Center for Regenerative Therapies, Berlin, Germany *RESEARCH ASSISTANT* *Topic: Cellular Biomechanics*

01/2010 – 03/2011	Julius Wolff Institute, Charité - Universitätsmedizin Berlin, Berlin-Brandenburg Center for Regenerative Therapies, Berlin, Germany *MASTER STUDENT/RESEARCH ASSISTANT* *Master thesis title: The influence of the biophysical environment on the migration behavior of human mesenchymal stem cells.*
07/2009 – 12/2009	Julius Wolff Institut, Charité - Universitätsmedizin Berlin, Berlin-Brandenburg Center for Regenerative Therapies, Berlin, Germany *TECHNICAL ASSISTANT* *Topic: Longitudinal 4D monitoring of bone defect healing in rat femora*
12/2008 – 03/2009	Robert Koch-Institute, Centre for Biological Safety in Berlin, Germany *INTERNSHIP* *Topic: Establishment of a Western blot for the detection of specific proteins of the Ljungan virus*
02/2008 – 04/2008	Co.don AG in Teltow, Germany *INTERNSHIP* *Topic: Tissue engineering of cartilage*
04/2006 – 04/2008	JPT Peptide Technologies GmbH in Berlin, Germany *TECHNICAL ASSISTANT* *Topic: Peptide-based Services*
08/2007 – 12/2007	Technische Universität Berlin, Department of Environmental Technology, Berlin, Germany *STUDENT RESEARCH PROJECT* *Project title: Studies on the conjugative plasmid transfer mechanisms in gram-positive bacteria - Localization of a protein component in the cellular membrane.*

LABORATORY EXPERTISE

▪ cell culture	(stem) cell isolation and maintenance, 3D cell culture under static conditions and in bioreactors, cell preservation, flow cytometry, FACS
▪ animal models	chorioallantoic membrane (CAM) assay
▪ molecular biology	PCR, Real-time PCR, Western blot

▪ histology	fixation, embedding, and sectioning of paraffin-embedded and frozen samples, classical stainings, immunocytochemistry, immunohistochemistry, immunofluorescent stainings
▪ imaging	widefield and confocal light microscopy, microCT

TEACHING ACTIVITIES

07/2014 – Present	Supervision of four master students of Dental Medicine, University of Zurich, Zurich, Switzerland
2014/2015	Supervision of Short Term Scientific Missions (up to 3 months) of seven scientists from European Universities or Research Institutes funded by the European Cooperation in Science and Technology (COST)
02/2013 – 05/2013	Teaching assistant of the practical course in Organic Chemistry for bachelor students in Biology, University of Zurich, Zurich, Switzerland (135 teaching hours)

SKILLS AND COMPETENCES

Foreign Languages	German	Mother Tongue
	Polish	Mother Tongue
	English	Excellent Knowledge
	French	Basic Knowledge
Computer Skills	MS-Office	Excellent Knowledge
	LaTeX	Basic Knowledge
	Photoshop	Advanced Knowledge
	Image J	Advanced Knowledge
	GraphPad	Good Knowledge
	SPSS	Basic Knowledge

SCHOLARSHIPS AND GRANTS

04/2013	Training School of the European Cooperation in Science and Technology (COST) in Ancona, Italy
10/2012-11/2012	Short Term Scientific Mission granted by the European Cooperation in Science and Technology (COST) at the Department of Experimental Medicine, Section of Histology and Embryology, Second University of Naples, Naples, Italy

EDITORIAL RESPONSIBILITIES

11/2014 – Present	Reviewer for the *International Journal of Molecular Sciences*

MEMBERSHIPS

05/2014 – Present	European Orthopaedic Research Society
04/2009 – 03/2011	Member of the extended Academic Senate at Technische Universität Berlin, Berlin, Germany

PUBLICATIONS

Woloszyk A, Buschmann J, Waschkies C, Stadlinger B, Mitsiadis TA (2016). Human dental pulp stem cells and gingival fibroblasts seeded into silk fibroin scaffolds have the same ability in attracting vessels. Front Physiol. (accepted)

Woloszyk A, Liccardo D, Mitsiadis TA (2016). Three-dimensional imaging of the developing vasculature within stem cell-seeded scaffolds cultured in ovo. Front Physiol. (accepted)

Petersen A, Princ A, Ellinghaus A, Woloszyk A, Korus G, Leemhuis H, Schmidt-Bleek K, Heschel I, Duda GN (2016). Mimicking the growth plate extracellular matrix structure enables endochondral bone growth in a critical size defect. Nat Mater. (under revision)

Mitsiadis TA, Woloszyk A (2015). Odyssey of human dental pulp stem cells and their remarkable ability to survive in extremely adverse conditions. Front Physiol. 2015 Mar 26;6:99.

Kivrak Pfiffner F, Waschkies C, Tian Y, Woloszyk A, Calcagni M, Giovanoli P, Rudin M, Buschmann J (2014). A new in vivo MRI method to non-invasively monitor and quantify the perfusion capacity of 3D-biomaterials grown on the chorioallantoic membrane of chick embryos. Tissue Eng Part C Methods. 2015 Apr;21(4):339-46.

Woloszyk A, Holsten Dircksen S, Bostanci N, Müller R, Hofmann S, Mitsiadis TA (2014). Influence of mechanical environment on the engineering of mineralized tissues using human dental pulp stem cells and silk fibroin scaffolds. PLoS One. 2014 Oct 29;9(10):e111010.

Jimenez-Rojo L, Granchi Z, Woloszyk A, Filatova A, Pagella P, Mitsiadis TA. Regenerative dentistry: stem cells meet nanotechnology. (In book: Horizons in Clinical Nanomedicine. Editors: Pan Stanford Publishing. Edition: 1st edition, 2014)

Mitsiadis TA, Woloszyk A, Jiménez-Rojo L (2012). Nanodentistry: combining nanostructured materials and stem cells for dental tissue regeneration. Nanomedicine (Lond). 2012 Nov;7(11):1743-53.

Schiraldi C, Stellavato A, D'Agostino A, Tirino V, d'Aquino R, Woloszyk A, De Rosa A, Laino L, Papaccio G and Mitsiadis TA (2012). Fighting for Territories: Time-lapse Analysis of Dental Pulp and Dental Follicle Stem Cells in Co-Culture Reveals Specific Migratory Capabilities. Eur Cell Mater. Vol. 24 (pages 426-440).

CONFERENCE PROCEEDINGS

Woloszyk A, Mitsiadis TA, Angiogenic potential of human dental pulp stem cells. Conference of the Italian Society for Biomaterials, Ancona, Italy, June 2015. *(Oral presentation by T.A.M.)*

Woloszyk A, Buschmann J, Mitsiadis TA, From teeth to vessels: The angiogenic potential of dental pulp stem cells. 11th International Conference on Nanosciences & Nanotechnologies, Thessaloniki, Greece, July 2014. *(Oral presentation)*

Pagella P, Neto E, Woloszyk A, Lamghari M, Mitsiadis TA, A microfluidic co-culture system for the study of orofacial innervation. 11th International Conference on Nanosciences & Nanotechnologies, Thessaloniki, Greece, July 2014. *(Poster presentation)*

Woloszyk A, Buschmann J, Mitsiadis TA, The Angiogenic Potential of Dental Pulp Stem Cells: in ovo studies. 13th Day of Clinical Research, Zurich, Switzerland, June 2014. *(Oral presentation)*

Woloszyk A, Buschmann J, Mitsiadis TA, Angiogenic properties of human dental pulp stem cells: in ovo studies. 10th annual meeting of the Swiss Stem Cell Network, Geneva, Switzerland, June 2014. *(Poster presentation)*

Pagella P, Woloszyk A, Neto E, Lamghari M, Mitsiadis TA, Interactions between trigeminal sensory innervation and mesenchymal stem cells of different origins. 10th annual meeting of the Swiss Stem Cell Network, Geneva, Switzerland, June 2014. *(Poster presentation)*

Woloszyk A, Bostanci N, Holsten Dircksen S, Papaccio G, Hofmann S, Müller R, Mitsiadis TA, The potential of dental pulp stem cells in regenerative medicine. TERMIS-EU, Istanbul, Turkey, June 2013. *(Poster presentation)*

Woloszyk A, Bostanci N, Holsten Dircksen S, Papaccio G, Hofmann S, Müller R, Mitsiadis TA, The potential of dental pulp stem cells in regenerative medicine. 11th International Conference on Tooth Morphogenesis and Differentiation, La Londe les Maures, France, May 2013. *(Poster presentation)*

Pagella P, Woloszyk A, Neto E, Lamghari M, Mitsiadis TA, Cross talk between sensory innervation and mesenchymal stem cells for orofacial regeneration in a microfluidics co-culture system. 12th Day of Clinical Research, Zurich, Switzerland, April 2013. *(Poster presentation)*

Petersen A, Woloszyk A, Ellinghaus A, Duda GN (2012). The potential of highly orientated scaffold pore architecture for bone tissue regeneration, TERMIS World Congress, Vienna, Austria, September 2012.

Woloszyk A, Petersen A, Duda GN, Migration of human mesenchymal stem cells is influenced by Wnt3a and mechanical stimulation, TERMIS-EU, Granada, Spain, June 2011. *(Oral presentation)*

Mehta M, Heyland M, Woloszyk A, Peters A, Lienau J, Fratzl P, Duda GN, Longitudinal monitoring of bone defect healing in rat femora (4D monitoring), Orthopedic Research Society, New Orleans, Louisiana, March 2010. *(Poster presentation)*

13. References

Abe, S., Yamaguchi, S., and Amagasa, T. (2007). Multilineage Cells from Apical Pulp of Human Tooth with Immature Apex. *Oral Science International*, *4*(1), 45–58.

About, I., Bottero, M.-J., de Denato, P., Camps, J., Franquin, J.-C., and Mitsiadis, T. A. (2000). Human dentin production in vitro. *Experimental Cell Research*, *258*, 33–41.

About, I., Laurent-Maquin, D., Lendahl, U., and Mitsiadis, T. A. (2000). Nestin Expression in Embryonic and Adult Human Teeth under Normal and Pathological Conditions. *The American Journal of Pathology*, *157*(1), 287–295.

Adams, R. H., and Alitalo, K. (2007). Molecular regulation of angiogenesis and lymphangiogenesis. *Nature Reviews Molecular Cell Biology*, *8*, 464–478.

Alge, D. L., Zhou, D., Adams, L. L., Wyss, B. K., Shadday, M. D., Woods, E. J., Chu, T. M. G., and Goebel, W. S. (2010). Donor-matched comparison of dental pulp stem cells and bone marrow-derived mesenchymal stem cells in a rat model. *Journal of Tissue Engineering and Regenerative Medicine*, *4*(1), 73–81.

Allt, G., and Lawrenson, J. G. (2001). Pericytes : Cell Biology and Pathology. *Cells Tissues Organs*, *169*, 1–11.

Almubarak, S., Nethercott, H., Freeberg, M., Beaudon, C., Jha, A., Jackson, W., Marcucio, R., Miclau, T., Healy, K., and Bahney, C. (2016). Tissue engineering strategies for promoting vascularized bone regeneration. *Bone*, *83*, 197–209.

Altman, G. H., Diaz, F., Jakuba, C., Calabro, T., Horan, R. L., Chen, J., Lu, H., Richmond, J., and Kaplan, D. L. (2003). Silk-based biomaterials. *Biomaterials*, *24*, 401–416.

Alvarez, O. M., Fahey, C. B., Auletta, M. J., and Fernández-Obregón, A. (1998). A novel treatment for venous leg ulcers. *Journal of Foot and Ankle Surgery*, *37*(4), 319–324.

Anderson-Berry, A., Brien, E. A. O., Bleyl, S. B., Lawson, A., Gundersen, N., Ryssman, D., Sweeley, J., Dahl, M. J., Drake, C. J., Schoenwolf, G. C., and Albertine, K. H. (2005). Vasculogenesis Drives Pulmonary Vascular Growth in the Developing Chick Embryo. *Developmental Dynamics*, *233*, 145–153.

Armulik, A., Abramsson, A., and Betsholtz, C. (2005). Endothelial/Pericyte Interactions. *Circulation Research*, *97*(6), 512–523.

Asahara, T. (1997). Isolation of Putative Progenitor Endothelial Cells for Angiogenesis. *Science*, *275*, 964–966.

Asahara, T., and Kawamoto, A. (2004). Endothelial progenitor cells for postnatal vasculogenesis. *American Journal of Physiology - Cell Physiology*, *287*, C572–C579.

Asahara, T., Kawamoto, A., and Masuda, H. (2011). Concise Review: Circulating Endothelial Progenitor Cells for Vascular Medicine. *Stem Cells*, *29*, 1650–1655.

Atala, A., Bauer, S. B., Soker, S., Yoo, J. J., and Retik, A. B. (2006). Tissue-engineered autologous bladders for patients needing cystoplasty. *The Lancet*, *367*, 1241–1246.

Bento, L. W., Zhang, Z., Imai, A., Nör, F., Dong, Z., Shi, S., Araujo, F. B., and Nör, J. E. (2013). Endothelial Differentiation of SHED Requires MEK1/ERK Signaling. *Journal of Dental Research*, *92*(1), 51–7.

Berthiaume, F., Maguire, T. J., and Yarmush, M. L. (2011). Tissue engineering and regenerative medicine: history, progress, and challenges. *Annual Review of Chemical and Biomolecular Engineering*, *2*, 403–30.

Bianco, P., Riminucci, M., Gronthos, S., and Gehron Robey, P. (2001). Bone Marrow Stromal Stem Cells: Nature, Biology, and Potential Applications. *Stem Cells*, *19*, 180–192.

Bolland, B. J. R. F., Kanczler, J. M., Dunlop, D. G., and Oreffo, R. O. C. (2008). Development of in vivo μCT evaluation of neovascularisation in tissue engineered bone constructs. *Biomaterials*, *43*, 195–202.

Brignier, A. C., and Gewirtz, A. M. (2010). Embryonic and adult stem cell therapy. *Journal of Allergy and Clinical Immunology*, *125*, S336–44.

Bronckaers, A., Hilkens, P., Fanton, Y., Struys, T., Gervois, P., Politis, C., Martens, W., and Lambrichts, I. (2013). Angiogenic Properties of Human Dental Pulp Stem Cells. *PloS One*, *8*(8), e71104.

Burke, Z. D., Thowfeequ, S., Peran, M., and Tosh, D. (2007). Stem cells in the adult pancreas and liver. *The Biochemical Journal*, *404*, 169–178.

Buschmann, J., Welti, M., Hemmi, S., Neuenschwander, P., Baltes, C., Giovanoli, P., Rudin, M., and Calcagni, M. (2011). Three-Dimensional Co-Cultures of Osteoblasts and Endothelial Cells in DegraPol Foam: Histological and High-Field Magnetic Resonance Imaging Analyses of Pre-Engineered Capillary Networks in Bone Grafts. *Tissue Engineering. Part A*, *17*(3-4), 291–299.

Cao, Y., Vacanti, J. P., Paige, K. T., Upton, J., and Vacanti, C. A. (1997). Transplantation of Chondrocytes Utilizing a Polymer-Cell Construct to Produce Tissue-Engineered Cartilage in the Shape of a Human Ear. *Plastic &amp Reconstructive Surgery*, *100*(2), 297–302.

Caplan, A. I. (1991). Mesenchymal Stem Cells. *Journal of Orthopaedic Research*, *9*(5), 641–50.

Carmeliet, P., and Jain, R. K. (2000). Angiogenesis in cancer and other diseases. *Nature*, *407*, 249–257.

Carmeliet, P., and Jain, R. K. (2011). Molecular mechanisms and clinical applications of angiogenesis. *Nature*, *473*, 298–307.

Chagastelles, P. C., and Nardi, N. B. (2011). Biology of stem cells: an overview. *Kidney International Supplements*, *1*(3), 63–67.

Chan, B. P., and Leong, K. W. (2008). Scaffolding in tissue engineering: general approaches and tissue-specific considerations. *European Spine Journal*, *17*(4), S467–479.

Chang, D.-J., Oh, S.-H., Lee, N., Choi, C., Jeon, I., Kim, H. S., Shin, D. A., Lee, S. E., Kim, D., and Song, J. (2013). Contralaterally transplanted human embryonic stem cell-derived neural precursor cells (ENStem-A) migrate and improve brain functions in stroke-damaged rats. *Experimental & Molecular Medicine*, *45*(11), e53.

Chen, T. S. N., and Chen, P. S. Y. (1994). The myth of prometheus and the liver. *Journal of the Royal Society of Medicine*.

Cheng, W., Yan-hua, R., Fang-gang, N., and Guo-an, Z. (2011). The content and ratio of type I and III collagen in skin differ with age and injury. *African Journal of Biotechnology*, *10*(13), 2524–2529.

Cordeiro, M. M., Dong, Z., Kaneko, T., Zhang, Z., Miyazawa, M., Shi, S., Smith, A. J., and Nör, J. E. (2008). Dental Pulp Tissue Engineering with Stem Cells from Exfoliated Deciduous Teeth. *Journal of Endodontics*, *34*(8), 962–9.

Costa-Almeida, R., Granja, P. L., Soares, R., and Guerreiro, S. G. (2014). Cellular strategies to promote vascularisation in tissue engineering applications. *European Cells and Materials*, *28*, 51–67.

d'Aquino, R., De Rosa, A., Lanza, V., Tirino, V., Laino, L., Graziano, A., Desiderio, V., Laino, G., and Papaccio, G. (2009). Human mandible bone defect repair by the grafting of dental pulp stem/progenitor cells and collagen sponge biocomplexes. *European Cells and Materials*, *18*, 75–83.

d'Aquino, R., Graziano, A., Sampaolesi, M., Laino, G., Pirozzi, G., De Rosa, A., and Papaccio, G. (2007). Human postnatal dental pulp cells co-differentiate into osteoblasts and endotheliocytes: a pivotal synergy leading to adult bone tissue formation. *Cell Death and Differentiation*, *14*(6), 1162–71.

De Berdt, P., Vanacker, J., Ucakar, B., Elens, L., Diogenes, A., Leprince, J. G., Deumens, R., and des Rieux, A. (2015). Dental Apical Papilla as Therapy for Spinal Cord Injury. *Journal of Dental Research*, *94*(11), 1575–1581.

Derringer, K. A., and Linden, R. W. A. (2004). Vascular endothelial growth factor, fibroblast growth factor 2, platelet derived growth factor and transforming growth factor beta released in human dental pulp following orthodontic force. *Archives of Oral Biology*, *49*, 631–641.

Dew, L., MacNeil, S., and Chong, C. K. (2015). Vascularization strategies for tissue engineers. *Regenerative Medicine*, *10*(2), 211–24.

Dominici, M., Le Blanc, K., Mueller, I., Slaper-Cortenbach, I., Marini, F., Krause, D., Deans, R., Keating, A., Prockop, D. J., and Horwitz, E. (2006). Minimal criteria for defining multipotent mesenchymal stromal cells. The International Society for Cellular Therapy position statement. *Cytotherapy*, *8*(4), 315–317.

Eckfeldt, C. E., Mendenhall, E. M., and Verfaillie, C. M. (2005). The molecular repertoire of the "almighty" stem cell. *Nature Reviews Molecular Cell Biology*, *6*(9), 726–737.

Egusa, H., Sonoyama, W., Nishimura, M., Atsuta, I., and Akiyama, K. (2012). Stem cells in dentistry-Part I: Stem cell sources. *Journal of Prosthodontic Research*, *56*(3), 151–65.

Ehrbar, M., Djonov, V. G., Schnell, C., Tschanz, S. A., Martiny-Baron, G., Schenk, U., Wood, J., Burri, P. H., Hubbell, J. A., and Zisch, A. H. (2004). Cell-Demanded Liberation of VEGF121 from Fibrin Implants Induces Local and Controlled Blood Vessel Growth. *Circulation Research*, *94*(8), 1124–1132.

El-Gendy, R., Kirkham, J., Newby, P. J., Mohanram, Y., Boccaccini, A. R., and Yang, X. B. (2015). Investigating the Vascularization of Tissue-Engineered Bone Constructs Using Dental Pulp Cells and 45S5 Bioglass® Scaffolds. *Tissue Engineering. Part A*, *21*(13-14), 2034–43.

Evans, M. J., and Kaufman, M. H. (1981). Establishment in culture of pluripotential cells from mouse embryos. *Nature*, *292*(5819), 154–156.

Ferrara, N. (1996). Vascular Endothelial Growth Factor. *European Journal of Cancer*, *32A*(14), 2413–2422.

Ferrari, G., Terushkin, V., Wolff, M. J., Zhang, X., Valacca, C., Poggio, P., Pintucci, G., and Mignatti, P. (2012). TGF-b1 Induces Endothelial Cell Apoptosis by Shifting VEGF Activation of p38MAPK from the Prosurvival p38b to Proapoptotic p38a. *Molecular Cancer Research*, *10*(5), 605–614.

Fong, H., Hohenstein, K. A., and Donovan, P. J. (2008). Regulation of Self-Renewal and Pluripotency by Sox2 in Human Embryonic Stem Cells. *Stem Cells*, *26*(8), 1931–8.

Friedenstein, A. J., Piatetzky-Shapiro, I. I., and Petrakova, K. V. (1966). Osteogenesis in transplants of bone marrow cells. *Journal of Embryology and Experimental Morphology*, *16*(3), 381–90.

Fulco, I., Miot, S., Haug, M. D., Barbero, A., Wixmerten, A., Feliciano, S., Wolf, F., Jundt, G., Marsano, A., Farhadi, J., Heberer, M., Jakob, M., Schaefer, D. J., and Martin, I. (2014). Engineered autologous cartilage tissue for nasal reconstruction after tumour resection: an observational first-in-human trial. *The Lancet*, *384*, 337–346.

Gaengel, K., Genové, G., Armulik, A., and Betsholtz, C. (2009). Endothelial-Mural Cell Signaling in Vascular Development and Angiogenesis. *Arteriosclerosis, Thrombosis, and Vascular Biology*, *29*(5), 630–638.

Gasiorowski, J. Z., Murphy, C. J., and Nealey, P. F. (2013). Biophysical cues and cell behavior: the big impact of little things. *Annual Review of Biomedical Engineering*, *15*, 155–76.

Geckil, H., Xu, F., Zhang, X., Moon, S., and Demirci, U. (2011). Engineering hydrogels as extracellular matrix mimics. *Nanomedicine*, *5*(3), 469–484.

Ghanaati, S., Unger, R. E., Webber, M. J., Barbeck, M., Orth, C., Kirkpatrick, J. A., Booms, P., Motta, A., Migliaresi, C., Sader, R. A., and Kirkpatrick, C. J. (2011). Scaffold vascularization in vivo driven by primary human osteoblasts in concert with host inflammatory cells. *Biomaterials*, *32*, 8150–60.

Gilbert, P. M., Havenstrite, K. L., Magnusson, K. E. G., Sacco, A., Leonardi, N. A., Kraft, P., Nguyen, N. K., Thrun, S., Lutolf, M. P., and Blau, H. M. (2010). Substrate Elasticity Regulates Skeletal Muscle Stem Cell Self-Renewal in Culture. *Science*, *329*, 1078–81.

Giuliani, A., Manescu, A., Langer, M., Rustichelli, F., Desiderio, V., Paino, F., De Rosa, A., Laino, L., D'Aquino, R., Tirino, V., and Papaccio, G. (2013). Three Years After Transplants in Human Mandibles, Histological and In-Line Holotomography Revealed That Stem Cells Regenerated a Compact Rather Than a Spongy Bone: Biological and Clinical Implications. *Stem Cells Translational Medicine*, *2*, 316–24.

Graziano, A., d'Aquino, R., Laino, G., and Papaccio, G. (2008). Dental Pulp Stem Cells: A Promising Tool for Bone Regeneration. *Stem Cell Reviews*, *4*(1), 21–6.

Gronthos, S., Brahim, J., Li, W., Fisher, L. W., Cherman, N., Boyde, A., DenBesten, P., Gehron Robey, P., and Shi, S. (2002). Stem Cell Properties of Human Dental Pulp Stem Cells. *Journal of Dental Research*, *81*(8), 531–535.

Gronthos, S., Mankani, M., Brahim, J., Gehron Robey, P., and Shi, S. (2000). Postnatal human dental pulp stem cells (DPSCs) in vitro and in vivo. *Proceedings of the National Academy of Sciences*, *97*(25), 13625–30.

Haegebarth, A., and Clevers, H. (2009). Wnt Signaling, Lgr5, and Stem Cells in the Intestine and Skin. *The American Journal of Pathology*, *174*(3), 715–721.

Hall, D. A. (1981). Gerontology: Collagen disease. *Clinics in Endocrinology and Metabolism*, *10*(1), 23–55.

Hamrahi, V. F., Goverman, J., Jung, W., Wu, J. C., Fischman, A. J., Tompkins, R. G., Yu, Y. Y., Fagan, S. P., and Carter, E. A. (2012). In Vivo Molecular Imaging of Murine Embryonic Stem Cells Delivered to a Burn Wound Surface via Integra® Scaffolding. *Journal of Burn Care & Research*, *33*(2), e49–e54.

Heo, J. S., Choi, S.-M., Kim, H. O., Kim, E. H., You, J., Park, T., Kim, E., and Kim, H.-S. (2013). Neural transdifferentiation of human bone marrow mesenchymal stem cells on hydrophobic polymer-modified surface and therapeutic effects in an animal model of ischemic stroke.

Neuroscience, *238*, 305–18.

Hewett, P. W. (2009). Vascular Endothelial Cells from Human Micro- and Macrovessels: Isolation, Characterisation and Culture. In S. Martin & C. Murray (Eds.), *Methods in Molecular Biology, Angiogenesis Protocols* (2nd ed., Vol. 467, pp. 95–111). Humana Press.

Hilkens, P., Fanton, Y., Martens, W., Gervois, P., Struys, T., Politis, C., Lambrichts, I., and Bronckaers, A. (2014). Pro-angiogenic impact of dental stem cells in vitro and in vivo. *Stem Cell Research*, *12*(3), 778–90.

Hofmann, S., Hagenmüller, H., Koch, A. M., Müller, R., Vunjak-Novakovic, G., Kaplan, D. L., Merkle, H. P., and Meinel, L. (2007). Control of in vitro tissue-engineered bone-like structures using human mesenchymal stem cells and porous silk scaffolds. *Biomaterials*, *28*(6), 1152–1162.

Hombach-Klonisch, S., Panigrahi, S., Rashedi, I., Seifert, A., Alberti, E., Pocar, P., Kurpisz, M., Schulze-Osthoff, K., Mackiewicz, A., and Los, M. (2008). Adult stem cells and their trans-differentiation potential-perspectives and therapeutic applications. *Journal of Molecular Medicine*, *86*(12), 1301–1314.

Huang, G. T.-J., Gronthos, S., and Shi, S. (2009). Mesenchymal Stem Cells Derived from Dental Tissues vs. Those from Other Sources: Their Biology and Role in Regenerative Medicine. *Journal of Dental Research*, *88*(9), 792–806.

Huang, G. T.-J., Sonoyama, W., Chen, J., and Park, S. H. (2006). In vitro characterization of human dental pulp cells: various isolation methods and culturing environments Received: *Cell and Tissue Research*, *324*(2), 225–236.

Huang, G. T.-J., Yamaza, T., Shea, L. D., Djouad, F., Kuhn, N. Z., Tuan, R. S., and Shi, S. (2010). Stem/Progenitor Cell–Mediated De Novo Regeneration of Dental Pulp with Newly Deposited Continuous Layer of Dentin in an In Vivo Model. *Tissue Engineering. Part A*, *16*(2), 605–15.

Ingber, D. E. (1997). Tensegrity: the architectural basis of cellular mechanotransduction. *Annual Review of Physiology*, *59*, 575–599.

Iohara, K., Zheng, L., Ito, M., Ishizaka, R., Nakamura, H., Into, T., Matsushita, K., and Nakashima, M. (2009). Regeneration of dental pulp after pulpotomy by transplantation of CD31(-)/ CD146(-) side population cells from a canine tooth. *Regenerative Medicine*, *4*(3), 377–85.

Jackson, K. A., Majka, S. M., Wang, H., Pocius, J., Hartley, C. J., Majesky, M. W., Entman, M. L., Michael, L. H., Hirschi, K. K., and Goodell, M. A. (2001). Regeneration of ischemic cardiac muscle and vascular endothelium by adult stem cells. *Journal of Clinical Investigation*, *107*, 1395–1402.

Janik, H., and Marzec, M. (2015). A review: Fabrication of porous polyurethane scaffolds. *Materials Science and Engineering C*, *48*, 586–591.

Janković, B. D., Isaković, K., Lukić, M. L., Vujanović, N. L., Petrović, S., and Marković, B. M. (1975). Immunological Capacity of the Chicken Embryo I. Relationship Between the Maturation of Lymphoid Tissues and the Occurrence of Cell-Mediated Immunity in the Developing Chicken Embryo. *Immunology*, *29*(3), 497–508.

Ji, P., Manupipatpong, S., Xie, N., and Li, Y. (2016). Induced Pluripotent Stem Cells: Generation Strategy and Epigenetic Mystery behind Reprogramming. *Stem Cells International*, 1–11.

Jiménez-Rojo, L., Granchi, Z., Graf, D., and Mitsiadis, T. A. (2012). Stem cell fate determination during development and regeneration of ectodermal organs Lucía. *Frontiers in Physiology*, *3*(107), 1–11.

Jin, K., Li, B., Lou, L., Xu, Y., Ye, X., Yao, K., Ye, J., and Gao, C. (2016). In vivo vascularization of MSC-loaded porous hydroxyapatite constructs coated with VEGF-functionalized collagen/heparin multilayers. *Scientific Reports*, *6*(19871), 1–13.

Jones, D. L., and Wagers, A. J. (2008). No place like home: anatomy and function of the stem cell niche. *Nature Reviews Molecular Cell Biology*, *9*(1), 11–21.

Kajstura, J., Leri, A., Finato, N., Di Loreto, C., Beltrami, C. A., and Anversa, P. (1998). Myocyte proliferation in end-stage cardiac failure in humans. *Proceedings of the National Academy of Sciences*, *95*(15), 8801–5.

Kalluri, R. (2003). Basement Membranes: Structure, Assembly and Role in Tumour Angiogenesis. *Nature Reviews Cancer*, *3*, 422–433.

Kässmeyer, S., Plendl, J., Custodis, P., and Bahramsoltani, M. (2009). New insights in vascular development: vasculogenesis and endothelial progenitor cells. *Anatomia, Histologia, Embryologia*, *38*, 1–11.

Katari, R., Peloso, A., and Orlando, G. (2015). Tissue engineering and regenerative medicine: semantic considerations for an evolving paradigm. *Frontiers in Bioengineering and Biotechnology*, *2*, 1–6.

Kémoun, P., Laurencin-Dalicieux, S., Rue, J., Farges, J.-C., Gennero, I., Conte-Auriol, F., Briand-Mesange, F., Gadelorge, M., Arzate, H., Narayanan, a S., Brunel, G., and Salles, J.-P. (2007). Human dental follicle cells acquire cementoblast features under stimulation by BMP-2/-7 and enamel matrix derivatives (EMD) in vitro. *Cell and Tissue Research*, *329*(2), 283–94.

Kivrak Pfiffner, F., Waschkies, C., Tian, Y., Woloszyk, A., Calcagni, M., Giovanoli, P., Rudin, M., and Buschmann, J. (2015). A New In Vivo Magnetic Resonance Imaging Method to Noninvasively Monitor and Quantify the Perfusion Capacity of Three-Dimensional Biomaterials Grown on the Chorioallantoic Membrane of Chick Embryos. *Tissue Engineering. Part C*, *21*(4), 339–346.

Korpisalo, P., and Ylä-Herttuala, S. (2010). Stimulation of functional vessel growth by gene therapy. *Integrative Biology*, *2*, 102–112.

Krause, D. S., Theise, N. D., Collector, M. I., Henegariu, O., Hwang, S., Gardner, R., Neutzel, S., and Sharkis, S. J. (2001). Multi-Organ, Multi-Lineage Engraftment by a Single Bone Marrow-Derived Stem Cell. *Cell*, *105*(3), 369–377.

Ku, C. H., Johnson, P. H., Batten, P., Sarathchandra, P., Chambers, R. C., Taylor, P. M., Yacoub, M. H., and Chester, A. H. (2006). Collagen synthesis by mesenchymal stem cells and aortic valve interstitial cells in response to mechanical stretch. *Cardiovascular Research*, *71*, 548–556.

Laino, G., d'Aquino, R., Graziano, A., Lanza, V., Carinci, F., Naro, F., Pirozzi, G., and Papaccio, G. (2005). A New Population of Human Adult Dental Pulp Stem Cells: A Useful Source of Living Autologous Fibrous Bone Tissue (LAB). *Journal of Bone and Mineral Research*, *20*(8), 1394–1402.

Lambert, V., Gouadon, E., Capderou, A., Le Bret, E., Ly, M., Dinanian, S., Renaud, J.-F., Pucéat, M., and Rücker-Martin, C. (2015). Right ventricular failure secondary to chronic overload in congenital heart diseases: Benefits of cell therapy using human embryonic stem cell–derived cardiac progenitors. *The Journal of Thoracic and Cardiovascular Surgery*, *149*(3), 708–715.

Lane, S. W., Williams, D. A., and Watt, F. M. (2014). Modulating the stem cell niche for tissue regeneration. *Nature Biotechnology*, *32*(8), 795–803.

Larsen, W. J. (1998). *Essentials of Human Embryology* (2nd ed.). New York: Churchill Livingstone.

Laschke, M. W., Harder, Y., Amon, M., Martin, I., Farhadi, J., Ring, A., Torio-Padron, N., Schramm, R., Rücker, M., Junker, D., Häufel, J. M., Carvalho, C., Heberer, M., Germann, G., Vollmar, B., and Menger, M. D. (2006). Angiogenesis in Tissue Engineering: Breathing Life into Constructed Tissue Substitutes. *Tissue Engineering*, *12*(8), 2093–2104.

Laschke, M. W., and Menger, M. D. (2012). Vascularization in Tissue Engineering: Angiogenesis versus Inosculation. *European Surgical Research*, *48*(2), 85–92.

Laschke, M. W., and Menger, M. D. (2015). Prevascularization in tissue engineering: Current concepts and future directions. *Biotechnology Advances*, *34*(2), 112–121.

Lau, A. N., Goodwin, M., Kim, C. F., and Weiss, D. J. (2012). Stem Cells and Regenerative Medicine in Lung Biology and Diseases. *Molecular Therapy*, *20*(6), 1116–1130.

Lee, H. S., Jeon, M., Kim, S. O., Kim, S. H., Lee, J. H., Ahn, S. J., Shin, Y., and Song, J. S. (2015). Characteristics of stem cells from human exfoliated deciduous teeth (SHED) from intact cryopreserved deciduous teeth. *Cryobiology*, *71*(3), 374–383.

Lee, O. K., Kuo, T. K., Chen, W.-M., Lee, K.-D., Hsieh, S.-L., and Chen, T.-H. (2004). Isolation of multipotent mesenchymal stem cells from umbilical cord blood. *Blood*, *103*(5), 1669–1675.

Liang, L., Wang, J., Zhang, Y., Shen, Z., Zheng, J., Li, J., Su, Z., Cai, J., Jiang, W., and Sun, M. (2015). Transdifferentiation of bone marrow-derived mesenchymal stem cells into salivary gland-like cells using a novel culture method. *Biotechnology Letters*, *37*(7), 1505–1513.

Liu, L., Wei, X., Ling, J., Wu, L., and Xiao, Y. (2011). Expression Pattern of Oct-4, Sox2, and c-Myc in the Primary Culture of Human Dental Pulp Derived Cells. *Journal of Endodontics*, *37*(4), 466–72.

Liu, Y., Zheng, Y., Ding, G., Fang, D., Zhang, C., Bartold, P., Gronthos, S., Shi, S., and Wang, S. (2008). Periodontal Ligament Stem Cell-Mediated Treatment for Periodontitis in Miniature Swine. *Stem Cells*, *26*(4), 1065–1073.

Livak, K. J., and Schmittgen, T. D. (2001). Analysis of Relative Gene Expression Data Using Real-Time Quantitative PCR and the 2-DDCT Method. *Methods*, *25*(4), 402–408.

Lizier, N. F., Kerkis, A., Gomes, C. M., Hebling, J., Oliveira, C. F., Caplan, A. I., and Kerkis, I. (2012). Scaling-Up of Dental Pulp Stem Cells Isolated from Multiple Niches. *PloS One*, *7*(6), e39885.

Loh, Q. L., and Choong, C. (2013). Three-Dimensional Scaffolds for Tissue Engineering Applications: Role of Porosity and Pore Size. *Tissue Engineering. Part B*, *19*(6), 485–502.

Lois, C., and Alvarez-Buylla, A. (1993). Proliferating subventricular zone cells in the adult mammalian forebrain can differentiate into neurons and glia. *Proceedings of the National Academy of Sciences*, *90*(5), 2074–2077.

Lovett, M., Lee, K., Edwards, A., and Kaplan, D. L. (2009). AVascularization Strategies for Tissue Engineering Michael. *Tissue Engineering. Part B*, *15*(3), 353–70.

Maraldi, T., Riccio, M., Resca, E., Pisciotta, A., La Sala, G. B., Ferrari, A., Bruzzesi, G., Motta, A., Migliaresi, C., Marzona, L., and De Pol, A. (2011). Human Amniotic Fluid Stem Cells Seeded in Fibroin Scaffold Produce In Vivo Mineralized Matrix. *Tissue Engineering. Part A*, *17*(21-22), 2833–2843.

Martin, P. (1997). Wound Healing-Aiming for Perfect Skin Regeneration. *Science*, *276*(5309), 75–81.

Mason, C., and Dunnill, P. (2008). A brief definition of regenerative medicine. *Regenerative Medicine*, *3*(1), 1–5.

McKay, W. F., Peckham, S. M., and Badura, J. M. (2007). A comprehensive clinical review of recombinant human bone morphogenetic protein-2 (INFUSE Bone Graft). *International Orthopaedics*, *31*(6), 729–34.

Meirelles, L. da S., and Beyer Nardi, N. (2009). Methodology, biology and clinical applications of mesenchymal stem cells. *Frontiers in Bioscience*, *14*, 4281–4298.

Menicanin, D., Mrozik, K. M., Wada, N., Marino, V., Shi, S., Bartold, P. M., and Gronthos, S. (2014). Periodontal-Ligament-Derived Stem Cells Exhibit the Capacity for Long-Term Survival, Self-Renewal, and Regeneration of Multiple Tissue Types in Vivo. *Stem Cells and Development*, *23*(9), 1001–11.

Merkle, F. T., Mirzadeh, Z., and Alvarez-Buylla, A. (2007). Mosaic Organization of Neural Stem Cells in the Adult Brain. *Science*, *317*(5836), 381–4.

Messina, E., De Angelis, L., Frati, G., Morrone, S., Chimenti, S., Fiordaliso, F., Salio, M., Battaglia, M., Latronico, M. V. G., Coletta, M., Vivarelli, E., Frati, L., Cossu, G., and Giacomello, A. (2004). Isolation and Expansion of Adult Cardiac Stem Cells From Human and Murine Heart. *Circulation Research*, *95*(9), 911–921.

Michiels, C. (2003). Endothelial Cell Functions. *Journal of Cellular Physiology*, *196*(3), 430–443.

Mitsiadis, T. A., Barrandon, O., Rochat, A., Barrandon, Y., and De Bari, C. (2007). Stem cell niches in mammals. *Experimental Cell Research*, *313*(16), 3377–85.

Mitsiadis, T. A., Feki, A., Papaccio, G., and Catón, J. (2011). Dental pulp stem cells, niches, and notch signaling in tooth injury. *Advances in Dental Research*, *23*(3), 275–9.

Mitsiadis, T. A., and Graf, D. (2009). Cell Fate Determination During Tooth Development and Regeneration. *Birth Defects Research. Part C*, *87*(3), 199–211.

Mitsiadis, T. A., Woloszyk, A., and Jiménez-Rojo, L. (2012). Nanodentistry: combining nanostructured materials and stem cells for dental tissue regeneration. *Nanomedicine*, *7*(11), 1743–53.

Miura, M., Gronthos, S., Zhao, M., Lu, B., Fisher, L. W., Robey, P. G., and Shi, S. (2003). SHED: Stem cells from human exfoliated deciduous teeth. *Proceedings of the National Academy of Sciences*, *100*(10), 5807–12.

Morrison, S. J., Shah, N. M., and Anderson, D. J. (1997). Regulatory Mechanisms in Stem Cell Biology. *Cell*, *88*, 287–298.

Morsczeck, C., Götz, W., Schierholz, J., Zeilhofer, F., Kühn, U., Möhl, C., Sippel, C., and Hoffmann, K. H. (2005). Isolation of precursor cells (PCs) from human dental follicle of wisdom teeth. *Matrix Biology*, *24*(2), 155–65.

Mundy, G. (1999). Stimulation of Bone Formation in Vitro and in Rodents by Statins. *Science*, *286*(5446), 1946–1949.

Murphy, C. M., O'Brien, F. J., Little, D. G., and Schindeler, A. (2013). Cell-scaffold interactions in the bone tissue engineering triad. *European Cells and Materials*, *26*, 120–132.

Nadri, S., Soleimani, M., Kiani, J., Atashi, A., and Izadpanah, R. (2008). Multipotent mesenchymal stem cells from adult human eye conjunctiva stromal cells. *Differentiation; Research in Biological Diversity*, *76*(3), 223–31.

Nanci, A. (2012). *Ten Cate's Oral Histology: Development, Structure, and Function* (8th ed.). Mosby.

Nazarov, R., Jin, H.-J., and Kaplan, D. L. (2004). Porous 3-D scaffolds from regenerated silk fibroin. *Biomacromolecules*, *5*(3), 718–26.

Novosel, E. C., Kleinhans, C., and Kluger, P. J. (2011). Vascularization is the key challenge in tissue engineering. *Advanced Drug Delivery Reviews*, *63*(4-5), 300–11.

Nowak-Sliwinska, P., Segura, T., and Iruela-Arispe, M. L. (2014). The chicken chorioallantoic membrane model in biology, medicine and bioengineering. *Angiogenesis*.

O'Brien, F. J. (2011). Biomaterials & scaffolds for tissue engineering. *Materials Today*, *14*(3), 88–95.

Oh, J., Lee, Y. D., and Wagers, A. J. (2014). Stem cell aging: mechanisms, regulators and therapeutic opportunities. *Nature Medicine*, *20*(8), 870–880.

Orlando, G., Wood, K. J., Stratta, R. J., Yoo, J. J., Atala, A., and Soker, S. (2011). Regenerative Medicine and Organ Transplantation: Past, Present, and Future. *Transplantation*, *91*(12), 1310–1317.

Pardali, E., Goumans, M. J., and ten Dijke, P. (2010). Signaling by members of the TGF-β family in vascular morphogenesis and disease. *Trends in Cell Biology*, *20*(9), 556–567.

Pellegrini, G., and De Luca, M. (2014). Eyes on the Prize: Limbal Stem Cells and Corneal Restoration. *Cell Stem Cell*, *15*(2), 121–122.

Pellettieri, J., and Alvarado, A. S. (2007). Cell Turnover and Adult Tissue Homeostasis: From Humans to Planarians. *Annual Review of Genetics*, *41*(1), 83–105.

Pepper, M. S., Vassalli, J.-D., Orci, L., and Montesano, R. (1993). Biphasic Effect of Transforming Growth Factor-β1 on in Vitro Angiogenesis. *Experimental Cell Research*, *204*, 356–363.

Pessina, A., and Gribaldo, L. (2006). The key role of adult stem cells: therapeutic perspectives. *Current Medical Research and Opinion*, *22*(11), 2287–2300.

Phelps, E. A., and García, A. J. (2010). Engineering more than a cell: Vascularization strategies in tissue engineering. *Current Opinion in Biotechnology*, *21*(5), 704–709.

Pittenger, M. F. (1999). Multilineage Potential of Adult Human Mesenchymal Stem Cells. *Science*, *284*(5411), 143–147.

Pokrywczynska, M., Lewandowska, M. A., Krzyzanowska, S., Jundzill, A., Rasmus, M., Warda, K., Gagat, M., Deptula, A., Helmin-Basa, A., Holysz, M., Nowacki, M., Buchholz, L., Bodnar, M., Marszalek, A., Grzanka, A., Jozwicki, W., Michalkiewicz, J., and Drewa, T. (2015). Transdifferentiation of Bone Marrow Mesenchymal Stem Cells into the Islet-Like Cells: the Role of Extracellular Matrix Proteins. *Archivum Immunologiae et Therapiae Experimentalis*, *63*(5), 377–384.

Poss, K. D. (2010). Advances in understanding tissue regenerative capacity and mechanisms in animals. *Nature Reviews Genetics*, *11*(10), 710–722.

Priest, C. A., Manley, N. C., Denham, J., Wirth, E. D., and Lebkowski, J. S. (2015). Preclinical safety of human embryonic stem cell-derived oligodendrocyte progenitors supporting clinical trials in spinal cord injury. *Regenerative Medicine*, *10*, 939–958.

Raff, M. (2003). Adult Stem Cell Plasticity: Fact or Artifact? *Annual Review of Cell and Developmental Biology*, *19*(1), 1–22.

Raya-Rivera, A., Esquiliano, D. R., Yoo, J. J., Lopez-Bayghen, E., Soker, S., and Atala, A. (2011). Tissue-engineered autologous urethras for patients who need reconstruction: an

observational study. *Lancet (London, England)*, *377*(9772), 1175–82.

Rezai-Rad, M., Bova, J. F., Orooji, M., Pepping, J., Qureshi, A., Del Piero, F., Hayes, D., and Yao, S. (2015). Evaluation of bone regeneration potential of dental follicle stem cells for treatment of craniofacial defects. *Cytotherapy*, *17*(11), 1572–1581.

Ribatti, D. (2014). The chick embryo chorioallantoic membrane as a model for tumor biology. *Experimental Cell Research*, *328*(2), 314–324.

Riccio, M., Maraldi, T., Pisciotta, A., La Sala, G. B., Ferrari, A., Bruzzesi, G., Motta, A., Migliaresi, C., and De Pol, A. (2012). Fibroin Scaffold Repairs Critical-Size Bone Defects In Vivo Supported by Human Amniotic Fluid and Dental Pulp Stem Cells Massimo. *Tissue Engineering. Part A*, *18*, 1006–13.

Risau, W. (1997). Mechanisms of angiogenesis. *Nature*.

Robinton, D. A., and Daley, G. Q. (2012). The promise of induced pluripotent stem cells in research and therapy. *Nature*, *481*, 295–305.

Romanoff, A. L. (1960). *The Avian Embryo: Structural and Funtional Development* (1st ed.). The Macmillan Co, New York.

Rouwkema, J., Rivron, N. C., and van Blitterswijk, C. A. (2008). Vascularization in tissue engineering. *Trends in Biotechnology*, *26*(8), 434–441.

Sakai, K., Yamamoto, A., Matsubara, K., Nakamura, S., Naruse, M., Yamagata, M., Sakamoto, K., Tauchi, R., Wakao, N., Imagama, S., Hibi, H., Kadomatsu, K., Ishiguro, N., and Ueda, M. (2012). Human dental pulp-derived stem cells promote locomotor recovery after complete transection of the rat spinal cord by multiple neuro-regenerative mechanisms. *The Journal of Clinical Investigation*, *122*(1), 80–90.

Sanchez-Ramos, J., Song, S., Cardozo-Pelaez, F., Hazzi, C., Stedeford, T., Willing, A., Freeman, T. B., Saporta, S., Janssen, W., Patel, N., Cooper, D. R., and Sanberg, P. R. (2000). Adult Bone Marrow Stromal Cells Differentiate into Neural Cells in Vitro. *Experimental Neurology*, *164*(2), 247–256.

Sangaralingham, S. J., Ritman, E. L., McKie, P. M., Ichiki, T., Lerman, A., Scott, C. G., Martin, F. L., Harders, G. E., Bellavia, D., and Burnett Jr., J. C. (2012). Cardiac Micro-Computed Tomography Imaging of the Aging Coronary Vasculature. *Circulation. Cardiovascular Imaging*, *5*(4), 518–524.

Scadden, D. T. (2006). The stem-cell niche as an entity of action. *Nature*, *441*, 1075–9.

Schiraldi, C., Stellavato, A., D'Agostino, A., Tirino, V., d'Aquino, R., Woloszyk, A., De Rosa, A., Laino, L., Papaccio, G., and Mitsiadis, T. A. (2012). Fighting for territories: time-lapse analysis of dental pulp and dental follicle stem cells in co-culture reveals specific migratory capabilities. *European Cells and Materials*, *24*, 426–40.

Schofield, R. (1978). The relationship between the spleen colony-forming cell and the haemopoietic stem cell. *Blood Cells*, *4*(1-2), 7–25.

Schwartz, R. E., Reyes, M., Koodie, L., Jiang, Y., Blackstad, M., Lund, T., Lenvik, T., Johnson, S., Hu, W.-S., and Verfaillie, C. M. (2002). Multipotent adult progenitor cells from bone marrow differentiate into functional hepatocyte-like cells. *The Journal of Clinical Investigation*, *109*(10), 1291–302.

Schwartz, S. D., Regillo, C. D., Lam, B. L., Eliott, D., Rosenfeld, P. J., Gregori, N. Z., Hubschman, J.-P., Davis, J. L., Heilwell, G., Spirn, M., Maguire, J., Gay, R., Bateman, J., Ostrick, R. M., Morris, D.,

Vincent, M., Anglade, E., Del Priore, L. V, and Lanza, R. (2015). Human embryonic stem cell-derived retinal pigment epithelium in patients with age-related macular degeneration and Stargardt's macular dystrophy: follow-up of two open-label phase 1/2 studies. *The Lancet*, *385*(9967), 509–516.

Seo, B.-M., Miura, M., Gronthos, S., Bartold, P. M., Batouli, S., Brahim, J., Young, M., Robey, P. G., Wang, C.-Y., and Shi, S. (2004). Investigation of multipotent postnatal stem cells from human periodontal ligament. *Lancet*, *364*(9429), 149–55.

Seo, B.-M., Sonoyama, W., Yamaza, T., Coppe, C., Kikuiri, T., Akiyama, K., Lee, J. S., and Shi, S. (2008). SHED repair critical-size calvarial defects in mice. *Oral Diseases*, *14*(5), 428–434.

Seydoux, G., and Braun, R. E. (2006). Pathway to Totipotency: Lessons from Germ Cells. *Cell*, *127*(5), 891–904.

Shi, Q., Wu, M. H.-D., Hayashida, N., Wechezak, A. R., Clowes, A. W., and Sauvage, L. R. (1994). Proof of fallout endothelialization of impervious dacron grafts in the aorta and inferior vena cava of the dog. *Journal of Vascular Surgery*, *20*(4), 546–557.

Shi, S., Robey, P. G., and Gronthos, S. (2001). Comparison of Human Dental Pulp and Bone Marrow Stromal Stem Cells by cDNA Microarray Analysis. *Bone*, *29*(6), 532–9.

Shimono, M., Ishikawa, T., Ishikawa, H., Matsuzaki, H., Hashimoto, S., Muramatsu, T., Shima, K., Matsuzaka, K.-I., and Inoue, T. (2003). Regulatory Mechanisms of Periodontal Regeneration. *Microscopy Research and Technique*, *60*(5), 491–502.

Shin'oka, T., Imai, Y., and Ikada, Y. (2001). Transplantation of a tissue-engineered pulmonary artery. *The New England Journal of Medicine*, *344*(7), 532–3.

Sidney, L. E., Branch, M. J., Dunphy, S. E., Dua, H. S., and Hopkinson, A. (2014). Consise Review: Evidence for CD34 as a Common Marker for Diverse Progenitors. *Stem Cells*, *32*, 1380–1389.

Silver, F. H., and Landis, W. J. (2011). Deposition of apatite in mineralizing vertebrate extracellular matrices: A model of possible nucleation sites on type I collagen. *Connective Tissue Research*, *52*, 242–254.

Smith, A. G. (2001). Embryo-Derived Stem Cells: Of Mice and Men. *Annual Review of Cell and Developmental Biology*, *17*, 435–62.

Sofia, S., McCarthy, M. B., Gronowicz, G., and Kaplan, D. L. (2001). Functionalized silk-based biomaterials for bone formation. *Journal of Biomedical Materials Research*, *54*(1), 139–48.

Sonoyama, W., Liu, Y., Fang, D., Yamaza, T., Seo, B.-M., Zhang, C., Liu, H., Gronthos, S., Wang, C.-Y., Wang, S., and Shi, S. (2006). Mesenchymal Stem Cell-Mediated Functional Tooth Regeneration in Swine. *PloS One*, *1*(1), e79.

Sonoyama, W., Liu, Y., Yamaza, T., Tuan, R. S., Wang, S., Shi, S., and Huang, G. T.-J. (2008). Characterization of the Apical Papilla and Its Residing Stem Cells from Human Immature Permanent Teeth: A Pilot Study. *Journal of Endodontics*, *34*(2), 166–71.

Stoppato, M., Stevens, H. Y., Carletti, E., Migliaresi, C., Motta, A., and Guldberg, R. E. (2013). Effects of silk fibroin fiber incorporation on mechanical properties, endothelial cell colonization and vascularization of PDLLA scaffolds. *Biomaterials*, *34*(19), 4573–4581.

Szot, G. L., Yadav, M., Lang, J., Kroon, E., Kerr, J., Kadoya, K., Brandon, E. P., Baetge, E. E., Bour-Jordan, H., and Bluestone, J. A. (2014). Tolerance Induction and Reversal of Diabetes in Mice Transplanted with Human Embryonic Stem Cell-Derived Pancreatic Endoderm. *Cell Stem Cell*, *16*(2), 148–157.

Takahashi, K., Tanabe, K., Ohnuki, M., Narita, M., Ichisaka, T., Tomoda, K., and Yamanaka, S. (2007). Induction of Pluripotent Stem Cells from Adult Human Fibroblasts by Defined Factors. *Cell*, *131*(5), 861–72.

Takahashi, K., and Yamanaka, S. (2006). Induction of Pluripotent Stem Cells from Mouse Embryonic and Adult Fibroblast Cultures by Defined Factors. *Cell*, *126*(4), 663–76.

Tatullo, M., Marrelli, M., Shakesheff, K. M., and White, L. J. (2015). Dental pulp stem cells: function, isolation and applications in regenerative medicine. *Journal of Tissue Engineering and Regenerative Medicine*, *9*(11), 1205–1216.

Thomson, J. A., Itskovitz-Eldor, J., Shapiro, S. S., Waknitz, M. A., Swiergiel, J. J., Marshall, V. S., and Jones, J. M. (1998). Embryonic Stem Cell Lines Derived from Human Blastocysts. *Science*, *282*(5391), 1145–1147.

Tirino, V., Paino, F., De Rosa, A., and Papaccio, G. (2012). Identification, isolation, characterization, and banking of human dental pulp stem cells. *Methods in Molecular Biology*, *879*, 443–463.

Vacanti, J. P., Morse, M. A., Saltzman, W. M., Domb, A. J., Perez-Atayde, A., and Langer, R. (1988). Selective Cell Transplantation Using Bioabsorbable Artificial Polymers as Matrices By. *Journal of Pediatric Surgery*, *23*(1), 3–9.

Vaes, B., Van't Hof, W., Deans, R., and Pinxteren, J. (2012). Application of MultiStem® allogeneic cells for iImmunomodulatory therapy: clinical progress and pre-clinical challenges in prophylaxis for graft versus host disease. *Frontiers in Immunology*, *3*, 345.

Virtej, A., Løes, S., Iden, O., Bletsa, A., and Berggreen, E. (2013). Vascular endothelial growth factors signalling in normal human dental pulp: a study of gene and protein expression. *European Journal of Oral Sciences*, *121*, 92–100.

Wagers, A. J., and Weissman, I. L. (2004). Plasticity of Adult Stem Cells. *Cell*, *116*, 639–648.

Walthers, C. M., Nazemi, A. K., Patel, S. L., Wu, B. M., and Dunn, J. C. Y. (2014). The Effect of Scaffold Macroporosity on Angiogenesis and Cell Survival in Tissue-Engineered Smooth Muscle. *Biomaterials*, *35*(19), 5129–5137.

Wang, J., Wang, X., Sun, Z., Wang, X., Yang, H., Shi, S., and Wang, S. (2010). Stem Cells from Human-Exfoliated Deciduous Teeth Can Differentiate into Dopaminergic Neuron-Like Cells. *Stem Cells and Development*, *19*(9), 1375–83.

Watt, F. M., and Driskell, R. R. (2010). The therapeutic potential of stem cells. *Philosophical Transactions of the Royal Society. Series B*, *365*(1537), 155–63.

Watt, F. M., and Hogan, B. L. M. (2000). Out of Eden: Stem Cells and Their Niches. *Science*, *287*, 1427–1430.

Weissman, I. L. (2000). Stem Cells: Units of Development, Units of Regeneration, and Units in Evolution. *Cell*, *100*(1), 157–68.

Weissman, I. L., Anderson, D. J., and Gage, F. (2001). Stem and Progenitor Cells: Origins, Phenotypes, Lineage Commitments, and Transdifferentiations. *Annual Review of Cell and Developmental Biology*, *17*, 387–403.

Welm, B., Behbod, F., Goodell, M. A., and Rosen, J. M. (2003). Isolation and characterization of functional mammary gland stem cells. *Cell Proliferation*, *36*, 17–32.

Wiese, C., Rolletschek, A., Kania, G., Blyszczuk, P., Tarasov, K. V., Tarasova, Y., Wersto, R. P., Boheler, K. R., and Wobus, A. M. (2004). Nestin expression-a property of multi-lineage progenitor cells? *Cellular and Molecular Life Sciences*, *61*(19-20), 2510–2522.

Wobus, A. M., and Boheler, K. R. (2005). Embryonic Stem Cells: Prospects for Developmental Biology and Cell Therapy. *Physiological Reviews*, *85*(2), 635–678.

Woloszyk, A., Holsten Dircksen, S., Bostanci, N., Müller, R., Hofmann, S., and Mitsiadis, T. A. (2014). Influence of the Mechanical Environment on the Engineering of Mineralised Tissues Using Human Dental Pulp Stem Cells and Silk Fibroin Scaffolds. *PloS One*, *9*(10), e111010.

Woods, E. J., Perry, B. C., Hockema, J. J., Larson, L., Zhou, D., and Goebel, W. S. (2009). Optimized cryopreservation method for human dental pulp-derived stem cells and their tissues of origin for banking and clinical use. *Cryobiology*, *59*(2), 150–7.

Xin, J., Ding, W., Hao, S., Jiang, L., Zhou, Q., Wu, T., Shi, D., Cao, H., Li, L., and Li, J. (2015). Human bone marrow mesenchymal stem cell-derived hepatocytes express tissue inhibitor of metalloproteinases 4 and follistatin. *Liver International*, *35*(10), 2301–2310.

Xuan, J. W., Bygrave, M., Jiang, H., Valiyeva, F., Dunmore-Buyze, J., Holdsworth, D. W., Izawa, J. I., Bauman, G., Moussa, M., Winter, S. F., Greenberg, N. M., Chin, J. L., Drangova, M., Fenster, A., and Lacefield, J. C. (2007). Functional Neoangiogenesis Imaging of Genetically Engineered Mouse Prostate Cancer Using Three-Dimensional Power Doppler Ultrasound. *Cancer Research*, *67*(6), 2830–2839.

Zhang, L., Kahn, C. J. F., Chen, H., Tran, N., and Wang, X. (2008). Effect of uniaxial stretching on rat bone mesenchymal stem cell: Orientation and expressions of collagen types I and III and tenascin-C. *Cell Biology International*, *32*, 344–352.

Zhang, W., Walboomers, X. F., Shi, S., Fan, M., and Jansen, J. A. (2006). Multilineage Differentiation Potential of Stem Cells Derived from Human Dental Pulp after Cryopreservation. *Tissue Engineering*, *12*(10), 2813–23.

Zuk, P. A., Zhu, M., Ashjian, P., De Ugarte, D. A., Huang, J. I., Mizuno, H., Alfonso, Z. C., Fraser, J. K., Benhaim, P., and Hedrick, M. H. (2002). Human Adipose Tissue Is a Source of Multipotent Stem Cells. *Molecular Biology of the Cell*, *13*, 4279–4295.

14. Appendix

14.1 Publications

14.1.1 Schiraldi et al., Eur Cell Mater, 2012

Fighting for Territories: Time-lapse Analysis of Dental Pulp and Dental Follicle Stem Cells in Co-Culture Reveals Specific Migratory Capabilities (PAPER)

Dental pulp stem cells (DPSCs) and dental follicle stem cells (DFSCs) are two dental mesenchymal stem cell populations that can be isolated from human teeth. Previous studies have shown that these two cell populations may have different functions when used for tissue repair *in vivo*. The presented project investigated the migratory and proliferative behavior of both cell populations in mono- and co-culture setups *in vitro*. Low and irregular migration profiles were observed when DPSCs and DFSCs were cultured alone. However, in co-cultures DFSCs but not DPSCs increased their migration activity and velocity and surrounded the DPSCs. This behavior resembles the *in vivo* embryonic developmental process of odontogenesis, where follicle cells encircle both the dental papilla and the enamel organ of the developing tooth germ. Together with a gene expression analysis of regulatory genes involved in dental cell migration and differentiation, the findings prove that stem cell populations isolated from distinct tissues behave differently according to their environment, retain their genetic memory, and compete with each other to acquire the appropriate territory. Therefore, these specific characteristics of stem cell populations have to be considered when selecting them for the future repair and regeneration of particular dental tissues in the clinic.

During the preparation of the paper I was responsible for the revision and editing of the manuscript.

FIGHTING FOR TERRITORIES: TIME-LAPSE ANALYSIS OF DENTAL PULP AND DENTAL FOLLICLE STEM CELLS IN CO-CULTURE REVEALS SPECIFIC MIGRATORY CAPABILITIES

Chiara Schiraldi[1], Antonietta Stellavato[1], Antonella D'Agostino[1], Virginia Tirino[2], Riccardo d'Aquino[2], Anna Woloszyk[4], Alfredo De Rosa[3], Luigi Laino[3], Gianpaolo Papaccio[2*] and Thimios A. Mitsiadis[4*]

[1]Department of Experimental Medicine, Section of Biotechnology, Second University of Naples, Italy
[2]Department of Experimental Medicine, Section of Medical Histology and Embryology, TERM laboratory, Second University of Naples, Italy
[3]Department of Dentistry, Second University of Naples, Italy
[4]Institute of Oral Biology, ZZM, Faculty of Medicine, University of Zurich, Switzerland
[*]Equal senior authors

Abstract

Stem cell migration is a critical step during the repair of damaged tissues. In order to achieve appropriate cell-based therapies for tooth and periodontal ligament repair it is necessary first to understand the dynamics of tissue-specific stem cell populations such as dental pulp stem cells (DPSC) and dental follicle stem cells (DFSC). Using time-lapse imaging, we analysed migratory and proliferative capabilities of these two human stem cell lines *in vitro*. When cultured alone, both DPSC and DFSC exhibited low and irregular migration profiles. In co-cultures, DFSC, but not DPSC, spectacularly increased their migration activity and velocity. DFSC rapidly surrounded the DPSC, thus resembling the *in vivo* developmental process, where follicle cells encircle both dental epithelium and pulp. Cell morphology was dependent on the culture conditions (mono-culture or co-culture) and changed over time. Regulatory genes involved in dental cell migration and differentiation such as *TWIST1*, *MSX1*, *RUNX2*, *SFRP1* and *ADAM28*, were also evaluated in co-cultures. *MSX1* up-regulation indicates that DPSC and DFSC retain their odontogenic potential. However, DPSC lose their capacity to differentiate into odontoblasts in the presence of DFSC, as suggested by *RUNX2* up-regulation and *TWIST1* down-regulation. In contrast, the unchanged levels of *SFRP1* expression suggest that DFSC retain their potential to form periodontal tissues even in the presence of DPSC. These findings demonstrate that stem cells behave differently according to their environment, retain their genetic memory, and compete with each other to acquire the appropriate territory. Understanding the mechanisms involved in stem cell migration may lead to new therapeutic approaches for tooth repair.

Keywords: Tooth; odontoblast; dental follicle; periodontal ligament; dental pulp; dental stem cells; tooth repair; regeneration.

*Addresses for correspondence:
Prof. Thimios A. Mitsiadis,
University of Zurich, Faculty of Medicine, Institute of Oral Biology, ZZM,
Plattenstrasse 11, 8032 Zurich, Switzerland.
Telephone Number: +41 44 6343390
FAX Number: +41 44 6344310
E-mail: thimios.mitsiadis@zzm.uzh.ch

Prof. Gianpaolo Papaccio,
Department of Experimental Medicine, Medical Histology and Embryology,
TERM Laboratory, Second University of Naples,
Via L. Armanni 5, 80138 Naples, Italy.
Telephone Number: +39 081 5666014
FAX Number: +39 0815666014
Email:gianpaolo.papaccio@unina2.it

Introduction

Cell migration is a widespread, highly dynamic and complex process that is crucial for the appropriate development of organs and tissues (Aman and Piotrowski, 2010; Binamé *et al.*, 2010). Aberrant cell migration often results in severe morphogenetic defects and/or diseases (Friedl and Gilmour, 2009). Reactivation of cell migration underlies tissue repair processes, as well as several pathological conditions, such as metastatic cancers, thus making the study of cell movement clinically relevant.

In order to understand better the mechanisms involved in tissue repair and/or regeneration *in vivo*, *in vitro* assay systems have been developed that can bring considerable information about motility and directional migration of cells (Okumoto, 2010; Stephens and Allan, 2003; Wang *et al.*, 2008). Cellular dynamics and functions (e.g. cell migration, proliferation, apoptosis) can be visualised and quantitatively analysed through computational live image processing (Huth *et al.*, 2011; Wang *et al.*, 2008), thus allowing us to obtain biochemical and biophysical information about different cell populations at precise temporo-spatial windows (Aman and Piotrowski, 2010).

Tooth development results from sequential and reciprocal interactions between the oral epithelium and the cranial neural crest-derived mesenchyme (Bluteau *et al.*, 2008; Mitsiadis and Graf, 2009; Mitsiadis and Luder, 2011; Thesleff *et al.*, 1989; Thesleff *et al.*, 1991; Thesleff *et al.*, 1995). Epithelial cells give rise to the enamel producing ameloblasts, while mesenchymal cells are involved in the formation of the dental pulp and dental follicle. Odontoblasts originated by the dental pulp produce the dentin matrix, whereas dental follicle cells contribute to the formation of cementum, periodontal ligament, and alveolar bone (Diep *et al.*, 2009). Periodontal ligament occupies the space between the tooth root and the alveolar bone and serves for tooth anchorage to the bone and masticatory

force distribution. Although it has been shown that dental follicle cells express a plethora of regulatory molecules (Liu and Wise, 2007; Morsczeck and Schmalz, 2010), the mechanisms controlling their *in vivo* behaviour (e.g., cell proliferation, migration, and differentiation) remains elusive. Dental follicle cells are in close contact with cells of the dental papilla and root dentin during odontogenesis (Mitsiadis and Luder, 2011; Thesleff *et al*., 1989), and it has been demonstrated that these interactions constitute an important step for dental follicle differentiation (Bai *et al*., 2010). Signalling molecules, derived from the dental papilla and root dentin, could be responsible for the proliferation and differentiation of dental follicle cells *in vivo* (Bai *et al*., 2010; Mitsiadis and Rahiotis, 2004).

During tooth repair after injury or carious lesion, numerous genes that are expressed throughout embryonic tooth development are reactivated. For example, nestin and Notch molecules are re-expressed in the dental pulp during the reparative processes (Mitsiadis and Rahiotis, 2004). Tooth repair also involves activation of various dental stem cell populations (Mitsiadis *et al*., 2011). During tissue repair and/or regeneration, stem cells self-replicate, generate daughter cells and finally re-populate the damaged tissue (Laird *et al*., 2008; Smith, 2001; Smith, 2005). This process requires the oriented or directed movement of stem cells toward this particular anatomic destination (Laird *et al*., 2008). In human teeth, stem cell populations have been isolated and characterised from dental pulp and dental follicle (Gronthos *et al*., 2000; Handa *et al*., 2002; Laino *et al*., 2005; Miura *et al*., 2003; Papaccio *et al*., 2006; Takeda *et al*., 2008). Dental pulp stem cells (DPSC) and dental follicle stem cells (DFSC) were sorted by FACS using cell-surface markers such as CD117, CD34 and flk-1 for DPSC (d'Aquino *et al*., 2007; Graziano *et al*., 2008; Tirino *et al*., 2011) and SSEA4, OCT-4, TRA1-80 and TRA1-81 for DFSC (d'Aquino *et al*., 2011). These stem cell populations reside in various niches within the dental pulp and follicle (Lovschall *et al*., 2007; Mitsiadis *et al*., 2011). DPSC are very flexible and can differentiate into chondrocytes, adipocytes, neurons, muscles, odontoblasts and bone cells. *In vivo*, DPSC can form a vascularised pulp-like tissue that is surrounded by odontoblast-like cells (Nakashima and Iohara, 2011). The first clinical trial was successfully performed a few years ago, where DPSC from patients were capable to fully repair their own alveolar bone defects (d'Aquino *et al*., 2009). Similarly to the DPSC, DFSC exhibit a great differentiation potential (e.g. adipocytes, myoblasts, neurons, glial cells, cementoblasts, periodontal ligament fibroblasts), with the exception of bone formation (d'Aquino *et al*., 2011; Morsczeck *et al*., 2005; Yao *et al*., 2008). Indeed, DFSC are not capable of differentiating into osteoblasts unless a specific culture medium is used (Bai *et al*., 2010; d'Aquino *et al*., 2011; Yagyuu *et al*., 2010; Wu *et al*., 2008). Taken together these findings indicate that DPSC and DFSC may have different functions when used for tissue repair *in vivo*. Thus, it is desirable to understand their behaviour *in vitro* better, before any future clinical application.

In this study we applied time-lapse cell imaging, in an attempt to understand complex biological phenomena related to dental injury and repair/regeneration. We have found that DPSC and DFSC in co-culture behave differently from in mono-culture and compete with each other to increase their vital territory. The fact that DFSC rapidly migrate and occupy most of the culture space by surrounding and restraining the DPSC suggests new criteria for the clinical use of the various stem cell populations during tooth repair.

Materials and Methods

Subjects, stem cell extraction, digestion, and culture

Dental pulps were extracted from intact teeth of 21 to 45 year-old healthy individuals. Dental follicles were collected from wisdom tooth germs with not yet formed roots from 18 to 40 year-old healthy individuals. Dental pulps as well as dental follicles were incubated in a digestive solution composed of 3 mg/mL type I collagenase and 4 mg/mL dispase in phosphate buffered saline (PBS) for 1 h at 37 °C. After enzymatic digestion, the solution was filtered through 70 µm Falcon strainers (Becton & Dickinson, Milan, Italy) and then cells were immersed in DMEM culture medium supplemented with 10 % foetal bovine serum (FBS) (Lonza, Milan, Italy), 100 mM 2P-ascorbic acid, 2 mM L-glutamine, 100 U/mL penicillin, 100 µg/mL streptomycin (Invitrogen, San Giuliano Milanese, Milan, Italy) and cultured in 75 cm^2 flasks with filtered valves (Papaccio *et al*., 2006). FGF2 (20 ng/mL) was added to the medium for the culture of the dental follicles. Cells were cultured at 37 °C in a 5 % CO_2 incubator. The culture medium was renewed twice per week. Upon confluence, cells were used either for cell sorting or for time-lapse experiments (generally, at the first passage). Digested tissues were permitted to achieve near confluence (90 % of flask surface), which corresponds to $4x10^5$ cells/25 cm^2 for both cell populations. However, the average doubling time for DPSC is about 3 d while for DFSC it is 1 d (for details see Tirino *et al*., 2011).

Colony efficiency assays and proliferation potential

To evaluate colony efficiency and proliferation potential, single cells obtained by limiting dilutions were plated. After three weeks of culture, cells were stained with 0.1 % (w/v) toluidine blue in 1 % paraformaldehyde (PFA) and the number of clones (>50 cells) was counted.

Fluorescence-activated cell sorting (FACS)

For the collection of DPSC, approximately $1x10^6$ dental pulp cells per sample were detached from the flasks, washed and incubated with the CD117 and CD34 antibodies for 30 min at 4 °C. After incubation, CD34 and CD117 co-expressing cells were sorted using a FACS Aria II BD (BD Biosciences, Milan, Italy). The purity of these sorted cell populations was 90 %. The $CD34^+/CD117^+$cells were cultured in DMEM supplemented with 10 % FBS and then used for the time-lapse experiments.

For the collection of DFSC, nearly $1x10^6$ follicle cells per sample were detached from the flask using 0.02 % EDTA in PBS, pelleted (10 min at 1,000 rpm), washed in 0.1 % bovine serum albumin (BSA) in PBS at 4 ºC, and then incubated with the SSEA4 antibody for 30 min at 4 °C.

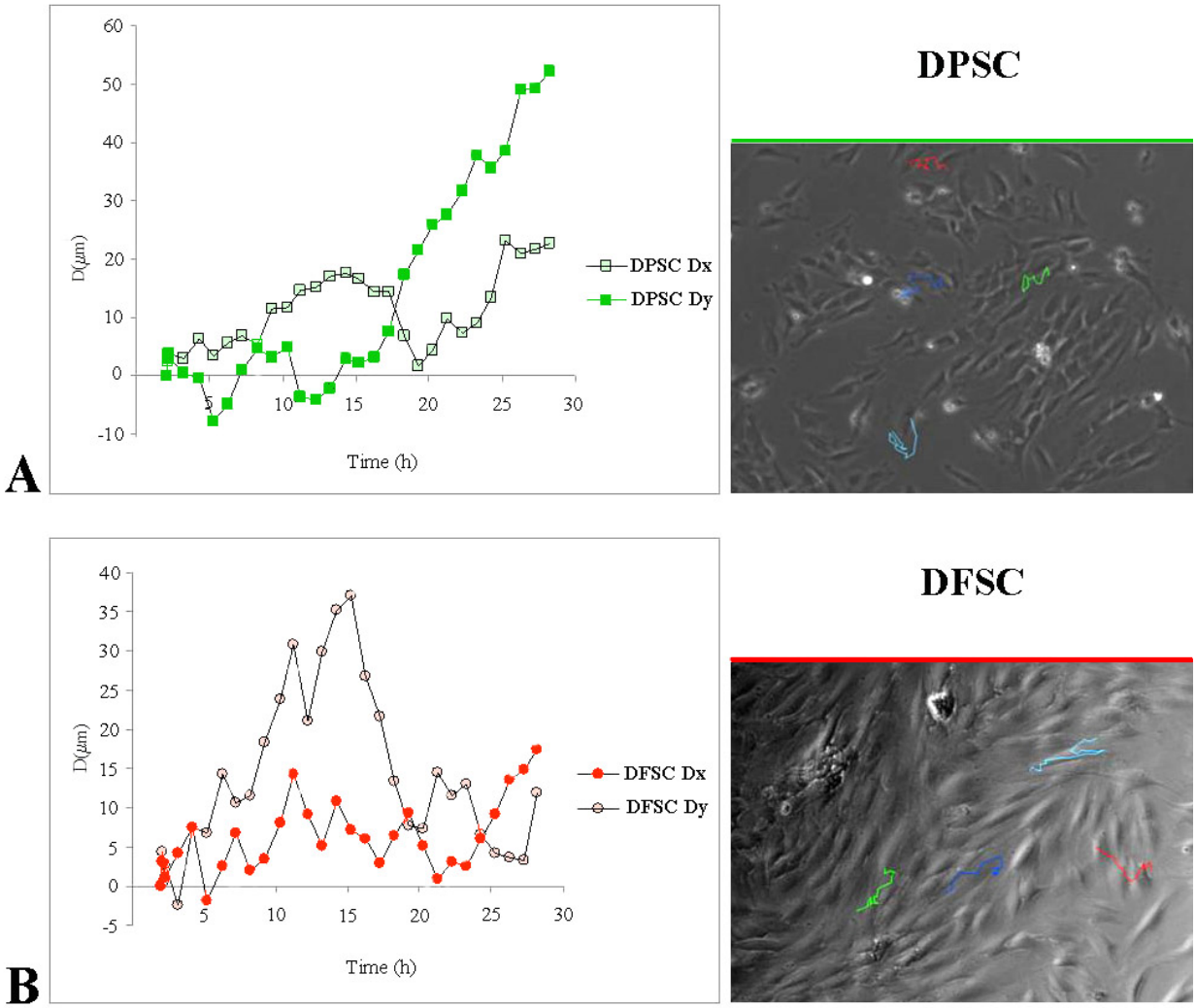

Fig. 1. Cell movement and orientation of DPSC and DFSC cultured alone. (**A**) When cultured alone, DPSC exhibit a random and restricted motility through the x or y axes. Coloured lines (right image) are representative of extracted cell tracks for DPSC in overall time (30 h). (**B**) When cultured alone, DFSC show circular movements. Coloured lines (right image) represent extracted cell tracks for DFSC in overall time (30 h).

After washing, the cells were analysed by flow cytometry and sorted by FACS. The purity of the sorted SSEA4$^+$ population was 90 %. SSEA4$^+$ cells were cultured in DMEM at 10 % FBS and used for time-lapse experiments.

Dye staining

Lipophilic cell tracking dyes such as PKH26 and PKH67 (Sigma Aldrich, Milan, Italy), use membrane-labelling technology to stabilise the incorporation of a fluorescent dye into the lipid regions of the cell membrane. Lipophilic cell labelling is simple to use and allows the follow up of the tagged cells *in vitro* and/or *in vivo*. Therefore, it constitutes a powerful tool for studying the kinetics and behaviour of various cell populations in a heterogeneous environment. DPSC and DFSC were stained with the PKH26 and PKH67 dyes, respectively, at a final concentration of $2x10^{-6}$ M and $3x10^5$ cells/mL according to the manufacturer's instructions. Diluent C is the labelling vehicle provided with the kit, an isosmotic aqueous solution designed to maintain cell viability and maximise dye solubility and staining efficiency (Lee-MacAry *et al*., 2001).

Time-lapse co-culture experiments

DPSC were cultured together with DFSC in a standard 24-well culture plate with μ-dish (35 mm, high) culture-insert (Ibidi, Integrated BioDiagnostics, Munich, Germany). In order to identify the behaviour of these two specific dental stem cell populations in this co-culture system, a series of cell mixtures with different ratio of DPSC/DFSC (i.e.$1.7x10^2$ cells/mm^2/$1.7x10^3$ cells/mm^2{1:10}, $1.7x10^3$ cells/mm^2/$1.7x10^2$ cells/mm^2 {10:1}, $2.8x10^2$ cells/mm^2/$2.8x10^2$ cells/mm^2{1:1}) were prepared (Fig. 1). Briefly, adherent cells were removed from flasks after 24 h of culture, using proteolytic enzymes (trypsin/EDTA; Invitrogen, Milan, Italy), immediately re-suspended and either plated as such or labelled prior to seeding. The labelling procedure consists in re-suspending centrifuged cells in 1 mL of staining solutions (i.e. PKH26 and PKH67) for 5 min, washing in culture medium for fluorescent dye excess removal, and finally seeding and incubating at 37 °C. After 2 h of incubation, fluorescence microscopy images were taken to analyse the morphology of the cells. The cells were observed for 30 h on Oko-Full time-lapse

in bright field and in fluorescence. In particular, the images in bright field were captured every 1 h (Δt), while those in fluorescence were captured every 4 h. This feature allowed us to reduce sample photo-bleaching and cell damage. It is possible to change the acquisition time of the images through a Ludl shutter controlled by the Oko-Vision software. The latter is an optical video-microscopy station, composed of a microscope (Zeiss Axiovert 200), with a 10x objective in phase contrast, equipped with motorised "stage incubator" for automated sample positioning, a stage incubator where the temperature and the atmosphere were kept at 37 °C and 5 % CO_2, respectively, and controlled humidity. The sequential images were captured by a CCD video camera (ORCA ER, Hamamatsu Photonics, Hamamatsu City, Japan). The monolayer was imaged using phase contrast, while the fluorescently labelled stem cells were imaged using Chroma Filters multi-channel (86013V2), for FITC (excitation BP 450-490 nm, emission LP 515 nm) and TRITC (excitation BP 550 nm, emission LP 580 nm).

Cell tracking software and analysis

The time-lapse video microscopy system represents a novel fully automated high-throughput approach for a precise and detailed cell tracking. In time-lapse video microscopy, manual cell tracking remains the most common method for analysing migratory behaviour of cell populations. Cell-Tracker, automatic tracking and analysis software was implemented using oko-vision (version 2009) and consists of a graphical, cross-platform open source application, adjustable to various types of microscopy images and video files. A modular architecture allows for the expansion of image processing and independent tracking. The Graphicator allows plotting of cell coordinates *versus* time, cell velocity and orientation. Cell-Tracker software allows easy following of cell movement in an interactive way. The cell trajectory is superimposed on the images, for visual validation of the analysis.

Manual tracking was performed with a custom viewing program that enabled storage of x and y coordinates by clicking on cells in sequential images with a computer mouse. Manual cell tracking was performed for a total of 4 cells for each field of view (object), for a total of four objects selected in each well. Generally, each condition was repeated at least three times. In addition, each experiment was performed for all cells located within the preselected regions of analysis, during the considered recording time (i.e. 30 h - 30 tracks).

The speed and motility of DPSC and DFSC in separate wells were analysed using the above-mentioned software. The speed, area, deformation, trajectory and detailed tracking of the cells were computed and displayed for analysis. The interaction of the two dental stem cell populations was studied in different conditions in the same well. Tabulated data of tracking results were exported into Microsoft Excel for further numerical analysis and evaluated statistically using Student's *t*-test. The conversion factor for measured pixels to microns (1.06 for 10x objective) was determined using a stage micrometer.

Cell-Tracker was plotted as cell coordinates (x and y) *versus* time. The cell velocity along x axis (vector) was calculated by the following equation:

$$v_x = \frac{Dx}{t_f - t_0}$$

where Dx denotes the last cell tracker, t_f and t_o represent final time and initial time, respectively.

Analyses were performed considering the ratio DPSC/DFSC ($1.7x10^3$ cells/mm^2/$1.7x10^2$ cells/mm^2 and $1.7x10^2$ cells/mm^2/$1.7x10^3$ cells/mm^2) per well and the major cell number ($1.7x10^3$ cells/mm^2). Data represent the mean ± SD of three independent experiments.

Isolation of total RNA and quantitative real-time (qRT)-PCR

Total RNA was extracted by using 1 mL of TRIzol® (Invitrogen, Milan, Italy), according to the manufacturer's instructions. The precipitate was then re-suspended in nuclease-free water. The concentration of the extracted RNA was determined using a Nanodrop spectrophotometer (Celbio, Milan, Italy), and qualitative analysis of the RNA was accomplished by 1 % agarose-gel (w/v) electrophoresis. For cDNA synthesis, performed with the Reverse Transcription System Kit (Promega, Milan, Italy), 1 μg of DNase-digested total RNA was used (DNA-free kit; Ambion-Applied Biosystems, Monza, Italy). Quantitative RT-PCR was obtained by using the iQ™ SYBR® Green Supermix (Bio-Rad Laboratories, Milan, Italy) to analyse the expression of *TWIST1*, *MSX1*, *RUNX2*, *ADAM28* and *SFRP1*. BLAST query permitted the specificity analysis of

Table 1. Oligonucleotide primers for real time PCR.

Primers	Sequence	Gene Function	T °C Annealing
TWIST-1	Sense GGCACCATCCTCACACCTCTG Antisense TGGCTGATTGGCACGACCTC	Cell lineage determination, cell differentiation	57 °C
MSX-1	Sense ACTGAGACGCAGGTGAAGATATGG Antisense CCGCCGAGAGGGAAGGAGAG	Craniofacial development, odontogenesis	55 °C
RUNX-2	Sense ACCAGCAGCACTCCATATCTCTAC Antisense CTTCCATCAGCGTCAACACCATC	Osteoblastic differentiation, skeletal morphogenesis	55 °C
SFRP-1	Sense TGTAATCCAGTCGGCTTGTTCTTG Antisense GGCTGCTGCTCCACATTGC	Regulation in cancer, dental follicle development	55 °C
ADAM-28	Sense TTGTGGTGGTTGCTATGGTAATCC Antisense GGCTTCATCTGACTCATCTCTTGG	Cell-cell and cell-matrix interactions.	56 °C

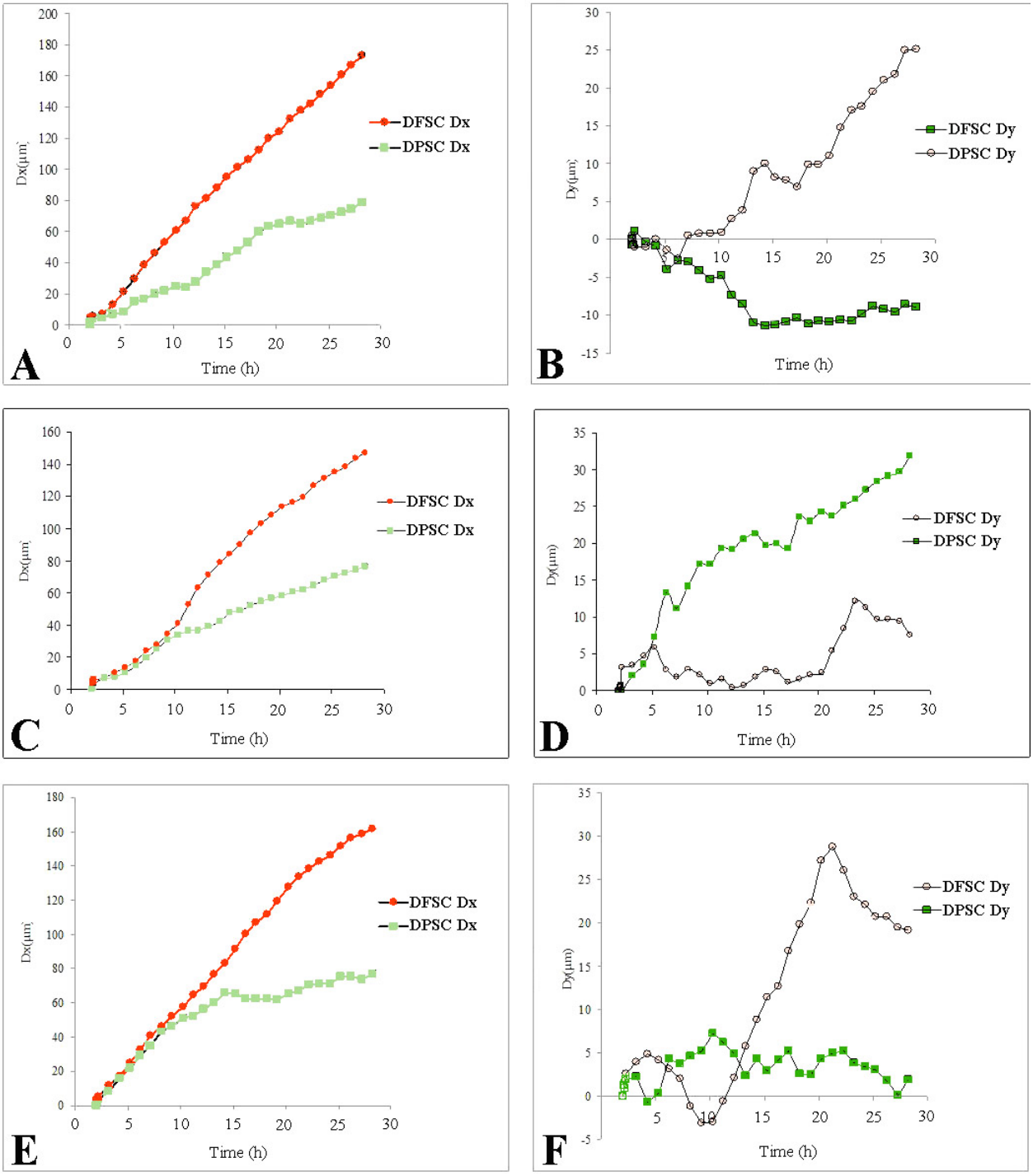

Fig. 2. Cell motility in co-culture of DPSC and DFSC. The graphs show the cell tracker analyses of DPSC and DFSC co-cultured at a ratio 1:1 along x **(A)** and y axis **(B)**, at a ratio 10:1 along x **(C)** and y axis **(D)**, and at ratio 1:10 along x (**E**) and y axis (**F**).

each qRT-PCR primer pair, and corresponding sequences were designed by Beacon Designer™ software. The primer sequences are shown in Table 1. All reactions were carried out in triplicate, and the expression of specific mRNA relative to the control was determined after normalisation with respect to GAPDH gene. The fold-change of test gene mRNA expression was calculated by considering the efficiency of each primer (between 80 and 110 %), and by using the comparative threshold method (ΔΔCt = difference of ΔCt between co-cultured cells and single cell populations used as controls). The results were expressed as normalised fold expression, calculated by the ratio of crossing points of amplification curves of several genes and internal standard, by using the Bio-Rad iQ™5 software (Bio-Rad Laboratories Srl).

Results

Colony efficiency assays and proliferation potential

To assess the proliferation and clonogenic potential of DPSC and DFSC, we performed a limiting dilution

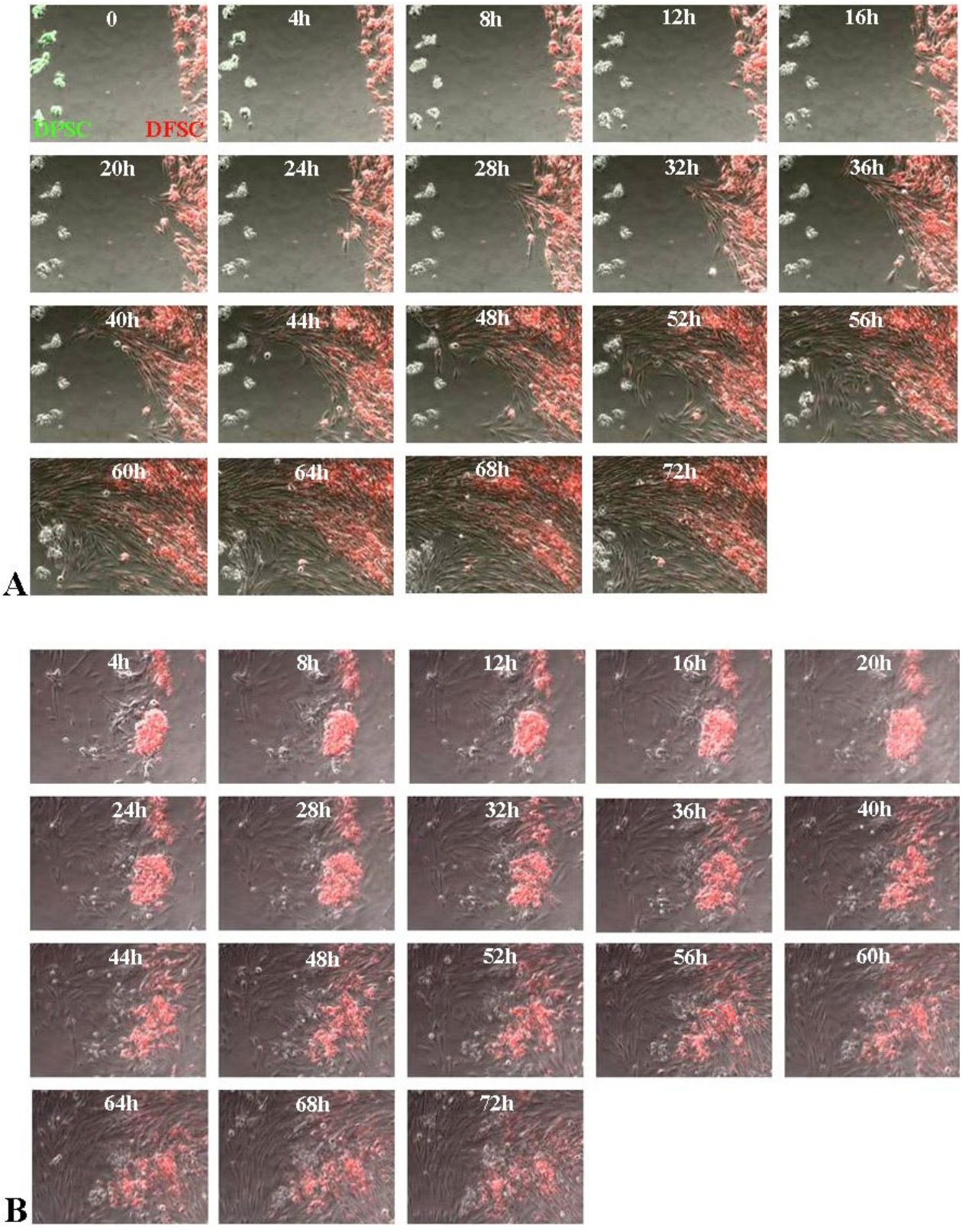

Fig. 3. Time-lapse panel images. (**A**) DPSC and DFSC in co-culture at a ratio $1.7x10^2$ cells/mm^2/$1.7x10^3$ cells/mm^2 (1:10). Note that DFSC completely surround DPSC. (**B**) DPSC and DFSC in co-culture at a ratio $1.7x10^2$ cells/mm^2/$1.7x10^2$ cells/mm^2 (1:1). Note that DPSC do not move, building up a wall slide by slide. Merge micrographs (bright field, FITC and TRITC) captured at 4 h intervals.

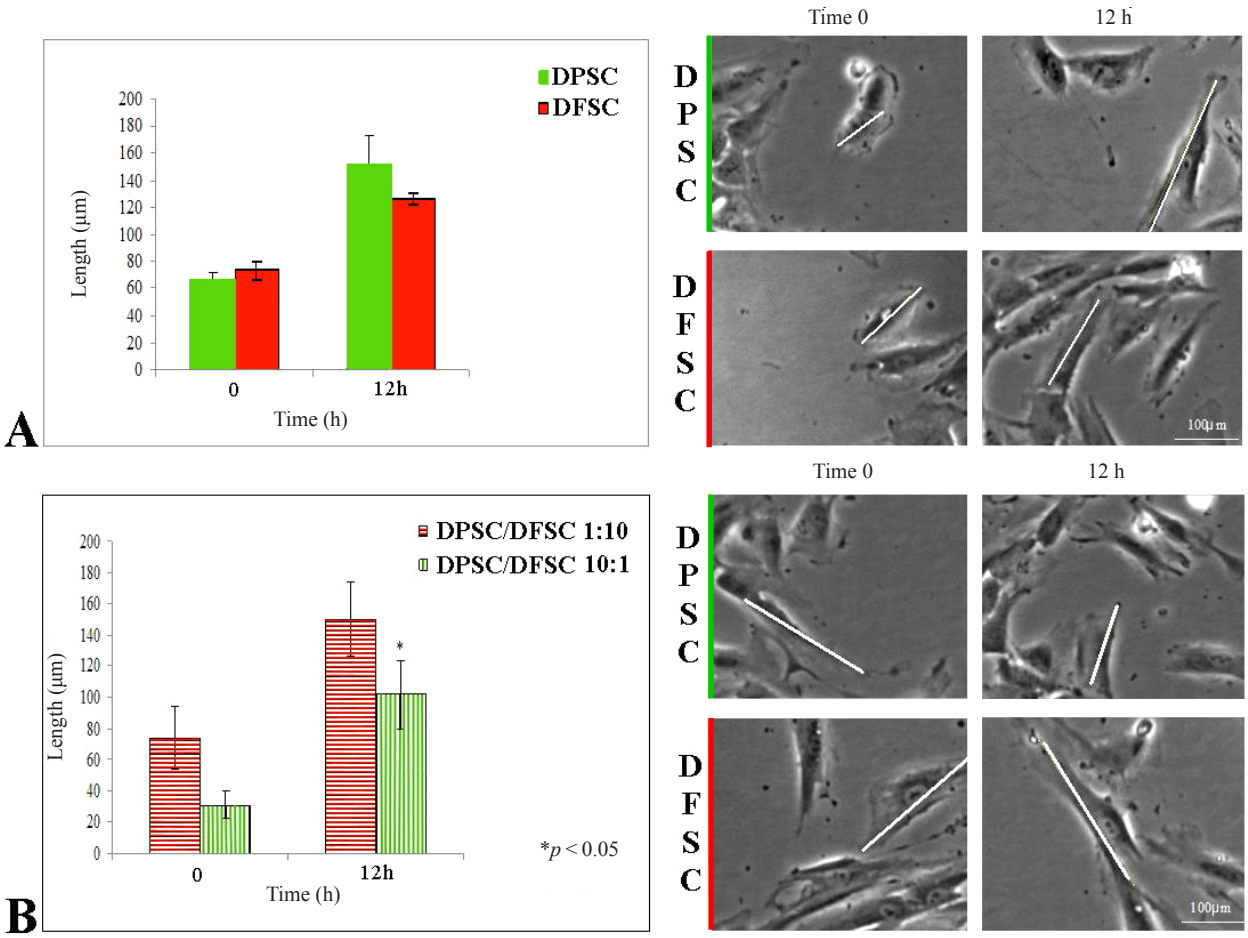

Fig. 4. Cell dimension analysis. (**A**) Major axis averaged sizes during time of DPSC and DFSC cultured alone, demonstrating that in both populations cells become elongated. (**B**) Major axis averaged dimensions during time of DPSC and DFSC co-cultured at a ratio 1:10 and 10:1. In both cases DFSC significantly ($p < 0.05$) increase their sizes, whereas DPSC shorten them.

assay. After 3 weeks of culture, 92 % of the wells (442 of 480), which were initially plated with one or two DPSC, contained colonies (formed of >50 cells), with a doubling time of ≈2.6 d. For DFSC, 93 % of the wells (445 of 480) contained colonies with a doubling time of ≈2.4 d.

Cytometry assay

To isolate DPSC, dental pulp cells were detected and sorted for co-expression of CD34 and CD117 markers at passage 1 of culture. The positivity of these antigens was ~15 % of the total cell population. To isolate DFSC, dental follicle cells were detected and sorted for SSEA4 expression at passage 1 of culture. The percentage of SSEA4 positivity was ~80 %. DPSC and DFSC were sorted and then used for time-lapse and RT-PCR experiments.

Time-lapse observations

In order to observe the behaviour of DPSC and DFSC *in vitro* (i.e. cell movement, orientation, morphology and velocity), time-lapse video-microscopy analyses were performed on 6-8 tracks for each image (4 fields of view per well). These two stem cell populations were cultured either alone or together in various cell ratios. As a control, $1x10^4$ DPSC or DFSC per well (200 mm^2) were used. In co-cultures, DPSC and DFSC were seeded separately using a spacer (Culture-Insert). In a first set of experiments, the cell ratio was fixed at 1:1, 1:10 and 10:1 along x and y axes, and each stem cell population was stained with a different dye (green colour for DPSC, red colour for DFSC). Analyses of the DPSC and DFSC behaviour were performed on the side of the well containing the greater number of cells ($1.7x10^3$ cells/mm^2).

Cell movement and orientation

When cultured alone, DPSC and DFSC moved trivially for short distances and often returned in their point of origin (Fig. 1A and B). More precisely, DPSC showed random and small motility through the x or y axes (Fig. 1A), while most of the DFSC displayed circular movements within a small perimeter (Fig. 1B). The behaviour of DPSC and DFSC changed significantly in the co-culture experiments, and this was dependent on both the number and ratio of cultured cells.

DPSC/DFSC 1:1 co-culture

A substantial and interesting change of cell movements was observed when the two stem cell populations were seeded at the same density. In this case, a better linear progression was detected for DFSC movements along both coordinates (x and y axis), as confirmed by curve analyses, although

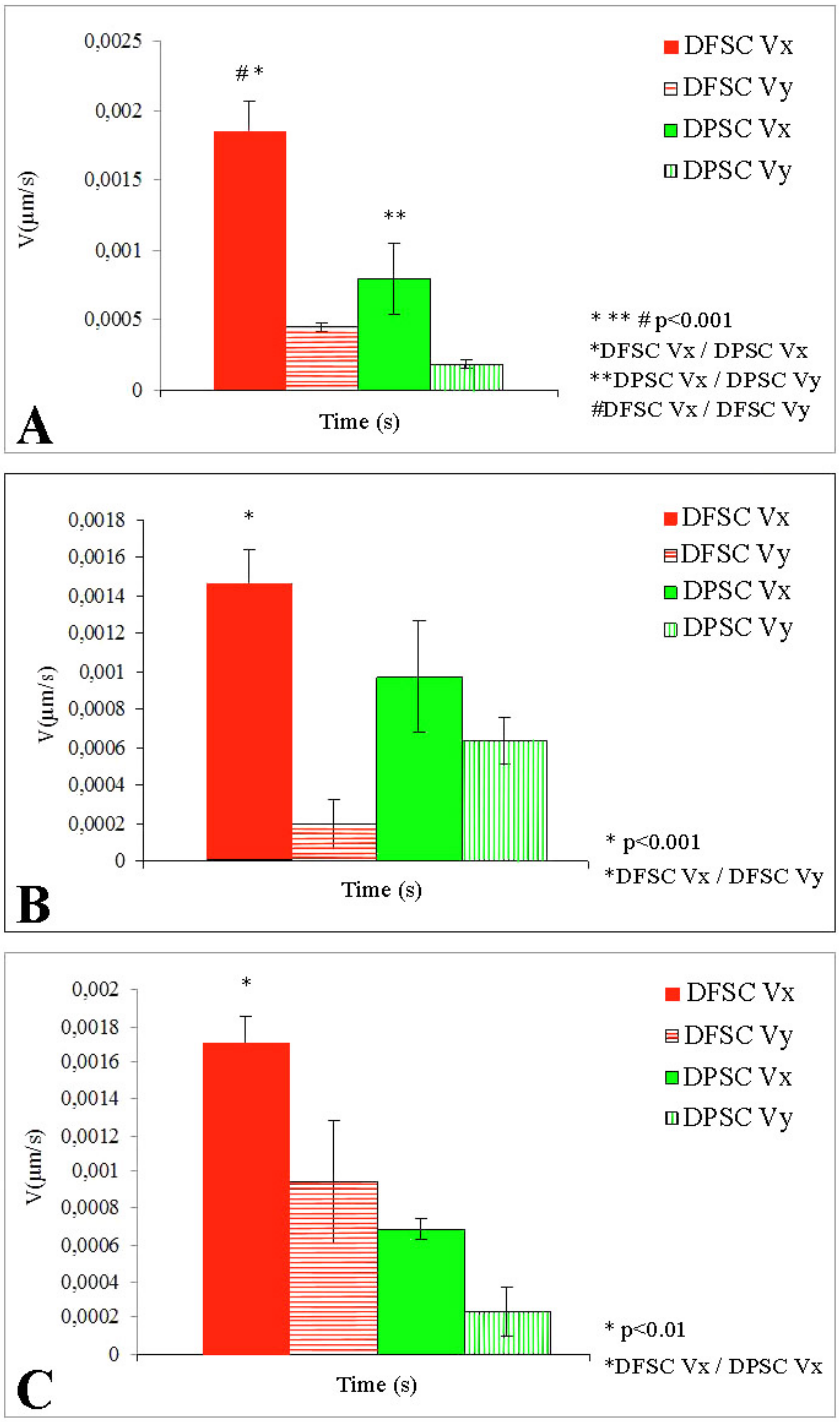

Fig. 5. Cell velocity analysis. DPSC and DFSC in co-culture at a ratio 1:10 (**A**), 10:1 (**B**), and 1:1 (**C**). DFSC result in 2-fold horizontal velocity in comparison with DPSC and even 3-fold along the vertical axis. Data represent the mean ± SD of three independent experiments. The groups are significantly different according to Student's *t*-test ($p < 0.001$).

DFSC moved oppositely to DPSC along the y axis. The track of DPSC along the x axis (Dx) was more linear than the track along the y axis (Dy) (Fig. 2A and B).

DPSC/DFSC 10:1 co-culture

When DPSC and DFSC were co-cultured at a 10:1 ratio, both cell populations exhibited a linear progression along the x axis (Dx), while cell movements were highly irregular along the y axis. More precisely, DPSC showed only short irregular movements, and remained practically in the same position. In contrast, DFSC covered a long distance, and although their initial movement was irregular it finally became linear and unidirectional (Fig. 2C and D).

DPSC/DFSC 1:10 co-culture

When DPSC and DFSC were co-cultured at the 1:10 ratio, both cell types showed a linear progression of their movements along the x axis (Dx), while their movements were irregular along the y axis (Dy). However, DFSC moved more than DPSC along the y axis (Fig. 2E and F).

Image analyses

The observation of the panels (Fig. 3) confirmed that there is an interaction between DFSC and DPSC in terms of motility. We observed that DFSC movement was mainly directed along the horizontal axis on the way to surround the DPSC, almost embracing or moving them out, occupying the whole territory in a short period of time (Fig. 3A). In contrast, the movement of DPSC was comparable to a plug flow along the x axis, being much slower than that of DFSC. The images clearly showed that DPSC migration was less directional than the DFSC migration (Fig. 3B). At the initial stages of the co-culture (day 1), we have observed "pioneer" DFSC moving towards DPSC (Fig. 3A). These "pioneer cells" quickly returned to the DFSC territory once they approached or contacted the DPSC. This step may represent a stimulatory signal to the whole DFSC population for starting their migration towards DPSC (see also supplementary movies 1, 2 and 3 on the kinetics of DFSC "red cells" and DPSC "green cells" – on the web page for this paper).

Cell morphology

Another important point that has been addressed in this study concerns the morphological modifications (i.e. shapes and dimensions) of DPSC and DFSC when cultured either alone or together. We have observed that, when cultured alone, both DPSC and DFSC (which are slightly longer than the DPSC at the starting point) changed their shapes during movement and became considerably flattened and elongated after 12 h (Fig. 4A). More precisely, cells increased their length by up to 1.7-fold (Table 2). In all co-culture variants, DFSC significantly ($p < 0.05$) increased their size (2-fold higher; Table 2), became elongated and acquired a spindle shape (Fig. 4B). The enveloping attitude of DFSC seemed to induce this restricted elongation of DPSC in co-culture: DPSC decreased in size ($p < 0.05$) and assumed a polygonal shape (Fig. 4B).

Cell velocity

Concerning cell velocity, in co-cultures of DPSC and DFSC at a ratio 1:10, DFSC were twice as fast as DPSC ($p < 0.001$) on the x axis. On the y axis, cell movement was slower when compared with the x axis but also, in this case, DFSC were faster than DPSC (Fig. 5A). In co-cultures of DPSC and DFSC at a ratio 10:1, DPSC v_y was greater than DFSC v_y (Fig. 5B), while at a ratio 1:1, DFSC were significantly faster than DPSC, in both x and y axes (Fig. 5C). Specifically, DFSC v_x resulted in a 2-fold increase over DPSC horizontal velocity, and even 3-fold along the vertical axis (Fig. 5C). This confirms that DFSC are more active when compared with DPSC.

Real-time PCR observations

The expression of several genes that are regulators of cell proliferation, migration and differentiation during odontogenesis was evaluated by RT-PCR in our culture system (Table 1). We have used the comparative threshold method (ΔΔCt = difference of ΔCt between co-cultured cells and single cell populations used as controls) and the results were expressed as normalised fold expression, calculated by the ratio of crossing points of amplification curves of several genes and internal standard. *TWIST1* was markedly up-regulated in DPSC at 24 h, while it was down-regulated at 48 h (Fig. 6A). In contrast, *MSX1* and *RUNX2* expression showed a strong down-regulation at 24 h that changed into a significant up-regulation at 48 h (Fig. 6A). The expression of *SFRP1* was up-regulated at 24 h and 48 h of culture (Fig. 6A). *ADAM28* expression was drastically up-regulated in DPSC after 48 h of culture (Fig. 6A).

Analysis of the same profiles of gene expression in co-cultures with prevalent DFSC has shown that the expression of *TWIST1* was slightly decreased at 24 h and 48 h of culture, whereas expression of *MSX1* and *ADAM28* were significantly up-regulated after 48 h of culture (Fig. 6B). *RUNX2* expression was initially decreased (24 h) and thereafter increased (48 h). *SFRP1* expression was slightly decreased after 48 h of culture.

Discussion

Cell-based dental tissue repair or regeneration is an attractive approach that complements traditional restorative and surgical techniques for replacement of injured or pathologically damaged tissues. Such therapeutic approaches often require large numbers of stem cells that after injection migrate towards the injury site following a gradient of directional stimuli. However, a frequent problem of these therapies is the integration of the injected stem cells with the injured or pathological site (Mitsiadis *et al.,* 2012). A deeper appreciation of the mechanisms involved in stem cell behaviour will certainly facilitate cell-based treatments for tissue repair.

In this study, we investigated the *in vitro* behaviour of two different dental stem cell populations, DPSC and DFSC, using time-lapse imaging. This technique offers an ideal platform for understanding stem cell kinetics in response to injuries and cell-based therapeutic interventions (Aman and Piotrowski, 2010; Wang *et al*., 2008). The ability of DPSC and DFSC to actively migrate, either randomly or directionally, and fill the empty space during dental tissue repair is an important biological parameter in pathological contexts (Huth *et al*., 2011). The vast majority of DPSC and DFSC did not show any peculiar or systematic migratory behaviour when cultured separately *in vitro*. Both DPSC and DFSC exhibit tumbling phases: DPSC showed a limited and random migratory activity, while DFSC followed a circular mode of movement to explore their local environment and often returned to their

Table 2. DPSC and DFSC dimensions when cultured either alone or together.

Major axis length	**T = 0**	**T = 12** h
DPSC	67.1 ± 4.1	151.5 ± 21.7
DFSC	73.6 ± 7.3	126.3 ± 4.4
DPSC/DFSC 10:1	67.1 ± 8.7	87.8 ± 8.2
DPSC/DFSC 1:10	73.7 ± 20.1	150.0 ± 23.1

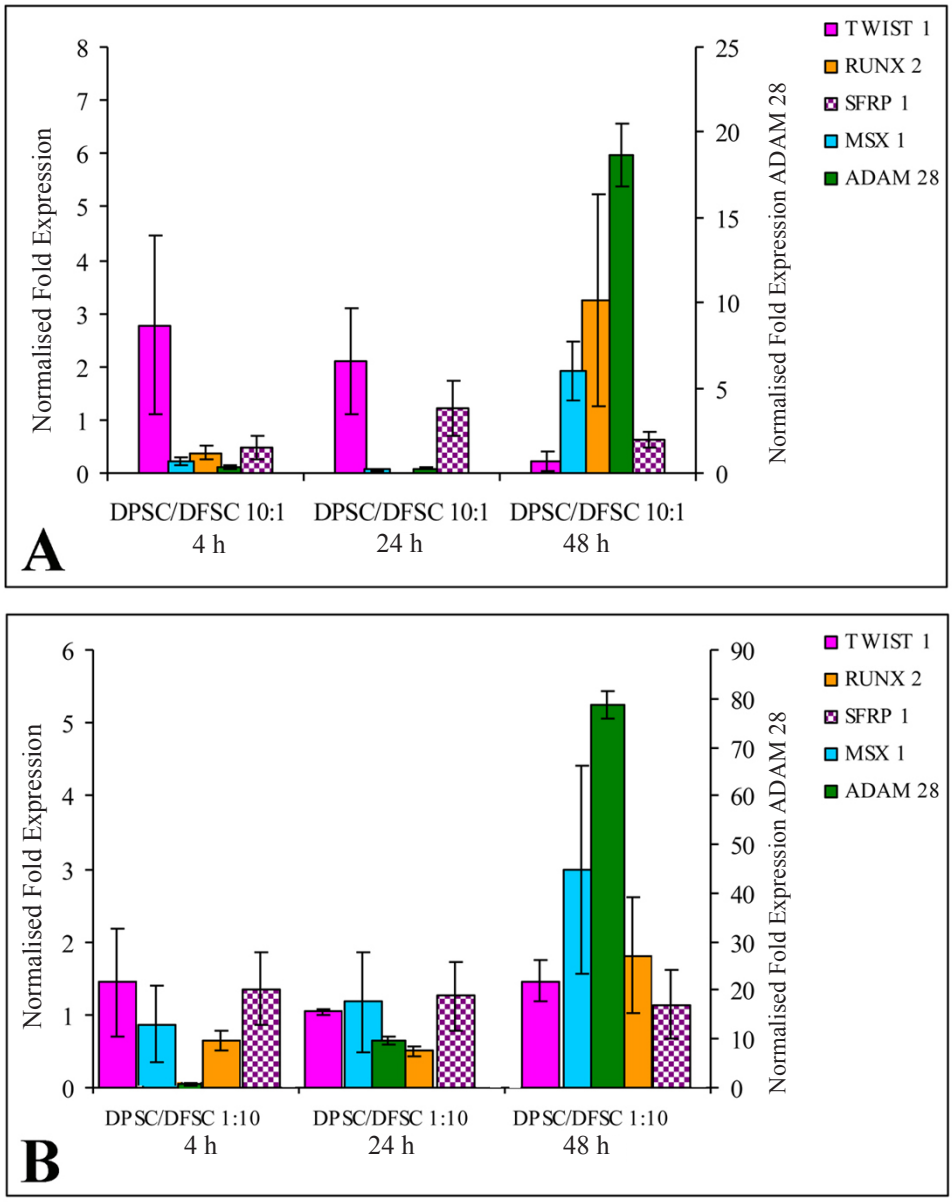

Fig. 6. Gene expression analysis. Images showing normalised fold expression for the genes *TWIST 1*, *MSX 1*, *RUNX 2, SFRP1* and *ADAM 28* in co-cultures of DPSC and DFSC containing (**A**) a prevalent population of DPSC (DPSC/DFSC at a ratio 10:1) and (**B**) a prevalent population of DFSC (DPSC/DFSC at a ratio 1:10).

point of origin. It has been shown that the tumbling phase is cell-autonomous and independent of directional cues such as chemokine signalling (Reichman-Fried *et al*., 2004). DPSC and DFSC motion was tortuous, probably due to the frequent reversals in directions caused by successive protrusions with opposing orientations. Reduction of direction reversals makes cell movement less tortuous and cells adopt an oriented trajectory towards a chemical or electric signal (Aman and Piotrowski, 2010; Arocena *et al*., 2010; Zhao *et al*., 2011a). Indeed, the co-culture of DPSC and DFSC stimulated their migration abilities, particularly when these two stem cell populations were seeded in equal cell numbers. DPSC showed limited proliferation and migration capabilities, and adopted a non-directed random "walk". In contrast, DFSC exhibited quick spreading and directionally migrated towards DPSC. Pre-migratory DFSC started to extend protrusions for guidance and traction in a non-directed fashion. Early DFSC migration serves to populate the empty Petri-dish space, whereas late migration apparently relies on directional cues emanating from DPSC. It has been shown that the direction of late cell migration is established by gradients of repulsive and/or attractant molecules diffusing from the target tissue (Aman and Piotrowski, 2010; Kuriyama and Mayor, 2008). In addition to guidance cues, cell movement requires physical forces that are established through interactions of cells with their environment (Grashoff *et al*., 2010; Hoffman *et al*., 2011). In collectively migrating cells, only a few pioneer (or leading) cells perceive guidance cues (Aman and Piotrowski, 2010; Binamé *et al*., 2010; Friedl and Gilmour, 2009). Indeed, in our co-culture system DFSC started to migrate collectively after getting spatial and directional information from pioneer cells. Migration of pioneer DFSC initially occurred with no interactions with

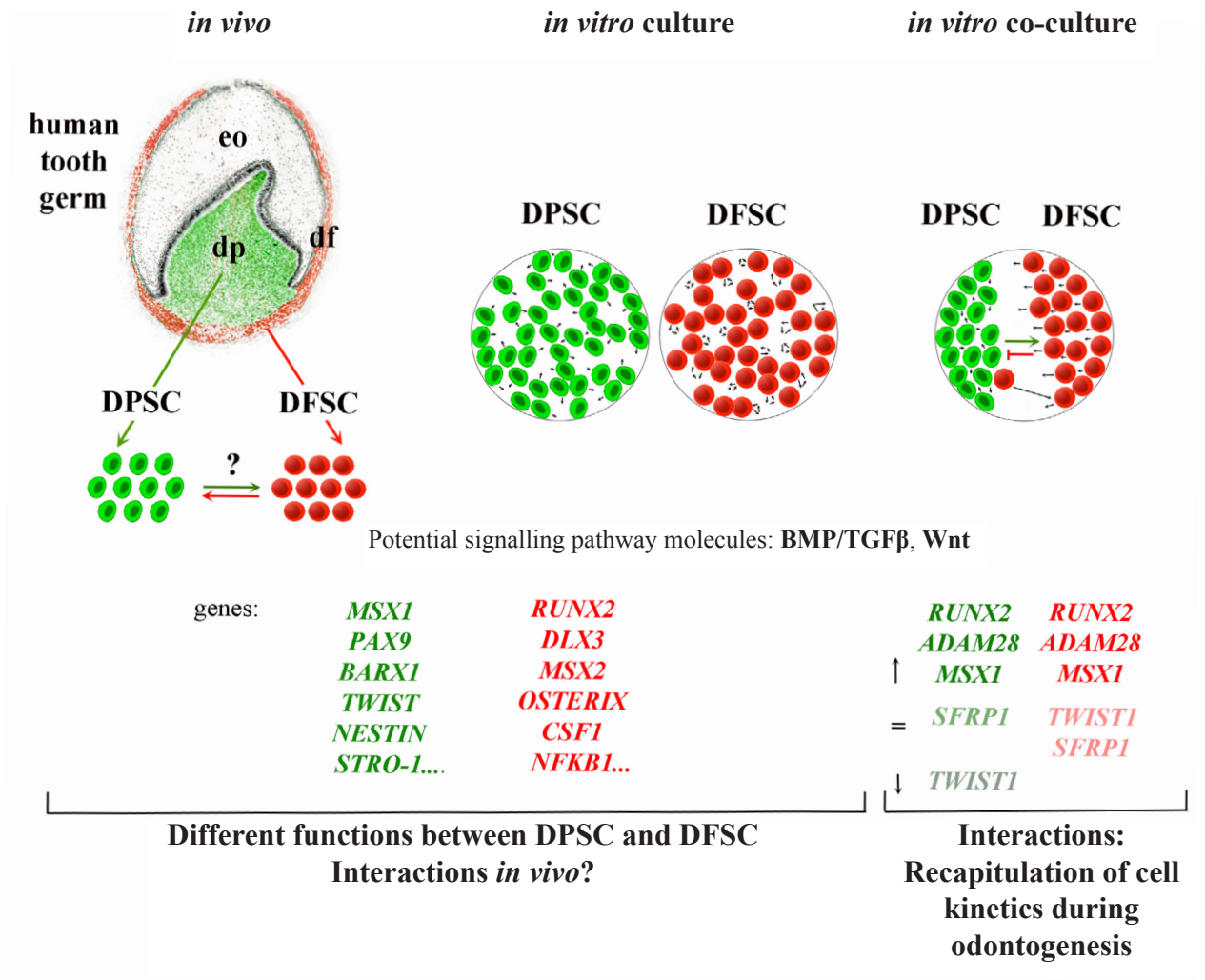

Fig. 7. Schematic representation showing DPSC and DFSC cultured alone or together *in vitro*. DPSC are isolated from the dental pulp (dp, green colour) and DFSC from the dental follicle (df, red colour), which surrounds both the enamel organ (eo) and dental pulp of the developing tooth. *In vivo*, the functions of these two stem cell populations are tissue specific, DPSC control repair/regeneration of the dentin-pulp complex, while DFSC operate for the homeostasis and repair of the periodontium. Genes are differentially expressed in dental pulp (e.g. *MSX1, PAX9* etc., in green) and dental follicle cells (*DLX3, MSX2* etc., in red). Signalling pathways such as BMP/TGFβ and Wnt regulate the expression of these genes. It is not yet known if there are interactions between DPSC and DFSC *in vivo* after tooth eruption. However, these two stem cell populations interact in co-cultures: DFSC migrate fast (small arrows) towards DPSC (probably due to DPSC-derived attractant signals, green arrow) and finally embrace them. In contrast, DPSC stay on place (possibly because of DFSC-derived repulsive signals, red symbol). This movement recapitulates the kinetics of the dental follicle and dental papilla cells during odontogenesis. Expression of several genes was up-regulated (up looking arrow), unchanged (=), or down-regulated (down looking arrow) in co-cultured DPSC and DFSC.

the trailing DFSC. These pioneer DFSC travel until they reach the DPSC territory, and immediately after contacting DPSC they move back to their point of origin where they transmit the acquired information for an oriented DFSC migration towards DPSC. Shortly afterwards, the trailing DFSC migrate fast as cohorts, occupy most of the empty territory, and finally embrace and restrain the DPSC. This DFSC motion closely resembles that of dental follicle cells during odontogenesis, where they encircle the enamel organ and the dental papilla of the developing tooth germ (Fig. 7). Thus, a step of embryonic tooth development was reiterated in the *in vitro* co-culture model. The fact that DFSC are isolated from a developing and not yet differentiated tissue that surrounds the not erupted tooth germ might explain the greater migration activity of DFSC compared with DPSC, which are isolated from the mature pulp tissue. Although collectively migrating cells often lose their motility as they reach their target (Aman and Piotrowski, 2010), DFSC at the end of the migratory pathway were still motile.

Tooth damage is the result of different mechanisms of injury combined with the incapacity for intrinsic dental tissue repair. In autologous stem cell-based approaches, patient-related factors, such as the healthy or pathological condition of the dental pulp and periodontal ligament, may influence the quality of the therapeutic preparation

(Catón *et al*., 2011). Regeneration of dental pulp does not yet constitute a treatment modality in the clinical field of endodontics. The use of DPSC holds a strong promise in this respect. These cells can differentiate into odontoblasts that will form new dentin, endothelial cells that would support the re-vascularisation and neurons that will re-innervate the regenerated pulp tissue (Catón *et al*., 2011; Nakashima and Iohara, 2011). If DPSC are injected into the injured area they do not have to migrate fast or over long distances since the pulp space is delimited by the dental mineral structures, thus making DPSC the most appropriate choice for pulp regeneration. Another major challenge in dentistry is the regeneration of the disease-affected periodontal tissues (i.e. tooth root cementum, alveolar bone and periodontal ligament), in a manner that recapitulates embryonic tooth development. Periodontium acts as a suspension for the tooth, adapting to the mechanical and masticatory loads. DFSC are capable of differentiating into all cell types composing the periodontal tissues, they can travel fast and far away from the site of injection, thus ensuring a quick and appropriate tissue recovery.

To improve the use of DPSC for dentin repair and DFSC for periodontal regeneration, it is important to replicate the permissive signals that initiate the differentiation of pulp cells into odontoblasts and of follicle cells into periodontal ligament fibroblasts, respectively (Fig. 7). Such a strategy is likely to restore better the damaged soft and hard dental tissues. WNT proteins are regulators of cell proliferation, migration and differentiation during tooth development and regeneration (Dassule and McMahon, 1998; Sarkar and Sharpe, 2000), and have a great therapeutic potential for hard tissue remodelling and regeneration after injury (Long, 2011; Reya and Clevers, 2005). Recent clinical therapeutic strategies focus on the inhibition of the WNT antagonists such as the Secreted-Frizzled Related Protein-1 (SFRP1), which is expressed in dental follicle cells during odontogenesis (Liu and Wise, 2007; Liu *et al*., 2012; Morsczeck and Schmalz, 2010). *SFRP1* expression is regulated by TGFβ/BMP signalling molecules (Li *et al*., 2011a) that are involved in dental cell specification and differentiation (Huang *et al*., 2010; Ko *et al*., 2007; Mitsiadis and Graf, 2009; Thesleff *et al*., 1995). For example, aberrant BMP signalling affects odontoblast differentiation and induces ectopic bone formation that replaces normal dentin (Li *et al*., 2011b). In dental mesenchyme, BMP4 regulates the expression of *MSX1* (Vainio *et al*., 1993), which is a crucial gene for tooth formation since its point mutation in humans causes partial anodontia (Vastardis *et al*., 1996). The interplay between TGFβ/BMP and WNT signalling pathways is needed to ensure dental stem cell specification during tooth repair (Du *et al*., 2012; Silvério *et al*., 2012). In our co-culture model, expression of *MSX1* was significantly up-regulated in both DFSC and DPSC, indicating that these two stem cell populations have a great capacity to form dental structures. TWIST1 could promote the odontogenic potential of DPSC by antagonising the function of RUNX2 that favours osteoblast differentiation (Li *et al*., 2011b; Pan *et al*., 2010; Zhao *et al*., 2005). However, the co-culture of DPSC and DFSC resulted in down-regulation of *TWIST1* and significant up-regulation of *RUNX2* expression, suggesting that DPSC lose their capacity to differentiate into odontoblasts in the presence of DFSC. *SFRP1* expression in DFSC was not altered when DFSC were co-cultured with various ratios of DPSC, indicating that DFSC retain their potential to form periodontal tissues in the presence of DPSC. Recent studies have shown that *ADAM28* overexpression has opposite effects on DPSC and DFSC: ADAM28 promotes proliferation of DFSC (Zhao *et al*., 2010), while it inhibits proliferation and induces differentiation of DPSC (Zhao *et al*., 2011b). In co-cultures, *ADAM28* expression was increased dramatically in both DFSC and DPSC, indicating that the proliferative potential resides within DFSC.

Conclusions

In conclusion, our observations have highlighted that DFSC and DPSC behave differently in co-culture from when cultured alone and compete with each other in order to replenish the free territory. The fact that DFSC migrate faster than DPSC and dominate them establishes new criteria for the selection and use of specific stem cell populations for the repair and regeneration of particular dental tissues in the clinic. These results, based on dental stem cell lines, could be extrapolated for the controlled regeneration of organs that have important vital functions.

Acknowledgements

The authors wish to thank the European Science Foundation (ESF) COST Action 1005 NAMABIO, where T.A. Mitsiadis is a management committee member and the representative of Switzerland. This study was supported by the Swiss National Foundation (SNSF) grants 31003A_135633 and 3100A0_118332 (T.A.M.), and by funds from the University of Zurich (T.A.M., A.W.), Second University of Naples (Ateneo 2010) (G.P.), and PON EU Funds "PROMETEO" (01_02834). The authors wish to thank Prof. Mario de Rosa, Director of the CSGA (Centro Servizi Grandi Apparecchiature, Ateneo SUN Napoli, Italy) for providing the time-lapse facilities, Prof. Stefano Guido and Prof. Marino Simeone for helping with the software for image analysis and experimental set-up. We wish to confirm that there are no known conflicts of interest associated with this publication and there has been no significant financial support for this work that could have influenced its outcome.

References

Aman A, Piotrowski T (2010) Cell migration during morphogenesis. Dev Biol **341**: 20-33.

Arocena M, Zhao M, Collinson JM, Song B (2010) A time-lapse and quantitative modelling analysis of neural stem cell motion in the absence of directional cues and in electric fields. J Neurosci Res **88**: 3267-3274.

Bai Y, Bai Y, Matsuzaka K, Hashimoto S, Kokubu E, Wang X, Inoue T (2010) Formation of bone-like tissue by

dental follicle cells co-cultured with dental papilla cells. Cell Tissue Res **342**: 221-231.

Binamé F, Pawlak G, Roux P, Hibner U (2010) What makes cells move: requirements and obstacles for spontaneous cell motility. Mol Biosyst **6**: 648-661.

Bluteau G, Luder HU, De Bari C, Mitsiadis TA (2008) Stem cells for tooth engineering. Eur Cell Mater **16**: 1-9.

Catón J, Bostanci N, Remboutsika E, De Bari C, Mitsiadis TA (2011) Future dentistry: cell therapy meets tooth and periodontal repair and regeneration. J Cell Mol Med **15**: 1054-1065.

Dassule HR, McMahon AP (1998) Analysis of epithelial-mesenchymal interactions in the initial morphogenesis of the mammalian tooth. Dev Biol **202**: 215-227.

d'Aquino R, Graziano A, Sampaolesi M, Laino G, Pirozzi G, De Rosa A, Papaccio G (2007) Human postnatal dental pulp cells co-differentiate into osteoblasts and endotheliocytes: a pivotal synergy leading to adult bone tissue formation. Cell Death Differ **14**: 1162-1171.

d'Aquino R, De Rosa A, Lanza V, Tirino V, Laino L, Graziano A, Desiderio V, Laino G, Papaccio G (2009) Human mandible bone defect repair by the grafting of dental pulp stem/progenitor cells and collagen sponge biocomplexes. Eur Cell Mater **18**: 75-83.

d'Aquino R, Tirino V, Desiderio V, Studer M, De Angelis GC, Laino L, De Rosa A, Di Nucci D, Martino S, Paino F, Sampaolesi M, Papaccio G (2011) Human neural crest-derived postnatal cells exhibit remarkable embryonic attributes either *in vitro* or *in vivo*. Eur Cell Mater **21**: 304-316.

Diep L, Matalova E, Mitsiadis TA, Tucker AS (2009) Contribution of the tooth bud mesenchyme to alveolar bone. J Exp Zool B Mol Dev Evol **312B**: 510-517.

Du Y, Ling J, Wei X, Ning Y, Xie N, Gu H, Yang F (2012) Wnt/β-catenin signaling participates in cementoblast/osteoblast differentiation of dental follicle cells. Connect Tissue Res **53**: 390-397.

Friedl P, Gilmour D (2009) Collective cell migration in morphogenesis, regeneration and cancer. Nat Rev Mol Cell Biol **10**: 445-457.

Grashoff C, Hoffman BD, Brenner MD, Zhou R, Parsons M, Yang MT, McLean MA, Sligar SG, Chen CS, Ha T, Schwartz MA (2010) Measuring mechanical tension across vinculin reveals regulation of focal adhesion dynamics. Nature **466**: 263-266.

Graziano A, d'Aquino R, Laino G, Proto A, Giuliano MT, Pirozzi G, De Rosa A, Di Napoli D, Papaccio G (2008) Human CD34+ stem cells produce bone nodules *in vivo*. Cell Prolif **41**: 1-11.

Gronthos S, Mankani M, Brahim J, Robey PG, Shi S (2000) Postnatal human dental pulp stem cells (DPSCs) *in vitro* and *in vivo*. Proc Natl Acad Sci USA **97**: 13625-13630.

Handa K, Saito M, Tsunoda A, Yamauchi M, Hattori S, Sato S, Toyoda M, Teranaka T, Narayanan AS (2002) Progenitor cells from dental follicle are able to form cementum matrix *in vivo*. Connect Tissue Res **43**: 406-408.

Hoffman BD, Grashoff C, Schwartz MA (2011) Dynamic molecular processes mediate cellular mechanotransduction. Nature **475**: 316-323.

Huang X, Xu X, Bringas P Jr, Hung YP, Chai Y (2010) Smad4-Shh-Nfic signaling cascade-mediated epithelial-mesenchymal interaction is crucial in regulating tooth root development. J Bone Miner Res **25**: 1167-1178.

Huth J, Buchholz M, Kraus JM, Mølhave K, Gradinaru C, v Wichert G, Gress TM, Neumann H, Kestler HA (2011) TimeLapseAnalyzer: multi-target analysis for live-cell imaging and time-lapse microscopy. Comput Methods Programs Biomed **104**: 227-234.

Ko SO, Chung IH, Xu X, Oka S, Zhao H, Cho ES, Deng C, Chai Y (2007) Smad4 is required to regulate the fate of cranial neural crest cells. Dev Biol **312**: 435-447.

Kuriyama S, Mayor R (2008) Molecular analysis of neural crest migration. Philos Trans R Soc Lond B Biol Sci **363**: 1349-1362.

Laino G, d'Aquino R, Graziano A, Lanza V, Carinci F, Naro F, Pirozzi G, Papaccio G (2005) A new population of human adult dental pulp stem cells: a useful source of living autologous fibrous bone tissue (LAB). J Bone Miner Res **20**: 1394-1402.

Laird DJ, von Andrian UH, Wagers AJ (2008) Stem cell trafficking in tissue development, growth, and disease. Cell **132**: 612-630.

Lee-MacAry AE, Ross EL, Davies D, Laylor R, Honeychurch J, Glennie MJ, Snary D, Wilkinson RW (2001) Development of a novel flow cytometric cell-mediated cytotoxicity assay using the fluorophores PKH-26 and TO-PRO-3 iodide. J Immunol Methods **252**: 83-92.

Li J, Huang X, Xu X, Mayo J, Bringas P Jr, Jiang R, Wang S, Chai Y (2011a) SMAD4-mediated WNT signaling controls the fate of cranial neural crest cells during tooth morphogenesis. Development **138**: 1977-1989.

Li Y, LuY, MaciejewskaI, GallerK, CavenderA, D'SouzaRN (2011b) *TWIST1* promotes odontoblast differentiation. Adv Dent Res **23**: 280-284.

Liu D, Wise GE (2007) A DNA microarray analysis of chemokine and receptor genes in the rat dental follicle--role of secreted frizzled-related protein-1 in osteoclastogenesis. Bone **41**: 266-272.

Liu D, Yao S, Wise GE (2012) Regulation of SFRP-1 expression in the rat dental follicle. Connect Tissue Res **53**: 366-372.

Long F (2011) Building strong bones: molecular regulation of the osteoblast lineage. Nat Rev Mol Cell Biol **13**: 27-38.

Lovschall H, Mitsiadis TA, Poulsen K, Jensen KH, Kjeldsen AL (2007) Coexpression of Notch3 and Rgs5 in the pericyte-vascular smooth muscle cell axis in response to pulp injury. Int J Dev Biol **51**: 715-721.

Mitsiadis TA, Graf D (2009) Cell fate determination during tooth development and regeneration. Birth Defects Res C Embryo Today **87**: 199-211.

Mitsiadis TA, Luder H (2011) Genetic basis for tooth malformations: from mice to men and back again. Clin Genet **80**: 319-329.

Mitsiadis TA, Rahiotis C (2004) Parallels between tooth development and repair: conserved molecular mechanisms following carious and dental injury. J Dent Res **83**: 896-902.

Mitsiadis TA, Feki A, Papaccio G, Catón J (2011) Dental pulp stem cells, niches, and notch signaling in tooth injury. Adv Dent Res **23**: 275-279.

Mitsiadis TA, Woloszyk A, Jiménez-Rojo L (2012) Nanodentistry: combining nanostructured materials and stem cells for dental tissue regeneration. Nanomedicine **7**: 1-11.

Miura M, Gronthos S, Zhao M, Lu B, Fisher LW, Robey PG, Shi S (2003) SHED: stem cells from human exfoliated deciduous teeth. Proc Natl Acad Sci USA **100**: 5807-5812.

Morsczeck C, Schmalz G (2010) Transcriptomes and proteomes of dental follicle cells. J Dent Res **89**: 445-456.

Morsczeck C, Götz W, Schierholz J, Zeilhofer F, Kühn U, Möhl C, Sippel C, Hoffmann KH (2005) Isolation of precursor cells (PCs) from human dental follicle of wisdom teeth. Matrix Biol **24**: 155-165.

Nakashima M, Iohara K (2011) Regeneration of dental pulp by stem cells. Adv Dent Res **23**:313-319.

Okumoto S (2010) Imaging approach for monitoring cellular metabolites and ions using genetically encoded biosensors. Curr Opin Biotechnol **21**: 45-54.

Pan K, Sun Q, Zhang J, Ge S, Li S, Zhao Y, Yang P (2010) Multilineage differentiation of dental follicle cells and the roles of *RUNX2* over-expression in enhancing osteoblast/cementoblast-related gene expression in dental follicle cells. Cell Prolif **43**: 219-228.

Papaccio G, Graziano A, d'Aquino R, Graziano MF, Pirozzi G, Menditti D, De Rosa A, Carinci F, Laino G (2006) Long-term cryopreservation of dental pulp stem cells (SBP-DPSCs) and their differentiated osteoblasts: a cell source for tissue repair. J Cell Physiol **208**: 319-325.

Reichman-Fried M, Minina S, Raz E (2004) Autonomous modes of behavior in primordial germ cell migration. Dev Cell **6**: 589-596.

Reya T, Clevers H (2005) Wnt signalling in stem cells and cancer. Nature **434**: 843-850.

Sarkar L, Sharpe PT (2000) Inhibition of Wnt signaling by exogenous Mfrzb1 protein affects molar tooth size. J Dent Res **79**: 920-925.

Silvério KG, Davidson KC, James RG, Adams AM, Foster BL, Nociti FH Jr, Somerman MJ, Moon RT (2012) Wnt/β-catenin pathway regulates bone morphogenetic protein (BMP2)-mediated differentiation of dental follicle cells. J Periodontal Res **47**: 309-319.

Smith AG (2001) Embryo-derived stem cells: of mice and men. Annu Rev Cell Dev Biol **17**: 435-462.

Smith GH (2005) Stem cells and mammary cancer in mice. Stem Cell Rev **1**: 215-223.

Stephens DJ, Allan VJ (2003) Light microscopy techniques for live cell imaging. Science **300**: 82-86.

Takeda T, Tezuka Y, Horiuchi M, Hosono K, Iida K, Hatakeyama D (2008) Characterization of dental pulp stem cells of human tooth germs. J Dent Res **87**: 676-681.

Thesleff I, Vainio S, Jalkanen M (1989) Cell-matrix interactions in tooth development. Int J Dev Biol **33**: 91-97.

Thesleff I, Partanen AM, Vainio S (1991) Epithelial-mesenchymal interactions in tooth morphogenesis: the roles of extracellular matrix, growth factors, and cell surface receptors. J Craniofac Genet Dev Biol **11**: 229-237.

Thesleff I, Vaahtokari A, Partanen AM (1995) Regulation of organogenesis. Common molecular mechanisms regulating the development of teeth and other organs. Int J Dev Biol **39**: 35-50.

Tirino V, Paino F, d'Aquino R, Desiderio V, De Rosa A, Papaccio G (2011) Methods for the identification, characterization and banking of human DPSCs: current strategies and perspectives. Stem Cell Rev **7**: 608-615.

Vainio S, Karavanova I, Jowett A, Thesleff I (1993) Identification of BMP-4 as a signal mediating secondary induction between epithelial and mesenchymal tissues during early tooth development. Cell **75**: 45-58.

Vastardis H, Karimbux N, Guthua SW, Seidman JG, Seidman CE (1996) A human MSX1 homeodomain missense mutation causes selective tooth agenesis. Nat Genet **13**: 417-421.

Wang Y, Shyy JY, Chien S (2008) Fluorescence proteins, live-cell imaging, and mechanobiology: seeing is believing. Annu Rev Biomed Eng **10**: 1-38.

Wu J, Jin F, Tang L, Yu J, Xu L, Yang Z, Wu G, Duan Y, Jin Y (2008) Dentin non-collagenous proteins (dNCPs) can stimulate dental follicle cells to differentiate into cementoblast lineages. Biol Cell **100**: 291-302.

Yagyuu T, Ikeda E, Ohgushi H, Tadokoro M, Hirose M, Maeda M, Inagake K, Kirita T (2010) Hard tissue-forming potential of stem/progenitor cells in human dental follicle and dental papilla. Arch Oral Biol **55**: 68-76.

Yao S, Pan F, Prpic V, Wise GE (2008) Differentiation of stem cells in the dental follicle. J Dent Res **87**: 767-771.

Zhao Z, Zhao M, Xiao G, Franceschi RT (2005) Gene transfer of the Runx2 transcription factor enhances osteogenic activity of bone marrow stromal cells *in vitro* and *in vivo*. Mol Ther **12**: 247-253.

Zhao Z, Wang Y, Wang D, Liu H (2010) The regulatory role of a disintegrin and metalloproteinase 28 on the biologic property of human periodontal ligament stem cells. J Periodontol **81**: 934-944.

Zhao Z, Watt C, Karystinou A, Roelofs AJ, McCaig CD, Gibson IR, De Bari C (2011a) Directed migration of human bone marrow mesenchymal stem cells in a physiological direct current electric field. Eur Cell Mater **22**: 344-358.

Zhao Z, Liu H, Wang D (2011b) ADAM28 manipulates proliferation, differentiation, and apoptosis of human dental pulp stem cells. J Endod **37**: 332-339.

Discussion with Reviewers

Reviewer I: As the authors are experts in the dental field, could they discuss the possibility of using mixed populations of DPSC and DFSC in transplantations targeting tooth repair?

Authors: Dental follicle cells and dental papilla cells are in close contact during odontogenesis. Signalling molecules from the dental papilla could promote proliferation and differentiation of dental follicle cells during development. Indeed, in our co-culture model we have shown that DPSC stimulated the migration abilities of DFSC. In addition, previous results have shown that, in co-culture, DPSC can promote differentiation of DFSC and formation of hard tissues (Bai *et al*., 2010). We hypothesise that the use of mixed DFSC and DPSC populations for tooth repair may accelerate cytodifferentiation and hard matrix deposition

events. However, it is of importance to carefully define the appropriate percentage and dosage of DFSC and DPSC according to the targeted dental tissue (dental pulp or periodontal tissues). Taking these parameters into account, repair of the dentin-pulp complex and/or periodontal tissues could occur in a faster than normal way.

In the co-culture, DFSC motion closely resembles that of dental follicle cells during odontogenesis. Dental follicle cells encircle the enamel organ and the dental papilla of the developing tooth germ. DFSC could also be used for the regeneration of a follicle around a tooth germ formed *in vitro* (recombination of dental epithelium with dental papilla mesenchyme: formation of a brand new tooth). Once the follicle will form around the tooth germ, the explant could be implanted into the alveolar bone *in vivo*. This technique will probably allow the development and eruption of a new tooth with all appropriate tissues and possible functions.

Reviewer II: DPSC and DFSC seem to be both originated from mesenchymal stem cells because they share similar surface markers and give rise to similar cell types. However, they do have different migration activity *in vitro*. What mechanisms underly the different migration capacity? How this can be used in regenerative medicine?
Authors: Briefly, the difference in the migration activity in the *in vitro* co-culture system can be explained by the fact that DFSC are isolated from a developing tissue (neural crest-derived mesenchymal tissue that forms the dental sac, which surrounds the epithelial enamel organ and the mesenchymal dental papilla of the developing tooth germ before eruption) and might thus exhibit a greater migration activity than DPSC, which belong to a tissue that is already developed and mature.

In the recent literature there are not many articles concerning this topic. In particular, there is a description of receptors and soluble factors involved in the migration but there is not a substantial difference between the two stem cell populations (DPSC and DFSC). To our knowledge, this is the first study on the co-culture of human DPSC and DFSC, thus allowing the investigation of specific/mediated interactions between these two stem cell populations. In fact, we highlighted that their behaviour differs in single population cultures compared with the co-culture assay, which allows an insight on cell kinetics and gene expression modulation. Several recent papers have reported on the migration of DPSC in the presence of different chemoattractants (EMPs) and/or induced migration of DPSC by selective cytokines (e.g. Howard *et al*., 2010; Suzuki *et al*., 2011). However, the migration of DFSC, as well as the migration in a co-culture model, have not been explored in these or other papers. It has been demonstrated that TGFβ1, an important signalling molecule for tissue regeneration and a marker for functional odontoblasts (Melin *et al*., 2000), and SPARC, a non-collagenous protein localised in dentin and bone, are able to stimulate DPSC migration (Pavasant *et al*., 2008). However, these studies report on DPSC migration, but not in DFSC. The role of the various signalling molecules (IGF, EGF, FGF etc) involved in DPSC and DFSC migration is still unknown.

It is well known that *in vivo*, DPSC and DFSC are localised in specific compartments of the tooth organ and their roles are distinct. The *in vitro* interaction between DPSC and DFSC could be useful for better understanding the complex *in vivo* mechanisms involved in repair of specific dental tissues. Few reports hypothesise such interactions between different cell populations of the craniofacial complex. For example, Tancharoen *et al*. (2005) have studied the influence of neuropeptides released from dental pulp cells in the periodontal tissue and suggested a link between periodontitis and pulp inflammation. The results of the study show that DFSC and DPSC in our *in vitro* co-culture system recapitulate the *in vivo* kinetics during odontogenesis, where dental follicle cells surround the dental pulp before the eruption of the tooth. This property of DFSC may be used for the reconstitution of tooth germs *in vitro* or *ex vivo*, thus allowing their implantation into the alveolar bone for the replacement of missing teeth (Mitsiadis and Papagerakis, 2011).

Additional References

Howard C , Murray P and Kenneth NN (2010) Dental pulp stem cell migration. J Endod **36:** 1963-1966.

Melin M, Joffre-Romeas A, Farges JC, Couble ML, Magloire H, Bleicher F.(2000) Effects of TGFbeta1 on dental pulp cells in cultured human tooth slices. J Dent Res **79:** 1689-1696.

Mitsiadis and Papagerakis (2011) Regenerated teeth: the future of tooth replacement? Regen Med **6:** 135-139.

Pavasant P, Yongchaitrakul T. (2008) Secreted protein acidic, rich in cysteine induces pulp cell migration *via* alphavbeta3 integrin and extracellular signal-regulated kinase. Oral Dis **14:** 335-430.

Suzuki T, Lee CH, Chen M, Zhao W, Fu SY, Qi JJ, Chotkowski G, Eisig SB, Wong A, Mao JJ. (2011) Induced migration of dental pulp stem cells for *in vivo* pulp regeneration. J Dent Res **90:** 1013-1018.

Tancharoen S, Sarker KP, Imamura T, Biswas KK, Matsushita K, Tatsuyama S, Travis J, Potempa J, Torii M, Maruyama I. (2005) Neuropeptide release from dental pulp cells by RgpB *via* proteinase-activated receptor-2 signaling. J Immunol **174:** 5796-5804.

14.1.2 Mitsiadis et al., Nanomedicine, 2012

Nanodentistry: combining nanostructured materials and stem cells for dental tissue regeneration (REVIEW)

The presented review about the application of nanotechnology for therapeutical purposes in dentistry describes benefits and future possibilities of the combinatorial use of stem cells and nanomaterials. It covers the pathology and regenerative potential of dental tissues, describes stem cell populations within the dental pulp and periodontal tissues, presents promising stem cell-based dental tissue regeneration studies performed in animal models, and discusses safety and efficacy issues of stem cell-based therapies in dentistry. Furthermore, it informs about potential applications of nanomedicine including the monitoring of stem cells after transplantation, gene, protein, and drug delivery, as well as nanobiomimetics.
My contribution includes the literature research with a focus on the different dental stem cell populations, as well as the co-writing and co-editing of the manuscript.

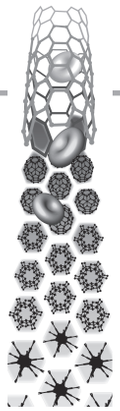

Nanodentistry: combining nanostructured materials and stem cells for dental tissue regeneration

Regenerative dentistry represents an attractive multidisciplinary therapeutic approach that complements traditional restorative/surgery techniques and benefits from recent advances in stem cell biology, molecular biology, genomics and proteomics. Materials science is important in such advances to move regenerative dentistry from the laboratory to the clinic. The design of novel nanostructured materials, such as biomimetic matrices and scaffolds for controlling cell fate and differentiation, and nanoparticles for diagnostics, imaging and targeted treatment, is needed. The combination of nanotechnology, which allows the creation of sophisticated materials with exquisite fine structural detail, and stem cell biology turns out to be increasingly useful in regenerative medicine. The administration to patients of dynamic biological agents comprising stem cells, bioactive scaffolds and/or nanoparticles will certainly increase the regenerative impact of dental pathological tissues. This overview briefly describes some of the actual benefits and future possibilities of nanomaterials in the emerging field of stem cell-based regenerative dentistry.

KEYWORDS: dentin ■ dentistry ■ nanomaterials ■ nanotechnology ■ odontoblast ■ periodontium ■ regenerative medicine ■ scaffolds ■ stem cells ■ tooth

Thimios A Mitsiadis*[1], Anna Woloszyk[1] & Lucia Jiménez-Rojo[1]

[1]Institute of Oral Biology, Department of Orofacial Development & Regeneration, ZZM, Faculty of Medicine, University of Zurich, Zurich, Switzerland
**Author for correspondence:*
Tel.: +41 44 634 33 90
Fax: +41 44 634 43 10
thimios.mitsiadis@zzm.uzh.ch

Pathology & natural regenerative potential of dental tissues

Two of the hardest tissues of the body, the enamel and dentin, form as a result of sequential and reciprocal interactions between cells of the oral epithelium and the cranial neural crest-derived mesenchyme [1]. Mesenchymal cells give rise to the dental follicle and dental pulp, while the oral epithelium forms the ameloblasts. A part of the dental pulp cells differentiates into odontoblasts that produce dentin matrix, whilst ameloblasts form the enamel. When the mineralization of the tooth crown is complete, the tooth root starts to develop and subsequently the tooth erupts in the oral cavity. Once root development and cementum deposition have been accomplished, the tooth anchors to the surrounding alveolar bone through the periodontal ligament (PDL), which contains extracellular matrix (ECM) and a great variety of cells such as fibroblasts, epithelial rests of Malassez (ERM) and endothelial cells.

The mineralized dental tissues are vulnerable to various external harmful agents, such as bacteria and acids, but also to traumatic injuries that jeopardize tooth integrity. Although the mitotic and secretory activities of dental pulp and periodontal cells are reduced in adult teeth, these biological processes can be reactivated in pathological conditions (e.g., periodontal and carious diseases) or following traumatic injury [2]. After a mild lesion, such as early caries, surviving postmitotic odontoblasts can produce new dentin through a process known as reactionary dentinogenesis. However, a severe dental injury leads to odontoblast apoptosis, which activates dental pulp stem cells to differentiate into new odontoblasts, which produce the reparative dentin [2]. Periodontal regeneration is a complex process that involves the interaction of several populations of cells that control the specific ECM components. Cell-occlusive barriers ranging from cellulose to synthetic absorbable materials, which restrict the repopulation of the periodontium from epithelial cells and favor growth of PDL cells and cementoblasts, are commonly used for periodontium regeneration in dental clinics. These materials are often used in conjunction with biological factors to enhance the regeneration of the alveolar bone. Damaged enamel cannot be repaired naturally since ameloblasts are not present in humans after tooth eruption. Thus, a common practice in dental clinics is to substitute the damaged enamel with biomaterials, ceramics and precious metals.

It is evident that the natural regenerative capacity of dental tissues is often insufficient to entirely restore damaged teeth. In such cases, stem cell biology combined with tissue engineering technology could be useful for the development of innovative strategies for cell-based dental tissue regeneration [3,4].

Future Medicine part of fsg

Stem cell populations within dental & periodontal tissues

Stem cells are undifferentiated cells characterized by their ability to self-replicate throughout life and their capacity to differentiate into diverse specialized cell types [5]. Adult stem cells are found in various tissues of the human body of both epithelial and mesenchymal origin, including skin [6], adipose tissue [7], periosteum [8] and cartilage [9]. Owing to their ability to give rise to every cell type in a given tissue, adult stem cells are responsible for tissue/organ homeostasis and regeneration.

Mesenchymal stem cells have been isolated from different locations within adult or postnatal dental tissues. Dental mesenchymal stem cells have been isolated from the pulp of adult teeth (dental pulp stem cells [DPSCs]) and deciduous teeth [10], the apical part of dental papilla [11,12], the dental follicle [13] and the PDL (Figure 1) [14,15]. All these dental stem cell populations express typical mesenchymal stem cell markers such as STRO-1, MUC-18 or Cd146, and Cd44 [16], but some of them also express other markers including Cd90, Cd73, Cd29 and Cd24 [11,17]. However, the marker or combination of markers that reliably identifies dental stem cells has not been established yet. Thus, dental mesenchymal stem cells are often recognized by their ability to give rise to odontogenic [10,16,18–21], adipogenic [16,22], chondrogenic [22], osteogenic [23], myogenic [24] and neurogenic [16,25] lineages *in vitro* or to regenerate dental tissues *in vivo* [11,17].

Since most dental epithelial cells disappear shortly after tooth eruption, identifying epithelial stem cells within adult dental tissues constitutes a major challenge. Putative epithelial stem cell populations have been isolated from third molars [26] and, most surprisingly, dental pulp [27]. However, to date, ERM located in the PDL (Figure 1), appear as the more promising source of epithelial stem cells [28,29].

Recently, pluripotent stem cells, named dental pulp pluripotent stem cells, have been isolated from the dental pulp of third molars [30]. These cells show the ability to differentiate into tissues that derive from embryonic mesodermal, endodermal and ectodermal layers, suggesting their potential utility for the regeneration of both epithelial and mesenchymal dental tissues.

Stem cell-based dental tissue regeneration

Harmful agents (e.g., caries) damage the hard tissues of the tooth first and then reach the dental pulp. The affected dental pulp is usually amputated (pulpotomy) or extracted (pulpectomy) and substituted with an artificial material after disinfection of the pulp cavity [3]. Although the tooth is preserved in its normal position, it is not vital anymore and it cannot completely fulfill its role [3]. Thus, the regeneration of the dentin–pulp complex represents the ideal solution and this process requires the revascularization and reinnervation of the pulp, as well as the deposition of newly generated dentin. As previously mentioned, DPSCs have the ability to differentiate into odontoblasts, endothelial cells and neurons, among other cell types. In mice, transplantation of DPSCs can regenerate both pulp and dentin tissues *in vivo* after pulpotomy [31]. DPSCs and the apical part of dental papillas isolated from human third molars, seeded on a poly-D,L-lactide/glycole scaffold and transplanted into the empty root canal space of mouse teeth, were able to refill the empty space with a newly formed vascularized pulp [17,32]. A continuous layer of mineralized tissue resembling dentin was deposited in the existing dental walls of the canals [17,32]. Although these results prove that DPSCs can regenerate the dental pulp, further studies are clearly required to investigate their potential clinical applications.

Periodontitis is one of the most common infectious diseases in humans. Periodontitis is triggered by micro-organisms that attach to the teeth, cause chronic inflammation and eventually destroy the periodontal tissues [3]. Studies in immunocompromised mice have shown that transplanted PDL stem cells were able to regenerate the periodontium, thus indicating their huge potential for future cell-based therapies in the dental clinic [3]. However, severe damage of the periodontal tissues often results in tooth loss, so it is still necessary to develop new strategies in order to potentially use entirely regenerated teeth in clinics. This could be achieved either by generating a tooth germ *in vitro* before implanting it *in vivo*, or by grafting dental stem cells in the oral cavity. In this last case, dental stem cells could be carried on tooth-shaped biomimetic scaffolds [3]. Using different scaffolds it has been possible to induce differentiation of PDL stem cells and DPSCs into the various cell types composing the root and/or the periodontal tissues both *in vitro* and *in vivo* [33,34]. DPSCs were implanted subcutaneously onto the back of severe combined immunodeficient mice (CB-17/Icr-SCID/SCID mice) [33]. Regarding regeneration of dental epithelium, it has been shown that ERM derived from porcine

mandible can differentiate into ameloblasts after co-culture with dental pulp cells *in vitro*. These ameloblast-like cells were positive for keratin 14 and amelogenin. Moreover, after transplantation of ERM cells combined with primary dental pulp cells an enamel-like tissue was produced in the implant. Histological analysis revealed that appropriate stages of amelogenesis, from initiation to maturation, were present in all implants. Thick enamel–dentin structures were clearly recognized, and ameloblast-like cells expressing keratin 14 and amelogenin were found 8 weeks post-transplantation [29].

Equally important for the development of stem cell-based therapies in dentistry is the use of signaling molecules. Several molecules involved in periodontal development are already in use in the clinical practice. A long time ago, it was shown that PDGF molecules were able to stimulate periodontal healing and regeneration [35,36]. Since then, other molecules, such as BMPs [37–39] and amelogenins [40], have been used for the stimulation of periodontal tissue regeneration.

Current studies focus on the identification of the correct population of cells, suitable signaling molecules and desirable scaffold materials that will be used as carriers for specific cell types.

Safety & efficacy issues of stem cell-based therapies in dentistry

Stem cell-based therapies are both promising and challenging. The engraftment of exogenous therapeutic cells in patients must obey strict safety rules, exclude tumor formation and avoid or minimize rejection [41,42]. The purity, biological activity and quantity of the injected cells should be optimized to ensure cell functionality. Cell functionality should be tested both *in vitro* and *in vivo* in various animal models. Defined strategies should also be developed to monitor the behavior and fate of the engrafted cells before any clinical trial. There is a consensus that differentiated cells that originate from stem cells rather than undifferentiated stem cells should be used directly for transplantation in the clinics [42]. Even if stem cell injection or transplantation is successful in animal models, it is important to optimize and secure stem cell-based therapeutic strategies before clinical trials.

An optimal engraftment strategy must avoid (or minimize) immune response in the host. Grafted or injected stem cells are recognized as foreign material by the immune system of the host, thus generating a cascade of events resulting in the destruction and rejection of the transplanted cells. This process can compromise the immune status of the recipient. Immunosuppressive treatments that increase graft survival are undesirable, since it has been shown that a correlation exists between the length of exposure to immunosuppressive drugs and the risk of malignancy after stem cell transplantation. Recent results have shown that mesenchymal stem cells from umbilical cord blood, dental pulp, PDL and bone marrow have immunosuppressive properties *in vitro* [43–45]. Moreover, the clonogenic nature of adult stem cells represents an advantage over heterogeneous stem cell populations resulting in a more reproducible, potent immunosuppressive effect in patients [46]. Autologous cell-based therapies are

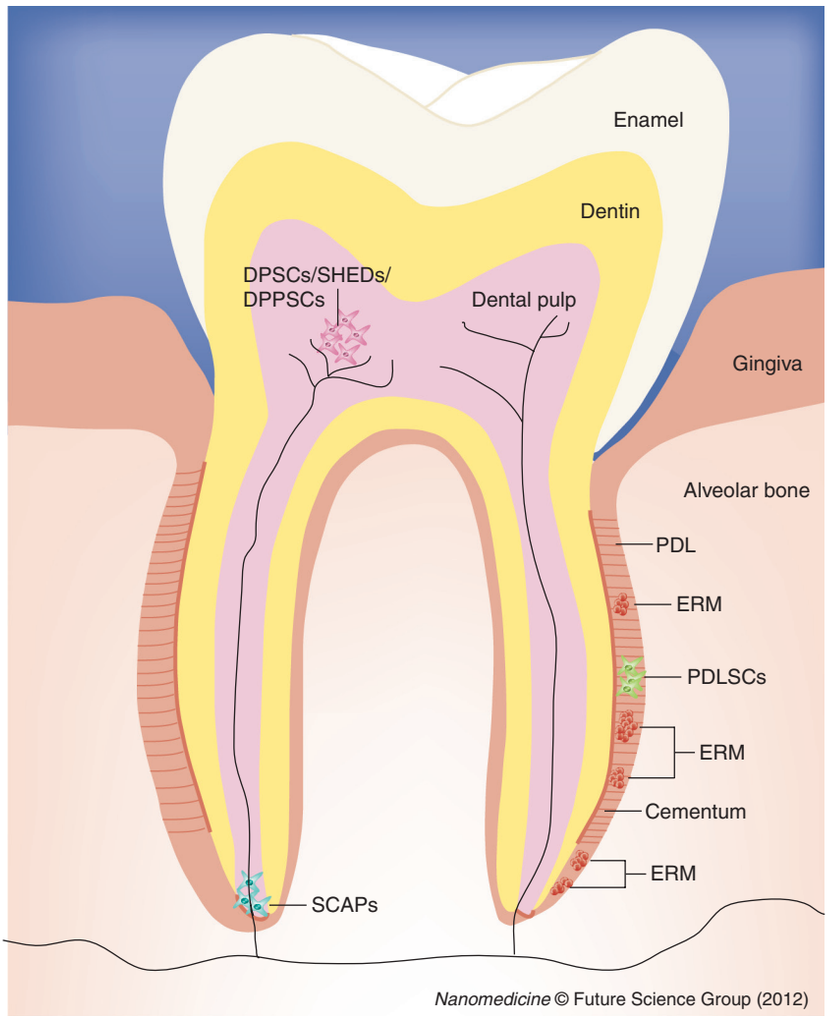

Figure 1. The various dental stem populations within an adult human tooth.
DPPSC: Dental pulp pluripotent stem cell; DPSC: Dental pulp stem cell; ERM: Epithelial cell rest of Malassez; PDL: Periodontal ligament; PDLSC: Periodontal ligament stem cell; SCAP: Stem cell from the apical papilla; SHED: Stem cell from human exfoliated deciduous teeth.

advantageous because there is minimal risk of immunological rejection and disease transmission. However, the outcome of all tissue engineering approaches using autologous stem cell transplantation is subjective to the patient since the patient is both (at the same time) the source and the recipient of the cells that will be used for his/her own treatment. Factors related to the age and general health status of the patient, health condition of the dental pulp and periodontium at the moment of surgery, as well as the size and site of the injury, may influence the efficacy of stem cell-based dental treatments. The influence of these factors on the efficacy of cell preparations for cell-based dental treatments has not been investigated exhaustively.

The generation of induced pluripotent stem cells (iPSCs) by reprogramming somatic cells via a cocktail of transcription factors could be advantageous towards cell-based regenerative therapies [47,48]. Somatic cells have been reprogrammed and turned into pluripotent cells by the overexpression of a cocktail of four transcription factors (Oct4, Sox2, c-Myc and Klf4) [47]. It has recently been shown that mouse iPSCs can give rise to neural crest-like cells that can be further differentiated into odontogenic mesenchymal cells [49]. iPSCs could be generated from somatic cells of the patient, who will be the donor and recipient simultaneously, thus overcoming the problems associated with allogeneic immune rejection [50]. Although tempting, this potential has not yet been proven, since there is not clear understanding of the effects that the reprogrammed cells could have on the immune system [51]. For example, studies in animal models have shown immunoreactivity towards grafted iPSCs of the same genetic background [52]. Both adult dental stem cells and iPSCs represent an attractive source of cells for regenerative dentistry. Nevertheless, there are still safety and immunogenicity issues that should be overcome before their use in the clinic.

Although promising advances have been made in dental stem cell isolation and expansion, it is still necessary to refine these procedures. It is noteworthy that stem cells from every individual patient should be considered as specific pools and be quality controlled accordingly. It is obvious that there is not yet an ideal and unique approach for cell-based repair of dental tissues. However, rapid progress in stem cell biology and biomaterial sciences might allow the development of new methods and protocols for personalized dental treatments.

Nanomedicine: a giant leap forward in disease diagnosis & treatment

Nanomedicine represents a subfield of nanotechnology that uses particles in the size range of 1–1000 nm for the treatment, diagnosis, monitoring and control of various diseases [53,54]. Nanoparticles, which are similar in scale to biological macromolecules such as DNA and proteins [53], can be used for targeted therapy through DNA, protein and drug delivery, *in vivo* imaging, and diagnostics, as well as for the creation of active scaffolds and implants [55–57]. Nanoparticles can be composed of organic materials (e.g., lipids), inorganic materials (e.g., iron oxide or gold), or a combination of both types. Novel and improved nanostructured materials can be tailored by engineering their characteristics such as structure, stability, size, shape and surface properties in order for them to be selectively delivered to precise sites (target regions) of the body [58]. This can be achieved through passive or active targeting mechanisms: passive targeting is enabled by enhanced vascular permeability during neo-angiogenesis of injured or pathological body sites, while active targeting benefits from overexpression in the infectious or damaged areas of several cell surface molecules that can bind specifically to precoated nanoparticle ligands [58,59]. Recently, a dual modular system that mimics the communication-dependent recruitment of inflammatory cells to regions of disease has been developed to improve the tissue target efficiency of nanoparticles [60]. Another more recent study has demonstrated the programming and assembly of DNA-based nanorobots that are able to carry molecular loads, transport chemical ingredients to target cells and stimulate their intracellular alterations [61].

These sophisticated biomaterials are increasingly being incorporated into the stem cell biology field. The combination of stem cells with innovative nanotechnology holds great promise for applications in the biomedical arena. Fundamental challenges include stem cell expansion *in vitro* without using feeder layers, enhancement of stem cells survival after transplantation and reproducible regulation of their fate in the body [55]. The development of nanomaterials could be helpful in detecting and manipulating stem cells that will be used for tissue repair in the clinic. Nanomaterials are being used to precisely define the stem cell microenvironment through the provision of morphogenetic gradients and cell adhesion molecules, to direct stem cell fates and to provide

a template for stem cells for the formation of new tissues and organs. Furthermore, internalization of nanoparticles, previously labeled with chelated ions, small molecules, metals and nanocrystals, by stem cells enables their detection by imaging. The physical, chemical and biological properties of nanomaterials can be exploited to influence proliferation, attachment, fate and differentiation of stem cells [62]. This multidisciplinary approach allowed scientists to create a fully synthetic organ for transplantation after soaking a porous polymer nanocomposite tracheobronchial replica in a solution of bone marrow stem cells [63]. Although these new developments are encouraging, long-term studies are necessary before we can exploit such synthetic nanosystems in the clinic. For example, it is important to verify nontoxicity, exclude tumorigenic potential [64] and adverse side effects on a systemic level of nanoparticles, and study their interference with the self-renewal ability of stem cells. In addition, the pharmaceutical industry, has been reticent to engage with the cell-based regenerative medicine industry probably because of the complex regulatory and ethical issues [65]. This leads to uncertainty regarding the cost and time that will be required to successfully gain market approval for nanomedicine.

Monitoring of stem cells after transplantation: magnetic nanoparticles & quantum dots

Stem cell-based regenerative therapies necessitate thorough testing in animals and, then in humans. For the evaluation of the therapeutic efficacy of the transplanted stem cells, it is important to track their survival, migration, fate and regenerative impact *in vivo*. Transplanted stem cells can be assessed for long-term periods using noninvasive imaging techniques [66,67]. Stem cells can be tracked *in vivo* after their transplantation using different strategies: initial labeling of stem cells with fluorescent dyes or magnetic nanoparticles, such as superparamagnetic iron oxide, and stem cell transfection with several reporter genes such as the *LacZ* and green fluorescent protein (*GFP*) [68,69]. The visualization of the labeled stem cells requires either simple, or complex and sophisticated imaging systems such as MRI [66,70,71], computed tomography imaging [72], PET and single-photon emission computed tomography imaging [73]. Superparamagnetic iron oxide nanoparticles (60–150 nm in diameter) are composed of biodegradable and recyclable iron and are coated with dextran or carboxydextran to prevent aggregation and ensure aqueous solubility [74,75]. Magnetic nanoparticles can attach to the stem cell surface, but are also capable of being internalized by phagocytosis or, more often, by endocytosis [76], a process that is often facilitated by the use of coating and membrane receptor-binding agents [69,77]. Endocytosis of magnetic nanoparticles does not affect stem cell viability, growth, fate or differentiation [78].

Quantum dots (QDs) are cadmium selenide semiconductor fluorescence-emitting nanostructures (less than 10 nm in diameter) that are used for long-term labeling of stem cells [79–81]. QDs present a number of advantages over conventional organic dyes (e.g., 1,1'-dioctadecyl-3,3,3'3'-tetramethylindocarbocyanine perchlorate) and fluorescent proteins (e.g., green fluorescent protein): high brightness, superb photostability and a single excitation wavelength for multiple colors [82]. Due to their excellent optical properties, the detection of QD-labeled stem cells relies on imaging systems that are less sophisticated and complex than MRI. QDs have been used to monitor in real time the dynamics of various cell components [83]. Information concerning participation and clustering of multiple cell surface molecules involved in stem cell migration and differentiation may be useful for the design of innovative scaffolds for homing stem cells before transplantation. QDs are also internalized by endocytosis, which is improved by the use of specific peptides such as RGD, phospholipids and cholera toxin [84–86]. A number of internalized QDs are transported via endosomes to the perinuclear region [87], while QDs that will not be used by the cells display an oxidative degradation [68] that could lead to mitochondria dysfunction and, ultimately, cell death [88]. It is possible that the composition and physical properties of QDs and magnetic nanoparticles lead to unique toxic responses [53,85,87]. To date there is no conclusive evidence of known human toxic responses that are exclusively caused by nanomaterials [53]. Furthermore, most of the studies demonstrated no interference of these nanoparticles with stem cell differentiation [84,85]. However, variations in the composition, structure, size and surface coating of nanoparticles may influence stem cell behavior and fate [88,89].

Magnetic nanoparticles and QDs may provide valuable information about stem cell migration, anchorage, fate and differentiation in the context of dental pathology (e.g., periodontitis, pulpitis and traumatic injury) and repair [3,5,90].

For example, internalized nanoparticles would allow monitoring of the kinetics and fate of the labeled stem cells that were injected into the periodontal space or pulp chamber following dental injury (Figure 2). These approaches are necessary to evaluate the therapeutic effects of stem cells when exposed to a specific microenvironment before their application in dental clinics.

Targeting therapy: gene, protein & drug intracellular delivery

One of the most attractive concepts in manipulating the fate of stem cells and directing their differentiation into specific cell populations is the use of nanomaterials for intracellular gene delivery (e.g., RNAi and DNA) [91,92]. Generally, viral (e.g., adenoviruses, lentiviruses and retroviruses) and nonviral vectors (e.g., lipids and polymers) can be used for cellular transfection and/or nucleofection, thus offering durable gene expression within stem cells [93–96]. Nonviral carriers have a number of advantages over viral vectors, since they exhibit low-risk immunogenicity and insertional mutagenesis, controllable toxicity, and excellent gene-carrying capacity [95]. Many efforts for the improvement of nonviral vectors are focused on cationic polymers that interact with negatively charged DNA or RNAi. Polymers, including poly(L-lysine)-palmitic acid, poly(L-lysine) and polyethylenimine, condense the genetic material into particles of 200–300 nm in diameter, protect them from enzymes and facilitate cellular entrance [94,97]. These complexes of polymers and genetic material (called 'polyplexes') have a transfection efficiency that is equivalent to adenoviral vectors [97].

Nanoparticles, carbon nanotubes and silicon nanowire arrays have also been used for gene delivery [98,99]. The apatite particles coated with E-cadherin and fibronectin, ensure high gene delivery capacity in stem cells [100].

Polymeric, biodegradable nanoparticles of 100–300 nm in diameter could also serve as platforms to incorporate and deliver proteins and chemicals within stem cells. It has been shown that, after internalization, these nanoparticles accumulate in the perinuclear region and have minimal effect on the viability and proliferation of stem cells, but a high impact on their differentiation [68].

The cytotoxicity of 'polyplexes', nanoparticles and nanotubes has been evaluated in stem cells and the results showed that, in general, the toxicity correlates with the chemistry, concentration, size, shape and coating of the nanomaterials [97,98].

Nanobiomimetics: design of bioactive scaffolds & artificial stem cell niches

The behavior of stem cells is tightly controlled by a specialized microenvironment called the 'stem cell niche' [5]. This microenvironment regulates the survival, proliferation and differentiation of stem cells.

Injection of stem cells into the injured or pathological tissue limits their spread and does not ensure their good engraftment [101]. Injected cells could die due to the absence of trophic factors or oxygen, or lack of a suitable ECM for their adhesion. This can be avoided by placing stem cells in biocompatible and biodegradable nanofiber scaffolds that temporarily recreate the fibrous 3D network of the ECM and mimic the structural aspects of the stem cell niche. Hence, stem cells are anchored to the nanofibers of the scaffolds, which behave as artificial stem cell niches, and then transplanted to the lesion site. This will improve stem cell survival, migration and differentiation potentials, and finally their 3D organization [101]. Stem cells cultured on nanofiber scaffolds exhibit high viability and lower mobility, and differ in morphology when compared with cells cultured on conventional substrates (e.g., polystyrene) [102,103]. Nanofibers with a controlled diameter (e.g., 300–1000 nm) are composed of either natural polymers, such as collagen and silk, or synthetic polymers including poly(lactic acid) and poly(amide) [102,104,105]. The 3D organization, surface and chemistry of these scaffolds result in stem cell self-renewal, migration and differentiation. Nanofiber scaffolds have high porosity and specific surfaces that offer an ideal environment for stem cell homing.

Identifying the appropriate stem cell populations and providing the suitable microenvironment that allows them to repair or regenerate an injured tissue is the key for a successful cell-based therapy. Nanotechnology may be used to create artificial microenvironments that will direct stem cells or progenitor cells towards a precise fate and function. A big challenge is to engineer materials that resemble the structural complexity of stem cell niches, which represent specific anatomic locations homing stem cells and preventing them from exiting the mitotic cycle [106]. ECM molecules, such as collagen, fibronectin, laminin and proteoglycans, represent the noncellular components of the niches and are important for the creation of a particular microenvironment (e.g., tooth or bone). ECM provides nanoscale structures, such as

the 15–300 nm in diameter collagen fibrils that allow cell adhesion (via integrins) and immobilization of signaling molecules, thus influencing the fate and behavior (i.e., proliferation, migration and differentiation) of stem cells [107]. The concentration, size, spacing, surface chemistry and shape (e.g., ridges, grooves, pores and pits) of the artificial nanostructures (e.g., nanotubes and nanolines) are important parameters for the development of cell adhesion sites that monitor stem cell behavior [108–110]. For example, it has been shown that surface irregularity (e.g., nanoline grating) and diverse surface chemistries (e.g., silica and poly[methyl methacrylate]) are capable of enhancing adhesion, alignment, growth and differentiation of stem cells [108,109].

In vivo transplantation of stem cells anchored to nanofiber-based scaffolds is a technique successfully used in regenerative medicine [111,112]. Transplanted biodegradable scaffolds act as temporary niches that guide, by controlling stem cell behavior, the formation of a new specific ECM for tissue repair. The design of tissue-specific artificial niches offers new perspectives to stem cell-based applications in dentistry for the treatment of peculiar anatomic sites (e.g., alveolar bone, dentin–pulp complex, enamel and periodontium). Furthermore, nanomaterials could be successfully used for the generation of new nanotextured 'osteogenic coating' dental implants that may lead to direct bone material contact and also bone healing in those cases in which bone is compromised. The variety of adult stem cell populations within dental tissues indicates that their differentiation potential and response to nanoscale materials may be different. However, there are not yet methodical comparative studies that will allow the assessment of nanomaterials on the various dental stem cell lines. The lack of this crucial information delays the application of stem cell-based therapies in dental clinics.

Conclusion

There is no doubt that nanotechnology offers enormous benefits and a plethora of exciting perspectives to cell-based regenerative medicine. Recent advances in nanoscale materials increase the potential to control stem cell fate, improve DNA and drug delivery, modulate the immune response to implanted cells, and create advanced scaffolds for the treatment of various diseases. Nanomaterials and cell-based products must be regulated and manufactured at a low-cost scale to ensure their successful application in clinics. Dentists could benefit from the use of nanoparticles to label stem cells, which, after being placed on scaffolds, could be further implanted into damaged dental tissues

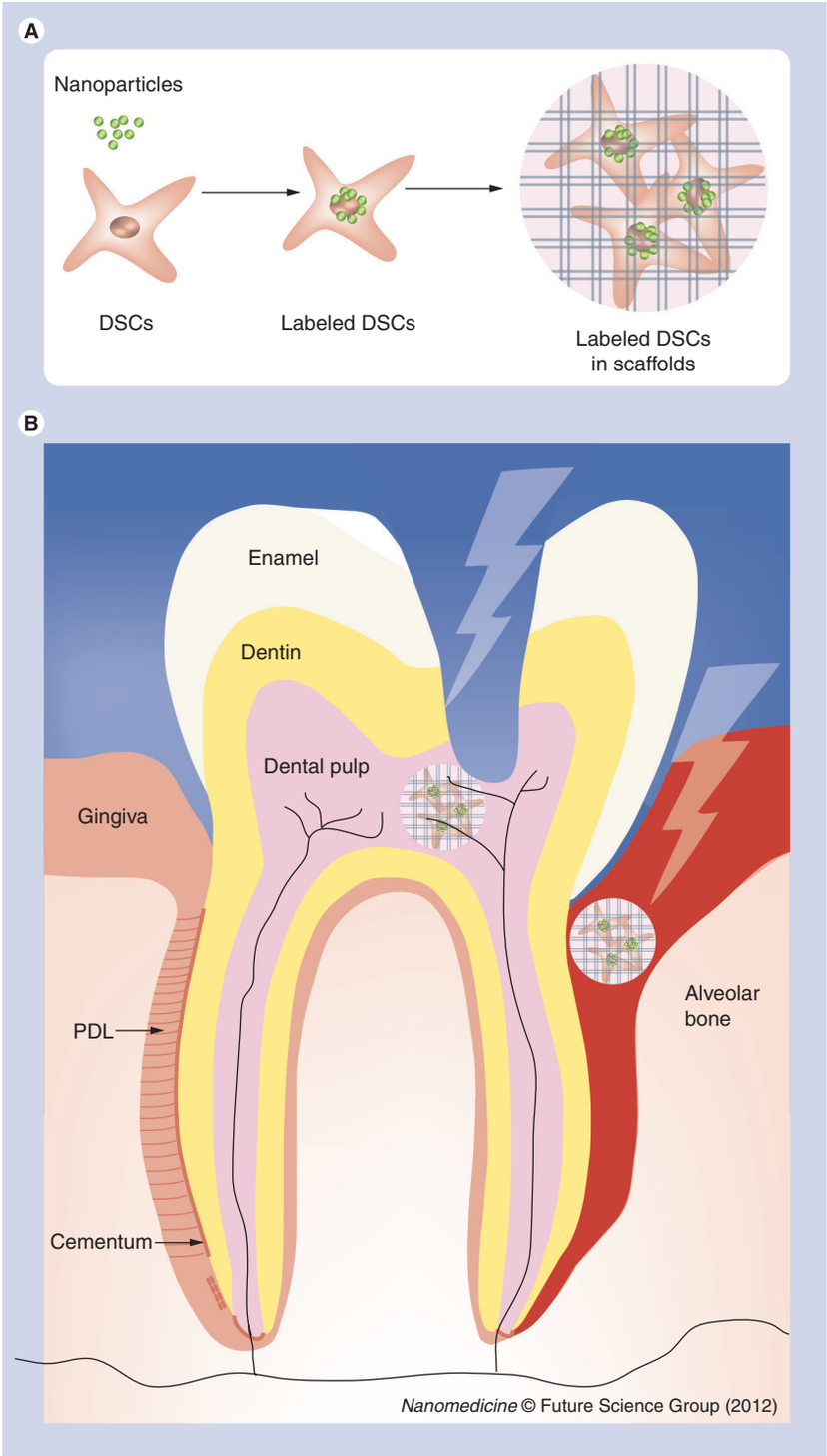

Figure 2. Nanotechnology in regenerative dentistry. (A) DSCs can be labeled with nanoparticles before placing them into biomimetic scaffolds. **(B)** Afterwards, those scaffolds that contain labeled DSCs could be transplanted to repair damaged dental tissues. Tooth crown, pulp and periodontium are the most commonly affected dental tissues.
DSC: Dental stem cell; PDL: Periodontal ligament.

in order to regenerate them (Figure 2). The application of nanotechnology for dental purposes (nanodentistry) holds great promise as a type of personalized medicine for the management of target-specific treatment and imaging of dental tissues.

Future perspective

Dental clinics could benefit in the near future from the combinatorial use of stem cells and nanostructures (e.g., creation of specific scaffolds). These devices, which will contain cells, could be implanted into damaged dental sites in order to regenerate them. However, there are serious issues concerning standardization of techniques, nanoparticles and stem cells that have to be solved before their clinical application in humans.

Acknowledgements

The authors wish to thank the European Science Foundation (ESF) COST Action 1005 NAMABIO, where TA Mitsiadis is a management committee member and the representative of Switzerland.

Financial & competing interests disclosure

This work was supported by the Swiss National Foundation (SNSF) grants 31003A_118332 (TA Mitsiadis) and 31003A-135633 (TA Mitsiadis), and funds from the University of Zurich (L Jiménez-Rojo, A Woloszyk and TA Mitsiadis). The authors have no other relevant affiliations or financial involvement with any organization or entity with a financial interest in or financial conflict with the subject matter or materials discussed in the manuscript apart from those disclosed.

No writing assistance was utilized in the production of this manuscript.

Executive summary

Pathology & natural regenerative potential of dental tissues

- The mineralized dental tissues are vulnerable to various external harmful agents such as bacteria and acids, but also to traumatic injuries that jeopardize tooth integrity. The natural regenerative capacity of dental tissues is often insufficient to entirely restore damaged teeth.

Stem cell populations within dental & periodontal tissues

- Dental mesenchymal stem cells have been isolated from the pulp of adult and deciduous teeth, the apical part of dental papilla, the dental follicle and the periodontal ligament.
- Putative epithelial stem cell populations have been isolated from dental pulp. However, epithelial cell rests of Malassez, located in the periodontal ligament, appear as the more promising source of epithelial stem cells.

Stem cell-based dental tissue regeneration

- Studies in animals have shown that transplanted dental mesenchymal stem cells were able to regenerate the periodontium and dental pulp *in vivo*, thus indicating their huge potential for future cell-based therapies in dental clinics.

Safety & efficacy issues of stem cell-based therapies in dentistry

- There are still safety and efficacy issues that need to be solved before the application of stem cell-based therapies in clinics. Immunogenicity of the transplanted cells is one example. The potential use of induced pluripotent stem cells in regenerative dentistry is discussed.

Nanomedicine: a giant leap forward in disease diagnosis & treatment

- Nanomedicine represents a subfield of nanotechnology that uses particles in the size range 1–1000 nm for the treatment, diagnosis, monitoring and control of various diseases. Different sophisticated biomaterials are increasingly being incorporated into the stem cell biology field.

Monitoring of stem cells after transplantation: magnetic nanoparticles & quantum dots

- For the evaluation of the therapeutic efficacy of the transplanted stem cells it is important to track their survival, migration, fate and regenerative impact *in vivo*. Stem cells can be tracked *in vivo* after their transplantation using different types of nanoparticles, such as superparamagnetic iron oxide or quantum dots.

Targeting therapy: gene, protein & drug intracellular delivery

- Polyplexes, nanoparticles, carbon nanotubes and silicon nanowire arrays can be used for gene delivery to stem cells before transplanting them *in vivo*.

Nanobiomimetics: design of bioactive scaffolds & artificial stem cell niches

- Biocompatible and biodegradable nanofiber scaffolds constitute artificial stem cell niches that influence the survival, self-renewal and differentiation of stem cells.

Conclusion

- The use of nanotechnology for dental purposes (nanodentistry) holds great promise as a type of personalized medicine for the management of target-specific treatment and imaging of dental tissues. However, there are still certain safety issues to be solved before any clinical application.

References

Papers of special note have been highlighted as:
- ▪ of interest
- ▪▪ of considerable interest

1 Jiménez-Rojo L, Granchi Z, Graf D, Mitsiadis TA. Stem cell fate determination during development and regeneration of ectodermal organs. *Front. Physiol.* 3, 107 (2012).

2 Mitsiadis TA, De Bari C, About I. Apoptosis in developmental and repair-related human tooth remodeling: a view from the inside. *Exp. Cell Res.* 314(4), 869–877 (2008).

3 Caton J, Bostanci N, Remboutsika E, De Bari C, Mitsiadis TA. Future dentistry: cell therapy meets tooth and periodontal repair and regeneration. *J. Cell. Mol. Med.* 15(5), 1054–1065 (2011).

4 Mitsiadis TA, Papagerakis P. Regenerated teeth: the future of tooth replacement? *Regen. Med.* 6(2), 135–139 (2011).

▪▪ **Discusses the main advances in dental regeneration.**

5 Mitsiadis TA, Feki A, Papaccio G, Caton J. Dental pulp stem cells, niches, and notch signaling in tooth injury. *Adv. Dental Res.* 23(3), 275–279 (2011).

6 Toma JG, Akhavan M, Fernandes KJ *et al.* Isolation of multipotent adult stem cells from the dermis of mammalian skin. *Nat. Cell Biol.* 3(9), 778–784 (2001).

7 Zuk PA, Zhu M, Ashjian P *et al.* Human adipose tissue is a source of multipotent stem cells. *Mol. Biol. Cell* 13(12), 4279–4295 (2002).

8 De Bari C, Dell'accio F, Luyten FP. Human periosteum-derived cells maintain phenotypic stability and chondrogenic potential throughout expansion regardless of donor age. *Arthritis Rheum.* 44(1), 85–95 (2001).

9 Alsalameh S, Amin R, Gemba T, Lotz M. Identification of mesenchymal progenitor cells in normal and osteoarthritic human articular cartilage. *Arthritis Rheum.* 50(5), 1522–1532 (2004).

10 Miura M, Gronthos S, Zhao M *et al.* SHED: stem cells from human exfoliated deciduous teeth. *Proc. Natl Acad. Sci. USA* 100(10), 5807–5812 (2003).

11 Sonoyama W, Liu Y, Fang D *et al.* Mesenchymal stem cell-mediated functional tooth regeneration in swine. *PLoS ONE* 1, e79 (2006).

12 Sonoyama W, Liu Y, Yamaza T *et al.* Characterization of the apical papilla and its residing stem cells from human immature permanent teeth: a pilot study. *J. Endodontics* 34(2), 166–171 (2008).

13 Morsczeck C, Gotz W, Schierholz J *et al.* Isolation of precursor cells (PCs) from human dental follicle of wisdom teeth. *Matrix Biol.* 24(2), 155–165 (2005).

14 Seo BM, Miura M, Gronthos S *et al.* Investigation of multipotent postnatal stem cells from human periodontal ligament. *Lancet* 364(9429), 149–155 (2004).

15 Wang L, Shen H, Zheng W *et al.* Characterization of stem cells from alveolar periodontal ligament. *Tissue Eng. Part A* 17(7–8), 1015–1026 (2011).

16 Gronthos S, Brahim J, Li W *et al.* Stem cell properties of human dental pulp stem cells. *J. Dental Res.* 81(8), 531–535 (2002).

17 Huang GT, Yamaza T, Shea LD *et al.* Stem/progenitor cell-mediated *de novo* regeneration of dental pulp with newly deposited continuous layer of dentin in an *in vivo* model. *Tissue Eng. Part A* 16(2), 605–615 (2010).

18 Gronthos S, Mankani M, Brahim J, Robey PG, Shi S. Postnatal human dental pulp stem cells (DPSCs) *in vitro* and *in vivo*. *Proc. Natl Acad. Sci. USA* 97(25), 13625–13630 (2000).

▪▪ **Dental mesenchymal stem cells are isolated and characterized for the first time.**

19 About I, Bottero MJ, De Denato P, Camps J, Franquin JC, Mitsiadis TA. Human dentin production *in vitro*. *Exp. Cell Res.* 258(1), 33–41 (2000).

▪ **First study showing production of human dentin *in vitro*.**

20 Alliot-Licht B, Bluteau G, Magne D *et al.* Dexamethasone stimulates differentiation of odontoblast-like cells in human dental pulp cultures. *Cell Tissue Res.* 321(3), 391–400 (2005).

21 Tecles O, Laurent P, Zygouritsas S *et al.* Activation of human dental pulp progenitor/stem cells in response to odontoblast injury. *Arch. Oral Biol.* 50(2), 103–108 (2005).

22 Waddington RJ, Youde SJ, Lee CP, Sloan AJ. Isolation of distinct progenitor stem cell populations from dental pulp. *Cells Tissues Organs* 189(1–4), 268–274 (2009).

23 De Mendonca Costa A, Bueno DF, Martins MT *et al.* Reconstruction of large cranial defects in nonimmunosuppressed experimental design with human dental pulp stem cells. *J. Craniofac. Surg.* 19(1), 204–210 (2008).

24 Kerkis I, Ambrosio CE, Kerkis A *et al.* Early transplantation of human immature dental pulp stem cells from baby teeth to golden retriever muscular dystrophy (GRMD) dogs: local or systemic? *J. Transl Med.* 6, 35 (2008).

25 Nosrat IV, Widenfalk J, Olson L, Nosrat CA. Dental pulp cells produce neurotrophic factors, interact with trigeminal neurons *in vitro*, and rescue motoneurons after spinal cord injury. *Dev. Biol.* 238(1), 120–132 (2001).

26 Honda MJ, Shinohara Y, Hata KI, Ueda M. Subcultured odontogenic epithelial cells in combination with dental mesenchymal cells produce enamel-dentin-like complex structures. *Cell Transplant.* 16(8), 833–847 (2007).

27 Nam H, Lee G. Identification of novel epithelial stem cell-like cells in human deciduous dental pulp. *Biochem. Biophys. Res. Comm.* 386(1), 135–139 (2009).

28 Nam H, Kim J, Park J *et al.* Expression profile of the stem cell markers in human Hertwig's epithelial root sheath/epithelial rests of Malassez cells. *Mol. Cells* 31(4), 355–360 (2011).

29 Shinmura Y, Tsuchiya S, Hata K, Honda MJ. Quiescent epithelial cell rests of Malassez can differentiate into ameloblast-like cells. *J. Cell Physiol.* 217(3), 728–738 (2008).

30 Atari M, Gil-Recio C, Fabregat M *et al.* Dental pulp of the third molar: a new source of pluripotent-like stem cells. *J. Cell Sci.* 125(Pt 14), 3343–3356 (2012).

31 Huang GT, Shagramanova K, Chan SW. Formation of odontoblast-like cells from cultured human dental pulp cells on dentin *in vitro*. *J. Endodontics* 32(11), 1066–1073 (2006).

32 Volponi AA, Pang Y, Sharpe PT. Stem cell-based biological tooth repair and regeneration. *Trends Cell Biol.* 20(12), 715–722 (2010).

33 Washio K, Iwata T, Mizutani M *et al.* Assessment of cell sheets derived from human periodontal ligament cells: a pre-clinical study. *Cell Tissue Res.* 341(3), 397–404 (2010).

34 Yang B, Chen G, Li J *et al.* Tooth root regeneration using dental follicle cell sheets in combination with a dentin matrix-based scaffold. *Biomaterials* 33(8), 2449–2461 (2012).

35 Howell TH, Fiorellini JP, Paquette DW, Offenbacher S, Giannobile WV, Lynch SE. A Phase I/II clinical trial to evaluate a combination of recombinant human platelet-derived growth factor-BB and recombinant human insulin-like growth factor-I in patients with periodontal disease. *J. Periodontol.* 68(12), 1186–1193 (1997).

36 Lynch SE, Williams RC, Polson AM *et al.* A combination of platelet-derived and insulin-like growth factors enhances periodontal regeneration. *J. Clin. Periodontol.* 16(8), 545–548 (1989).

37 Nakashima M, Mizunuma K, Murakami T, Akamine A. Induction of dental pulp stem cell differentiation into odontoblasts by electroporation-mediated gene delivery of growth/differentiation factor 11 (Gdf11). *Gene Ther.* 9(12), 814–818 (2002).

38 Jin QM, Anusaksathien O, Webb SA, Rutherford RB, Giannobile WV. Gene therapy of bone morphogenetic protein for periodontal tissue engineering. *J. Periodontol.* 74(2), 202–213 (2003).

39 Ripamonti U, Crooks J, Petit JC, Rueger DC. Periodontal tissue regeneration by combined applications of recombinant human osteogenic protein-1 and bone morphogenetic protein – a pilot study in Chacma baboons (*Papio ursinus*). *Eur. J. Oral Sci.* 109(4), 241–248 (2001).

40 Veis A, Tompkins K, Alvares K *et al.* Specific amelogenin gene splice products have signaling effects on cells in culture and in implants *in vivo*. *J. Biol. Chem*. 275(52), 41263–41272 (2000).

41 Grad I, Hibaoui Y, Jaconi M *et al.* NANOG priming before full reprogramming may generate germ cell tumours. *Eur. Cells Mater.* 22, 258–274; discussion 274 (2011).

42 Forsberg M, Hovatta O. Challenges for the therapeutic use of pluripotent stem derived cells. *Front. Physiol.* 3, 19 (2012).

43 Wada N, Menicanin D, Shi S, Bartold PM, Gronthos S. Immunomodulatory properties of human periodontal ligament stem cells. *J. Cell Physiol.* 219(3), 667–676 (2009).

44 Le Blanc K, Ringden O. Immunomodulation by mesenchymal stem cells and clinical experience. *J. Inter. Med.* 262(5), 509–525 (2007).

45 Wang M, Yang Y, Yang D *et al.* The immunomodulatory activity of human umbilical cord blood-derived mesenchymal stem cells *in vitro*. *Immunology* 126(2), 220–232 (2009).

46 Davies LC, Lonnies H, Locke M *et al.* Oral mucosal progenitor cells are potently immunosuppressive in a dose-independent manner. *Stem Cells Dev.* 21(9), 1478–1487 (2012).

47 Takahashi K, Yamanaka S. Induction of pluripotent stem cells from mouse embryonic and adult fibroblast cultures by defined factors. *Cell* 126(4), 663–676 (2006).

▪▪ **Induced pluripotent stem cells were generated for the first time.**

48 Takahashi K, Okita K, Nakagawa M, Yamanaka S. Induction of pluripotent stem cells from fibroblast cultures. *Nat. Protocols* 2(12), 3081–3089 (2007).

49 Otsu K, Kishigami R, Oikawa-Sasaki A *et al.* Differentiation of induced pluripotent stem cells into dental mesenchymal cells. *Stem Cells Dev.* 21(7), 1156–1164 (2012).

50 Li SC, Zhong JF. Twisting immune responses for allogeneic stem cell therapy. *World J. Stem Cells* 1(1), 30–35 (2009).

51 Okita K, Yamanaka S. Induced pluripotent stem cells: opportunities and challenges. *Philos. Trans. R. Soc. Lond. Series B Biol. Sci.* 366(1575), 2198–2207 (2011).

52 Zhao T, Zhang ZN, Rong Z, Xu Y. Immunogenicity of induced pluripotent stem cells. *Nature* 474(7350), 212–215 (2011).

53 Kim BY, Rutka JT, Chan WC. Nanomedicine. *N. Engl. J. Med.* 363(25), 2434–2443 (2010).

▪▪ **Discusses the applications of nanomaterials in medicine.**

54 Xia Y. Nanomaterials at work in biomedical research. *Nat. Mater.* 7(10), 758–760 (2008).

55 Huebsch N, Mooney DJ. Inspiration and application in the evolution of biomaterials. *Nature* 462(7272), 426–432 (2009).

56 Moghimi SM, Hunter AC, Murray JC. Nanomedicine: current status and future prospects. *FASEB J.* 19(3), 311–330 (2005).

57 Moghimi SM, Hunter AC, Andresen TL. Factors controlling nanoparticle pharmacokinetics: an integrated analysis and perspective. *Ann. Rev. Pharm. Toxicol.* 52, 481–503 (2012).

58 Wang Y, Brown P, Xia Y. Nanomedicine: swarming towards the target. *Nat. Mater.* 10(7), 482–483 (2011).

59 Petros RA, Desimone JM. Strategies in the design of nanoparticles for therapeutic applications. *Nat. Rev. Drug Discov.* 9(8), 615–627 (2010).

▪▪ **Review of the various strategies for designing nanoparticles destined for clinical use.**

60 Von Maltzahn G, Park JH, Lin KY *et al.* Nanoparticles that communicate *in vivo* to amplify tumour targeting. *Nat. Mater.* 10(7), 545–552 (2011).

61 Douglas SM, Bachelet I, Church GM. A logic-gated nanorobot for targeted transport of molecular payloads. *Science* 335(6070), 831–834 (2012).

▪ **Elegant and smart design of nanorobots for targeted transport.**

62 Oh S, Brammer KS, Li YS *et al.* Stem cell fate dictated solely by altered nanotube dimension. *Proc. Natl Acad. Sci. USA* 106(7), 2130–2135 (2009).

63 Jungebluth P, Alici E, Baiguera S *et al.* Tracheobronchial transplantation with a stem-cell-seeded bioartificial nanocomposite: a proof-of-concept study. *Lancet* 378(9808), 1997–2004 (2011).

64 Andon FT, Fadeel B. Programmed cell death: molecular mechanisms and implications for safety assessment of nanomaterials. *Acc. Chem. Res.* doi:10.1021/ar300020b (2012) (Epub ahead of print).

65 Prescott C. Regenerative nanomedicines: an emerging investment prospective? *J. R. Soc. Inter. R. Soc.* 7(Suppl. 6), S783–S787 (2010).

66 Arbab AS, Janic B, Haller J, Pawelczyk E, Liu W, Frank JA. *In vivo* cellular imaging for translational medical research. *Curr. Med. Imaging Rev.* 5(1), 19–38 (2009).

67 Gera A, Steinberg GK, Guzman R. *In vivo* neural stem cell imaging: current modalities and future directions. *Regen. Med.* 5(1), 73–86 (2010).

68 Ferreira L, Karp JM, Nobre L, Langer R. New opportunities: the use of nanotechnologies to manipulate and track stem cells. *Cell Stem Cell* 3(2), 136–146 (2008).

69 Thu MS, Bryant LH, Coppola T *et al.* Self-assembling nanocomplexes by combining ferumoxytol, heparin and protamine for cell tracking by magnetic resonance imaging. *Nat. Med.* 18(3), 463–467 (2012).

70 Lewin M, Carlesso N, Tung CH *et al.* Tat peptide-derivatized magnetic nanoparticles allow *in vivo* tracking and recovery of progenitor cells. *Nat. Biotechnol.* 18(4), 410–414 (2000).

71 Terreno E, Castelli DD, Viale A, Aime S. Challenges for molecular magnetic resonance imaging. *Chem. Rev.* 110(5), 3019–3042 (2010).

72 Yu SB, Watson AD. Metal-based x-ray contrast media. *Chem. Rev.* 99(9), 2353–2378 (1999).

73 Chen K, Conti PS. Target-specific delivery of peptide-based probes for PET imaging. *Adv. Drug Del. Rev.* 62(11), 1005–1022 (2010).

74 Reimer P, Balzer T. Ferucarbotran (Resovist): a new clinically approved RES-specific contrast agent for contrast-enhanced MRI of the liver: properties, clinical development, and applications. *Eur. Radiol.* 13(6), 1266–1276 (2003).

75 Wang YX, Hussain SM, Krestin GP. Superparamagnetic iron oxide contrast agents: physicochemical characteristics and applications in MR imaging. *Eur. Radiol.* 11(11), 2319–2331 (2001).

76 Hsiao JK, Tai MF, Chu HH *et al.* Magnetic nanoparticle labeling of mesenchymal stem cells without transfection agent: cellular behavior and capability of detection with clinical 5 T magnetic resonance at the single cell level. *Magn. Reson. Med.* 58(4), 717–724 (2007).

77 Arbab AS, Yocum GT, Kalish H *et al.* Efficient magnetic cell labeling with protamine sulfate complexed to ferumoxides for cellular MRI. *Blood* 104(4), 1217–1223 (2004).

78 Song YS, Ku JH. Monitoring transplanted human mesenchymal stem cells in rat and rabbit bladders using molecular magnetic resonance imaging. *Neurourol. Urodynamics* 26(4), 584–593 (2007).

79 Bruchez MP. Quantum dots find their stride in single molecule tracking. *Curr. Opin Chem. Biol.* 15(6), 775–780 (2011).

80 Lin S, Xie X, Patel MR *et al.* Quantum dot imaging for embryonic stem cells. *BMC Biotechnol.* 7, 67 (2007).

81 Zhang H, Yee D, Wang C. Quantum dots for cancer diagnosis and therapy: biological and clinical perspectives. *Nanomedicine (Lond.)* 3(1), 83–91 (2008).

82 Alivisatos P. The use of nanocrystals in biological detection. *Nat. Biotechnol.* 22(1), 47–52 (2004).

83 Chen H, Titushkin I, Stroscio M, Cho M. Altered membrane dynamics of quantum dot-conjugated integrins during osteogenic differentiation of human bone marrow derived progenitor cells. *Biophys. J.* 92(4), 1399–1408 (2007).

84 Chakraborty SK, Fitzpatrick JA, Phillippi JA *et al.* Cholera toxin B conjugated quantum dots for live cell labeling. *Nano Lett.* 7(9), 2618–2626 (2007).

85 Shah BS, Mao JJ. Labeling of mesenchymal stem cells with bioconjugated quantum dots. *Meth. Mol. Biol.* 680, 61–75 (2011).

86 Slotkin JR, Chakrabarti L, Dai HN *et al.* *In vivo* quantum dot labeling of mammalian stem and progenitor cells. *Dev. Dyn.* 236(12), 3393–3401 (2007).

87 Hsieh SC, Wang FF, Lin CS, Chen YJ, Hung SC, Wang YJ. The inhibition of osteogenesis with human bone marrow mesenchymal stem cells by CdSe/ZnS quantum dot labels. *Biomaterials* 27(8), 1656–1664 (2006).

88 Maysinger D, Lovric J, Eisenberg A, Savic R. Fate of micelles and quantum dots in cells. *Eur. J. Pharm. Biopharm.* 65(3), 270–281 (2007).

89 Ruoslahti E, Bhatia SN, Sailor MJ. Targeting of drugs and nanoparticles to tumors. *J. Cell Biol.* 188(6), 759–768 (2010).

90 Mitsiadis TA, Rahiotis C. Parallels between tooth development and repair: conserved molecular mechanisms following carious and dental injury. *J. Dental Res.* 83(12), 896–902 (2004).

91 Derfus AM, Chen AA, Min DH, Ruoslahti E, Bhatia SN. Targeted quantum dot conjugates for siRNA delivery. *Bioconjugate Chem.* 18(5), 1391–1396 (2007).

92 Harris TJ, Green JJ, Fung PW, Langer R, Anderson DG, Bhatia SN. Tissue-specific gene delivery via nanoparticle coating. *Biomaterials* 31(5), 998–1006 (2010).

93 Clements MO, Godfrey A, Crossley J, Wilson SJ, Takeuchi Y, Boshoff C. Lentiviral manipulation of gene expression in human adult and embryonic stem cells. *Tissue Eng.* 12(7), 1741–1751 (2006).

94 Clements BA, Incani V, Kucharski C, Lavasanifar A, Ritchie B, Uludag H. A comparative evaluation of poly-L-lysine-palmitic acid and Lipofectamine 2000 for plasmid delivery to bone marrow stromal cells. *Biomaterials* 28(31), 4693–4704 (2007).

95 Glover DJ, Lipps HJ, Jans DA. Towards safe, non-viral therapeutic gene expression in humans. *Nat. Rev. Gene* 6(4), 299–310 (2005).

96 Gropp M, Reubinoff B. Lentiviral vector-mediated gene delivery into human embryonic stem cells. *Meth. Enzymol.* 420, 64–81 (2006).

97 Aliabadi HM, Landry B, Sun C, Tang T, Uludag H. Supramolecular assemblies in functional siRNA delivery: where do we stand? *Biomaterials* 33(8), 2546–2569 (2012).

98 Bianco A, Kostarelos K, Prato M. Making carbon nanotubes biocompatible and biodegradable. *Chem. Commun. (Camb.)* 47(37), 10182–10188 (2011).

99 Kostarelos K. Carbon nanotubes: fibrillar pharmacology. *Nat. Mater.* 9(10), 793–795 (2010).

100 Kutsuzawa K, Akaike T, Chowdhury EH. The influence of the cell-adhesive proteins E-cadherin and fibronectin embedded in carbonate-apatite DNA carrier on transgene delivery and expression in a mouse embryonic stem cell line. *Biomaterials* 29(3), 370–376 (2008).

101 Mooney DJ, Vandenburgh H. Cell delivery mechanisms for tissue repair. *Cell Stem Cell* 2(3), 205–213 (2008).

102 Kuo SW, Lin HI, Hui-Chun Ho J *et al.* Regulation of the fate of human mesenchymal stem cells by mechanical and stereo-topographical cues provided by silicon nanowires. *Biomaterials* 33(20), 5013–5022 (2012).

103 Shih YR, Chen CN, Tsai SW, Wang YJ, Lee OK. Growth of mesenchymal stem cells on electrospun type I collagen nanofibers. *Stem Cells* 24(11), 2391–2397 (2006).

104 Dzenis Y. Materials science. Structural nanocomposites. *Science* 319(5862), 419–420 (2008).

105 Murugan R, Ramakrishna S. Design strategies of tissue engineering scaffolds with controlled fiber orientation. *Tissue Eng.* 13(8), 1845–1866 (2007).

106 Mitsiadis TA, Barrandon O, Rochat A, Barrandon Y, De Bari C. Stem cell niches in mammals. *Exp. Cell Res.* 313(16), 3377–3385 (2007).

107 Kraehenbuehl TP, Langer R, Ferreira LS. Three-dimensional biomaterials for the study of human pluripotent stem cells. *Nat. Methods* 8(9), 731–736 (2011).

▪ **The construction and benefits of artificial stem cell niches.**

108 Dalby MJ, Andar A, Nag A *et al.* Genomic expression of mesenchymal stem cells to altered nanoscale topographies. *J. R. Soc. Inter. R. Soc.* 5(26), 1055–1065 (2008).

109 Dickinson LE, Kusuma S, Gerecht S. Reconstructing the differentiation niche of embryonic stem cells using biomaterials. *Macromol. Biosci.* 11(1), 36–49 (2011).

110 Lipski AM, Pino CJ, Haselton FR, Chen IW, Shastri VP. The effect of silica nanoparticle-modified surfaces on cell morphology, cytoskeletal organization and function. *Biomaterials* 29(28), 3836–3846 (2008).

111 Hashi CK, Zhu Y, Yang GY *et al.* Antithrombogenic property of bone marrow mesenchymal stem cells in nanofibrous vascular grafts. *Proc. Natl Acad. Sci. USA* 104(29), 11915–11920 (2007).

112 Hashi CK, Derugin N, Janairo RR *et al.* Antithrombogenic modification of small-diameter microfibrous vascular grafts. *Arterioscler. Thromb. Vasc. Biol.* 30(8), 1621–1627 (2010).

14.1.3 Woloszyk et al., PLoS One, 2014

Influence of mechanical environment on the engineering of mineralized tissues using human dental pulp stem cells and silk fibroin scaffolds (PAPER)

This paper describes the findings of a collaborative project between the Institute of Oral Biology (University of Zurich) and the Institute for Biomechanics (ETH Zurich), which was mostly performed by Sabrina Holsten Dircksen within the framework of her Master Thesis. To finalize the project, I used frozen samples from the study for RNA extraction in order to study the gene expression within the different groups, which are typically expressed in mineralized tissues like bone, dentin, and cementum. Based on the manuscript of Sabrina Holsten Dircksen and my gene expression analysis, I compiled all the results and figures, and rewrote the manuscript in order to adapt it for publication in PLoS ONE.

This study investigated the influence of the mechanobiological environment of human dental pulp stem cells *in vitro* on their mineralization potential when seeded on a 3D silk fibroin scaffold. Mechanical stimulation was provided by a spinner flask bioreactor, while osteogenic differentiation medium was used as a biological stimulus. Histological analyses and micro-computed tomography (microCT) of the samples showed low levels of mineralisation when samples were cultured in static conditions, while their culture in a dynamic environment with osteogenic medium and weekly microCT scans significantly increased the formation of homogeneously mineralised structures, which was also confirmed by the elevated calcium levels. The gene expression analysis suggested that hDPSCs are able to adapt a non-dental identity by changing the culture conditions only. Taken together, the presented findings showed that the mechanically dynamic environment can direct hDPSCs towards the osteogenic lineage significantly stronger than osteogenic medium alone. However, the combination of mechanical and biological stimuli yields the highest amount of mineralization, suggesting a synergistic effect.

OPEN ACCESS Freely available online

PLOS ONE

Influence of the Mechanical Environment on the Engineering of Mineralised Tissues Using Human Dental Pulp Stem Cells and Silk Fibroin Scaffolds

Anna Woloszyk[1], Sabrina Holsten Dircksen[2], Nagihan Bostanci[3], Ralph Müller[2], Sandra Hofmann[2,4,5], Thimios A. Mitsiadis[1]*

1 Orofacial Development and Regeneration, Institute of Oral Biology, Centre of Dental Medicine, University of Zurich, Zurich, Switzerland, **2** Institute for Biomechanics, ETH Zurich, Zurich, Switzerland, **3** Oral Translational Research, Institute of Oral Biology, Centre of Dental Medicine, University of Zurich, Zurich, Switzerland, **4** Department of Biomedical Engineering, Eindhoven University of Technology, Eindhoven, the Netherlands, **5** Institute for Complex Molecular Sciences, Eindhoven University of Technology, Eindhoven, the Netherlands

Abstract

Teeth constitute a promising source of stem cells that can be used for tissue engineering and regenerative medicine purposes. Bone loss in the craniofacial complex due to pathological conditions and severe injuries could be treated with new materials combined with human dental pulp stem cells (hDPSCs) that have the same embryonic origin as craniofacial bones. Optimising combinations of scaffolds, cells, growth factors and culture conditions still remains a great challenge. In the present study, we evaluate the mineralisation potential of hDPSCs seeded on porous silk fibroin scaffolds in a mechanically dynamic environment provided by spinner flask bioreactors. Cell-seeded scaffolds were cultured in either standard or osteogenic media in both static and dynamic conditions for 47 days. Histological analysis and micro-computed tomography of the samples showed low levels of mineralisation when samples were cultured in static conditions (0.16±0.1 BV/TV%), while their culture in a dynamic environment with osteogenic medium and weekly µCT scans (4.9±1.6 BV/TV%) significantly increased the formation of homogeneously mineralised structures, which was also confirmed by the elevated calcium levels (4.5±1.0 *vs.* 8.8±1.7 mg/mL). Molecular analysis of the samples showed that the expression of tooth correlated genes such as *Dentin Sialophosphoprotein* and *Nestin* were downregulated by a factor of 6.7 and 7.4, respectively, in hDPSCs when cultured in presence of osteogenic medium. This finding indicates that hDPSCs are able to adopt a non-dental identity by changing the culture conditions only. Also an increased expression of *Osteocalcin* (1.4x) and *Collagen type I* (1.7x) was found after culture under mechanically dynamic conditions in control medium. In conclusion, the combination of hDPSCs and silk scaffolds cultured under mechanical loading in spinner flask bioreactors could offer a novel and promising approach for bone tissue engineering where appropriate and rapid bone regeneration in mechanically loaded tissues is required.

Citation: Woloszyk A, Holsten Dircksen S, Bostanci N, Müller R, Hofmann S, et al. (2014) Influence of the Mechanical Environment on the Engineering of Mineralised Tissues Using Human Dental Pulp Stem Cells and Silk Fibroin Scaffolds. PLoS ONE 9(10): e111010. doi:10.1371/journal.pone.0111010

Editor: Irina Kerkis, Instituto Butantan, Brazil

Received July 3, 2014; **Accepted** September 25, 2014; **Published** October 29, 2014

Data Availability: The authors confirm that all data underlying the findings are fully available without restriction. All relevant data are within the paper and its Supporting Information files.

Funding: This work was supported by funds from University of Zurich, funds from ETH Zurich. The funders had no role in study design, data collection and analysis, decision to publish, or preparation of the manuscript.

Competing Interests: The authors have declared that no competing interests exist.

* Email: thimios.mitsiadis@zzm.uzh.ch

Introduction

Hard tissues of the craniofacial complex are subjected to physical, chemical and biological health risk factors of the surrounding environment. Examples are high mechanical impact resulting in fractures, smoking as a risk factor for osteoporosis and bone fracture [1], as well as microbiological infections of the periodontal tissues resulting in alveolar bone and subsequent tooth loss [2]. Repair of these bones requires the reconstruction of their anatomical, physiological, and functional properties, which cannot yet be fully accomplished by current treatment strategies [3]. For this reason, a considerable effort has been made during the last two decades to generate innovative engineering products that could be used together with specific populations of stem/progenitor cells and growth factors in order to form the most adequate and physiological substitutes for bone repair.

Mesenchymal cells forming craniofacial bones and dental tissues (e.g. dentin) have the same embryonic origin and share many biochemical and molecular properties [4–6]. These tissues are composed mostly of collagen type I and, to a lesser degree, of other tissue-specific extracellular matrix components that with the progressive deposition of hydroxyapatite crystals become highly mineralised [7,8]. As for all other tissues, their homeostasis is based on the presence of sufficient vasculature [9], innervation [10], and specific stem cell populations. These cells are characterised by their ability to self-renew without losing their potency to differentiate into various cell types [11].

Bones undergo constant remodelling by a well-orchestrated interplay of stem cell-derived osteoblasts and osteoclasts [12]. In contrast to that, dentin is not remodelled but continuously deposited by odontoblasts throughout the life of a tooth [13,14]. Following serious dental injuries or carious lesions, disintegrated odontoblasts can be replaced by newly-formed odontoblasts that originate from stem cells residing in the dental pulp [5,14–16].

Bone marrow stem cells (BMSCs) were the first to be used in clinics with success for the treatment of leukemias since the 1950 s [17] and thus constitute the golden standard in stem cell research. Since the discovery of dental pulp stem cells (DPSCs) comparative studies have shown that both BMSCs and DPSCs have almost identical properties in terms of gene expression and differentiation potential (e.g. osteogenic, chondrogenic, adipogenic, myogenic, neurogenic) [15,18,19]. However, DPSCs exhibit higher clonogenic and proliferative potential when compared to BMSCs [20]. In contrast to BMSCs that originate from the mesoderm, DPSCs are derived from cranial neural crest (CNC) cells, as demonstrated by the expression of markers characteristic for CNC-derived stem cells like GFAP, HNK-1, nestin, P75, and S-100 [11,21]. Common embryonic origin together with the Hox gene expression profile was shown to play a key role in determining progenitor cell fate during adult bone regeneration [22]. It was demonstrated that Hox-negative neural crest-derived skeletal stem cells adopted a Hox-positive profile and differentiated into osteoblasts after transplantation into a defect in the mesoderm-derived tibia. On the contrary, Hox-positive mesoderm-derived skeletal stem cells did not adopt a Hox-negative profile and differentiated into chondroblasts after transplantation into a defect in the neural crest-derived mandible [22]. This proves that stem cells differ in plasticity and that they have a 'positional memory' that depends on their Hox gene expression profile [23]. The use of DPSCs is thus important for reconstitution of craniofacial tissues and presumably much more appropriate than the use of BMSCs. Furthermore, DPSCs are easily accessible after routine tooth extraction procedures resulting in little morbidity and therefore a realistic autologous cell source, while BMSC isolation requires invasive and painful surgery. Optimising the combination of DPSCs, scaffolds, growth factors, and the use of mechanical loading for the generation of particular hard tissues is currently a great challenge.

Numerous types of silk fibroin scaffolds have been used for tissue engineering purposes in the last two decades [24,25]. Important advantages of silk compared to other biomaterials are the excellent biocompatible and mechanical properties, load-bearing capacity, and lack of releasing toxic by-products during silk degradation [26]. Silk scaffolds have been used in combination with a variety of cell types to obtain the most desirable effects for specific tissue repair. The behaviour and fate of stem cells closely depend on the geometry and composition of the scaffolds, as well as the applied forces [27]. For example, BMSCs were incorporated in hexafluoro-2-propanol based porous silk scaffolds for optimal bone regeneration [28–31]. Mechanical cues, including shear stress, substrate stiffness and nano-topography, have been shown to also stimulate osteogenesis [32]. Mechanotransduction is carried out through several mechanoreceptors, like integrins, cadherins, gap junctions, and Ca^{2+} channels, which are able to alter gene expression in response to loading or stretching [33–35]. A tool for imposing shear stress on cells during *in vitro* culture conditions is the spinner flask bioreactor through increased turbulent fluid flow, generated by stirring of the medium. Compared to static cultures, the bioreactor improves the culture conditions since it allows better control in terms of temperature, pH, pressure, nutrient and oxygen supply as well as waste removal [36,37].

After investigating the osteogenic potential of human DPSCs seeded in silk scaffolds cultured in both static and dynamic conditions, in the present study we were able to show that these cells are reactive to mechanical loading, which is an important component of both the bone and the tooth environment and is able to increase the mineralisation of silk scaffolds by human DPSCs *in vitro*.

Materials and Methods

Preparation of silk fibroin scaffolds

Silk fibroin scaffolds were prepared as previously described [29]. Briefly, silkworm cocoons (Trudel Inc., Zurich, Switzerland) were boiled 2 times for 1 h in an aqueous solution of 0.02 M Na_2CO_3 (Fluka, Buchs SG, Switzerland) and rinsed with ultrapure water (UPW) to extract sericin. Lyophilized silk was dissolved in hexafluoro-2-propanol (HFIP) (abcr GmbH & Co., Karlsruhe, Germany) to obtain a 17% (w/v) silk fibroin solution. NaCl crystals (224–315 μm in diameter) (Sigma-Aldrich, Buchs SG, Switzerland) were weighed in Teflon containers and silk fibroin/HFIP solution was added at a ratio of 20: 1 (NaCl/silk fibroin). After complete evaporation of the solvent NaCl/silk fibroin blocks were immersed in 90% (v/v) methanol (Sigma-Aldrich, Buchs SG, Switzerland) in UPW for 30 min, dried and NaCl was leached by incubation in UPW for 2 days resulting in scaffolds with more than 90% porosity [38]. 25 disk shaped scaffolds were punched (10 mm diameter, 1–2 mm thick) and autoclaved at 121°C and 1 bar for 20 min.

Isolation, culture and characterisation of dental pulp stem cells (DPSCs)

DPSCs were obtained from dental pulps of clinically healthy teeth from 14–16 year old patients who had their teeth extracted due to orthodontic treatment. The procedure was reviewed and approved by the Institutional Review Board of the Centre of Dental Medicine, University of Zurich and was performed with guardians' and underage patients' written informed consent abiding by the guidelines for studies with human cells of irreversibly anonymous origin. Written consents are stored in the dental faculty for all anonymized studies. After removal of the dental pulp from the tooth, DPSCs were isolated, expanded and characterized as described earlier [39]. All experiments were performed with DPSCs at passage 3 (P3) or P4.

Scaffold seeding

25 silk fibroin scaffolds were pre-wetted in Dulbecco's Modified Eagle Medium (DMEM) for 36 hours at room temperature before seeding them with DPSCs (5 scaffolds per group) at a density of 5×10^6 cells per scaffold in 50 μL of control medium (DMEM, 10% FBS, 1% Pen-Strep and 50 ng/mL fungizone). To allow attachment of DPSCs to the scaffolds, they were incubated for 90 min in a humidified incubator at 37°C. Thereafter, 1 mL culture medium per well (12-well-plate) was added and scaffolds were incubated for additional 24 h. Subsequently, scaffolds were placed in spinner flask bioreactors with a stirring speed of 120 rpm (referred to as dynamic) or in spinner flask bioreactors without stirring (referred to as static) and were cultured in either control or osteogenic medium (control medium plus 50 μg/mL ascorbic acid-2-phosphate, 100 nM dexamethasone, 7 mM β-glycerolphosphate) at 37°C with 5% CO_2. All cell culture ingredients were obtained from Gibco Invitrogen, Basel, Switzerland.

Sample analysis

Micro-computed tomography (μCT). μCT measurements were performed on a μCT80 imaging system (Scanco Medical, Brüttisellen, Switzerland). Samples were scanned either weekly starting from day 19 (groups Sp.O.W, Sp.C.W) or on the last day of the experiment only to determine potential x-ray effects on cell development (groups Sp.O.E, St.O.E, St.C.E) ($n = 5$–6 per group). Scanning was performed at an isotropic nominal resolution of 18 μm, energy level was set to 45 kVp, intensity to 177 μA, 200 ms integration time and two-fold frame averaging. A constrained Gaussian filter was applied to reduce part of the noise. Filter support was set to 1.0 and filter width sigma to 0.8. Segmentation was performed to distinguish mineralised tissue from non-mineralised tissue. A threshold that corresponded to a hydroxyapatite density of 145 mg HA/ccm was set after visual judgement of the grey images to identify mineralised structures. Components smaller than 50 voxels were filtered away by applying component labelling. Quantitative morphometry was performed to assess relative mineralised extracellular matrix volume of the entire construct using direct microstructural bone analysis as previously described for human bone biopsies [40].

After 47 days of culture, scaffolds were blotted on clean paper towels to determine the total wet weight. Scaffolds were weighed, cut into six pieces, weighed again and processed for various analyses ($n = 5$–6 per group). Where necessary, samples were disintegrated using steel balls and a Mini-Beadbeater (Biospec, Bartlesville, OK, USA) three times at 25,000 rpm for 10 s with cooling of the samples in between the cycles.

Cell proliferation and viability. Cell proliferation was determined by DNA analysis from disintegrated samples. DNA content was measured using the Quant-iT PicoGreen dsDNA Assay Kit (Life Technologies Europe B.V., Zug, Switzerland) and cell viability was evaluated using the AlamarBlue assay (Life Technologies Europe B.V., Zug, Switzerland) according to the manufacturer's instructions. Fluorescence was measured using a plate reader (Infinite 200 PRO, Tecan Group Ltd, Männedorf, Switzerland).

Osteogenic potential of DPSCs. To study the osteogenic capacity of DPSCs seeded into silk fibroin scaffolds we performed alkaline phosphatase (ALP) and calcium deposition assays additionally to the μCT evaluation. For this purpose, disintegrated scaffold pieces were used. ALP activity (Sigma-Aldrich, Buchs SG, Switzerland) was measured spectrophotometrically based on conversion of p-nitrophenyl phosphate to p-nitrophenol as previously described [29]. Quantification of calcium was performed with the Calcium (CPC) LiquiColor Test according to the manufacturer's instructions (DiaSys Greiner, Flacht, Germany). Collagen type I was assessed by staining the intact samples with Sirius Red (Sigma-Aldrich, Buchs SG, Switzerland) as described previously [41]. After washing the samples with UPW, the remaining colour in saturated picric acid was bleached in a 1: 1 mix of Methanol and 0.2 M NaOH (Sigma-Aldrich, Buchs SG, Switzerland).

Histology. After fixation of the constructs in 10% neutral buffered formalin at room temperature for 20 min and 5 times washing with UPW, samples were dehydrated and impregnated with paraffin over night by use of a tissue processor (TPC 15 Duo, Medite AG, Winter Garden FL, United States) before being embedded in paraffin using a paraffin embedding station (TES 99, Medite AG, Winter Garden, FL, USA). Paraffin sections of 6–7 μm (HM355S, Microm International, Walldorf, Germany) were stained with Haematoxylin and Eosin (H&E) (Sigma-Aldrich, Buchs SG, Switzerland) for a general overview. Collagen distribution was visualised by Sirius Red staining while mineralisation was shown with von Kossa staining (Sigma-Aldrich, Buchs SG, Switzerland).

Gene expression analysis. RNA was extracted using a RNA extraction kit (RNeasy Mini Kit, Qiagen, Basel, Switzerland) and then transcribed into cDNA (High Capacity cDNA Reverse Transcription Kit, Applied Biosciences, Foster City, CA, USA). Quantitative Real Time (qRT) PCR was performed using SYBR-Green-based protocols in a StepOne Real Time PCR System (Applied Biosystems, Life Technologies, Basel, Switzerland). Expression analysis of *ALP*, *Collagen type I*, *Dentin Sialophosphoprotein (DSPP)*, *Nestin*, *Osteocalcin* and *GAPDH* (housekeeping gene) were carried out using the qPCR SYBR Master Mix (Applied Biosystems, Carlsbad, USA) in combination with oligonucleotide primers (Tab. 1), specifically designed for the indicated genes. Expression levels were calculated by the comparative ΔCt method ($2^{-\Delta Ct}$ formula) after being normalised to the Ct-value of the *GAPDH* housekeeping gene.

Statistical analysis

Comparisons of the groups were performed using one-way analysis of variance (ANOVA). When there were significant differences ($p<0.05$), comparisons betweeen the groups were further assessed with Bonferroni multiple-comparison test. Data were considered statistically significant at $p<0.05$ and highly significant at $p<0.01$.

Results

Mineralised tissue formation by hDPSCs

Mineralisation was monitored by time-lapse μCT starting from day 19 of *in vitro* culture in two of the five experimental groups, which were both cultured in a mechanically dynamic system in either osteogenic (Sp.O.W) or control medium (Sp.C.W) (Fig. 1b). Cells grown in control medium formed mineralised matrix with a delay of 2 weeks (Fig. 1d). A comparison of all the groups (Fig. 1a) showed significantly higher mineralisation in samples cultured at 120 rpm (dynamic) than samples cultured at 0 rpm (static) ($p<0.01$) (Fig. 1c, 1e), being even more abundant in samples that were cultured additionally in osteogenic medium (Fig. 1b, 1d). Mineralisation followed a linear pattern (Fig. 1d) with correlation coefficients of 0.99 and 0.98 for samples cultured in osteogenic and control medium, respectively. Both qualitative and quantitative analyses of the bone-like tissue volume fraction for all groups demonstrated that mineralisation was significantly higher in DPSC-seeded scaffolds cultured in spinner flasks at 120 rpm in osteogenic medium with weekly μCT scans (Fig. 1c1, 1e) when compared to the static control samples (Fig. 1c4, 1c5, 1e) ($p<0.01$). Samples cultured at 120 rpm (Fig. 1c1–3) exhibited a more homogenous mineralisation than samples cultured at 0 rpm (Fig. 1c4, 1c5).

Histological analysis of the tissue formed by DPSCs

Haematoxylin and Eosin staining showed that in samples cultured in spinner flasks the cells were distributed all over the scaffolds (Fig. 2a1–2a3). In their centre these scaffolds presented larger hollow areas free of cells and extracellular matrix (ECM). The amount of cells and ECM appeared to be lower in samples cultured in control medium (Fig. 2a2, 2a5) when compared to cells grown in osteogenic medium (Fig. 2a1, 2a4). The von Kossa staining confirmed the presence of phosphate in all groups (Fig. 2b1–2b5) and the Sirius Red staining allowed the visualisation of collagen type I fibres in all groups (Fig. 2c1–2c5). Qualitatively, the most homogenous distribution of collagen fibres was found in samples cultured in osteogenic medium in spinner

Table 1. Primers used in the study.

Primers	Sequence	Function
Alkaline Phosphatase (ALP)	fw ATGAAGGAAAAGCCAAGCAG	marker for matrix mineralisation
	rv ATGGAGACATTCTCTCGTTC	
Collagen type I (Col1)	fw AAGATGGACTCAACGGTCTC	marker for bone formation
	rv CAGGAAGCTGAAGTCGAAAC	
Dentin sialophosphoprotein	fw GAATTCTGCTGGTATTCCAG	marker for dentinogenesis
(DSPP)	rv GCCATTAGATTCATCACTGC	
Glyceraldehyde 3-phosphate	fw ATCACTGCCACCCAGAAGAC	housekeeping gene
dehydrogenase (GAPDH)	rv ATGAGGTCCACCACCCTGTT	
Nestin	fw CCTGCAAAAGGAGAATCAAG	marker for cell proliferation/migration,
	rv GTTCTCAATGTCTCTTGGTC	marker for odontoblasts
Osteocalcin (OC)	fw TCTCTGCTCACTCTGCTGG	marker for osteoblasts
	rv GCGTTTGTAGGCGGTCTTC	

doi:10.1371/journal.pone.0111010.t001

flasks with weekly μCT scans (Fig. 2c1). Both controls showed a very weak signal due to the low amount of collagen produced by the cells (Fig. 2c2, 2c5), which was confirmed by the Sirius Red assay (results not shown) where average collagen concentrations

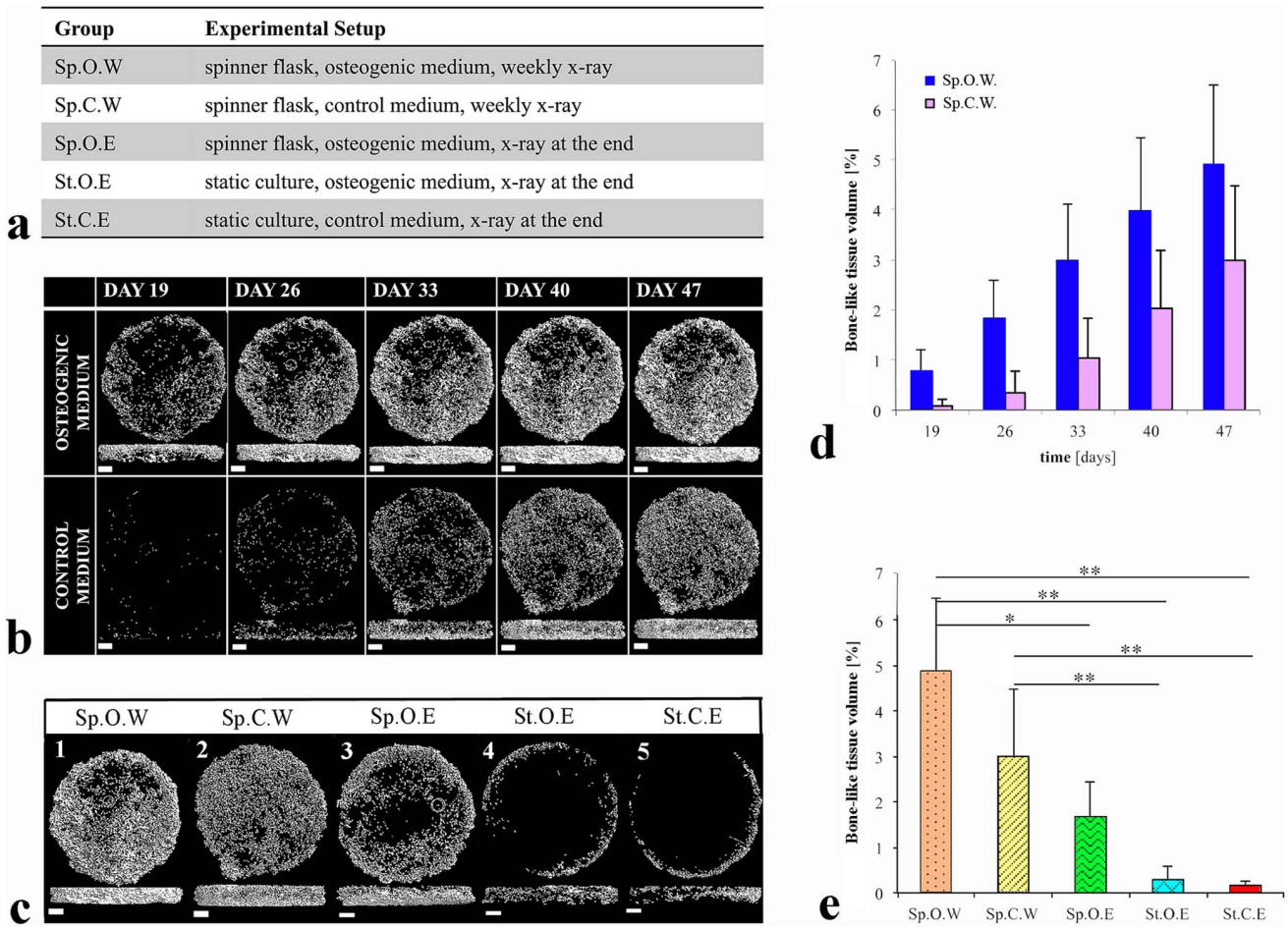

Figure 1. Mineralisation analysis using μCT. (**a**) Experimental groups. (**b**) Time-lapse μCT images of samples cultured in spinner flasks in either osteogenic (upper row) or control (lower row) medium. (**c**) μCT images of one representative sample per experimental group after 47 days of culture. (**d**) Time-dependent increase in bone-like tissue volume fraction as observed with weekly μCT scans. (**e**) Bone-like tissue volume fraction for all groups after 47 days of culture. Scale bars: 1 mm.
doi:10.1371/journal.pone.0111010.g001

were highest in groups that had been cultured in osteogenic medium. Collagen concentrations in both static and dynamic samples with μCT at the end of the culture (Sp.O.E, St.O.E) were shown to be significantly higher than the dynamic sample cultured in control medium with weekly μCT scans (Sp.C.W) with $p<0.05$ and $p<0.01$, respectively.

Biochemical analysis

The AlamarBlue assay showed that cell viability was not significantly different between the groups. However, cells cultured in the control medium were slightly more active than cells cultured in osteogenic medium (e.g. Sp.C.W = 107.2±89.8 *vs.* Sp.O.W = 54.3±32.5) (Fig. 3a). Furthermore, the number of cells was not significantly different between the groups except between samples cultured at 120 rpm in control medium with weekly μCT scans (Sp.C.W) and samples cultured at 0 rpm in osteogenic medium with one μCT scan in the end of the study (St.O.E) ($p<0.05$) (Fig. 3b). Calcium deposition was significantly increased 1.5–2 fold ($p<0.05$) when cells were cultured in osteogenic medium and/or in spinner flasks at 120 rpm (Fig. 3c). ALP activity, which is a marker for odontoblastic and osteoblastic differentiation, was negatively influenced by weekly μCT scans ($p<0.01$) as well as by static culture conditions ($p<0.05$). The highest level of ALP activity (13.5±2.7 μg p-nitrophenol/total DNA) was measured in samples cultured at 120 rpm with osteogenic medium and without weekly μCT scans (Fig. 3d).

Gene expression analysis

ALP, *DSPP* and *Nestin* expressions were downregulated in the experimental groups after 47 days of culture when compared to the control groups (Fig. 4a–c). *ALP* downregulation by a factor of 1.4–2.2 was not significant, whereas in the case of *DSPP* and *Nestin* the gene expression was significantly downregulated ($p<0.05$) in all groups except in the samples cultured at 120 rpm with control medium and weekly μCT scans (Sp.C.W). Similar expression patterns were observed between *Collagen type I* and *Osteocalcin* (Fig. 4d, e). In samples cultured dynamically (at 120 rpm) with control medium and weekly μCT scans (Sp.C.W) gene expression was higher by 1.6 fold and 1.4 fold ($p<0.01$), respectively, when compared to the control, with a highly significant increase in the case of *Collagen type I*. All remaining experimental groups were downregulated by a factor of 1.4–4.2, with only the samples cultured at 120 rpm in osteogenic medium with a μCT scan at the end of the experiment (Sp.O.E) being significantly different ($p<0.01$) for both *Collagen type I* and *Osteocalcin*.

Discussion

The dental pulp is an easily accessible source of multipotent cell populations. Therefore, the goal of this study was to investigate the potential of dental pulp stem cells (DPSCs) to be used for the regeneration of bone tissue and if mechanical loading could improve the behaviour of this cell population. For this purpose, human DPSCs (hDPSCs) were seeded on silk fibroin scaffolds that

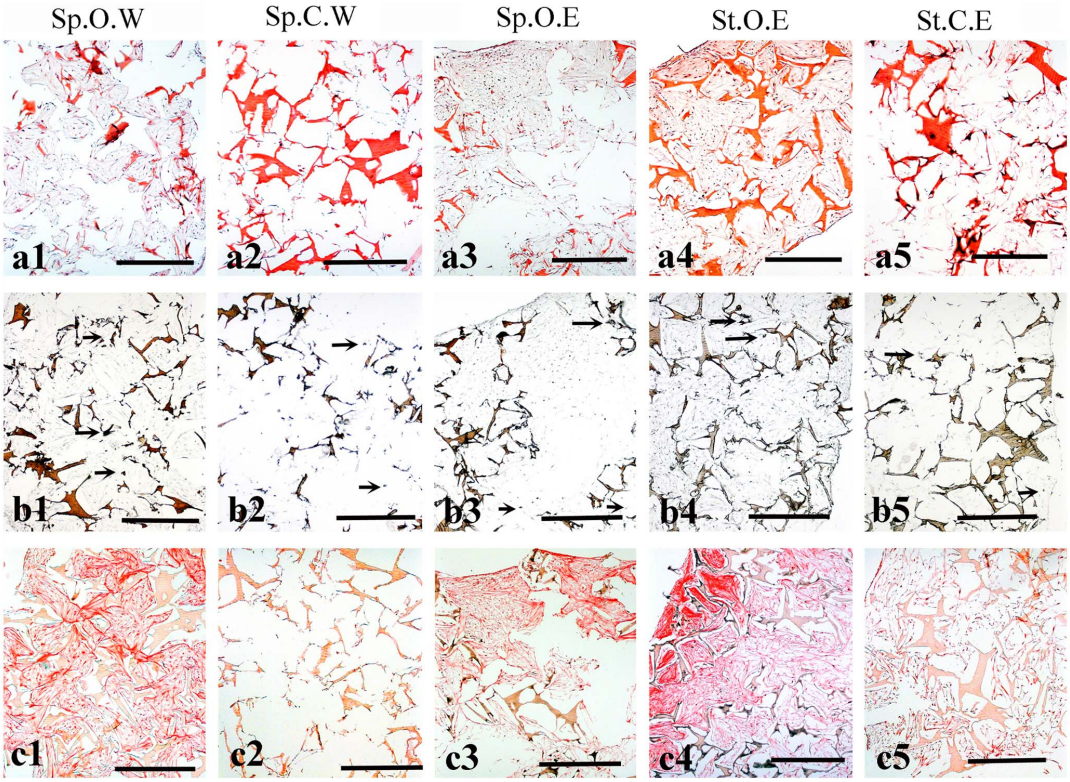

Figure 2. Histological analysis of hDPSCs seeded on silk fibroin scaffolds after 47 days of culture. (**a**) Haematoxylin and Eosin staining of histological sections from all groups. Extracellular matrix and silk scaffolds are stained red/pink. Cell nuclei are stained purple/violet. (**b**) Von Kossa staining. Silk scaffolds and mineralised nodules are stained in brown. Arrows indicate areas where phosphate is present. (**c**) Sirius Red staining showing the distribution of Collagen (red colour). Abbreviations: Sp.O.W: spinner flask culture in osteogenic medium with weekly x-ray; Sp.C.W: spinner flask culture in control medium with weekly x-ray; Sp.O.E: spinner flask culture in osteogenic medium with x-ray at the end; St.O.E: static culture in osteogenic medium with x-ray at the end; St.C.E: static culture in control medium with x-ray at the end. Scale bars: 500 μm.
doi:10.1371/journal.pone.0111010.g002

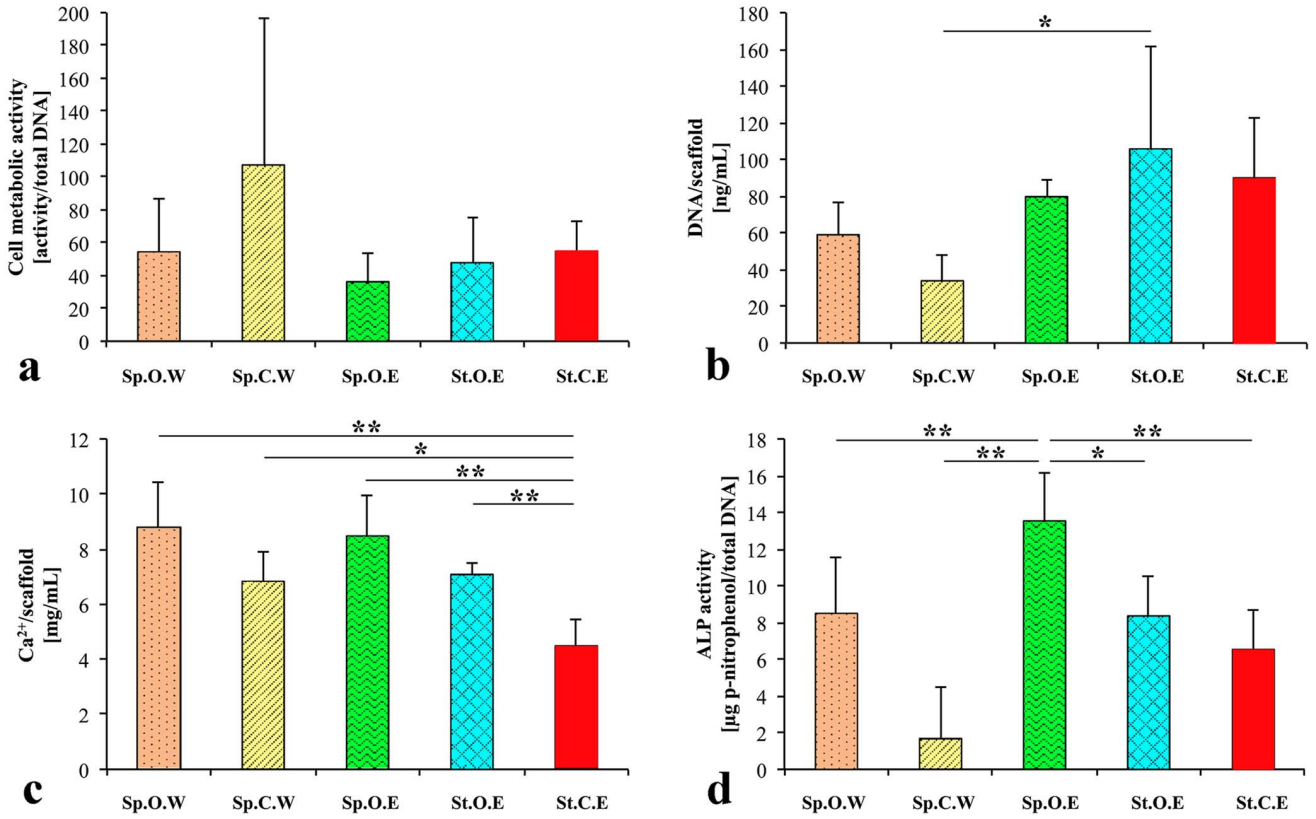

Figure 3. Biochemical analysis after 47 days of culture. (**a**) Cell metabolic activity [activity/total DNA]. (**b**) DNA content per scaffold [ng/mL]. (**c**) Calcium content per scaffold [mg/mL]. (**d**) ALP activity normalised to cell number [µg/p-nitrophenol/total DNA]. Data is shown as average ± standard deviation ($n = 5$). Asterisks indicate significant ($p<0.05$) or highly significant ($p<0.01$) difference between the groups. Abbreviations: Sp.O.W: spinner flask culture in osteogenic medium with weekly x-ray; Sp.C.W: spinner flask culture in control medium with weekly x-ray; Sp.O.E: spinner flask culture in osteogenic medium with x-ray at the end; St.O.E: static culture in osteogenic medium with x-ray at the end; St.C.E: static culture in control medium with x-ray at the end.
doi:10.1371/journal.pone.0111010.g003

offer a three-dimensional (3D) environment, which has been shown to allow proper cell adhesion and proliferation [42] and were cultured in static (0 rpm) and dynamic (120 rpm) conditions.

Mechanical loading has previously been shown to positively affect proliferation, differentiation, and ECM production when tension was applied on hDPSCs in two-dimensional (2D) and 3D cultures [43]. In line with the previous findings, the present study demonstrates that the application of mechanical loading in the form of turbulent flow accelerates the process of mineral deposition. Additionally, biochemical analyses have confirmed that the spinner flask culture conditions promote the differentiation capability of hDPSCs into mineral producing cells while they reduce their proliferation activity. This is not surprising since recent studies have shown that proliferation and differentiation cannot progress at the same time [44]. Indeed, hDPSCs that were exposed to uniaxial mechanical stretch increased their proliferation rate, while their differentiation into osteoblasts was dramatically decreased [45]. In contrast, hDPSCs stimulated by hydrostatic pressure increased their differentiation rate despite their reduced number and adhesion capacity [46]. In the present study we showed that the application of mechanical loading in the form of flow accelerated the process of mineral deposition. Biochemical analyses indicated higher cell proliferation activity in the statically cultured samples, while under dynamic culture conditions the differentiation capability of hDPSCs into mineral producing cells was promoted. This result was also confirmed by the amount of mineralised ECM deposition as evaluated by µCT. Statically (0 rpm) cultured scaffolds were mineralised only on their top and edges, whereas a stirring speed of 120 rpm resulted in a more homogeneous mineralisation in the scaffolds. These low levels of mineralisation in statically cultured samples could be explained by the limited nutrient supply in 3D scaffolds that exceed the size of 1 mm, as pointed out by previous *in vitro* studies where the formation of tissues was problematic in the centre of the scaffold [47,48]. By applying mechanical loading the nutrient supply could be improved.

Although there have been some attempts to regenerate lost alveolar bone (specialised bone structure that supports tooth) in patients using autologous hDPSCs seeded onto collagen sponge scaffolds [49], the results are still unsatisfactory. In these studies, hDPSCs have been isolated from third molars and seeded onto collagen sponge scaffolds before their implantation at the defective jaw sites. X-rays and histological analyses have shown that new bone was formed at the implantation sites three months post-surgery. Follow-up studies (three years post-surgery) have revealed that the regenerated bone was more compact than the physiological one [49]. These *in vivo* results clearly show that hDPSCs are able to differentiate into osteoblasts and repair bone defects in the orofacial area in a mechanically loaded environment. However, the density of the bone produced by hDPSCs when seeded onto collagen scaffolds was more compact than alveolar bone, which could compromise its metabolic functions due to the decrease in

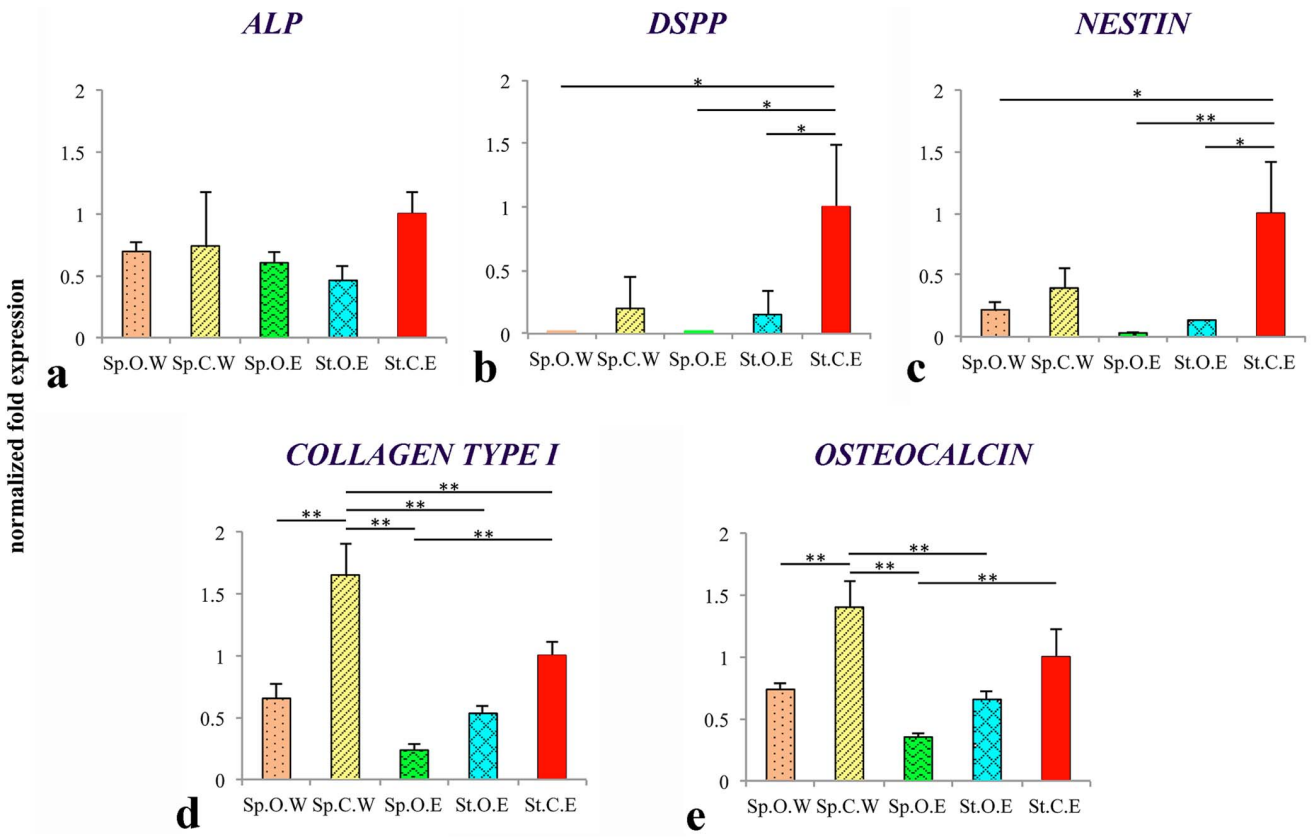

Figure 4. Gene expression analysis. Images showing normalised fold expression against *GAPDH* for the genes *ALP* (**a**), *DSPP* (**b**), *Nestin* (**c**), *Collagen type I* (**d**) and *Osteocalcin* (**e**). Data is shown as average ± standard deviation of three samples. Asterisks indicate significant ($p<0.05$) or highly significant ($p<0.01$) difference between the groups. Abbreviations: Sp.O.W: spinner flask culture in osteogenic medium with weekly x-ray; Sp.C.W: spinner flask culture in control medium with weekly x-ray; Sp.O.E: spinner flask culture in osteogenic medium with x-ray at the end; St.O.E: static culture in osteogenic medium with x-ray at the end; St.C.E: static culture in control medium with x-ray at the end.
doi:10.1371/journal.pone.0111010.g004

porosity. High bone density could be the result of the fast degradation time (4–5 weeks) of the collagen sponge [50], thus resulting in the lack of mechanical support before bone formation is completed.

Silk fibroin scaffolds could be an alternative to collagen materials since they perform better than collagen scaffolds sharing similar microstructures [51–53]. Silk fibroin is a biocompatible (after the removal of sericin) and biodegradable material whose physical and mechanical properties can be easily manipulated through structural readjustments [25,26,54]. Compared to collagen, silk fibroin offers a higher mechanical stability and a much slower degradation rate [25]. It has been demonstrated that bone-like tissue deposits occur appositionally to the silk fibroin scaffold, suggesting that the internal geometry of the scaffold might be used to determine the structure of the engineered bone [29,51]. At the same time this effect could not be accomplished with collagen scaffolds due to their faster degradation and the resulting loss of mechanical stability and geometrical guidance for the incorporated cells. Histological analyses confirmed high cell compatibility of silk fibroin scaffolds under dynamic conditions with a good amount of ECM being produced by hDPSCs over most of the scaffold volume.

Real Time PCR studies showed that hDPSCs cultured in osteogenic medium lost their dental genotypic profile, as indicated by the decreased levels of *DSPP* and *Nestin* expression when compared to the control. Even though *DSPP* has been also found to be expressed in bone, cementum, and certain non-mineralised tissues, the expression levels in these tissues were shown to be much lower than in dentin [55]. In contrast, expression of *Osteocalcin* that is mainly a bone-specific gene [56] and *Collagen type I*, which is expressed in both bone and dentin tissues, was upregulated in mechanically loaded samples. This has been already demonstrated in several previous studies and has been connected to the improved transport of nutrients [57–59].

Interestingly, a significantly positive effect of radiation on the mineralisation of the scaffold was observed during the μCT scans that contradicts previously reported results, where both hard tissue formation and cell survival were significantly reduced [60–62]. In a previous study where BMSCs were cultured on silk fibroin scaffolds μCT imaging had no impact on the osteogenic performance of the cells when compared to non-exposed samples [63].

Conclusion

In summary, by biochemical, histological, and μCT evaluations together with molecular analyses we have shown that hDPSCs have the potential to form mineralised matrix when grown on porous 3D silk fibroin scaffolds. This potential can be enhanced by mechanical loading and the addition of osteogenic factors in the culture medium. The clinical relevance lies in the availability of hDPSCs, their common embryonic origin with craniofacial tissues,

and the advantageous characteristics of the silk fibroin scaffold for applications in bone regeneration.

Supporting Information

File S1 Tables S1–S3. Table S1. Dataset of raw values for figure 1d. Table S2. Dataset of raw values for figure 1e and figures 3a–3d. Table S3. Dataset of raw values for figures 4a–4e. (DOCX)

Acknowledgments

The authors thank Professor Gianpaolo Papaccio (Second University of Naples, Italy) for sharing material and knowledge on human dental stem cells, Miss Verena Osterwalder (University of Zurich, Switzerland) for her technical assistance, and Trudel Silk Inc. (Zurich, Switzerland) for kindly providing silk cocoons.

Author Contributions

Conceived and designed the experiments: TM NB SH RM. Performed the experiments: SHD SH AW NB. Analyzed the data: SHD SH AW NB TM. Contributed reagents/materials/analysis tools: RM SH TM NB. Contributed to the writing of the manuscript: AW SHD TM NB SH RM.

References

1. Abate M, Vanni D, Pantalone A, Salini V (2013) Cigarette smoking and musculoskeletal disorders Corresponding author: Muscles Ligaments Tendons J 3: 63–69.
2. Catón J, Bostanci N, Remboutsika E, De Bari C, Mitsiadis TA (2011) Future dentistry: cell therapy meets tooth and periodontal repair and regeneration. J Cell Mol Med 15: 1054–1065. doi:10.1111/j.1582-4934.2010.01251.x.
3. Amini AR, Laurencin CT, Nukavarapu SP (2012) Bone tissue engineering: recent advances and challenges. Crit Rev Biomed Eng 40: 363–408. doi:10.1615/CritRevBiomedEng.v40.i5.10.
4. Akintoye SO, Lam T, Shi S, Brahim J, Collins MT, et al. (2006) Skeletal site-specific characterization of orofacial and iliac crest human bone marrow stromal cells in same individuals. Bone 38: 758–768. doi:10.1016/j.bone.2005.10.027.
5. Bluteau G, Luder HU, De Bari C, Mitsiadis T a (2008) Stem cells for tooth engineering. Eur Cell Mater 16: 1–9.
6. Mitsiadis TA, Graf D (2009) Cell fate determination during tooth development and regeneration. Birth Defects Res C Embryo Today 87: 199–211. doi:10.1002/bdrc.20160.
7. Silver FH, Landis WJ (2011) Deposition of apatite in mineralizing vertebrate extracellular matrices: A model of possible nucleation sites on type I collagen. Connect Tissue Res 52: 242–254. doi:10.3109/03008207.2010.551567.
8. Veis A (1993) Mineral-matrix interactions in bone and dentin. J Bone Miner Res 8 Suppl 2: S493–S497. doi:10.1002/jbmr.5650081312.
9. Krishnan L, Willett NJ, Guldberg RE (2014) Vascularization Strategies for Bone Regeneration. Ann Biomed Eng: 1–13. doi:10.1007/s10439-014-0969-9.
10. Pagella P, Jiménez-Rojo L, Mitsiadis T a (2014) Roles of innervation in developing and regenerating orofacial tissues. Cell Mol Life Sci 71: 2241–2251. doi:10.1007/s00018-013-1549-0.
11. Mitsiadis TA, Papagerakis P (2011) Regenerated teeth: the future of tooth replacement? Regen Med 6: 135–139. doi:10.2217/rme.10.101.
12. Remedios A (1999) Bone and bone healing. Vet Clin North Am Small Anim Pract 29: 1029–1044, v.
13. Opsahl Vital S, Gaucher C, Bardet C, Rowe PS, George A, et al. (2012) Tooth dentin defects reflect genetic disorders affecting bone mineralization. Bone 50: 989–997. doi:10.1016/j.bone.2012.01.010.
14. Mitsiadis TA, Rahiotis C (2004) Parallels between Tooth Development and Repair: Conserved Molecular Mechanisms following Carious and Dental Injury. J Dent Res 83: 896–902. doi:10.1177/154405910408301202.
15. Gronthos S, Mankani M, Brahim J, Robey PG, Shi S (2000) Postnatal human dental pulp stem cells (DPSCs) in vitro and in vivo. Proc Natl Acad Sci U S A 97: 13625–13630. doi:10.1073/pnas.240309797.
16. Mitsiadis TA, Feki A, Papaccio G, Catón J (2011) Dental pulp stem cells, niches, and notch signaling in tooth injury. Adv Dent Res 23: 275–279. doi:10.1177/0022034511405386.
17. Thomas ED, Lochte HL, Lu WC, Ferrebee JW (1957) Intravenous Infusion of Bone Marrow in Patients Receiving Radiation and Chemotherapy. N Engl J Med 257: 491–496. doi:10.1056/NEJM195709122571102.
18. Phinney DG, Prockop DJ (2007) Concise review: mesenchymal stem/multipotent stromal cells: the state of transdifferentiation and modes of tissue repair-current views. Stem Cells 25: 2896–2902. doi:10.1634/stemcells.2007-0637.
19. Dimarino AM, Caplan AI, Bonfield TL (2013) Mesenchymal Stem Cells in Tissue Repair. Front Immunol 4: 201. doi:10.3389/fimmu.2013.00201.
20. Tamaki Y, Nakahara T, Ishikawa H, Sato S (2013) In vitro analysis of mesenchymal stem cells derived from human teeth and bone marrow. Odontology 101: 121–132. doi:10.1007/s10266-012-0075-0.
21. Yu J, Wang Y, Deng Z, Tang L, Li Y, et al. (2007) Odontogenic capability: bone marrow stromal stem cells versus dental pulp stem cells. Biol Cell 99: 465–474. doi:10.1042/BC20070013.
22. Leucht P, Kim, Amasha R, James AW, Girod S, et al. (2008) Embryonic origin and Hox status determine progenitor cell fate during adult bone regeneration. Development 135: 2845–2854. doi:10.1242/dev.023788.
23. Grapin-Botton A, Bonnin MA, McNaughton LA, Krumlauf R, Le Douarin NM (1995) Plasticity of transposed rhombomeres: Hox gene induction is correlated with phenotypic modifications. Development 121: 2707–2721.
24. Minoura N, Aiba S, Higuchi M (1995) Attachment and growth of fibroblast cells on silk fibroin. Biochem Biophys Res Commun 208: 511–516.
25. Altman GH, Diaz F, Jakuba C, Calabro T, Horan RL, et al. (2003) Silk-based biomaterials. Biomaterials 24: 401–416. doi:10.1016/S0142-9612(02)00353-8.
26. Kundu B, Rajkhowa R, Kundu SC, Wang X (2013) Silk fibroin biomaterials for tissue regenerations. Adv Drug Deliv Rev 65: 457–470. doi:10.1016/j.addr.2012.09.043.
27. Mitsiadis TA, Woloszyk A, Jiménez-Rojo L (2012) Nanodentistry: combining nanostructured materials and stem cells for dental tissue regeneration. Nanomedicine (Lond) 7: 1743–1753. doi:10.2217/nnm.12.146.
28. Vunjak-Novakovic G, Meinel L, Altman G, Kaplan D (2005) Bioreactor cultivation of osteochondral grafts. Orthod Craniofacial Res 8: 209–218. doi:10.1111/j.1601-6343.2005.00334.x.
29. Hofmann S, Hagenmüller H, Koch A (2007) Control of in vitro tissue-engineered bone-like structures using human mesenchymal stem cells and porous silk scaffolds. Biomaterials 28: 1152–1162. doi:10.1016/j.biomaterials.2006.10.019.
30. Hofmann S, Hilbe M, Fajardo RJ, Hagenmüller H, Nuss K, et al. (2013) Remodeling of tissue-engineered bone structures in vivo. Eur J Pharm Biopharm 85: 119–129. doi:10.1016/j.ejpb.2013.02.011.
31. Rockwood DN, Gil ES, Park SH, Kluge JA, Grayson W, et al. (2010) Ingrowth of Human Mesenchymal Stem Cells into Porous Silk Particle Reinforced Silk Composite Scaffolds: An In Vitro Study. Acta Biomater 7: 144–151. doi:10.1016/j.actbio.2010.07.020.
32. Hung BP, Hutton DL, Grayson WL (2013) Mechanical control of tissue-engineered bone. Stem Cell Res Ther 4: 10. doi:10.1186/scrt158.
33. Pavalko FM, Norvell SM, Burr DB, Turner CH, Duncan RL, et al. (2003) A model for mechanotransduction in bone cells: the load-bearing mechanosomes. J Cell Biochem 88: 104–112. doi:10.1002/jcb.10284.
34. Papachristou DJ, Papachroni KK, Basdra EK, Papavassiliou AG (2009) Signaling networks and transcription factors regulating mechanotransduction in bone. Bioessays 31: 794–804. doi:10.1002/bies.200800223.
35. Steward AJ, Wagner DR, Kelly DJ (2013) Exploring the roles of integrin binding and cytoskeletal reorganization during mesenchymal stem cell mechanotransduction in soft and stiff hydrogels subjected to dynamic compression. J Mech Behav Biomed Mater. doi:10.1016/j.jmbbm.2013.07.020.
36. Haycock J (2011) 3D cell culture: a review of current approaches and techniques. Methods Mol Biol 695: 1–15. doi:10.1007/978-1-60761-984-0.
37. Rauh J, Milan F, Günther, Stiehler M (2011) Bioreactor systems for bone tissue engineering. Tissue Eng Part B Rev 17: 263–280. doi:10.1089/ten.teb.2010.0612.
38. Nazarov R, Jin, Kaplan DL (2004) Porous 3-D scaffolds from regenerated silk fibroin. Biomacromolecules 5: 718–726. doi:10.1021/bm034327e.
39. Tirino V, Paino F, De Rosa A, Papaccio G (2012) Identification, isolation, characterization, and banking of human dental pulp stem cells. Methods Mol Biol 879: 443–463.
40. Hildebrand T, Laib A, Müller R, Dequeker J, Rüegsegger P (1999) Direct three-dimensional morphometric analysis of human cancellous bone: microstructural data from spine, femur, iliac crest, and calcaneus. J Bone Miner Res 14: 1167–1174. doi:10.1359/jbmr.1999.14.7.1167.
41. Sittichokechaiwut A, Edwards JH, Scutt AM, Reilly GC (2010) Short bouts of mechanical loading are as effective as dexamethasone at inducing matrix production by human bone marrow mesenchymal stem cell. Eur Cell Mater 20: 45–57. doi:vol020a05 [pii].
42. Flemming R, Murphy C, Abrams G, Goodman S, Nealey P (1999) Effects of synthetic micro-and nano-structured surfaces on cell behavior. Biomaterials 20: 573–588.
43. Han, Seo, Yoon, Song, Park J-K (2008) Effect of mechanical tension on the human dental pulp cells. Biotechnol Bioprocess Eng 13: 410–417. doi:10.1007/s12257-008-0146-9.
44. Wang X, Ye K, Li Z, Yan C, Ding J (2013) Adhesion, proliferation, and differentiation of mesenchymal stem cells on RGD nanopatterns of varied nanospacings. Organogenesis 9. doi:26080 [pii].
45. Hata M, Naruse K, Ozawa S, Kobayashi Y, Nakamura N, et al. (2013) Mechanical stretch increases the proliferation while inhibiting the osteogenic

differentiation in dental pulp stem cells. Tissue Eng Part A 19: 625–633. doi:10.1089/ten.tea.2012.0099.
46. Yu V, Damek-Poprawa M, Nicoll SB, Akintoye SO (2009) Dynamic hydrostatic pressure promotes differentiation of human dental pulp stem cells. Biochem Biophys Res Commun 386: 661–665. doi:10.1016/j.bbrc.2009.06.106.
47. Kellner K, Liebsch G, Klimant I, Wolfbeis OS, Blunk T, et al. (2002) Determination of oxygen gradients in engineered tissue using a fluorescent sensor. Biotechnol Bioeng 80: 73–83. doi:10.1002/bit.10352.
48. Malda J, Rouwkema J, Martens DE, Le Comte EP, Kooy FK, et al. (2004) Oxygen Gradients in Tissue-Engineered PEGT/PBT Cartilaginous Constructs: Measurement and Modeling. Biotechnol Bioeng 86: 9–18. doi:10.1002/bit.20038.
49. Giuliani A, Manescu A, Langer M, Rustichelli F, Desiderio V, et al. (2013) Three years after transplants in human mandibles, histological and in-line holotomography revealed that stem cells regenerated a compact rather than a spongy bone: biological and clinical implications. Stem Cells Transl Med 2: 316–324. doi:10.5966/sctm.2012-0136.
50. Donzelli E, Salvadè A, Mimo P, Viganò M, Morrone M, et al. (2007) Mesenchymal stem cells cultured on a collagen scaffold: In vitro osteogenic differentiation. Arch Oral Biol 52: 64–73. doi:10.1016/j.archoralbio.2006.07.007.
51. Meinel L, Hofmann S, Karageorgiou V, Zichner L, Langer R, et al. (2004) Engineering cartilage-like tissue using human mesenchymal stem cells and silk protein scaffolds. Biotechnol Bioeng 88: 379–391. doi:10.1002/bit.20252.
52. Meinel L, Karageorgiou V, Fajardo R, Snyder B, Shinde-Patil V, et al. (2004) Bone tissue engineering using human mesenchymal stem cells: Effects of scaffold material and medium flow. Ann Biomed Eng 32: 112–122. doi:10.1023/B:ABME.0000007796.48329.b4.
53. Hofmann S, Knecht S, Langer R, Kaplan DL, Vunjak-Novakovic G, et al. (2006) Cartilage-like tissue engineering using silk scaffolds and mesenchymal stem cells. Tissue Eng 12: 2729–2738. doi:10.1089/ten.2006.12.ft-214.
54. Horan RL, Antle K, Collette AL, Wang Y, Huang J, et al. (2005) In vitro degradation of silk fibroin. Biomaterials 26: 3385–3393. doi:S0142-9612(04)00819-1 [pii] 10.1016/j.biomaterials.2004.09.020.
55. Qin C, Brunn JC, Cadena E, Ridall A, Butler WT (2003) Dentin sialoprotein in bone and dentin sialophosphoprotein gene expressed by osteoblasts. Connect Tissue Res 44: 179–183.
56. Orsini G, Ruggeri A, Mazzoni A, Nato F, Manzoli L, et al. (2012) A review of the nature, role, and function of dentin non-collagenous proteins. Part 1: proteoglycans and glycoproteins: 1–18.
57. Camps J, About I, Thonneman B, Mitsiadis TA, Schmaltz G, et al. (2002) Two-versus three-dimensional in vitro differentiation of human pulp cells into odontoblastic cells. Connect Tissue Res 43: 396–400.
58. Lizier NF, Kerkis A, Gomes CM, Hebling J, Oliveira CF, et al. (2012) Scaling-up of dental pulp stem cells isolated from multiple niches. PLoS One 7: e39885. doi:10.1371/journal.pone.0039885.
59. Bonnamain V, Thinard R, Sergent-Tanguy S, Huet P, Bienvenu G, et al. (2013) Human dental pulp stem cells cultured in serum-free supplemented medium. Front Physiol 4: 357. doi:10.3389/fphys.2013.00357.
60. Kraehenbuehl TP, Stauber M, Ehrbar M, Weber F, Hall H, et al. (2010) Effects of μCT radiation on tissue engineered bone-like constructs. Biomed Tech 55: 245–250. doi:10.1515/BMT.2010.031.
61. Muthna D, Soukup T, Vavrova J, Mokry J, Cmielova J, et al. (2010) Irradiation of adult human dental pulp stem cells provokes activation of p53, cell cycle arrest, and senescence but not apoptosis. Stem Cells Dev 19: 1855–1862. doi:10.1089/scd.2009.0449.
62. Abe S, Hamada K, Yamaguchi S, Amagasa T, Miura M (2011) Characterization of the radioresponse of human apical papilla-derived cells. Stem Cell Res Ther 2: 2. doi:10.1186/scrt43.
63. Hagenmüller H, Hofmann S, Kohler T, Merkle HP, Kaplan DL, et al. (2007) Non-invasive time-lapsed monitoring and quantification of engineered bone-like tissue. Ann Biomed Eng 35: 1657–1667. doi:10.1007/s10439-007-9338-2.

14.1.4 Kivrak Pfiffner et al., Tissue Eng Part C, 2015

A new in vivo MRI method to non-invasively monitor and quantify the perfusion capacity of 3D-biomaterials grown on the chorioallantoic membrane of chick embryos (PAPER)

The goal of this paper was to present a new *in vivo* MRI method for the non-invasive monitoring and quantification of the perfusion capacity of 3D biomaterials when cultured on the chorioallantoic membrane (CAM) of chicken embryos. To validate the method, which has been established based on the synthetic polymer DegraPol®, it was necessary to include measurements performed on a different type of scaffold.

We had started to use the CAM assay in the laboratory of Dr. Johanna Buschmann for our own studies, where we wanted to investigate the influence of human dental pulp stem cells (hDPSCs) on the vascularization efficiency of silk fibroin scaffolds. In order to complete the manuscript, the perfusion capacity of samples containing either empty silk scaffolds or hDPSC-seeded silk scaffolds were monitored and quantified using the *in vivo* MRI method after an incubation time of 7 days. I had extracted the hDPSCs from wisdom teeth, followed by cell expansion and cell seeding on the silk scaffolds, which were pre-incubated *in vitro*. Furthermore, I performed the CAM assay as well as the histological and immunohistological (anti-CD31 antibody) analysis and documentation of the samples after the *in vivo* MRI scan. While preparing the manuscript I provided the descriptions about 'Silk fibroin scaffolds' and 'Cells' in the 'Materials and Methods' section.

Interestingly, three to four times larger perfusion capacities were obtained in silk fibroin scaffolds when compared to DegraPol®, with a slightly higher perfusion capacity in hDPSC-seeded silk scaffolds. Similar to the DegraPol® scaffolds, the perfusion capacity measured within the silk fibroin scaffolds declined from the interface towards the surface region. The CD31-staining confirmed that functional vessels containing red blood cells of the chicken were present within the silk fibroin scaffold. The proof-of-principle in silk fibroin scaffolds showed that the *in vivo* MRI method developed by Kivrak Pfiffner et al. can be applied for the determination of the perfusion capacity in a large variety of bioengineered materials.

TISSUE ENGINEERING: Part C
Volume 21, Number 4, 2014

DOI: 10.1089/ten.tec.2014.0212

A New *In Vivo* Magnetic Resonance Imaging Method to Noninvasively Monitor and Quantify the Perfusion Capacity of Three-Dimensional Biomaterials Grown on the Chorioallantoic Membrane of Chick Embryos

Fatma Kivrak Pfiffner, MSc,[1,*] Conny Waschkies, PhD,[2,3,*] Yinghua Tian, PhD,[3] Anna Woloszyk, MSc,[4,5] Maurizio Calcagni, MD,[1] Pietro Giovanoli, MD,[1] Markus Rudin, PhD,[2] and Johanna Buschmann, PhD[1]

Adequate vascularization in biomaterials is essential for tissue regeneration and repair. Current models do not allow easy analysis of vascularization of implants *in vivo*, leaving it a highly desirable goal. A tool that allows monitoring of perfusion capacity of such biomaterials noninvasively in a cheap, efficient, and reliable *in vivo* model would hence add great benefit to research in this field. We established, for the first time, an *in vivo* magnetic resonance imaging (MRI) method to quantify the perfusion capacity of a model biomaterial, DegraPol® foam scaffold, placed on the embryonic avian chorioallantoic membrane (CAM) *in ovo*. Perfusion capacity was assessed through changes in the longitudinal relaxation rate before and after injection of a paramagnetic MRI contrast agent, Gd-DOTA (Dotarem®; Guerbet S.A.). Relaxation rate changes were compared in three different regions of the scaffold, that is, at the interface to the CAM, in the middle and on the surface of the scaffold ($p < 0.05$). The highest relaxation rate changes, and hence perfusion capacities, were measured in the interface region where the scaffold was attached to the CAM, whereas the surface of the scaffold showed the lowest relaxation rate changes. A strong positive correlation was obtained between relaxation rate changes and histologically determined vessel density ($R^2 = 0.983$), which corroborates our MRI findings. As a proof-of-principle, we measured the perfusion capacity in different scaffold materials, silk fibroin either with or without human dental pulp stem cells. For these, three to four times larger perfusion capacities were obtained compared to DegraPol; demonstrating that our method is sensitive to reveal such differences. In summary, we present a novel *in vivo* method for analyzing the perfusion capacity in three-dimensional-biomaterials grown on the CAM, enabling the determination of the perfusion capacity of a large variety of bioengineered materials.

Introduction

Tissue-engineered constructs for regenerative medicine are based on scaffolds that are used as a matrix for cells to attach and proliferate, so that these artificial grafts can be implanted at defect sites. For this purpose they should provide a high level of biocompatibility. Moreover, vascularization is often required, that is, the grafts should be easily vascularized after implantation and guarantee long-term functionality and survival of the implanted material and cells. To sustain the artificial graft in an environment as a functional tissue, it is necessary that the blood vessels penetrate the porous grafts from the surrounding tissue since the transport of oxygen and nutrients is dependent on a homogenously distributed vascular network in the implanted scaffold.[1–5]

Artificial engineered grafts can have different effects on vascularization. Not only the pore size, but also the size of the scaffold and the interconnectivity of the pores are important criteria for blood vessel ingrowth after implantation.[3,4] Numerous *ex vivo* and *in vivo* approaches have been established to monitor vascularization of tissue grafts including rodents, chicken, and fish.[6,7] *Ex vivo* assays are rapid but more limited because of the lack of inflammation and metabolic processes that may affect vascularization. Most of the currently available *in vivo* assays involve time,

This work was performed at University Hospital Zurich, Zurich, Switzerland.
[1]Plastic Surgery and Hand Surgery, University Hospital Zurich, Zurich, Switzerland.
[2]Institute for Biomedical Engineering, ETH and University of Zurich, Zurich, Switzerland.
[3]Visceral and Transplant Surgery, University Hospital Zurich, Zurich, Switzerland.
[4]Institute of Oral Biology, University of Zurich, Zurich, Switzerland.
[5]Molecular Life Sciences, University of Zurich and ETH Zurich, Zurich, Switzerland.
*These authors equally contributed to the work.

money, and repetitive animal sacrifice, and they are complex and sometimes not easy to compare.[3,8] The chorioallantoic membrane (CAM) of the chick embryo is a well-established model for studying vascularization *in vitro* and *in vivo* and is typically referred to as CAM assay.[9,10] It is a very useful model because of the easy accessibility of the vascular network. Moreover, its lack of immune competence enables studies dealing with tumor growth, wound healing, angiogenesis, antiangiogenesis, or biocompatibility of xenografts.[3,11,12] In addition, the CAM provides an excellent environment where the cells can attach and proliferate in three-dimensional (3D) scaffolds. Finally, the CAM assay is a rapid, simple, and low-cost screening method for tissue reactions toward biomaterials.[9]

An increasing amount of literature highlights the as yet unmet need to noninvasively monitor the vascularization extent of the implanted scaffolds to analyze the success of tissue regeneration *in vivo*.[13,14] To date, there are only few studies that use magnetic resonance imaging (MRI) as a nondestructive, noninvasive method to study biomaterials on the CAM.[9,10] Our current work presents for the first time the application of MRI to measure the perfusion capacity of CAM-implanted scaffolds *in situ* on the CAM in the living chicken embryo. This method allows a continuous, longitudinal monitoring of developing vessels and hence perfusion capacity in biomaterials *in vivo*.

The particular objectives of our study were (1) to quantify the perfusion capacity within a model scaffold biomaterial, DegraPol® foam, implanted for 7 days on the CAM by MRI *in ovo* and *in vivo* as a function of local distance from the CAM and as a function of time after contrast agent injection,(2) to correlate our MRI findings with histological analyses of vessel density, and (3) to apply the established method as a proof-of-principle to different biomaterials discovering the impact of human dental pulp stem cells (hDPSCs) on the perfusion capacity of a silk fibroin scaffold. In sum, we present a new and low cost screening method to study angiogenesis-related questions in the field of tissue-engineered biomaterials.

Materials and Methods

Scaffolds

DegraPol. The synthetic polyester-urethane DegraPol is a biocompatible and biodegradable material based on polyhydroxy-butyrate as a crystalline segment and ε-caprolactone as a soft segment.[15] Originally, its synthesis aimed at generating a suitable scaffold material for bone tissue engineering,[16] but has recently also been shown to be a beneficial scaffold material for cartilage,[17] nerves,[18] and tendons.[19]

DegraPol foams were kindly provided by *ab medica*, Italy. They were soaked in cyclohexane (Fluka, puriss) and frozen at −20°C overnight. They were cut into equal pieces of $8 \times 4 \times 3\,mm^3$ immediately after removal from the freezer and were dried at room temperature (evaporation of cyclohexane). All foams were sterilized with ethylenoxide before placing them carefully on the CAM.

Silk fibroin. Silk fibroin is a biocompatible (after the removal of sericin) and biodegradable material whose physical and mechanical properties can be easily manipulated through structural readjustments.[20,21] It is derived from silkworm cocoons of *Bombyx mori*, which contains at least two major fibroin proteins, light and heavy chains, 25 and 325 kDa, respectively.[22] Due to its versatility it has become a popular biomaterial for various applications, for example, in bone tissue engineering.[20] Silk fibroin scaffolds (Trudel Silk, Inc.) with a diameter of 5 mm, a height of 3 mm, and a pore size of 200–300 μm were used. They were prewetted for 36 h in phosphate-buffered solution to rehydrate them before use. After autoclaving (121°C, 1 bar, 20 min) scaffolds were immersed either in a cell suspension (0.5×10^6 cells/scaffold) or in cell-free culture medium, respectively. As culture medium, DMEM/F12 (D8437; Sigma) with 10% FBS (2602-P291705; PAN Biotech GmbH), 1% Pen/Strep (P0781; Sigma), 1% L-Glutamine (G7513; Sigma), and 0.02% fungizone (15290-018; Invitrogen) was used. Cell-seeded and cell-free scaffolds were placed in the incubator (37°C, 5% CO_2) to allow attachment of the cells. After 1 h scaffolds were washed in fresh culture medium and placed into a 24-well-plate with 0.8 mL of culture medium in the incubator overnight. After that the scaffolds were placed on the CAM of the fertilized chicken eggs.

Cells

hDPSCs were obtained from dental pulps of healthy teeth of adult patients after the extraction of impacted wisdom teeth. The procedure was approved by the Kantonale Ethikkommission of Zurich (reference number 2012-0588) and performed with written patients' consent. After the removal of the dental pulp from the tooth, hDPSCs were isolated, expanded, and characterized as described previously.[23]

CAM assay

Fertilized Lowman white LSL chick eggs (Animalco AG Geflügelzucht) were incubated at 37°C and 65% relative humidity. On incubation day (ID) 3.5 a circular window with a diameter of 40–45 mm was drilled into the eggshell after removing 2 mL albumen so that the developing CAM detached from the eggshell. The window in the eggshell was closed with a sterile Petri dish of 50 mm to prevent dehydration. On ID 7, DegraPol foam scaffolds, cell-seeded silk fibroin scaffolds and cell-free silk fibroin scaffolds were carefully placed on top of the CAM, one scaffold into each egg. The scaffolds were put in the middle of 1 cm-diameter plastic rings to flatten the surface of CAM (Fig. 1). Afterward the eggs were incubated for another 7 days until ID 14.

In vivo *assessment of perfusion capacity using MRI*

On ID 14, vascularization of the scaffold by capillaries of the chick embryo's CAM was studied *in situ* on the CAM ("*in ovo*") of the living chicken embryo ("*in vivo*") using MRI in eight samples. For the MRI examination, the eggs were placed onto a custom-built sliding bed and enveloped by warm water tubing to maintain the temperature of the chick embryo in a physiological range. To prevent motion of the chick embryos, they were sedated with five drops of 1:100 M ketamine (Ketasol-100; Graeub) dripped onto the CAM surface.

MRI was performed with a 4.7 T/16 cm Bruker PharmaScan small animal scanner (Bruker BioSpin) equipped with an actively decoupled two-coil system consisting of a 72 mm bird cage resonator for excitation and a 20 mm single loop surface coil for reception. The surface coil was fixed on

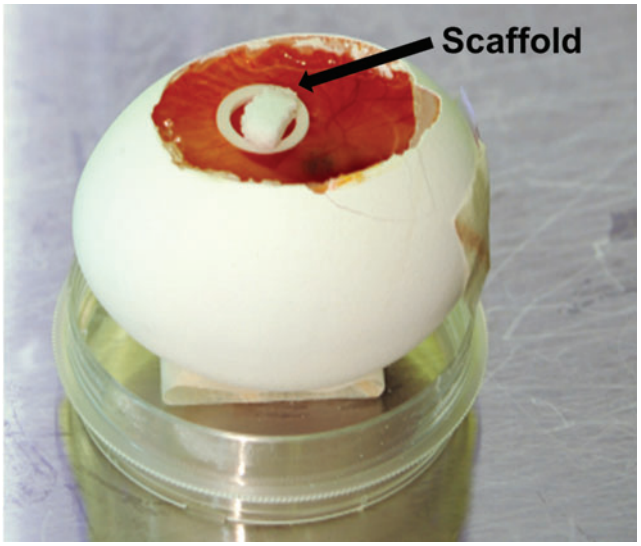

FIG. 1. DegraPol® foam scaffold (*arrow*) placed in the middle of a supportive plastic ring on top of the CAM on ID 7. CAM, chorioallantoic membrane; ID, incubation day. Color images available online at www.liebertpub.com/tec

the Petri dish that covered the eggshell window directly above the scaffold for optimal sensitivity.

Anatomical reference images were obtained in coronal, transversal, and sagittal slice orientations (FLASH sequence, TR/TE 200/3 ms, image matrix size 128×128, field of view $60 \times 60\,mm^2$, five slices, images reconstructed to a nominal resolution of $0.23 \times 0.23 \times 1\,mm^3$, total scan time 25 s). T_1-weighted MR images were acquired with a RARE sequence of variable TR and TE for quantitative T_1 and T_2 mapping (TR 200/400/800/1500/3000/4500 ms, TE 10/30/50/70/90 ms, RARE-factor 2, image matrix size 220×150, field of view $45 \times 30\,mm^2$, spatial resolution $0.2 \times 0.2\,mm^2$, slice thickness 1 mm, total scan time 9 min 40 s).

T_1 maps were acquired in eight DegraPol, four silk fibroin and four silk fibroin samples seeded with hDPSCs before and after i.v. injection 100 µL 0.05 M Gd-DOTA MRI contrast agent (Dotarem®; Guerbet S.A.). The time between Gd-DOTA injection and T_1 mapping was held constant at 25 min. An additional time series was acquired in three DegraPol samples with T_1 map acquired at 15, 25, 35, 45, and 60 min postinjection.

T_1 relaxation times were determined in three regions of interest at (1) the surface of the scaffold, (2) in the middle, and (3) at the interface of the scaffold with the CAM. Perfusion capacity in these three regions of interest was assessed through changes in the longitudinal relaxation rate, $\Delta R_1 = R_1 - R_{10}$, before and after injection of Gd-DOTA, as the relaxation rate changes with the amount of gadolinium present in the CAM:

$$R_1 = R_{10} + r_1 \cdot [Gd]$$

where

$$R_1 = 1/T_1$$

are the longitudinal relaxation rate after and R_{10} before contrast agent administration and r_1 the molar relaxivity of the contrast agent in $s^{-1}\,mol^{-1}\,L$ and [Gd] the concentration of Gd in mol L^{-1}.

Intravenous injection of Gd-DOTA

For intravenous injection of the MRI contrast agent, eggs were placed on a 37°C heating bed and i.v. injection was performed under a surgical microscope with 12–20× magnification. A big and straight vein on the surface was selected and grasped by a microsurgical forceps and 100 µL Gd-DOTA slowly injected with a 1.0 mL syringe and 30G needle. A cotton sticker was placed on the injection site of the vessel with slight pressure before the syringe was withdrawn to prevent bleeding.

Histological analyses

After completion of the MRI measurements the scaffold-CAM complex was fixed overnight using 4% formalin solution in phosphate-buffered saline, then excised, embedded in paraffin, cross sectioned in 5 µm slices, and stained with hematoxylin and eosin (H&E), CD31 (PECAM-1 [M-20]: sc-1506, Santa Cruz Biotechnology; staining procedure for paraffin sections of the VECTASTAIN Elite ABC Kit-Rabbit IgG [PK-6101; Vector Laboratories, Inc.]) and *Von Willebrand Faktor* (Factor VIII; Dako) according to established procedures.[24] Slices were obtained from three regions of the scaffold: (1) surface, (2) middle, and (3) interface to the CAM, and three to four slices for each region were analyzed. The vessel density was scored semi-quantitatively by counting the number of vessels manually under a light microscope (Leica DM 6000 B) equipped with a digital camera; with 0 = no vessels, $1 \leq 10$, 1.5 = 10–30, 2 = 30–50, 2.5 = 50–70, 3 = 70–90, 3.5 = 90–110, 4 = 110–130, 4.5 = 130–150, and $5 \geq 150$ vessels in a cross section of $32\,mm^2$.

Statistics

The correlation of capillarity densities and the change in relaxation rates, ΔR_1, was determined by linear regression using StatView 5.0.1. Moreover, one-way analysis of variance was conducted. Pairwise comparison probabilities (p) were calculated using the Fisher's PLSD. p-Values < 0.05 were considered significant.

Results

MRI measurements

The ability to quantify the perfusion capacity is crucial for assessing the biocompatibility of tissue-engineered grafts and biomaterials. Here, we used MRI to assess perfusion capacity through changes in the R_1 relaxation rates, ΔR_1, before and after injection of a paramagnetic MRI contrast agent, Gd-DOTA. In Figure 2, T_1-weighed images before and after injection are depicted. In the precontrast image, the scaffold and supportive plastic ring and head of the chick embryo can be distinguished, but are much better delineated in the postcontrast image, as the scaffold and embryonic structures show high contrast enhancement, while the adjacent tissue shows little uptake. As for the scaffold material implanted on the CAM, it is shown that contrast enhancement varies locally within the scaffold and

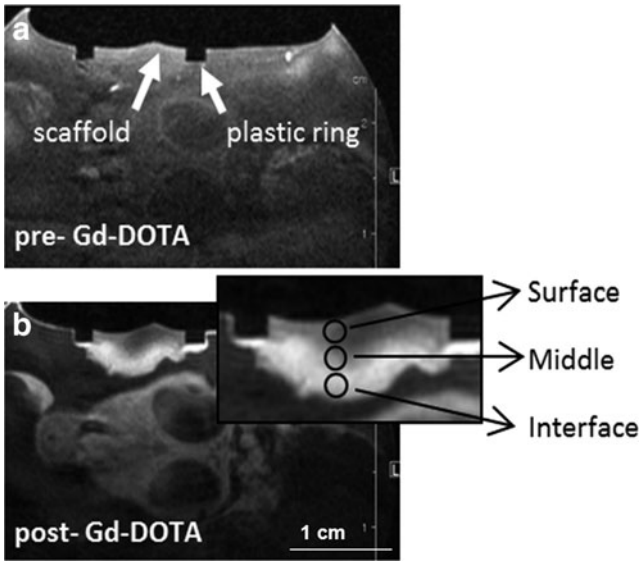

FIG. 2. *In ovo* T_1-weighted magnetic resonance images acquired 7 days postimplantation in an axial slice through the scaffold. **(a)** before **(b)** 25 min after i.v. injection of Gd-DOTA. Enlarged section: scaffold with regions of interest (*circles*) at the interface with the CAM, in the middle and on the surface of the scaffold.

that the largest signal change appears at the interface to the CAM (see enlarged section that zooms into the scaffold). Noteworthy to mention is the clear border of the contrast agent uptake at the interface to the CAM. While little Gd-DOTA uptake is found next to the scaffold implying little vascularization, there is a high contrast agent uptake at the interface. A quantitative analysis is summarized in Figure 3,

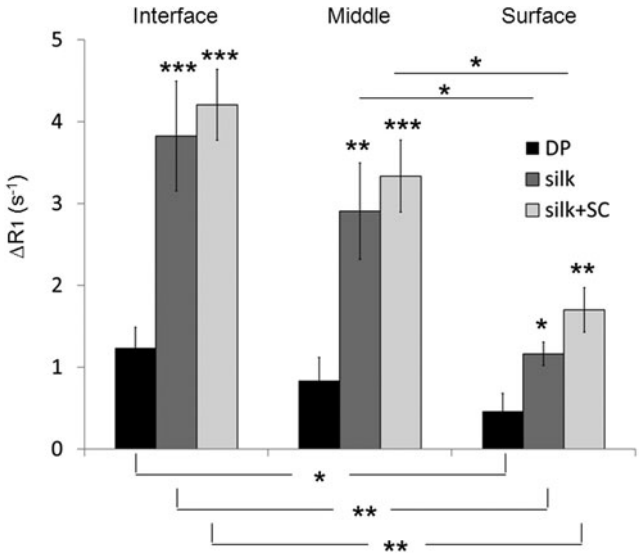

FIG. 3. Relaxation rate change ΔR_1 in three regions of interest at the interface, middle, and surface of the DegraPol and silk fibroin scaffolds either with or without human dental pulp stem cells (hDPSCs) grown for 1 week on the CAM. Values are given as mean ± standard deviation. *p*-Values are denoted as * is $p < 0.05$; ** $p < 0.01$; and *** $p < 0.001$. *Asterisks* without line refer to comparisons to DegraPol.

which shows that the relaxation rate change, ΔR_1, and hence perfusion capacity, declines from interface to the CAM toward the surface region of the scaffold ($n = 8$).

Finally, the relaxation rate change, ΔR_1, was monitored as a function of time after injection of Gd-DOTA ($n = 3$). As shown in Figure 4, the signal intensity reached a plateau at 35 min in all regions of interest studied.

Histology

Quantification of vessel density was accomplished by counting the number of blood vessels within cross sections of 8 × 4 mm stained by H&E (Fig. 5a). Vessels were identified as roundish blue structures lining endothelial cells. Representative images for each score level are available as Supplementary Data to this article (Supplementary Fig. S1; Supplementary Data are available online at www.liebertpub.com/tec). Vessel counts from H&E staining were also confirmed by an additional scoring in *von Willebrand Factor* immunostained corresponding sections (Fig. 5b). In addition, CD31 staining revealed the same vessel counts as determined by H&E and *von Willebrand Factor* stainings (Fig. 5c). These histological analyses revealed that the interface region of the implanted DegraPol scaffold with the CAM showed the highest number of small blood vessels compared with middle and surface, with an average vessel density score of 3.05 ± 1.34; 2.42 ± 1.15; and 1.47 ± 0.65, respectively. The surface region with the longest distance to the CAM had the lowest number of small blood vessels (Fig. 6). Therefore, the same regional pattern of vascularization was observed as in our MRI data. Furthermore, a strong correlation was obtained between relaxation rate changes, ΔR_1, and the histological scores for vessel density ($R^2 = 0.983$). Thus, the histology data corroborate the MRI findings.

Perfusion capacity in different biomaterials (proof-of-principle)

To apply the method to other biomaterials than DegraPol, relaxation rate changes, ΔR_1, of silk fibroin scaffolds (± hDPSCs) were measured for the same corresponding

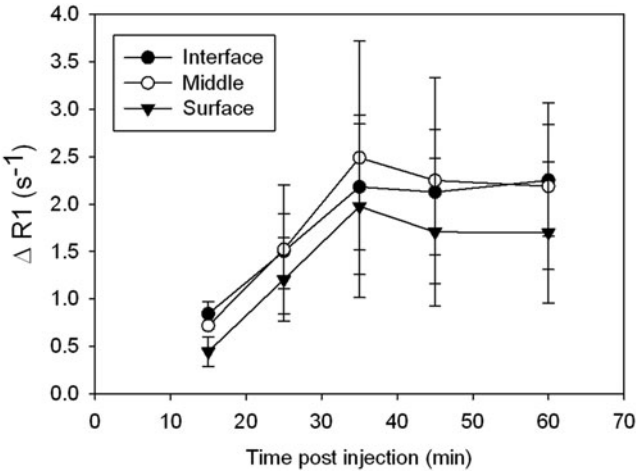

FIG. 4. Relaxation rate change ΔR_1 as a function of time after contrast agent injection in three regions of interest at the interface, middle, and surface of the DegraPol scaffold. Values are given as mean ± standard deviation.

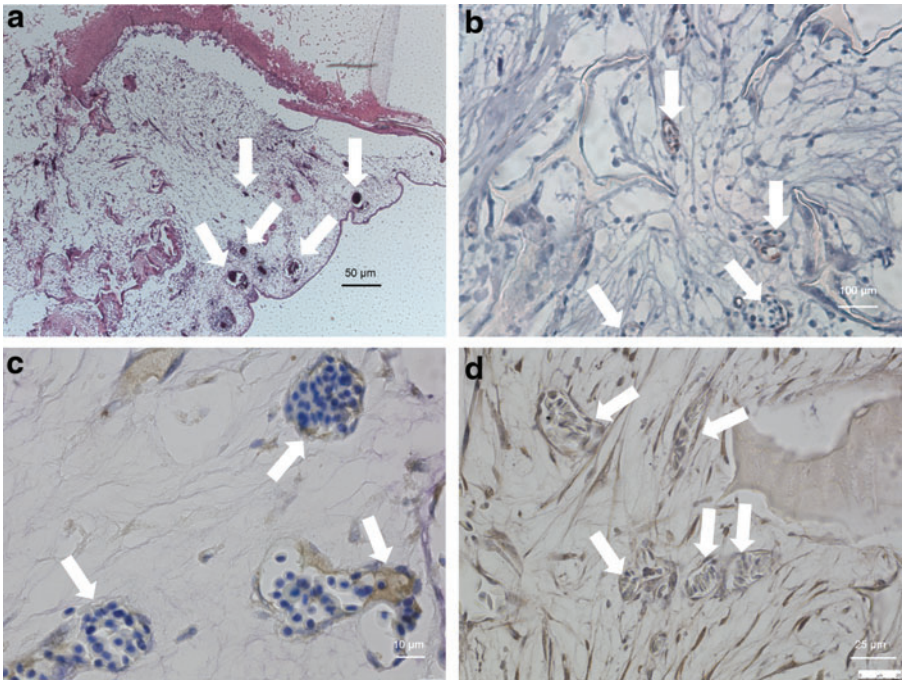

FIG. 5. Histological cross sections showing the capillaries in the scaffold material: **(a)** Hematoxylin and eosin staining of DegraPol at 100× magnification; **(b)** immunostaining with *von Willebrand Factor* of DegraPol at 200× magnification; **(c)** immunostaining with CD31 of DegraPol at 630× magnification (counterstaining Toluidine Blue) and **(d)** immunostaining with CD31 of silk fibroin seeded with hDPSCs (counterstaining hematoxylin) at 400× magnification. A few vessels are exemplarily highlighted by *arrows*. Color images available online at www.liebertpub.com/tec

scaffold regions (interface, middle, and surface, Fig. 3). For all three regions, the perfusion capacity of silk fibroin scaffolds was significantly higher compared with the DegraPol scaffolds (three to four times higher, $p < 0.0001$). However, the hDPSCs did not evoke a statistically significant higher perfusion of the silk fibroin scaffolds compared to the cell-free silk fibroin scaffolds ($p > 0.1$). Only a trend was noticed for all three regions, where the perfusion was higher in the presence of the hDPSCs compared to the cell-free scaffolds. CD31 staining clearly showed the vessels inside the silk fibroin scaffold seeded by hDPSCs (Fig. 5d). Finally, in both biomaterials, DegraPol and silk fibroin (±hDPSCs), perfusion capacity declines from the interface toward the surface, in line with the scaffolds being vascularized from the CAM toward the surface.

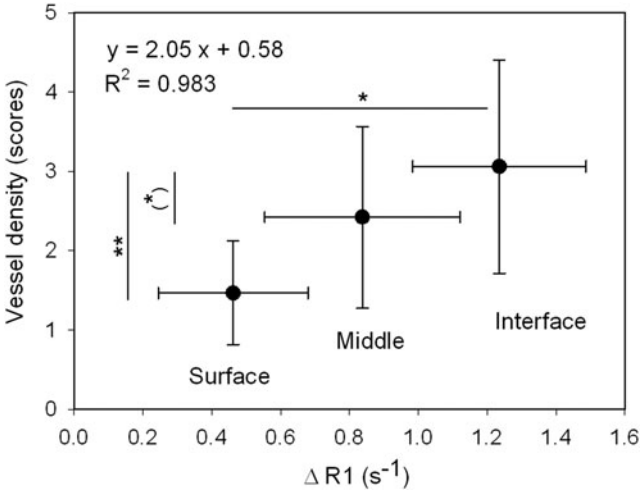

FIG. 6. Relaxation rate change ΔR_1 as a measure of perfusion capacity versus vessel density obtained by semiquantitative scoring of histological slices in three regions of interest at the interface, middle, and surface of the scaffold-CAM complex. Relaxation rate change and vessel density in the scaffold are highest at the interface to the CAM and decrease with distance from the CAM. Score $1 \leq 10$, score 1.5 = 10–30, score 2 = 30–50, score 2.5 = 50–70, score 3 = 70–90, score 3.5 = 90–110, score 4 = 110–130, score 4.5 = 130–150, and score $5 \geq 150$ vessels counted in a cross section of 32 mm^2. Values are given as mean ± standard deviation. *p*-Values are denoted as (*) is $p < 0.1$; $^*p < 0.05$; and $^{**}p < 0.01$.

Discussion

In this study, we present for the first time a cheap screening method for noninvasive quantification of the perfusion capacity of biomaterials with MRI *in vivo*. We found a strong positive correlation between local changes in T_1-based relaxation rates in biomaterials grown 1 week on the CAM and the vessel density determined by histology.

Vascularization in 3D biomaterials is a limiting factor for successful implantation and functionalization of these engineered tissues. The highly vascularized CAM of the chick embryo is a useful model to evaluate the tissue response and perfusion capacity of scaffolds placed on top of the CAM. Furthermore, this avian model provides a good nutritional environment to tissue-engineered materials. Compared to the traditional mammalian models, the CAM assay is cheap, more time efficient, and does not have any immune-system based reaction toward foreign bodies.[6] Thus, it allows—among many other applications—to work with human tumor cells to study tumor-induced angiogenesis[25] or chemoprevention.[26] Even in environmental pollution and health debates, it may serve as a valuable model.[27] Finally, the CAM assay has been well established,[6] is low priced, and predominantly used to study angiogenesis and anti-angiogenesis in response to different drugs, growth factors, and cell types.[3,28]

As a model biomaterial, we chose a biodegradable DegraPol foam because this polyester-urethane has been shown

to be biocompatible with respect to osteoblasts,[16] chondrocytes,[17] and tenocytes[29] among others. To date, many studies examined the tissue response toward biomaterials using the CAM model,[3,8] or tested different biomaterials such as PVC or modified polyurethanes with respect to angiogenesis and inflammatory response.[30] However, they often use ''end-point'' information such as histological analysis which necessitates the destruction of the tissue-engineered construct. In a previous study we therefore presented MRI as a nondestructive, analytical tool for studying vascularization *ex vivo* in the same biomaterial grown on the CAM.[10] While MRI has been employed *in vivo* to determine the mineralization of bone constructs placed on the CAM,[9] it has not been used so far for the assessment of the perfusion capacity. Our present study therefore shows for the first time MRI as a suitable method to examine the perfusion capacity in biomaterials placed on the CAM *in situ* in the living chicken embryo. The combination of the CAM model with an *in ovo* and *in vivo* MRI readout offers the potential to longitudinally monitor the perfusion capacity of biomaterials. In other words, the vascularization process can be followed *in vivo* by noninvasive MRI, thereby offering a novel screening method to quantify the perfusion capacity of a series of different biomaterials at different time points in the same sample.

In particular, our data show that the perfusion capacity of scaffolds grown for 1 week on the CAM can be quantified by analyzing relaxation rate changes, as these are dependent on the amount of contrast agent present in the vascular network. Inspection of contrast-enhancement within the scaffold revealed regional variations and a region of interest analysis of relaxation rate changes was performed to assess such heterogeneity more quantitatively. As such, perfusion capacity was found to be highest at the interface where the scaffold was attached to the CAM while it gradually decreased with distance from the interface with lowest perfusion capacity found at the surface of the scaffold. Presumably, DegraPol scaffolds were too large to be fully vascularized as has been found for smaller DegraPol foams (30 mm^3 as compared to 96 mm^3 used here) in our previous study.[10] Semi-quantitative histological analyses of vessel density in locally staggered histological sections taken from the interface, middle, and surface of the scaffold corroborates the MRI findings as the highest vessel density was found at the interface and lowest at the surface of the scaffold. Furthermore, histological scores were found to strongly correlate with the relaxation rate changes, providing further support for our notion that relaxation rate changes may be used as a simplified measure for perfusion capacity.

In order to apply this newly established method to a typical question in the field of tissue engineering (as a proof-of-principle), silk fibroin scaffolds either with or without hDPSCs were also analyzed with respect to their perfusion capacity by MRI. First of all, the differences in the relaxation rates between the two materials DegraPol and silk fibroin were significant; silk fibroin showed three to four times higher relaxation rates compared with DegraPol, which renders silk fibroin a much better scaffold material in terms of a fast vascularization. Second, silk fibroin seeded with hDPSCs had higher relaxation rates compared to cell-free constructs (trend), implying that an *in vitro* preseeding of only 1 day (!) has already a beneficial impact on the perfusion extent *in ovo*. The hDPSCs are involved in the building of new vessels inside the silk fibroin as confirmed by histological analysis of typical endothelial cell markers (von Willebrand Factor and CD31). Therefore, our method leads to remarkable changes in ΔR_1 for different scaffold materials and it is sensitive already for minor changes in preparation such as a 1-day preseeding by stem cells.

Some limitations of the *in ovo* CAM model as used in our study should be mentioned, however. First, only 30–40% of the windowed eggs survived the opening of the eggshell. This may mostly be attributed to eggshell dust contaminating the otherwise sterile egg cavity and its environment during windowing. Smaller windows might reduce the risk of contamination, however, larger windows allow minimizing the distance between the scaffold and the surface coil during MRI measurements and facilitate access to the vasculature during contrast agent injection, which is necessary for higher resolutions. Second, the injection of the contrast agent was a highly delicate process due to the small vessel size and flexibility within the egg yolk. An experienced microsurgeon (Y.T.) provided the required skills, but these can be also acquired by others through dedicated trainingThird, there is a limitation in size of the biomaterial under investigation; a size of $8 \times 4 \times 3$ mm^3 as used in case of the DegraPol scaffolds could have a bigger area placed on the CAM, however, the height (3 mm) cannot be increased much because during a time frame of 7 days, vessel growth starting from the CAM surface might not reach the top of the scaffold. Moreover, the timing between contrast agent injection and relaxation time measurement was set at 25 min. This time window was considered ample for the contrast agent to distribute in the microvasculature and extravascular compartment and the relaxation rate change, and hence perfusion signal, being not dominated by wash-in effects of bigger vessels. To assess possible effects of this specific time window we acquired a time series of relaxation rate changes between 15–60 min postinjection in three samples. These data reveal that contrast agent uptake is highest 35 min postinjection, indicating that other processes, such as diffusion, also contribute to the rather slow contrast agent uptake.[31] Thus, for highest contrast our preset time window of 25 min postinjection, which was preset such as to maximize uptake of contrast agent but also aimed at reducing necessary scantime, will be increased in future studies.

Finally it should be mentioned that in our study we did not take full advantage of our method's potential to perform longitudinal measurements that our *in ovo* CAM model combined with noninvasive *in vivo* MRI readout offers. To do so, a couple of legal, physiological, and technical issues will need to be tackled: Experimental procedures with fertilized eggs fall under the legislation of the Swiss federal ordinance on animal protection and welfare starting on ID 14 and hence the prerequisite legal framework needs to be set into place for experiments lasting longer than ID 14. On the physiological side it remains to be established how much the development of the vascular network and ultimately perfusion capacity is affected by stress induced by the handling of the egg, anesthesia, MRI measurement and contrast agent injection. Previous studies indicate that such effects exist and warrant further investigation.[32] And finally, contrast agent doses might need to be titrated down such as to enable repeated measurements, in particular as renal clearing rates in the avian embryo are not known and the

contrast agent supposedly remains in the closed environment of the egg.

Nevertheless, the method established here is really beneficial for tissue engineering and regeneration purposes because it allows performing a cheap and fast *in vivo* screening of the perfusion extent of any biomaterials or bioartificial constructs. It hence allows gathering valuable preclinical information about a material's potential long-term functionality and survival in the host tissue and therefore may steer early candidate selection for further development. Furthermore, for the benefit of the three Rs, it has become mandatory to evaluate cell-scaffold constructs prior to *in vivo* experiments.[33] With a cost of only 2 dollars per egg it is much cheaper compared with animal models such as mice (>25 dollars), rats (>35 dollars), or rabbits (>200 dollars). Moreover, vascularization of the biomaterials can be monitored as a function of time with noninvasive MRI and valuable information can be gathered within a time frame of only 2 weeks including 1 week of incubation and 1 week of monitoring angiogenesis in the material under view.

In sum, the CAM model's cost effectiveness and the absence of immune-defense reactions combined with the noninvasiveness of MRI to access the perfusion capacity of biomaterials and tissue-engineered constructs *in vivo* and *in ovo* will increase the attractiveness of this distinguished combination in the future. We conclude that the CAM assay together with noninvasive MRI presents a reliable *in vivo* model for monitoring the perfusion capacity of biomaterials. Further studies are planned with arrays of different biomaterials and differently pre-engineered biomaterials in our laboratory.

Acknowledgments

We would like to thank Ms. Pia Fuchs for H&E staining and Dr. Monika Hilbe for *von Willebrand Factor* staining. PD Dr. Andreas Boss is acknowledged for providing the contrast agent. Furthermore, Trudel Silk Inc., Zurich, Switzerland is highly acknowledged for providing silk fibroin and Dr. Sandra Hofmann, Eindhoven University of Technology, for manufacturing the scaffolds. We additionally thank PD Dr. Bernd Stadlinger of the clinic for dental medicine, for providing the teeth. The Matching Funds of University Hospital Zurich are highly acknowledged for financial support. We are thankful to *ab medica*, Italy, for providing the DegraPol foams.

Disclosure Statement

There are no competing financial interests.

References

1. Lemon, G., Howard, D., Tomlinson, M.J., Buttery, L.D., Rose, F.R.A.J., Waters, S.L., and King, J.R. Mathematical modelling of tissue-engineered angiogenesis. Math Biosci **221,** 101, 2009.
2. Borges, J., Tegtmeier, F.T., Padron, N.T., Mueller, M.C., Lang, E.M., and Stark, G.B. Chorioallantoic membrane angiogenesis model for tissue engineering: a new twist on a classic model. Tissue Eng **9,** 441, 2003.
3. Baiguera, S., Macchiarini, P., and Ribatti, D. Chorioallantoic membrane for *in vivo* investigation of tissue-engineered construct biocompatibility. J Biomed Mater Res Part B **100B,** 1425, 2012.
4. Rouwkema, J., Rivron, N.C., and van Blitterswijk, C.A. Vascularization in tissue engineering. Trends Biotechnol **26,** 434, 2008.
5. O'Brien, F.J. Biomaterials & scaffolds for tissue engineering. Mater Today **14,** 88, 2011.
6. Deryugina, E.I., and Quigley, J.P. Chick embryo chorioallantoic membrane models to quantify angiogenesis indued by inflammatory and tumor cells or purified effector molecules. Methods Enzymol **444,** 21, 2008.
7. Cole, R.W., Liu, F., and Herron, B.J. Imaging of angiogenesis: past, present and future. In: Méndez-Vilaz, A., and Diaz, J., eds. Microscopy: Science, Technology, Applications and Education. Madrid, Spain: FORMATEX, Vol. 1, 2010, pp. 885–896.
8. Valdes, T.I., Kreutzer, D., and Moussy, F. The chick chorioallantoic membrane as a novel *in vivo* model for the testing of biomaterials. J Biomed Mater Res **62,** 273, 2002.
9. Chesnick, I.E., Fowler, C.B., Mason, J.T., and Potter, K. Novel mineral contrast agent for magnetic resonance studies of bone implants grown on a chick chorioallantoic membrane. Magn Reson Imaging **29,** 1244, 2011.
10. Buschmann, J., Welti, M., Hemmi, S., Neuenschwander, P., Baltes, C., Rudin, M., Giovanoli, P., and Calcagni, M. 3D co-cultures of osteoblasts and endothelial cells in DegraPol foam: histological and high field MRI analyses of pre-engineered capillary networks in bone grafts. Tissue Eng Part A **17,** 291, 2011.
11. Klueh, U., Dorsky, D.I., Moussy, F., and Kreutzer, D.L. Ex ova chick chorioallantoic membrane as a novel model for evaluation of tissue responses to biomaterials and implants. J Biomed Mater Res Part A **67A,** 838, 2003.
12. Lokman, N.A., Elder, A.S.F., Ricciardelli, C., and Oehler, M.K. Chick chorioallantoic membrane (CAM) assay as an in vivo model to study the effect of newly identified molecules on ovarian cancer invasion and metastasis. Int J Mol Sci **13,** 9959, 2012.
13. Krishnan, R., Arora, R.P., Alexander, M., White, S.M., Lamb, M.W., Foster, C.E., Choi, B., and Lakey, J.R. Noninvasive evaluation of the vascular response to transplantation of alginate encapsulated islets using the dorsal skin-fold model. Biomaterials **35,** 891, 2014.
14. Sauerbier, S., Palmowski, M., Vogeler, M., Nagursky, H., Al-Ahmad, A., Fisch, D., Hennig, J., Schmelzeisen, R., Gutwald, R., and Fasol, U. Onset and maintenance of angiogenesis in biomaterials: *in vivo* assessment by dynamic contrast-enhanced MRI. Tissue Eng Part C Methods **15,** 455, 2009.
15. Milleret, V., Simonet, M., Bittermann, A.G., Neuenschwander, P., and Hall, H. Cyto- and hemocompatibility of a biodegradable 3D-scaffold material designed for medical applications. J Biomed Mater Res Part B **91B,** 109, 2009.
16. Saad, B., Casotti, M., Huber, T., Schmutz, P., Welti, M., Uhlschmid, G.K., Neuenschwander, P., and Suter, U.W. *In vitro* evaluation of the biofunctionality of osteoblasts cultured on DegraPol-foam. J Biomater Sci Polym Ed **11,** 787, 2000.
17. Saad, B., Moro, M., Tun-Kyi, A., Welti, M., Schmutz, P., Uhlschmid, G.K., Neuenschwander, P., and Suter, U.W. Chondrocyte-biocompatibility of DegraPol (R)-foam: *in vitro* evaluations. J Biomater Sci Polym Ed **10,** 1107, 1999.
18. Borkenhagen, M., Stoll, R.C., Neuenschwander, P., Suter, U.W., and Aebischer, P. *In vivo* performance of a new

biodegradable polyester urethane system used as a nerve guidance channel. Biomaterials **19,** 2155, 1998.
19. Buschmann, J., Meier-Bürgisser, G., Bonavoglia, E., Neuenschwander, P., Milleret, V., Giovanoli, P., and Calcagni, M. Cellular response of healing tissue to DegraPol tube implantation in rabbit Achilles tendon rupture repair: an *in vivo* histomorphometric study. J Tissue Eng Regen Med **7,** 413, 2013.
20. Hofmann, S., Hilbe, M., Fajardo, R.J., Hagenmueller, H., Nuss, K., Arras, M., Mueller, R., von Rechenberg, B., Kaplan, D.L., Merkle, H.P., and Meinel, L. Remodeling of tissue-engineered bone structures *in vivo*. Eur J Pharm Biopharm **85,** 119, 2013.
21. Kundu, B., Rajkhowa, R., Kundu, S.C., and Wang, X. Silk fibroin biomaterials for tissue regenerations. Adv Drug Deliv Rev **65,** 457, 2013.
22. Altman, G.H., Diaz, F., Jakuba, C., Calabro, T., Horan, R.L., Chen, J.S., Lu, H., Richmond, J., and Kaplan, D.L. Silk-based biomaterials. Biomaterials **24,** 401, 2003.
23. Tirino, V., Paino, F., De Rosa, A., and Papaccio, G. Identification, isolation, characterization, and banking of human dental pulp stem cells. In: Singh, S.R., ed. Somatic Stem Cells. Clifton, NJ: Humana Press, 2012, pp. 443–463.
24. Ribatti, D., Nico, B., Vacca, A., and Roncali, L. Localization of factor VIII-related antigen in the endothelium of the chick embryo chorioallantoic membrane. Histochem Cell Biol **112,** 447, 1999.
25. Subauste, M.C., Kupriyanova, T.A., Conn, E.M., Ardi, V.C., Quigley, J.P., and Deryugina, E.I. Evaluation of metastatic and angiogenic potentials of human colon carcinoma cells in chick embryo model systems. Clin Exp Metastasis **26,** 1033, 2009.
26. Wang, D., Taylor, E.W., Wang, Y., Wan, X., and Zhang, J. Encapsulated nanoepigallocatechin-3-gallate and elemental selenium nanoparticles as paradigms for nanochemoprevention. Int J Nanomed **7,** 1711, 2012.
27. Mousa, S.A., O'Connor, L., Rossman, T.G., and Block, E. Pro-angiogenesis action of arsenic and its reversal by selenium-derived compounds. Carcinogenesis **28,** 962, 2007.
28. Ribatti, D. Chick embryo chorioallantoic membrane as a useful tool to study angiogenesis. In: Jeon, K.W., ed. International Review of Cell and Molecular Biology, Vol. 270. San Diego: Elsevier Academic Press, Inc., 2008, pp. 181–224.
29. Sukthankar, A. DegraPol-btc/btgc: *In Vitro* Untersuchung der Biokompatibilität für Tenozyten Surgery Division University Hospital Zurich, University Hospital Zurich, Zurich, 1999.
30. Zwadlo-Klarwasser, G., Gorlitz, K., Hafemann, B., Klee, D., and Klosterhalfen, B. The chorioallantoic membrane of the chick embryo as a simple model for the study of the angiogenic and inflammatory response to biomaterials. J Mater Sci Mater Med **12,** 195, 2001.
31. Rudin, M., McSheehy, P.M.J., Allegrini, P.R., Rausch, M., Baumann, D., Becquet, M., Brecht, K., Brueggen, J., Ferretti, S., Schaeffer, F., Schnell, C., and Wood, J. PTK787/ZK222584, a tyrosine kinase inhibitor of vascular endothelial growth factor receptor, reduces uptake of the contrast agent GdDOTA by murine orthotopic B16/BL6 melanoma turnours and inhibits their growth *in vivo*. NMR Biomed **18,** 308, 2005.
32. Mohammad, F.K., Faris, G.A.M., and Al-Zubeady, A.Z. Developmental and behavioral effects of medetomidine following in ovo injection in chicks. Neurotoxicol Teratol **34,** 214, 2012.
33. Falkner, E., Eder, C., Kapeller, B., Fröschl, W., Schmatz, C., Macfelda, K., and Losert, U.M. The mandatory CAM testing of cells and scaffolds for tissue engineering: benefits for the three Rs of cooperation with the vaccine industry. Altern Lab Anim **32,** 573, 2004.

Address correspondence to:
Johanna Buschmann, PhD
Plastic Surgery and Hand Surgery
University Hospital Zurich
Sternwartstrasse 14
8091 Zürich
Switzerland

E-mail: johanna.buschmann@usz.ch

Received: April 15, 2014
Accepted: September 3, 2014
Online Publication Date: November 13, 2014

14.1.5 Mitsiadis and Woloszyk, Front Physiol, 2015

Odyssey of human dental pulp stem cells and their remarkable ability to survive in extremely adverse conditions (OPINION)

The goal of this communication was to inform the scientific community about an interesting observation we have made when shipping cells from Naples, Italy to Zurich, Switzerland. Instead of arriving within 24 hours the shipping of the cells took eight full days. Contrary to our expectations, the cells were not dead, but were still alive and continued proliferating after changing the medium, which suggests that human dental pulp stem cells are able to survive for prolonged periods of time in conditions of extreme stress.

I contributed by documenting the cell status after their arrival, performing literature research, as well as co-writing and co-editing the manuscript.

frontiers in Physiology

OPINION
published: 26 March 2015
doi: 10.3389/fphys.2015.00099

Odyssey of human dental pulp stem cells and their remarkable ability to survive in extremely adverse conditions

Thimios A. Mitsiadis and Anna Woloszyk*

Orofacial Development and Regeneration, Faculty of Medicine, Institute of Oral Biology, Center for Dentistry, University of Zurich, Zurich, Switzerland

Keywords: tooth, dental pulp stem cells, tissue regeneration, stem cells, stem cell niches, quiescent stem cells, hypoxia

Edited by:
Eumorphia Remboutsika, Biomedical Sciences Research Center "Alexander Fleming," Greece

Reviewed by:
Stavros Malas, Cyprus Institute of Neurology and Genetics, Cyprus
Angelo Putignano, Polytechnic University of Marche, Italy

****Correspondence:***
Thimios A. Mitsiadis, thimios.mitsiadis@zzm.uzh.ch

Specialty section:
This article was submitted to Craniofacial Biology, a section of the journal Frontiers in Physiology

Received: *03 March 2015*
Accepted: *12 March 2015*
Published: *26 March 2015*

Citation:
Mitsiadis TA and Woloszyk A (2015) Odyssey of human dental pulp stem cells and their remarkable ability to survive in extremely adverse conditions. Front. Physiol. 6:99. doi: 10.3389/fphys.2015.00099

Adult tissues contain stem cells, which proliferate to compensate for tissue loss throughout the life of the organism (Li and Clevers, 2010; Jiménez-Rojo et al., 2012). Therefore, adult stem cells are important for tissue repair and regeneration after injury. In seriously injured or carious teeth, stem cells residing in the dental pulp are responsible for the repair and regeneration of the damaged dental tissues (Catón et al., 2011; Mitsiadis et al., 2011). Dental pulp stem cells (DPSCs) can be isolated after labeling of the pulp cells with fluorescent mesenchymal stem cell (MSC) markers such as STRO-1, CD146, and CD44, followed by fluorescence-activated cell sorting (FACS) (Mitsiadis et al., 2012). Additional identification procedures include morphological criteria, adherence properties, proliferation, and differentiation potential, as well as tissue repair abilities of the sorted stem cell populations. The potential of DPSCs for the regeneration of bone tissue in patients has been demonstrated with a successful trial assay that has been realized in Napoli (Italy) several years ago (Catón et al., 2011; Mitsiadis et al., 2012).

We have established a close scientific collaboration with the Napoli stem cell team headed by Prof. Gianpaolo Papaccio for the exchange of knowledge and materials. Several months ago, we have requested for a bunch of freshly isolated DPSCs in order to complete a number of experiments that we are currently realizing in our laboratories in Zurich (Switzerland). DPSCs were shipped with an express delivery company on the 26/11/2014 from Napoli with destination to Zurich. The shipped DPSCs were grown as a monolayer in a 25 cm^2 culture flask containing the standard MSC culture medium. The flask that was sealed with Parafilm and left in ambient temperature should normally arrive to the destination the next day, but for unknown reasons the journey of DPSCs was longer and more exciting than expected. The DPSCs have followed an astonishing itinerary from Italy, to France (Paris), Great Britain, South Africa (Johannesburg), back to France, thereafter to Spain, France again. From France the cells finally arrived to Zurich Switzerland through Basel on the 4/12/2014. This itinerary can be considered as an Odyssey of DPSCs, which had to develop sophisticated mechanisms for their survival under these extremely adverse conditions.

Sometimes discoveries are arising by chance, following a mistake or having an unexpected behavior. It was expected that the flask, upon its late arrival, would contain only dead cells. However, surprisingly, DPSCs (or a big part of them) were still alive after their journey (**Figure 1A**). DPSCs were extremely proliferative and became confluent within 3 days, after changing the medium (**Figures 1B,C**). How this could be explained? Recent findings indicate that quiescent (reserve) and proliferating (active) stem cell pools may coexist in separate but adjacent compartments of many tissues (Li and Clevers, 2010). It has been proposed that stem cells can adopt a reversible quiescence state characterized by reduced metabolic activity in conditions such as lack of oxygen and/or nutrients (Cheung and Rando, 2013). However, the mechanisms that

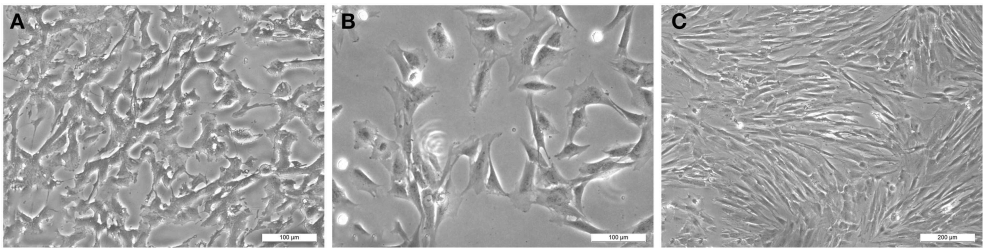

FIGURE 1 | Visualization of human dental pulp stem cells (hDPSCs): (A) upon arrival to Zurich (first passage), (B) after 6 h of culture (second passage), and (C) after 3 days of culture (second passage). Scale bars indicate the magnifications.

allow quiescent stem cells to survive metabolic or environmental stress, to preserve their cellular and genomic integrity and to assure long-term survival are not yet elucidated. It has been suggested that quiescence is an actively maintained state regulated by intrinsic mechanisms to sustain metabolic function during persistent environmental stress, and thus ensuring stem cell survival (Cheung and Rando, 2013). Viable stem cells were found in post-mortem tissues (Latil et al., 2012). These cells were able to maintain their functional properties after prolonged storage in anoxia *in vitro* and after transplantation (Latil et al., 2012). Similarly, it has been shown that several stem cell populations reside in poorly oxygenated niches (Simsek et al., 2010). Quiescent stem cells have the ability to sense environmental changes and respond by re-entering the cell cycle for proliferation (Cheung and Rando, 2013). Severe hypoxia could be critical for maintaining the viability of DPSCs. It is possible that mechanisms compatible with the low metabolic state of quiescence have allowed rapid responses for DMSCs re-activation.

This Odyssey revealed that DPSCs are able to survive for prolonged periods of time in conditions of extreme stress.

References

Catón, J., Bostanci, N., Remboutsika, E., De Bari, C., and Mitsiadis, T. A. (2011). Future dentistry: cell therapy meets tooth and periodontal repair and regeneration. *J. Cell Mol. Med*. 15, 1054–1065. doi: 10.1111/j.1582-4934.2010.01251.x

Cheung, T. H., and Rando, T. A. (2013). Molecular regulation of stem cell quiescence. *Nat. Rev. Mol. Cell Biol.* 14, 329–340. doi: 10.1038/nrm3591

Jiménez-Rojo, L., Granchi, Z., Graf, D., and Mitsiadis, T. A. (2012). Stem Cell Fate Determination during development and regeneration of ectodermal organs. *Front. Physiol.* 3:107. doi: 10.3389/fphys.2012.00107

Latil, M., Rocheteau, P., Châtre, L., Sanulli, S., Mémet, S., Ricchetti, M., et al. (2012). Skeletal muscle stem cells adopt a dormant cell state post mortem and retain regenerative capacity. *Nat. Commun*. 3:903. doi: 10.1038/ncomms1890.

Li, L., and Clevers, H. (2010). Coexistence of quiescent and active adult stem cells in mammals. *Science* 327, 542–545. doi: 10.1126/science.1180794.

Mitsiadis, T. A., Feki, A., Papaccio, G., and Catón, J. (2011). Dental pulp stem cells, niches, and notch signaling in tooth injury. *Adv. Dent. Res*. 23, 275–279. doi: 10.1177/0022034511405386

Mitsiadis, T. A., Woloszyk, A., and Jiménez-Rojo, L. (2012). Nanodentistry: combining nanostructured materials and stem cells for dental tissue regeneration. *Nanomedicine (Lond.)* 7, 1743–1753. doi: 10.2217/nnm.12.146

Simsek, T., Kocabas, F., Zheng, J., Deberardinis, R. J., Mahmoud, A. I., Olson, E. N., et al. (2010). The distinct metabolic profile of hematopoietic stem cells reflects their location in a hypoxic niche. *Cell Stem Cell* 7, 380–390. doi: 10.1016/j.stem.2010.07.011

Conflict of Interest Statement: The authors declare that the research was conducted in the absence of any commercial or financial relationships that could be construed as a potential conflict of interest.

14.1.6 Woloszyk and Buschmann et al., Front Physiol, 2016

Human dental pulp stem cells and gingival fibroblasts seeded into silk fibroin scaffolds have the same ability in attracting vessels (PAPER, shared first authorship)

In our previous studies we had observed that human dental pulp stem cell (hDPSC)-seeded silk fibroin scaffolds were able to attract more vessels than empty scaffolds. In order to test if this ability to attract vessels is unique to hDPSCs we wanted to compare the results to silk fibroin scaffolds seeded with another population of cells isolated from an oral-derived tissue, namely human gingival fibroblasts (hGFs). Similar to previous studies, the experimental part that I performed included the extraction of cells from the tissue of interest, i.e. human dental pulp and human gingiva, respectively, cell expansion, cell seeding of the scaffolds and culture of the cell-seeded samples on the CAM. The analyses of the samples were performed in close collaboration with Dr. Johanna Buschmann and her team at the University Hospital, who used an *in vivo* MRI technique to measure the perfusion capacity of the vascularized samples on the CAM of the living anesthetized chicken embryo after the injection of a contrast agent. After the MRI measurements, I continued with the sample analysis, which included histology and a manual blood vessel analysis. While preparing the manuscript I compiled the figures and contributed to the writing and literature research.

The results of both *in vivo* MRI and manual blood vessel analyses clearly demonstrated that hDPSCs and hGFs possess equal abilities in attracting blood vessels into silk fibroin scaffolds.

A possible explanation for a similar blood vessel attraction potential of both hDPSCs and hGFs is the fact that similar to hDPSCs also hGFs are derived from the cranial neural crest, and have been shown to possess stem cell properties before. Moreover, also hGFs are known to secrete angiogenic factors. Further studies are necessary in order to establish, which properties of a cell population are essential for the successful attraction of the host's vasculature into a 3D biomaterial and how this potential could be incorporated into future clinical strategies for the use of autologous tissue engineered implants for regenerative purposes.

frontiers in Physiology

ORIGINAL RESEARCH
published: 19 April 2016
doi: 10.3389/fphys.2016.00140

Human Dental Pulp Stem Cells and Gingival Fibroblasts Seeded into Silk Fibroin Scaffolds Have the Same Ability in Attracting Vessels

Anna Woloszyk[1]†, Johanna Buschmann[2]†, Conny Waschkies[3,4], Bernd Stadlinger[5] and Thimios A. Mitsiadis[1]*

[1] Orofacial Development and Regeneration, Center of Dental Medicine, Institute of Oral Biology, University of Zurich, Zurich, Switzerland, [2] Plastic Surgery and Hand Surgery, University Hospital Zurich, Zurich, Switzerland, [3] Institute for Biomedical Engineering, ETH and University of Zurich, Zurich, Switzerland, [4] Visceral and Transplant Surgery, University Hospital Zurich, Zurich, Switzerland, [5] Clinic of Cranio-Maxillofacial and Oral Surgery, University of Zurich, University Hospital Zurich, Zurich, Switzerland

OPEN ACCESS

Edited by:
Gianpaolo Papaccio, Second University of Naples, Italy

Reviewed by:
Francesco De Francesco, Second University of Naples, Italy
Vincenzo Desiderio, Seconda Università degli Studi di Napoli, Italy

***Correspondence:**
Anna Woloszyk
anna.woloszyk@zzm.uzh.ch

†*These authors have contributed equally to this work.*

Specialty section:
This article was submitted to Craniofacial Biology, a section of the journal Frontiers in Physiology

Received: *10 March 2016*
Accepted: *30 March 2016*
Published: *19 April 2016*

Citation:
Woloszyk A, Buschmann J, Waschkies C, Stadlinger B and Mitsiadis TA (2016) Human Dental Pulp Stem Cells and Gingival Fibroblasts Seeded into Silk Fibroin Scaffolds Have the Same Ability in Attracting Vessels. Front. Physiol. 7:140. doi: 10.3389/fphys.2016.00140

Neovascularization is one of the most important processes during tissue repair and regeneration. Current healing approaches based on the use of biomaterials combined with stem cells in critical-size bone defects fail due to the insufficient implant vascularization and integration into the host tissues. Therefore, here we studied the attraction, ingrowth, and distribution of blood vessels from the chicken embryo chorioallantoic membrane into implanted silk fibroin scaffolds seeded with either human dental pulp stem cells or human gingival fibroblasts. Perfusion capacity was evaluated by non-invasive *in vivo* Magnetic Resonance Imaging while the number and density of blood vessels were measured by histomorphometry. Our results demonstrate that human dental pulp stem cells and gingival fibroblasts possess equal abilities in attracting vessels within silk fibroin scaffolds. Additionally, the prolonged *in vitro* pre-incubation period of these two cell populations favors the homogeneous distribution of vessels within silk fibroin scaffolds, which further improves implant survival and guarantees successful healing and regeneration.

Keywords: regenerative medicine, vascularization, mesenchymal stem cells, human gingival fibroblasts (hGFs), human dental pulp stem cells (hDPSCs), silk fibroin scaffolds, chorioallantoic membrane (CAM)

INTRODUCTION

Classical bone defect treatments require the use of anatomically adapted devices that can establish tissue functionality and provide relief of symptoms to patients. However, the effectiveness and durability of treatments involving orthopedic or maxillofacial implants and transplantations of autologous bone grafts are still debatable. Indeed, the outcome of these regenerative solutions may be compromised by a variety of iatrogenic complications such as tissue morbidity and/or inflammation following implant or graft transplantation. Stem cell-based therapeutic approaches offer attractive alternatives in clinics since they can promise physiologically improved structural and functional outcomes. These therapies require a significant number of stem cell populations for implantation into specifically designed and composed scaffolds with various biological activities and compositions that can ensure their fast integration into the defect site. To avoid post-operative

complications it is essential to promote rapid, constant, and complete vascularization of these implantable constructs (Giannicola et al., 2010). Different strategies have been developed in order to enhance the vascularization capabilities of the various implanted materials. Cell seeding is one of the most popular and beneficial strategies to achieve this important goal. For example, it has been demonstrated that bone marrow stem cells (BMSCs) and endothelial cells seeded together in decalcified bone scaffolds can accelerate the vascularization process during calvaria bone repair (Koob et al., 2011). Similarly, it has been shown that human amniotic fluid-derived stem cells are able to enhance and stabilize vessel attraction and formation within collagen-chondroitin sulfate scaffolds (Lloyd-Griffith et al., 2015). Cell-seeded grafts may also have immunosuppressive functions that allow an improved healing procedure, as it has been already shown for adipose-derived stem cell-seeded scaffolds (Plock et al., 2015).

The use of human dental pulp stem cells (hDPSCs; Gronthos et al., 2000; Shi et al., 2001; Huang et al., 2009) and human gingival fibroblasts (hGFs; Xu et al., 2013; Chiquet et al., 2015) for regenerative purposes has been proposed as an alternative to BMSCs, since these cell populations exhibit similar properties and have the ability to adopt a variety of alternative fates in response to extrinsic factors. Indeed, it has been shown that hGFs have distinct functional activities in the regeneration and repair of periodontal tissues (Lee et al., 2013; Chiquet et al., 2015). Similarly, numerous studies have demonstrated that hDPSCs have the potential to differentiate into different cell types such as myocytes, chondrocytes, adipocytes, neurons, and osteoblasts both *in vitro* and *in vivo* (Gronthos et al., 2000; Zhang et al., 2006; d'Aquino et al., 2007; Bluteau et al., 2008; Mitsiadis et al., 2015). In addition, *in vitro* and *in vivo* studies have shown that hDPSCs may affect endothelial cell behavior by enhancing their migration and attraction toward them (Hilkens et al., 2014). The first clinical trial using autologous hDPSCs combined with commercially available collagen scaffolds (i.e., Gingistat®) for alveolar bone reconstruction has been successfully performed several years ago (d'Aquino et al., 2009). A 3 years follow-up study has shown that the structure of the regenerated bone at the grafted site was more compact than normal spongy alveolar bone (Giuliani et al., 2013), thus indicating that the choice of the appropriate scaffold and/or stem cell population is crucial for targeted, tissue-specific, regenerative procedures.

Silk fibroin scaffolds are commonly used in the medical field for a diverse set of applications such as vascular, neuronal, skin, cartilage, and bone regeneration (Altman et al., 2003; Kundu et al., 2013). Using bioreactor devices, we have previously shown that hDPSC-seeded silk fibroin scaffolds are able to form mineralized structures *in vitro* in a very short period of time (Woloszyk et al., 2014). In another recent study using the chicken embryo chorioallantoic membrane (CAM) assay combined with magnetic resonance imaging (MRI), we have demonstrated that hDPSCs can attract vessels within silk fibroin scaffolds (Kivrak Pfiffner et al., 2015).

Here we extended our previous studies and compared the capacity of hDPSCs and human gingival fibroblasts (hGFs) to attract vessels within silk fibroin scaffolds. Vascularization of the silk fibroin scaffolds was assessed using MRI and histomorphometric measurements. The results clearly demonstrated that hDPSCs and hGFs have similar abilities in attracting vessels and thus could be equally used in clinics for generating richly vascularized tissues.

MATERIALS AND METHODS

Production of Silk Fibroin Scaffolds

Silk fibroin scaffolds were produced using the salt leaching technique as previously described (Sofia et al., 2001; Nazarov et al., 2004; Hofmann et al., 2007). Briefly, silkworm cocoons (Trudel Inc., Zurich, Switzerland) were boiled in 0.02 M sodium carbonate (Fluka AG, Buchs SG, Switzerland) and rinsed with ultrapure water (UPW) to extract sericin. After drying, the silk was dissolved in 9 M lithium bromide and dialyzed against UPW for 36 h followed by lyophilization (Alpha 1-2, Martin Christ GMBH, Osterode am Harz, Germany). A 17% (w/v) silk fibroin solution was prepared by dissolving lyophilized silk in 1,1,1,3,3,3-hexafluoro-2-propanol (HFIP) (abcr GmbH & Co., Karlsruhe, Germany). This solution was added to Teflon containers filled with sodium chloride (Sigma-Aldrich Chemie GmbH, Buchs SG, Switzerland) at a ratio of 1:20 (silk fibroin:NaCl). After the evaporation of HFIP, the blocks were immersed in 90% methanol for 30 min (Sofia et al., 2001). The scaffolds were dried for at least 48 h before sodium chloride was leached out in five changes of UPW in 48 h resulting in scaffolds with more than 90% porosity (Nazarov et al., 2004). Wet silk fibroin scaffolds were cut into cylinders of 5 mm diameter and 3 mm height (59 mm^3) and were sterilized by autoclaving at 121°C and 1 bar for 20 min.

Cell Culture

The procedure for anonymized cell collection was approved by the Kantonale Ethikkommission of Zurich (reference number 2012-0588) and performed with written patients' consent. Human dental pulp stem cells (hDPSCs) were isolated from the dental pulp of extracted impacted wisdom teeth of healthy patients as previously described (Tirino et al., 2012). The dental pulps were enzymatically digested for 1 h at 37°C in a solution of collagenase (3 mg/mL; Life Technologies Europe B.V., Zug ZG, Switzerland) and dispase (4 mg/mL; Sigma-Aldrich Chemie GmbH, Buchs SG, Switzerland). A filtered single-cell suspension was plated in a 40 mm Petri dish with hDPSC growth medium containing DMEM/F12 (Sigma-Aldrich Chemie GmbH, Buchs SG, Switzerland) with 10% fetal bovine serum (FBS) (PAN Biotech GmbH, Aidenbach, Germany), 1% penicillin/streptomycin (P/S) (Sigma-Aldrich Chemie GmbH, Buchs SG, Switzerland), 1% L-glutamine (Sigma-Aldrich Chemie GmbH, Buchs SG, Switzerland), and 0.5 µg/ml fungizone (Life Technologies Europe B.V., Zug ZG, Switzerland) after washing away the enzyme solution. Healthy parts of gingiva were collected from biopsies. Gingival tissues were washed in phosphate buffered saline (PBS) (Life Technologies Europe B.V., Zug ZG, Switzerland), sectioned into small pieces and placed in 35 mm Petri dishes (TPP Techno Plastic Products AG, Trasadingen SH, Switzerland) for the outgrowth of human gingival fibroblasts (hGFs). The fibroblast growth medium is

composed by high glucose DMEM (Life Technologies Europe B.V., Zug ZG, Switzerland), 10% FBS, 1% P/S, and 1% HEPES (Sigma-Aldrich Chemie GmbH, Buchs SG, Switzerland). hDPSCs were cultured in DMEM/F12 (Sigma-Aldrich Chemie GmbH, Buchs SG, Switzerland) supplemented with 10% fetal bovine serum (FBS) (Biochrom AG, Berlin, Germany), 1% Penicillin/Streptamycin (P/S) (Sigma-Aldrich Chemie GmbH, Buchs SG, Switzerland), and 0.5 µg/mL fungizone (Thermo Fisher Scientific AG, Reinach BL, Switzerland). hGFs were expanded in DMEM high glucose (Thermo Fisher Scientific AG, Reinach BL, Switzerland) supplemented with 10% FBS, 1% P/S, and 1% HEPES (Thermo Fisher Scientific AG, Reinach BL, Switzerland). Cells were passaged at 80–90% confluence. All experiments were performed with cells from passages 4 and 5.

Scaffold Seeding

Sterile silk fibroin scaffolds were seeded with cells at a density of 0.5×10^6 per scaffold and then placed in a humidified incubator for 1 h at 37°C and 5% CO_2. The cells that were not attached to the scaffolds were washed away and then the seeded scaffolds were incubated for 1 week at 37°C before being placed on the CAM of fertilized chicken eggs. Empty scaffolds were used as controls (data not shown).

CAM Assay

No IACUC approval is necessary when performing experiments in chicken embryos until embryonic day 14 according to Swiss animal care guidelines (TSchV, Art. 112). Fertilized Lohman white LSL chicken eggs (Animalco AG, Staufen AG, Switzerland) were pre-incubated for 3 days at 38°C at a rotation speed of 360°/4 h (Bruja 3000, Brutmaschinen-Janeschitz GmbH, Hammelburg, Germany). On embryonic day 3 (ED 3) the eggs were processed for *in ovo* cultivation, which requires the opening of the shell with a drill (Dremel§, Conrad Electronic AG, Wollerau SZ, Switzerland). 2 mL of albumen was always removed with a syringe to increase the empty space under the top of the egg shell. The eggs were stabilized in 60 mm Petri dishes (Greiner Bio-One GmbH, Frickenhausen, Germany) and the created holes of the shells were covered with another 60 mm Petri dish that was fixed with a tape before the incubation of eggs at 37°C. On ED 7, empty and cell-seeded scaffolds were placed on the CAM (1-2/egg) in the middle of silicone rings that ensure a flat surface (**Figures 1A,B**) during their incubation period of 7 days.

In vivo Assessment of Perfusion Capacity Using MRI

Vascularization of the scaffolds by capillaries of the chicken embryo's CAM was studied on ED 14 using Magnetic Resonance Imaging (MRI) as previously described (Kivrak Pfiffner et al., 2015). The eggs were placed onto a custom-built sliding bed and enveloped by warm water tubing to maintain the temperature of the chicken embryo in a physiological range. To prevent motion, the chicken embryo was sedated with 5 drops of 1:100 M ketamine (Ketasol-100, Dr. E. Graeub AG, Bern BE, Switzerland) dripped onto the CAM surface. MRI was performed with a 4.7 T/16 cm Bruker PharmaScan small animal scanner (Bruker BioSpin MRI GmbH, Ettlingen, Germany) equipped with an actively decoupled two-coil system consisting of a 72 mm bird cage resonator for excitation and a 20 mm single loop surface coil for reception. Anatomical reference images were obtained in coronal, transversal, and sagittal slice orientations. T1-weighted MR images were acquired with a RARE sequence of variable TR and TE for quantitative T1 and T2 mapping. T1 maps were acquired in the samples before and after intravenous injection of 100 µL of 0.05 M Gd-DOTA MRI contrast agent (Dotarem®, Guerbet AG, Zuerich ZH, Switzerland). The time between Gd-DOTA injection and T1 mapping was kept constant at 25 min. T1 relaxation times were determined in three regions of interest: at the interface of the scaffold with the CAM (i.e., lower part), in the middle part of the scaffold, and finally at the surface of the scaffold (i.e., upper part). Perfusion capacity in these three regions was assessed through changes in the longitudinal relaxation rate $\Delta R1$ before and after injection of Gd-DOTA, as the relaxation rate changes with the amount of gadolinium present in the CAM.

Histological Analysis

The scaffold-CAM complex was fixed in 4% paraformaldehyde (PFA) at 4°C overnight. The cell-seeded constructs were excised from the CAM, embedded in paraffin (Haslab GmbH, Ostermundigen BE, Switzerland) and sectioned vertically in 5 µm thick sections. For histological evaluation, sections from the center of the scaffolds were stained with Hematoxylin and Eosin (H&E) (Mayer's hemalum solution, Merck KGaA, Darmstadt, Germany; Eosin Y, Sigma-Aldrich Chemie GmbH, Buchs SG, Switzerland). Pictures were taken using the Axio Scan.Z1 slidescanner (Carl Zeiss AG, Oberkochen, Germany), a Hitachi HV-F202FCL camera (Hitachi, Ltd., Tokyo, Japan), and the ZEN 2012 SP2 software (Carl Zeiss AG, Oberkochen, Deutschland) provided by the Center for Microscopy and Image analysis, University of Zurich.

Manual Vessel Analysis

The number of vessels and the percentage of vessels per scaffold area were determined by counting the number of vessels in longitudinal sections taken from the center of the scaffold (i.e., middle part). Each vessel was marked in black and ImageJ v1.48s (National Institutes of Health, USA) was used to analyze the number of marked vessels and their total area. Three sections of each sample (3 × hDPSCs, 3 × hGFs) were analyzed.

Statistics

For a comparison of the groups a one-way analysis of variance (ANOVA) was performed using GraphPad Prism v6.05 (GraphPad Software, Inc., La Jolla, CA, USA). A Bonferroni's multiple comparisons test was conducted to determine significant differences between the groups. Data were considered significant at $p < 0.05$ (*) and highly significant at $p < 0.01$ (**).

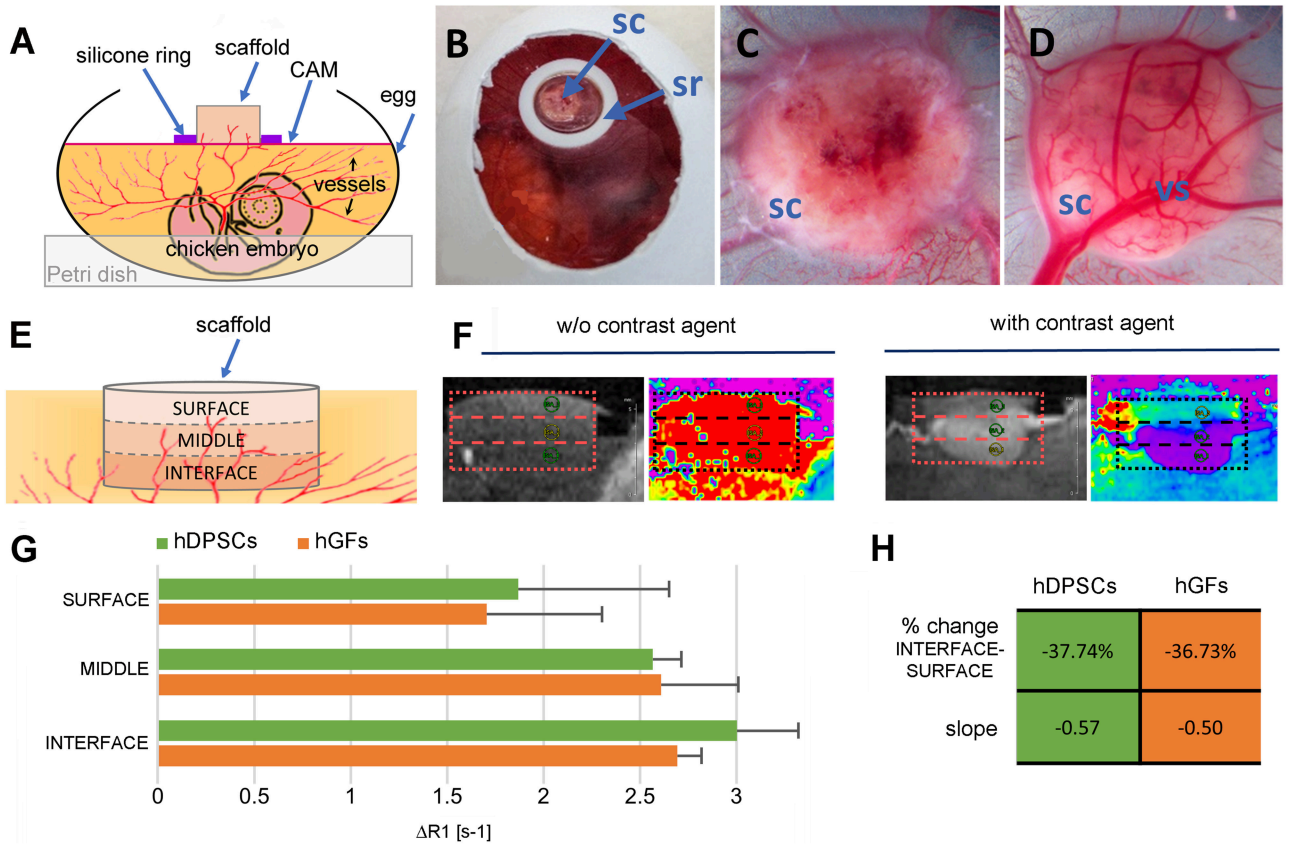

FIGURE 1 | Experimental setup and MRI analysis. (A,B) The scaffold is placed in the middle of a silicone ring on top of the CAM of a fertilized egg, which is stabilized in a Petri dish and incubated for 1 week. **(C)** Top and **(D)** bottom views of the scaffold after 1 week of incubation *in ovo*. **(E)** Scheme showing the analyzed parts of the samples. **(F)** Magnetic resonance image of the vascularized scaffold before and after the injection of the contrast agent Gd-DOTA. **(G)** Relaxation rate change ΔR1 in the interface, middle, and surface region of the scaffolds. Values are given as mean ± standard deviation. No statistically significant differences were found. **(H)** Percent change of the mean ΔR1 and slope of regression line between the interface and the surface layers within each group. CAM, chorioallantoic membrane; sc, scaffold; sr, silicone ring; vs, vessel; hDPSCs, human dental pulp stem cells; hGFs, human gingival fibroblasts.

RESULTS

Macroscopic Analysis

In growing vessels were visible on the surfaces of the hDPSC- and hGF-seeded silk fibroin scaffolds, both on the top (**Figure 1C**) and on the bottom (**Figure 1D**) of the samples after their CAM incubation for 1 week.

MRI Analysis

For a more precise analysis of the perfusion capacity of the samples, the scaffolds were divided into three equally sized regions, specified as "interface" (i.e., bottom of the scaffold touching the CAM), "middle," and "surface" (**Figure 1E**). Thereafter, their perfusion capacity was determined by calculating the change of R_1 relaxation rates (ΔR_1) measured by MRI before and after contrast enhancement by injected Gd-DOTA, a paramagnetic contrast agent (**Figure 1F**). The ΔR_1 values within the three regions of the scaffolds showed a gradual decrease of their perfusion capacity toward the surface region (**Figure 1G**). A comparison of the perfusion capacity between the hDPSC- and hGF-seeded silk fibroin scaffolds showed no significant differences of ΔR_1 within any of the three scaffold regions (**Figure 1G**). Both cell-seeded scaffolds showed only a percent change from interface to surface of approximately −37% (**Figure 1H**) resulting in much flatter slopes of −0.57 (hDPSCs) and −0.50 (hGFs) when compared to a slope of −1.33 observed in empty silk scaffolds (data not shown; Kivrak Pfiffner et al., 2015).

Histological and Manual Vessel Analysis

Qualitative and quantitative analyses of the vascularized scaffolds were performed using sections stained with Hematoxylin and Eosin (H&E). These histological sections showed large areas of tissue expansion (depicted by the blue dashed line) into the scaffold (depicted by the red dotted line) (**Figure 2A**). While in the samples seeded with hDPSCs the growing tissue filled approximately half of the scaffold areas (**Figure 2A1**), the tissue occupied roughly two-thirds of the scaffolds seeded with hGFs (**Figure 2A2**). CAM-derived blood vessels have penetrated both hDPSC- and hGF-seeded scaffolds (**Figures 2A3–6**). A manual analysis was performed in order to determine the number and

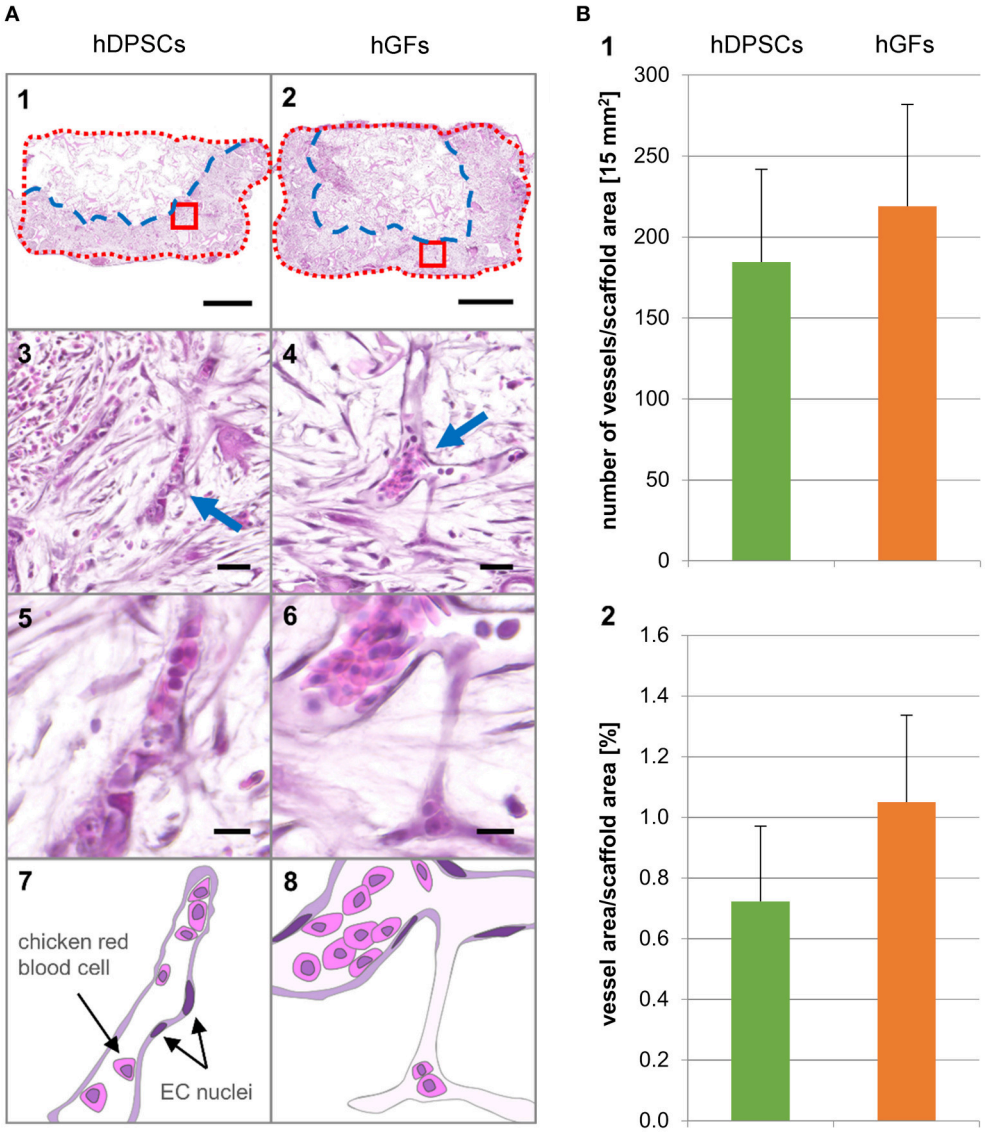

FIGURE 2 | Hematoxylin and Eosin stainings of longitudinal sections and histomorphometric analysis. ($A_{1,3,5,7}$) hDPSCs-seeded scaffolds. **($A_{2,4,6,8}$)** hGFs-seeded scaffolds. **($A_{1,2}$)** Scaffold section overview. Blue dashed line indicates the front line of the growing tissue. Red dotted line indicates the outline of the scaffold. Scale bar = 1 mm. **($A_{3,4}$)** Magnifications showing vascularization in the area marked with a red box in the corresponding overview picture. Arrows indicate capillaries. Scale bar = 25 μm. **($A_{5,6}$)** Magnifications showing single capillaries. Scale bar = 10 μm. **($A_{7,8}$)** Schematic representation of the capillaries shown in 5 and 6. **(B_1)** Number of vessels per scaffold area. **(B_2)** Percent vessel area per scaffold area. Values are given as mean ± standard deviation. No statistically significant differences were found. EC, endothelial cells; hDPSCs, human dental pulp stem cells; hGFs, human gingival fibroblasts.

the percent area occupied by the vessels within the three defined scaffold areas (**Figure 2B**). The corresponding graphs showed proportional values for scaffolds seeded with hDPSCs and hGFs. Although the average size of the counted vessels in both scaffolds was the same, a higher number of vessels was counted in hGFs-seeded scaffolds. This is due to the larger area occupied by the tissue in hGFs-seeded scaffolds when compared to the occupied tissue area in hDPSC-seeded scaffolds. The distribution of the vasculature along the horizontal axis of the scaffold was nearly homogeneous, whereas the vessel density decreased along the vertical axis following an interface-middle-surface gradient.

DISCUSSION

The use of biomaterials combined with stem cells aims at the successful healing and regeneration of injured or pathological tissues and organs (Stock and Vacanti, 2001; Griffith and Naughton, 2002). An essential prerequisite for effective tissue repair is the integration of the grafted material into the host tissue and its fast and effective vascularization, which ensures the constant supply of nutrients and oxygen, thus preventing necrosis of the newly formed tissue (Novosel et al., 2011). Therefore, it is essential and vital in stem cell-based

regenerative treatments to immediately attract blood vessels into the implanted cell-seeded scaffolds. Enhanced vascularization of the silk fibroin scaffolds has been achieved by integrating a mixture of endothelial cells with osteoblasts (Unger et al., 2010), but also by adding only one of these two cell populations (Unger et al., 2010; Ghanaati et al., 2011). Here we analyzed the capacity of human dental pulp stem cells (hDPSCs) and gingival fibroblasts (hGFs) seeded into silk fibroin scaffolds to attract vessels from the chicken embryo chorioallantoic membrane (CAM). Vascularization of the scaffolds was assessed with magnetic resonance imaging (MRI) and histomorphometric analyses demonstrating that both hDPSCs and hGFs have an equal capacity in attracting vessels within silk fibroin scaffolds. Small discrepancies between MRI and histomorphometric analysis data can be explained by the sample size that was evaluated: histomorphometry assesses only a part of the scaffold, whereas MRI measures the entire scaffold. The high perfusion capacity and the homogenous vessel distribution within hDPSC- or hGF-seeded silk fibroin scaffolds suggest an improved and faster regenerative outcome. The present results also indicate that a relatively long pre-incubation period (i.e., 1 week) of these cells is necessary for obtaining the homogeneous and abundant vascularization of the entire scaffold that favors its integration into the host tissue. Indeed, our previous studies based exclusively on MRI measurements have shown that a shorter pre-incubation period (i.e., 1 day) of hDPSCs is not leading to such a uniform distribution of vessels within silk scaffolds (Kivrak Pfiffner et al., 2015). Comparison between hDPSCs and hGFs seeded scaffolds did not result in obvious differences concerning the attraction of vessels. Similarly to the hDPSCs, hGFs are derived from cranial neural crest cells that possess stem cell properties (Xu et al., 2013; Chiquet et al., 2015; Mitsiadis et al., 2015) and exhibit a higher regenerative potential when compared to fibroblasts of non-oral origin (Eslami et al., 2009) that may explain the similarities observed in vessel attraction into the scaffolds by hDPSCs and hGFs. Previous studies based on gene expression analysis have compared the angiogenic properties of hDPSCs and hGFs and suggested that hDPSCs possess a stronger angiogenic potential (Hilkens et al., 2014). However, studies realized on the CAM have shown that the number of vessels growing into hDPSC- and hGF-containing Matrigel™ droplets was not variable (Hilkens et al., 2014). Vascular ingrowths have been observed into cell-free silk scaffolds after subcutaneous transplantation in mice, but these structures were mainly localized on the scaffold surface (Unger et al., 2010; Ghanaati et al., 2011).

Taken together the present findings clearly demonstrate that hDPSCs and hGFs possess equal capabilities in attracting vessels within silk fibroin scaffolds. Furthermore, these results show that the prolonged pre-incubation period of these two cell populations before their implantation, favors the homogeneous distribution of vessels within silk fibroin scaffolds, a process that guarantees successful tissue regeneration.

AUTHOR CONTRIBUTIONS

AW: experimental design, performance of experiments, writing of the manuscript, editing, discussing; JB: experimental design, MRI-measurements and analysis, writing of the manuscript, editing, discussing; CW: MRI-measurements and analysis, writing of the manuscript, editing, discussing; BS: experimental design, writing of the manuscript, editing, discussing; TM: experimental design, writing of the manuscript, editing, discussing.

FUNDING

This work was supported by the Swiss National Foundation (SNSF) grant 31003A_135633 (TM, AW), by institutional funds from University of Zurich (TM) and by the Matching Funds from the University of Zurich (JB, CW).

ACKNOWLEDGMENTS

The authors thank KD Dr. Michael Locher, Dr. Katharina Filo, and Dr. Philipp Sahrmann of the Clinic for Dental Medicine for providing teeth and gingival tissue, Dr. Yinghua Tian for the injection of the contrast agent. We are thankful to Prof. Ralph Müller, Prof. Sandra Hofmann, and Dr. Jolanda Baumgartner (Institute of Biomechanics, ETH Zurich) for manufacturing the silk scaffolds and Trudel Silk Inc. (Zurich, Switzerland) is highly acknowledged for providing silk fibroin. This work was supported by the Swiss National Foundation (SNSF) grant 31003A_135633 (TM, AW), by institutional funds from University of Zurich (TM), and by the Matching Funds from the University of Zurich (JB, CW). All authors contributed to the planning, writing, critical reading, and editing of the present manuscript. The authors confirm that there are no conflicts of interest associated with this work. Imaging was performed with equipment maintained by the Center for Microscopy and Image Analysis, University of Zurich.

REFERENCES

Altman, G. H., Diaz, F., Jakuba, C., Calabro, T., Horan, R. L., Chen, J. S., et al. (2003). Silk-based biomaterials. *Biomaterials* 24, 401–416. doi: 10.1016/S0142-9612(02)00353-8

Bluteau, G., Luder, H. U., De Bari, C., and Mitsiadis, T. A. (2008). Stem cells for tooth engineering. *Eur. Cells Mater.* 16, 1–9. doi: 10.5167/uzh-6570

Chiquet, M., Katsaros, C., and Kletsas, D. (2015). Multiple functions of gingival and mucoperiosteal fibroblasts in oral wound healing and repair. *Periodontology 2000* 68, 21–40. doi: 10.1111/prd.12076

Eslami, A., Gallant-Behm, C. L., Hart, D. A., Wiebe, C., Honardoust, D., Gardner, H., et al. (2009). Expression of integrin avb6 and TGF-Beta in scarless vs scar-forming wound healing. *J. Histochem. Cytochem.* 57, 543–557. doi: 10.1369/jhc.2009.952572

Ghanaati, S., Unger, R. E., Webber, M. J., Barbeck, M., Orth, C., Kirkpatrick, J. A., et al. (2011). Scaffold vascularization *in vivo* driven by primary human osteoblasts in concert with host inflammatory cells. *Biomaterials* 32, 8150–8160. doi: 10.1016/j.biomaterials.2011.07.041

Giannicola, G., Ferrari, E., Citro, G., Sacchetti, B., Corsi, A., Riminucci, M., et al. (2010). Graft vascularization is a critical rate-limiting step in skeletal stem

cell-mediated posterolateral spinal fusion. *J. Tissue Eng. Regen. Med.* 4, 273–283. doi: 10.1002/term.238

Giuliani, A., Manescu, A., Langer, M., Rustichelli, F., Desiderio, V., Paino, F., et al. (2013). Three graft vascularization is a critical rate-limiting step in skeletal stem cell-mediated posterolateral spinal fusion. *Stem Cells Transl. Med.* 2, 316–324. doi: 10.5966/sctm.2012-0136

Griffith, L. G., and Naughton, G. (2002). Tissue engineering-current challenges and expanding opportunities. *Science* 295, 1009–1014. doi: 10.1126/science.1069210

Gronthos, S., Mankani, M., Brahim, J., Robey, P. G., and Shi, S. (2000). Postnatal human dental pulp stem cells (DPSCs) *in vitro* and *in vivo*. *Proc. Natl. Acad. Sci. U.S.A.* 97, 13625–13630. doi: 10.1073/pnas.240309797

Hilkens, P., Fanton, Y., Martens, W., Gervois, P., Struys, T., Politis, I., et al. (2014). Pro-angiogenic impact of dental stem cells *in vitro* and *in vivo*. *Stem Cell Res.* 12, 778–790. doi: 10.1016/j.scr.2014.03.008

Hofmann, S., Hagenmüller, H., Koch, A. M., Müller, R., Vunjak-Novakovic, G., Kaplan, D. L., et al. (2007). Control of *in vitro* tissue-engineered bone-like structures using human mesenchymal stem cells and porous silk scaffolds. *Biomaterials* 28, 1152–1162. doi: 10.1016/j.biomaterials.2006.10.019

Huang, G. T., Gronthos, S., and Shi, S. (2009). Mesenchymal stem cells derived from dental tissues vs. those from other sources: their biology and role in regenerative medicine. *J. Dent. Res.* 88, 792–806. doi: 10.1177/0022034509340867

Kivrak Pfiffner, F., Waschkies, C., Tian, Y., Woloszyk, A., Calcagni, M., Giovanoli, P., et al. (2015). A new *in vivo* magnetic resonance imaging method to noninvasively monitor and quantify the perfusion capacity of three-dimensional biomaterials grown on the chorioallantoic membrane of chick embryos. *Tissue Eng. Part C Methods* 2, 339–346. doi: 10.1089/ten.TEC.2014.0212

Koob, S., Torio-Padron, N., Stark, G. B., Hannig, C., Stankovic, Z., and Finkenzeller, G. (2011). Bone formation and neovascularization mediated by mesenchymal stem cells and endothelial cells in critical-sized calvarial defects. *Tissue Eng. A* 17, 311–321. doi: 10.1089/ten.tea.2010.0338

Kundu, B., Rajkhowa, R., Kundu, S. C., and Wang, X. (2013). Silk fibroin biomaterials for tissue regenerations. *Adv. Drug Deliv. Rev.* 65, 457–470. doi: 10.1016/j.addr.2012.09.043.

Lee, I.-K., Lee, M.-J., and Jang, H. S. (2013). The interrelationship between human gingival fibroblast differentiation and cultivating time. *Tissue Eng. Regener. Med.* 10, 60–64. doi: 10.1007/s13770-013-0371-y

Lloyd-Griffith, C., McFadden, T. M., Duffy, G. P., Unger, R. E., Kirkpatrick, C. J., and O'Brien, F. J. (2015). The pre-vascularisation of a collagen-chondroitin sulphate scaffold using human amniotic fluid-derived stem cells to enhance and stabilise endothelial cell-mediated vessel formation. *Acta Biomater.* 26, 263–273. doi: 10.1016/j.actbio.2015.08.030.

Mitsiadis, T. A., Orsini, G., and Jimenez-Rojo, L. (2015). Stem cell-based approaches in dentistry. *Eur. Cells Mater.* 30, 248–257.

Nazarov, R., Jin, H. J., and Kaplan, D. L. (2004). Porous 3-D scaffolds from regenerated silk fibroin. *Biomacromolecules* 5, 718–726. doi: 10.1021/bm034327e

Novosel, E. C., Kleinhans, C., and Kluger, P. J. (2011). Vascularization is the key challenge in tissue engineering. *Adv. Drug Deliv. Rev.* 63, 300–311. doi: 10.1016/j.addr.2011.03.004

Plock, J. A., Schnider, J. T., Zhang, W., Schweizer, R., Tsuji, W., Kostereva, N., et al. (2015). Adipose- and bone marrow–derived mesenchymal stem cells prolong graft survival in vascularized composite allotransplantation. *Transplantation* 99, 1765–1773. doi: 10.1097/TP.0000000000000731

d'Aquino, R., De Rosa, A., Laino, G., Caruso, F., Guida, L., Rullo, R., et al. (2009). Human dental pulp stem cells: from biology to clinical applications. *J. Exp. Zool. B Mol. Dev. Evol.* 312, 408–415. doi: 10.1002/jez.b.21263.

d'Aquino, R., Graziano, A., Sampaolesi, M., Laino, G., Pirozzi, G., De Rosa, A., et al. (2007). Human postnatal dental pulp cells co-differentiate into osteoblasts and endotheliocytes: a pivotal synergy leading to adult bone tissue formation. *Cell Death Differ.* 14, 1162–1171. doi: 10.1038/sj.cdd.4402121

Shi, S., Robey, P. G., and Gronthos, S. (2001). Comparison of human dental pulp and bone marrow stromal stem cells by cDNA microarray analysis. *Bone* 29, 532–539. doi: 10.1016/S8756-3282(01)00612-3

Sofia, S., McCarthy, M. B., Gronowicz, G., and Kaplan, D. L. (2001). Functionalized silk-based biomaterials for bone formation. *J. Biomed. Mater. Res.* 54, 139–148.doi: 10.1002/1097-4636(200101)54:1<139::AID-JBM17>3.0.CO;2-7

Stock, U. A., and Vacanti, J. P. (2001). Tissue engineering: current state and prospects. *Annu. Rev. Med.* 52, 443–451. doi: 10.1146/annurev.med.52.1.443

Tirino, V., Paino, F., De Rosa, A., and Papaccio, G. (2012). Identification, isolation, characterization, and banking of human dental pulp stem cells. *Methods Mol. Biol.* 879, 443–463. doi: 10.1007/978-1-61779-815-3_26

Unger, R. E., Ghanaati, S., Orth, C., Sartoris, A., Barbeck, M., Halstenberg, S., et al. (2010). The rapid anastomosis between prevascularized networks on silk fibroin scaffolds generated *in vitro* with cocultures of human microvascular endothelial and osteoblast cells and the host vasculature. *Biomaterials* 31, 6959–6967. doi: 10.1016/j.biomaterials.2010.05.057

Woloszyk, A., Holsten Dircksen, S., Bostanci, N., Müller, R., Hofmann, S., and Mitsiadis, T. A. (2014). Influence of the mechanical environment on the engineering of mineralised tissues using human dental pulp stem cells and silk fibroin scaffolds. *PLoS ONE* 9:e111010. doi: 10.1371/journal.pone.0111010

Xu, X., Chen, C., Akiyama, K., Chai, Y., Le, A. D., Wang, Z., et al. (2013). Gingivae contain neural-crest- and mesoderm-derived mesenchymal stem cells. *J. Dent. Res.* 92, 825–832. doi: 10.1177/0022034513497961

Zhang, W., Walboomers, X. F., Shi, S., Fan, M., and Jansen, J. A. (2006). Multilineage differentiation potential of stem cells derived from human dental pulp after cryopreservation. *Tissue Eng.* 12, 2813–2823. doi: 10.1089/ten.2006.12.2813

Conflict of Interest Statement: The authors declare that the research was conducted in the absence of any commercial or financial relationships that could be construed as a potential conflict of interest.

14.1.7 Woloszyk et al., Front Physiol, 2016

Three-dimensional imaging of the developing vasculature within stem cell-seeded scaffolds cultured in ovo (METHODS ARTICLE)

In this paper we present our protocol, which we had established for the perfusion of vascularized 3D biomaterials when cultured on the chorioallantoic membrane (CAM) of developing chicken embryos followed by microcomputed tomography (microCT) imaging of the vasculature.

Previous publications had described a similar procedure for 3D biomaterials implanted in mammals (e.g. mice and rats). However, no protocol was available for 3D biomaterials incubated on the CAM of fertilized chicken eggs, which can be used to study the ingrowth and distribution of vessels into 3D scaffolds. In order to visualize the vascular network with microCT, a perfusion of the vascular system with a radiopaque compound was required. My literature research for an injectable radiopaque material suggested the use of MicroFil®, which cures once the samples are placed at 4°C overnight.

While preparing the manuscript I was responsible for the compilation of the figures and contributed to the writing and literature research. I provided a step-by-step protocol describing the seeding of 3D silk scaffolds with human dental pulp stem cells and their pre-culture *in vitro*, the *in ovo* culture conditions for the CAM assay, as well as the procedure for the MicroFil® perfusion, and microCT scanning. The optimization of this procedure included the fixation of the needle in the vessels of the CAM for successful perfusion, the adaptation of the proportions of the MicroFil® color and diluent for optimal filling of the vasculature, and the preparation of the samples for microCT scanning. The presented visualization method shows that a technique, which is commonly used in *in vivo* experiments performed in rodents, can also be applied in the cost-effective and easy to perform CAM assay. Therefore, it offers an additional analytical technique for the well-established *in ovo* angiogenesis assay, providing an easy but important tool for implant screening before *in vivo* testing, which helps to reduce the amount of animals needed for pre-clinical studies.

frontiers in Physiology

METHODS
published: 21 April 2016
doi: 10.3389/fphys.2016.00146

Three-Dimensional Imaging of the Developing Vasculature within Stem Cell-Seeded Scaffolds Cultured *in ovo*

Anna Woloszyk[1], *Davide Liccardo*[2] *and Thimios A. Mitsiadis*[1]*

[1] Orofacial Development and Regeneration, Centre for Dental Medicine, Institute of Oral Biology, University of Zurich, Zurich, Switzerland, [2] Section of Biotechnology and Medical Histology and Embryology, Department of Experimental Medicine, Second University of Naples, Naples, Italy

Successful tissue engineering requires functional vascularization of the three-dimensional constructs with the aim to serve as implants for tissue replacement and regeneration. The survival of the implant is only possible if the supply of oxygen and nutrients by developing capillaries from the host is established. The chorioallantoic membrane (CAM) assay is a valuable tool to study the ingrowth and distribution of vessels into scaffolds composed by appropriate biomaterials and stem cell populations that are used in cell-based regenerative approaches. The developing vasculature of chicken embryos within cell-seeded scaffolds can be visualized with microcomputed tomography after intravenous injection of MicroFil®, which is a radiopaque contrast agent. Here, we provide a step-by-step protocol for the seeding of stem cells into silk fibroin scaffolds, the CAM culture conditions, the procedure of MicroFil® perfusion, and finally the microcomputed tomography scanning. Three-dimensional imaging of the vascularized tissue engineered constructs provides an important analytical tool for studying the potential of cell seeded scaffolds to attract vessels and form vascular networks, as well as for analyzing the number, density, length, branching, and diameter of vessels. This *in ovo* method can greatly help to screen implants that will be used for tissue regeneration purposes before their *in vivo* testing, thereby reducing the amount of animals needed for pre-clinical studies.

Keywords: chorioallantoic membrane (CAM), vascularization, stem cells, biomaterials, 3D imaging, MicroFil®, microcomputed tomography, regenerative medicine

OPEN ACCESS

Edited by:
Sachiko Iseki,
Tokyo Medical and Dental University, Japan

Reviewed by:
Natalina Quarto,
Università di Napoli Federico II, Italy
Francesco De Francesco,
Second University of Naples, Italy

***Correspondence:**
Thimios A. Mitsiadis
thimios.mitsiadis@zzm.uzh.ch

Specialty section:
This article was submitted to Craniofacial Biology, a section of the journal Frontiers in Physiology

Received: *23 February 2016*
Accepted: *04 April 2016*
Published: *21 April 2016*

Citation:
Woloszyk A, Liccardo D and Mitsiadis TA (2016) Three-Dimensional Imaging of the Developing Vasculature within Stem Cell-Seeded Scaffolds Cultured in ovo. Front. Physiol. 7:146. doi: 10.3389/fphys.2016.00146

INTRODUCTION

The formation of new networks of blood vessels (i.e., angiogenesis) is essential in embryonic development, tissue homeostasis, pathology, and regeneration. Hematopoietic cells circulating within the vasculature supply the surrounding tissues with oxygen and nutrients, transport hormones, remove waste products, and CO_2, and protect the body from infections (Carmeliet and Jain, 2011). Successful engineering of tissue substitutes and transplantable organs depends on their rapid and adequate angiogenesis, since the appropriate supply of oxygen and nutrients is crucial for their long-term survival (Mitsiadis and Harada, 2015; Mitsiadis et al., 2015). A dense network of capillaries is formed in most tissues of the body that regulates the diffusion limit of

oxygen (Carmeliet and Jain, 2000; Novosel et al., 2011). Spontaneous vascular ingrowth from the host tissue to the transplanted devices (e.g., empty biodegradable implants) is very slow and limited to several tenths of micrometers per day (Rouwkema et al., 2008). Therefore, the improvement and acceleration of implant vascularization remains a key challenge in regenerative medicine.

Classical *in vivo* angiogenesis assays rely on small (e.g., mice, rats) and large (e.g., sheep, goats) animal models, where engineered constructs are most commonly implanted subcutaneously at their dorsal part (Staton et al., 2009; Jungraithmayr et al., 2013; Wang et al., 2015). However, these surgical procedures are time-consuming and often associated with high costs and repetitive animal sacrifice. The chorioallantoic membrane (CAM) is highly vascularized and serves as a transient gas exchange surface during the incubation period, similar to the lung (Romanoff, 1960). Originally, the CAM assay was used in order to study the developmental potential of embryonic tissue grafts (Rücker et al., 2006). As chicken embryos become immunocompetent only by day 18 of their development (Janković et al., 1975), various biological processes where vascularization plays a role can be studied without inducing an immune response, including insufficient vascularization (e.g., ischemic disorders) or excessive vessel formation (e.g., cancer), with the goal to either enhance or decrease vessel growth, respectively (Ribatti, 2014).

To visualize the three-dimensional (3D) development of the vasculature within implants cultured on the CAM, perfusion of the chicken embryos was performed with the radiopaque contrast agent MicroFil® followed by microcomputed tomography (microCT) of the implants. We demonstrate that this technique, which is commonly used in *in vivo* experiments performed in rodents (Bolland et al., 2008; Schmidt et al., 2009; Stoppato et al., 2013), can also successfully be applied in the CAM assay.

MATERIALS AND METHODS

Seeding of Human Dental Pulp Stem Cells

a. Defrost cryopreserved human dental pulp stem cells and culture in Dulbecco's Modified Eagle Medium: Nutrient Mixture F-12 (DMEM/F12) + 10% fetal bovine serum + 1% penicillin/streptamycin + 0.5 μg/mL fungizone in a humidified incubator at 37°C and 5% CO_2. Change the medium every 3–4 days.
b. At 80–90% confluency, trypsinize the cells, use a 70 μm strainer to obtain a single-cell suspension, centrifuge (1500 rpm, 5 min, RT), and resuspend the cell pellet at a concentration of 1×10^6 cells/50 μL.
c. Place the sterile cylindrical scaffold (silk fibroin, 5 mm diameter, 3 mm height) on a sterile filter paper to absorb any residual liquid and move the scaffold into the well of a 96-well-plate.
d. Seed the scaffold by pipetting 50 μL of the cell suspension on top of the scaffold, turn the scaffold, take up the cell suspension from the bottom of the well, and release it again on top of the scaffold.
e. For cell attachment, place the cell-seeded scaffolds in a humidified incubator for 1 h at 37°C and 5% CO_2. Wash the scaffold before placing it in a clean well of a 24-well-plate and adding 1 mL of medium. Culture for desired period of time and change medium every 3–4 days.

The procedure for anonymized cell collection was approved by the Kantonale Ethikkommission of Zurich and performed with written patients' consent.

Preparation of the Chicken Eggs for the CAM Assay and Placing of the Cell-Seeded Samples

a. Pre-incubate fertilized Lohman white LSL (Lohman Selected Leghorn) chicken eggs in an egg incubator for 3 days at 38°C at a rotation speed of 360°/4 h.
b. On embryonic day 3 (ED 3), stop the rotation in the morning and let the eggs rest in this position for 3 h to ensure that the embryo is on the top.
c. Mark the top of the egg with a pencil and carefully wipe the egg-shell with 70% ethanol without turning it.
d. Inside a clean bench, place the egg in a 60 mm Petri dish on top of a piece of tape to stabilize the egg.
e. Make a small hole in the shell with the tip of sterile pointy scissors and remove 4 mL of albumen using a syringe and a needle to lower the developing embryo.
f. Put Scotch™ tape on the area where you want to make the window.
g. Make another small hole, insert the scissors carefully and start cutting an oval hole while turning the egg with the other hand.
h. Remove the shell and cover the opening with a second 60 mm Petri dish, which needs to be fixed to the bottom lid with tape, and incubate in a humidified incubator at 37°C and 0% CO_2.
i. On ED 7, the cell-seeded scaffolds can be placed on the vascularized CAM. Remove the Petri dish lid, place a silicone ring (taken from sterile cryovials) on the CAM to ensure a flat surface, and position the sample in the middle of this ring.
j. Incubate for 7 days until ED 14 in a humidified incubator at 37°C and 0% CO_2.

Microfil® Perfusion and Microct Imaging

a. On ED 14, the chicken embryos are perfused with a mix of the MicroFil® components. Dilute the silicone rubber injection compound (yellow) 10-fold in MV-Diluent and add 10% (by weight) MV-Curing Agent right before use. Working time is at least 20 min and starts with the addition of curing agent.
b. Fill the MicroFil® mix into a 5 mL syringe and attach a three-way valve (Discofix® C) with a 10 cm tube for more flexibility between the 30G ½" needle and the syringe.
c. Using a stereoscope, fix a branch of the vitelline vasculature matching the diameter of the needle with blunt end tweezers and carefully insert the needle into the vessel. Apply a small drop of superglue where the needle enters the vasculature (**Figure 1**).
d. Inject the MicroFil® mix carefully into the vasculature until the pressure increases.

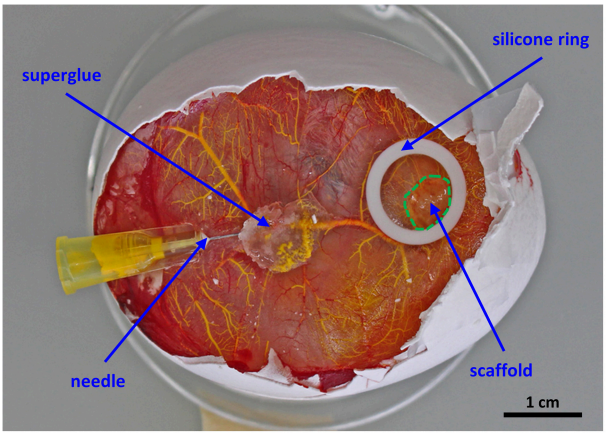

FIGURE 1 | Setup for the perfusion of the chorioallantoic membrane vasculature. The scaffold is placed in the middle of a silicone ring and cultured for 7 days *in ovo*. For proper perfusion a 30G ½" needle is fixed with a drop of superglue before MicroFil® (yellow) injection.

e. If filling of the vasculature is not sufficient, inject MicroFil® a second time into a non-perfused vessel. Remove the tube from the needle, which remains in the CAM, and attach a fresh needle to the tube. Repeat steps **c** and **d**.
f. Place the perfused chicken embryo overnight at 4°C for complete curing of the MicroFil®.
g. On the next day, remove the perfused scaffold samples from the CAM using scissors, wash in PBS, fix in 4% paraformaldehyde, wash in PBS, and place in 70% ethanol until microCT imaging.
h. Perform microCT scanning at an isotropic resolution of 20 µm, an energy level of 70 kVp, an intensity of 114 µA, and 300 ms integration time.

According to Swiss animal care guidelines experiments performed in chicken embryos until ED 14 do not need ethical approval (TSchV, Art. 112).

RESULTS

We have used the CAM assay to study the vascularization of a 3D biomaterial when placed in a highly vascularized environment. The perfusion of the vascular system was performed without pre-perfusion with phosphate buffered saline, as the blood was forced out by the injected MicroFil®. The initial perfusion efficiency with MicroFil® diluted according to the manufacturer's recommendation was improved by using a higher dilution of the silicone rubber injection compound, which required an increased amount of the MV-Curing Agent of 10% instead of 5% (by weight). If the perfusion was not complete after one injection, a second injection site was chosen to fill non-perfused areas (**Figures 2A,B**). Immunohistological stainings can still be performed on sections of paraffin-embedded samples after perfusion and microCT analysis (**Figure 2C**).

The microCT scan showed the MicroFil® perfused 3D vascular structure growing into the scaffold (red area in

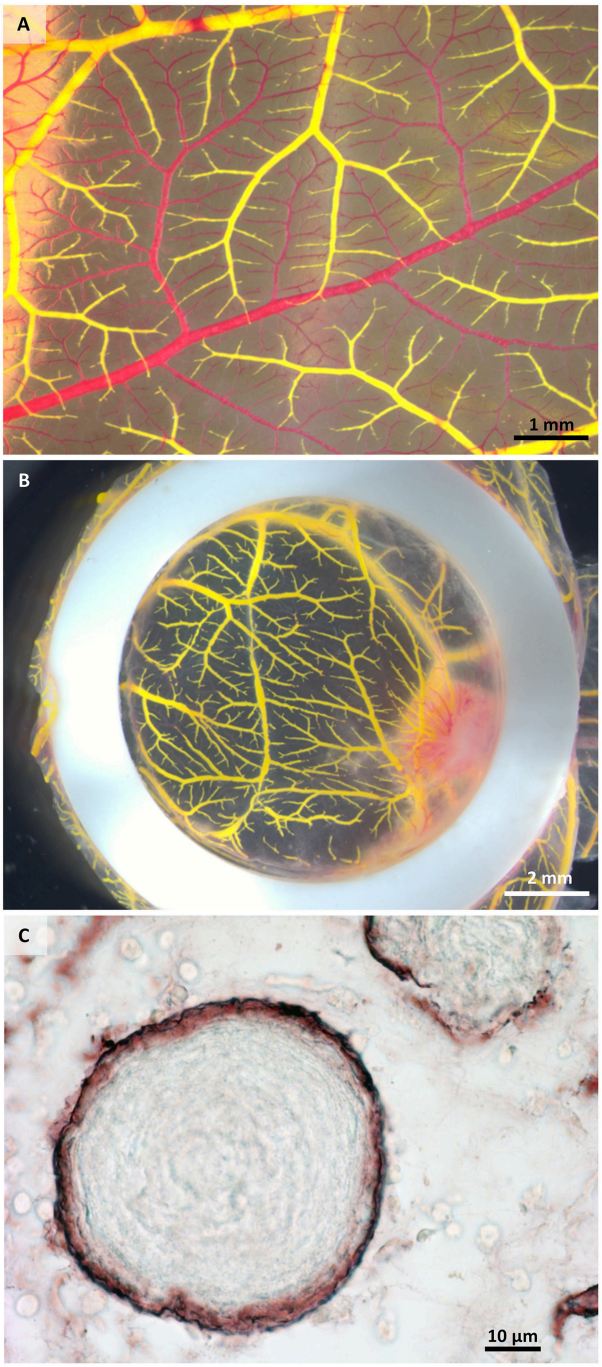

FIGURE 2 | Macroscopical and microscopical view of perfused samples. (A) Perfused (yellow) and non-perfused (red) vessels after one injection showing incomplete perfusion. **(B)** Exemplary sample after two injections of MicroFil®. **(C)** Histological section of a perfused sample showing vessels (brown) containing MicroFil®.

Figure 2B) from the bottom and from the sides within 7 days of *in ovo* culture. While the macroscopical image of the same sample *in ovo* (**Figure 3A**) provides only the information about the vascularization visible on the surface of the CAM, the microCT

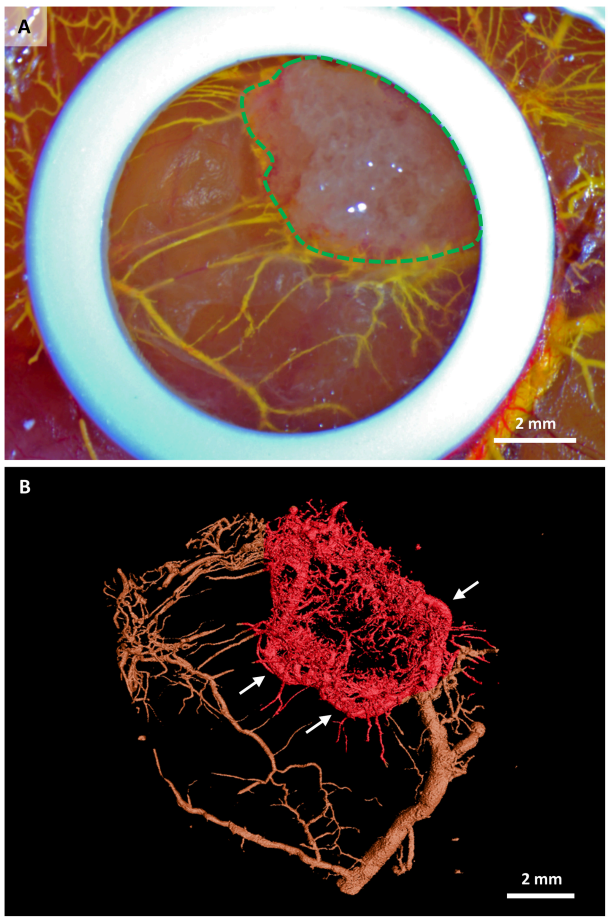

FIGURE 3 | Stem cell-seeded scaffolds perfused with MicroFil® after their *in ovo* culture. (A) Macroscopic view of a scaffold (green dashed line) immediately after perfusion with yellow MicroFil®. The silicone ring is seen in white, vasculature in yellow. **(B)** Microcomputed tomography image of the vascular cast within the scaffold (red color). Vasculature outside the scaffold area is marked in brown. New capillaries are sprouting from one large vessel that encircles the scaffold (white arrows).

image visualizes the whole vascular network. Interestingly, new capillaries are sprouting from one large vessel that encircles the scaffold, (**Figure 3B**, white arrows). The generated microCT data can be further used for complete morphometric characterization of the vascular network, including the number, length, branching, and diameter of vessels.

DISCUSSION

The generation of vascularized tissues and organs remains one of the key challenges in regenerative medicine (Novosel et al., 2011; Mitsiadis et al., 2012; Dew et al., 2015). Visualization of angiogenesis within implanted engineered devices aiming at tissue replacement and/or regeneration is pivotal for predicting and understanding the outcome of new regenerative approaches before their application in clinics.

Several techniques have been extensively used to study the vascular architecture of the whole body, as well as the microvasculature of specific organs and tissues in both health and disease. The development of new visualization methods using microcomputed tomography (microCT) improved our knowledge on specific tissue anatomy, physiology, and pathology tremendously. Further, developments using perfusion of tissues and organs before microCT scanning allowed additional analyses at the histological level and generated a plethora of volumetric and quantitative data (Garcia-Sanz et al., 1998). Therefore, the combination of vascular perfusion with microCT imaging and analysis has been applied in many fields, including embryonic vascular development (Anderson-Berry et al., 2005), cancer research (Xuan et al., 2007), cardiac disease models (Sangaralingham et al., 2012), and tissue engineering (Bolland et al., 2008; Stoppato et al., 2013). For example, the combination of MicroFil® perfusion with microCT imaging has been used to study angiogenesis in tissue engineered constructs implanted subcutaneously into immunosuppressed mice. Both natural allografts and osteosynthetic [poly (D,L)-lactic acid; PDLLA] grafts seeded with human bone marrow stromal cells (BMSCs) have been used for this study. The presence of BMSCs was able to increase the number of vessels within the implants (Bolland et al., 2008). Similarly, MicroFil® perfusion and microCT scanning have been performed in VEGF-treated porous polyurethane scaffolds implanted subcutaneously into rats (Schmidt et al., 2009). A more recent study using MicroFil® perfusion and microCT scanning has demonstrated that silk fibroin fibers combined with a PDLLA salt-leached sponge promoted vascularization when implanted subcutaneously into rats (Stoppato et al., 2013).

However, all these previous studies are based on rodents and therefore necessitate extensive animal care-taking, ethical approvals, as well as surgical skills and equipment. Moreover, a minimum of 10 days incubation time is needed in order to analyze implant vasculature. In contrast, the CAM assay is a simple, cost-effective, and highly reproducible method, which does not require ethical approval when performing experiments in chicken embryos until embryonic day 14 (Swiss animal care guidelines, TSchV, Art. 112). Even though the incubation time on the CAM is limited to a period of 7 days, it constitutes an excellent screening method to study the early phase of angiogenesis within implanted scaffolds. Following the "3Rs" principles of replacement, refinement, and reduction of animal use in research, the CAM assay combined with MicroFil® perfusion and microCT analysis as described in this protocol provides a valuable intermediate platform for initial assessments prior to pre-clinical studies in mammals.

This technique could be applied for the direct comparison of scaffolds (ceramics, synthetic polymers, and natural polymers) seeded with stem cell populations of different origins [e.g., adipose-derived stem cells (ASCs), bone marrow stem cells (BMSCs), DPSCs, periodontal ligament stem cells]. For example, it has been shown that BMSCs possess angiogenic potential (Oswald et al., 2004), but little is known about their capability to attract vessels in engineered structures. In contrast, ASCs have been demonstrated to promote the neovascularization when seeded in different scaffolds (De Francesco et al., 2009; Chan et al., 2016; Guo et al., 2016). In conclusion, the present method

can constitute a valuable tool for studying in detail cell-mediated vascularization efficiency.

AUTHOR CONTRIBUTIONS

AW: experimental design, performance of experiments, writing of the manuscript, editing, discussing. DL: experimental design, writing of the manuscript, editing, discussing. TM: experimental design, writing of the manuscript, editing, discussing.

FUNDING

This work was supported by the Swiss National Foundation (SNSF) grant 31003A_135633 (TM, AW), by institutional funds from University of Zurich (TM) and by funds from the Second University of Naples (SUN;DL).

ACKNOWLEDGMENTS

The authors thank Dr. Bernd Stadlinger and Dr. Philipp Sahrmann of the Clinic for Dental Medicine for providing teeth for dental pulp stem cell extraction. Furthermore, Trudel Silk Inc. (Zurich, Switzerland) is highly acknowledged for providing silk fibroin and the Institute of Biomechanics, ETH for manufacturing the scaffolds. Further, we thank Dr. Johanna Buschmann for technical advice and valuable discussions.

REFERENCES

Anderson-Berry, A., O'Brien, E. A., Bleyl, S. B., Lawson, A., Gundersen, N., Ryssman, D., et al. (2005). Vasculogenesis drives pulmonary vascular growth in the developing chick embryo. *Dev. Dyn.* 233, 145–153. doi: 10.1002/dvdy.20296

Bolland, B. J., Kanczler, J. M., Dunlop, D. G., and Oreffo, R. O. (2008). Development of *in vivo* μCT evaluation of neovascularisation in tissue engineered bone Constructs. *Biomaterials* 43, 195–202. doi: 10.1016/j.bone.2008.02.013

Carmeliet, P., and Jain, R. K. (2000). Angiogenesis in cancer and other diseases. *Nature* 407, 249–257. doi: 10.1038/35025220

Carmeliet, P., and Jain, R. K. (2011). Molecular mechanisms and clinical applications of angiogenesis. *Nature* 473, 298–307. doi: 10.1038/nature10144

Chan, E. C., Kuo, S. M., Kong, A. M., Morrison, W. A., Dusting, G. J., Mitchell, G. M., et al. (2016). Three dimensional collagen scaffold promotes intrinsic vascularisation for tissue engineering applications. *PLoS ONE* 11:e0149799. doi: 10.1371/journal.pone.0149799

De Francesco, F., Tirino, V., Desiderio, V., Ferraro, G., D'Andrea, F., Giuliano, M., et al. (2009). Human CD34+/CD90+ ASCs are capable of growing as sphere clusters, producing high levels of vegf and forming capillaries. *PLoS ONE* 4:e6537. doi: 10.1371/journal.pone.0006537

Dew, L., MacNeil, S., and Chong, C. K. (2015). Vascularization strategies for tissue engineers. *Regen. Med.* 10, 211–224. doi: 10.2217/rme.14.83

Garcia-Sanz, A., Rodriguez-Barbero, A., Bentley, M. D., Ritman, E. L., and Romero, J. C. (1998). Three-dimensional microcomputed tomography of renal vasculature in rats. *Hypertension* 31, 440–444. doi: 10.1161/01.HYP.31.1.440

Guo, L. Z., Kim, T. H., Han, S., and Kim, S. W. (2016). Angio-vasculogenic properties of endothelial-induced mesenchymal stem cells derived from human adipose tissue. *Circ. J.* 80, 998–1007. doi: 10.1253/circj.CJ-15-1169

Janković, B. D., Isaković, K., Lukić, M. L., Vujanović, N. L., Petrović, S., and Marković, B. M. (1975). Immunological capacity of the chicken embryo. I. Relationship between the maturation of lymphoid tissues and the occurrence of cell-mediated immunity in the developing chicken embryo. *Immunology* 29, 497–508.

Jungraithmayr, W., Laube, I., Hild, N., Stark, W. J., Mihic-Probst, D., Weder, W., et al. (2013). Bioactive nanocomposite for chest-wall replacement: cellular response in a murine model. *J. Biomater. Appl.* 29, 36–45. doi: 10.1177/0885328213513621

Mitsiadis, T. A., and Harada, H. (2015). Regenerated teeth: the future of tooth replacement. An update. *Regen. Med.* 10, 5–8. doi: 10.2217/rme.14.78

Mitsiadis, T. A., Orsini, G., and Jimenez-Rojo, L. (2015). Stem cell based approaches in dentistry. *Eur. Cell and Mat.* 30, 248–257.

Mitsiadis, T. A., Woloszyk, A., and Jiménez-Rojo, L. (2012). Nanodentistry: combining nanostructured materials and stem cells for dental tissue regeneration. *Nanomedicine (Lond).* 7, 1743–1753. doi: 10.2217/nnm.12.146

Novosel, E. C., Kleinhans, C., and Kluger, P. J. (2011). Vascularization is the key challenge in tissue engineering. *Adv. Drug Deliv. Rev.* 63, 300–311. doi: 10.1016/j.addr.2011.03.004

Oswald, J., Boxberger, S., Jørgensen, B., Feldmann, S., Ehninger, G., Bornhäuser, M., et al. (2004). Mesenchymal stem cells can be differentiated into endothelial cells *in vitro*. *Stem Cells* 22, 377–384. doi: 10.1634/stemcells.22-3-377

Ribatti, D. (2014). The chick embryo chorioallantoic membrane as a model for tumor biology. *Exp. Cell Res.* 328, 314–324. doi: 10.1016/j.yexcr.2014.06.010

Romanoff, A. L. (1960). *The Avian Embryo: Structural and Funtional Development*, *1st Edn*. New York, NY: The Macmillan Co.

Rouwkema, J., Rivron, N. C., and van Blitterswijk, C. A. (2008). Vascularization in tissue engineering. *Trends Biotechnol.* 26, 434–441. doi: 10.1016/j.tibtech.2008.04.009

Rücker, M., Laschke, M. W., Junker, D., Carvalho, C., Schramm, A., Mülhaupt, R., et al. (2006). Angiogenic and inflammatory response to biodegradable scaffolds in dorsal skinfold chambers of mice. *Biomaterials* 27, 5027–5038. doi: 10.1016/j.biomaterials.2006.05.033

Sangaralingham, S. J., Ritman, E. L., McKie, P. M., Ichiki, T., Lerman, A., Scott, C. G., et al. (2012). Cardiac micro-computed tomography imaging of the aging coronary vasculature. *Circ. Cardiovasc. Imaging* 5, 518–524. doi: 10.1523/JNEUROSCI.3593-07.2007.Omega-3

Schmidt, C., Bezuidenhout, D., Beck, M., Van der Merwe, E., Zilla, P., and Davies, N. (2009). Rapid three-dimensional quantification of VEGF-induced scaffold neovascularisation by microcomputed tomography. *Biomaterials* 30, 5959–5968. doi: 10.1016/j.biomaterials.2009.07.044

Staton, C. A., Reed, M. W., and Brown, N. J. (2009). A critical analysis of current *in vitro* and *in vivo* angiogenesis assays. *Int. J. Exp. Pathol.* 90, 195–221. doi: 10.1111/j.1365-2613.2008.00633.x

Stoppato, M., Stevens, H. Y., Carletti, E., Migliaresi, C., Motta, A., and Guldberg, R. E. (2013). Effects of Silk Fibroin Fiber Incorporation on Mechanical Properties, Endothelial Cell Colonization and Vascularization of PDLLA Scaffolds. *Biomaterials* 34, 4573–4581. doi: 10.1016/j.biomaterials.2013.02.009

Wang, K., Yu, L. Y., Jiang, L. Y., Wang, H. B., Wang, C. Y., and Luo, Y. (2015). The paracrine effects of adipose-derived stem cells on neovascularization and biocompatibility of a macroencapsulation device. *Acta Biomater.* 15, 65–76. doi: 10.1016/j.actbio.2014.12.025

Xuan, J. W., Bygrave, M., Jiang, H., Valiyeva, F., Dunmore-Buyze, J., and Holdsworth, D. W. (2007). Functional neoangiogenesis imaging of genetically engineered mouse prostate cancer using three-dimensional power doppler ultrasound. *Cancer Res.* 67, 2830–2839. doi: 10.1158/0008-5472.CAN-06-3944

Conflict of Interest Statement: The authors declare that the research was conducted in the absence of any commercial or financial relationships that could be construed as a potential conflict of interest.